Development of a low-cost marine pCO_2 sensor to characterise the natural variability of coastal carbonate chemistry in the context of global change

Kirsty Shona Hill

B.Sc. (Hons) University of the Highlands and Islands
B.Sc. (Hons) Heriot-Watt University

Submitted in fulfilment of the requirements for the Degree of Doctor of Philosophy

School of Geographical and Earth Sciences
College of Science and Engineering
University of Glasgow

January 2018

Dedication

This Ph.D. is dedicated to The Hills and David Brown

Abstract

Increasing concentrations of CO_2 are being released into the atmosphere from anthropogenic sources which consequently dissolves into the ocean creating carbonic acid. The effect of this is to decrease seawater pH and change the composition of marine carbonate chemistry as a whole. In certain areas of the world's ocean, there is already a substantial natural variability in carbonate chemistry which, in some cases, can exceed the projected figures for long-term anthropogenic acidification. This is especially true of coastal areas which can be subject to increased human activity but also a larger variation of naturally forced biological activity and hydrographically induced fluctuations of water column properties. Anthropogenic acidification will therefore be layered on top of this natural variability and this could have potentially adverse effects on the marine ecosystem. Studies of coastal areas can aid in ocean acidification research by highlighting how organisms cope under the decreasing levels of alkalinity. Because of this, it is vital that we characterise and quantify the drivers of the natural patterns in the marine carbonate system as well as the anthropogenically forced changes that are now evident. Partial pressure of CO_2 (pCO_2) is one of the most important parameters to be measured in conjunction with ocean acidification and carbonate chemistry research. High frequency temporal and spatial measurements of pCO_2 will provide some understanding of the fluxes and their variability and forcing parameters.

To aid the investigation into natural variability of coastal carbonate chemistry, pCO_2 sensors are an invaluable tool for ease of *in-situ* data collection. However, these sensors can require not only specific expertise of utilisation but are also inaccessible to many due to high cost. In lieu of an expensive sensor, the most common way to measure pCO_2 in seawater is with discrete sampling of water and subsequent analysis for two of the three parameters of the carbonate system (dissolved inorganic carbon (DIC), Total alkalinity (A_T) or pH) which is then used to calculate a final pCO_2 value. This method requires a substantial amount of cost, time and labour to not only retrieve seawater from depth, but also employ precise expertise in analyses with each step being potentially fraught with human error.

This research addressed these issues by developing a low-cost, easy-to-use sensor which efficiently and accurately measured coastal marine pCO_2. This required a research and development stage where the sensor and housing design was tested at The University of Glasgow (Chapter 2 and 3) and also deployed in a temperate (Chapter 4) and tropical (Chapter 5) field environment. Seawater samples were also taken and their carbonate chemistry analysed in conjunction with sensor readings to calibrate and confirm the accuracy of the sensor. Along with the developed sensor and the collection of *in-situ* pCO_2 data, other marine variables were also measured (pH, dissolved oxygen, chlorophyll, salinity, temperature, depth, photosynthetically active radiation, dissolved inorganic carbon and total alkalinity) to obtain a characterisation of the areas and an analysis of the drivers behind these variables.

The observed variability in the temperate area of Caol Scotnish, Loch Sween, Scotland was shown to be highly dependent on biological activity and the tidal action which exchanged different water masses into and out of the site. The observed variability in the tropical area of El Quseir, Egypt was shown to be highly dependent on biological activity, temperature and weather events. The sensor coped well in characterising the concentrations of pCO_2 in both sites. There is a larger fluctuation of pCO_2 in the tropical site than compared with the temperate site which is dictated by the relative hydrography in each area and the particular weather conditions experienced.

This research provides industry, scientists and interested parties with a means of monitoring pCO_2 levels in the marine environment in an efficient, easy and low-cost manner and contributes to the demand for the development of these sensors to monitor anthropogenically-forced global change which is layered over already in-flux natural carbonate chemistry.

Table of contents

List of figures

List of tables

Acknowledgements

Firstly, I thank the Engineering and Physical Sciences Research Council (EPSRC) and The University of Glasgow College Sensors Scholarship for providing the funding for this research. I also very gratefully received additional financial research support from the College of Science and Engineering Mobility fund at The University of Glasgow.

I extend the upmost gratitude and thanks to my supervisor Dr Nick Kamenos for the support provided throughout this long journey both academically and emotionally. Your knowledge and empathy was a crucial mix in helping me to the finish line. I would also like to thank Professor Craig Buttar for his invaluable advice and helping me feel my way through the long dark corridor of coding. Thank you also to Professor Maggie Cusack for support and being a truly inspirational figure in the world of academia. Additional academic support was provided by Dr Susan Fitzer who not only demonstrated invaluable laboratory techniques and provided lots of academic support but also gave some great craic on Friday Night Drinks. I was lucky enough to work alongside some fantastic laboratory wizards Harry Jackson (top forensic disposal expert and chemist), Charlotte Slaymark (DIC machine whisperer), Manon Trécu and Penne Donohue who provided some calm words whilst tending to mischievous aquaria. Marine field work is never easy and I am indebted to several people who helped make it not only smooth and successful but also enjoyable. Firstly, I thank Nick Kamenos for his diving expertise and practical instruction. I thank Dr Heidi Burdett for her mermaid tendencies and sampling skills on several field trips but mostly her wonderful companionship in Egypt. I extend gratitude to Heather Baxter who not only is a fantastic diver but supported me on my anxiety-filled crucial first long-term deployment of the sensor.

It has been a bumpy few years and I wholeheartedly thank Iain Ferguson of NHS Scotland for the physiotherapy required after slicing my hand open and nearly losing my thumb two-thirds of the way through the Ph.D. Not only is he a great physiotherapist but he gave fabulous life advice when faced with a panicked Ph.D. researcher. I also thank the (many!) amazing doctors, nurses and

consultants who exhibited the finest skills and care. Thank you to them and NHS Scotland which does the most brilliant work and should be applauded daily.

I now need to thank the excellent people who I have met along the way. Some brilliant office pals – Rebecca Skuce, Heather Rawcliffe, Charlotte McLean, Philippe Nauny, Eric Portenga, Charlie Gilles, Charlotte Slaymark, Alyssa Bell, Heather Baxter, Kate Schoenrock, Jinhua Mao, Bonnie Lewis, Nick Thomas and Callum Graham. A special mention to office angels Adrienne MacArtney for the intellectual chats and general sympatico we shared over wine and gin which eased the stresses of life, Southern Belle Sarah Simpson of which I was very proud to be bridesmaid to (friend for life), Hazel Long who is a superlative agony aunt and friend (and who makes the best Yorkshire strawberry compote), Crystal Smiley for the many gins and a good ear in The Chip and Caroline Miller for the many office chats. An extra special mention to Jill McColl who it would seem I have followed throughout my marine science journey from Oban to Glasgow. Jill was the best support a person could wish for in Glasgow and also the best friend a person could wish for – here's to the next ten years! A final mention to someone who has been and is still very influential in my life both personally and academically, Pete Taylor who not only introduced me to the delights of DIC and A_T analysis many years ago but also has extended to me fantastic friendship, support and quality malts. Away from the Ph.D. bubble I am lucky enough to have brilliant people around me – particularly Rachel Taylor, Laura Crockatt, Carol Anderson, Katie McFarlane-Slack, Eoina Rodgers, Jamie MacRae and many more who have influenced me and given me some of the best memories which will stay with me always.

I have left the best to last where I say the biggest thank you to the most special people a girl has ever had. My family have been superlative in every way throughout my whole life. Each of them has inspired me constantly in so many different ways and I feel like the luckiest person to have their support. My father Dennis has been an inspiration always. He is a caring, loving and supportive man who encouraged his girls to excel in anything they wanted. Both his daughters chose science (like him) and to say he was an inspiration is an understatement. An intellectual giant – I hope I have done him proud. My mother Shona has given me unconditional support and love and I couldn't be where I am now if it wasn't for her. To know even in the worst of times that you

have a Shona in your life, well that means you have the best life of anyone. A wonderful, strong woman who would do anything for anyone, I am so grateful I was born to her. I have always wanted to emulate my big sister Jacqueline (don't tell her). Growing up she was a firecracker of life and energy and always the person you would want to be around (and want to be). She would always protect me and guide me through the pitfalls of not only youth but also adulthood. I am so grateful I got to grow up with her. She wowed the world with her colour chemistry skills and received a Ph.D. for her troubles. As I'm here writing this now – she inspired me to reach the heights she managed. She still continues to reach heights I can only dream of. Thank you Hill Family.

Love and support provided by the inimitable David Brown is my final acknowledgement. He has been with me every step of the way throughout this Ph.D. and I thank him for everything.

Author's declaration

I declare that this thesis, except where acknowledged to others, represents my own work carried out in the School of Geographical and Earth Sciences, University of Glasgow. The research presented here has not been submitted for any other degree at The University of Glasgow, nor at any other institution. Any published or unpublished work by other authors has been given full acknowledgement in the text.

Kirsty Hill

Definitions and abbreviations

AIRICA	Automated Infrared Inorganic Carbon Analyser
ASH	Aragonite Saturation Horizon
A_T	Total alkalinity
$B(OH)_4^-$	Tetrahydroxyborate
$B(OH)_3$	Boric acid
c	Concentration of CO_2
$C_2H_4O_2$	Acetic acid (molecular formula)
$C_{12}H_{14}Br_4O_5S$	Bromocresol green
Ca^{2+}	Calcium ion
$CaCO_3$	Calcium carbonate
CCS	California Current System
CCS	Carbon capture and storage
CH_3COOH	Acetic acid (structural formula)
Chl-*a*	Chlorophyll-*a*
CO_2	Carbon dioxide
CO_3^{2-}	Carbonate ion
CRM	Certified Reference Material
DIC	Dissolved Inorganic Carbon
DO	Dissolved Oxygen
DOM	Dissolved Organic Matter
ENSO	El Niño Southern Oscillation
$f(CO_2)$	Fugacity of carbon dioxide
GND	Ground
GSS	Gas Sensing Solutions
H_2CO_3	Carbonic acid
H_2O	Water
H_3PO_4	Phosphoric acid
HAc	Acetic acid
HCl	Hydrochloric acid
HCO_3^-	Hydrogen carbonate ion (bicarbonate ion)
$HgCl_2$	Mercuric chloride
I_d	Intensity of radiation at 4.25 μm
I_o	Intensity of incoming radiation
IPCC	Intergovernmental Panel on Climate Change
IR	Infrared
ISFET	Ion Selective Field Effect Transistor
$K_{(x)}$	Equilibrium constant
l	Length of optical path from source to detector
MCU	Microcontroller
MISO	Master Input Slave Output
MOSI	Master Output Slave Input
N	Nitrogen
NaCl	Sodium chloride
NCM	Net Community Metabolism
NCP	Net Community Production
NDIR	Non-dispersive infrared
NiMH	Nickel metal hydride
OA	Ocean Acidification
OH^-	Hydroxide

PAR	Photosynthetically Active Radiation (μmol photons m^{-2} s^{-1})
pCO_2	Partial pressure of carbon dioxide
PIC	Particular Inorganic Carbon
POC	Particular Organic Carbon
PP	Primary Production
ppm	parts per million
PTFE	Polytetrafluoroethylene
PWM	Pulse Width Modulation
QICS	Quanitfying Impacts of Carbon Storage
RTC	Real-Time Clock
SCL	Serial Clock Line
SCLK	Serial Clock Line (output from master)
SCUBA	Self-Contained Underwater Breathing Apparatus
SDA	Serial Data Line
SOP	Standard Operating Procedure
SPI	Serial Peripheral Interface
SS	Slave Select
SST	Sea Surface Temperature
SW	Seawater
T-S	Temperature-Salinity
TTL	Transistor-Transistor Logic
UV	Ultraviolet
α	CO_2 absorption coefficient
Ω	Calcium carbonate saturation
ΩAr	Aragonite saturation state
ΩCa	Calcite saturation state
μatm	micro atmospheres

1 General Introduction

1.1 Background

Marine ecosystems are under threat from the potentially damaging consequences of anthropogenic climate forcing (e.g., Andersson *et al.*, 2008; Caldeira and Wickett, 2001; Doney *et al*, 2009; Hoffmann *et al.*, 2010; Johnson *et al.*, 2013). Greenhouse gas concentrations in the atmosphere from anthropogenic sources have risen unprecedentedly in the post-industrial period and are higher than at any time in the last 800 000 years (IPCC, 2014). These levels along with other anthropogenically forced factors are "*extremely likely*" to be the main driver of climate change since industrial times (IPCC, 2014).

Carbon dioxide (CO_2) is a vital component of the global carbon cycle and for the oceanic system as a whole. Carbon contributes to important biological processes within the ocean in the form of CO_2 gas. CO_2 is found in the oceans in a gas phase which is in equilibrium with the concentration of dissolved carbon dioxide. This is known as the partial pressure of CO_2 (pCO_2). The recent increasing concentrations of atmospheric CO_2 is changing the physical, biological and chemical characteristics of the marine environment and causing the oceans to become less alkaline (IPCC, 2014). This process is called ocean acidification (OA) and can have potentially damaging effects on marine ecology and the health of the oceans.

If this process continues unmitigated then it is projected by the year 2100 that there will be a decrease in oceanic surface water pH of between 0.14 and 0.35 units (Meehl *et al.*, 2007; Orr *et al.*, 2005; IPCC, 2014). Since pre-industrial times the global average concentration of CO_2 in the atmosphere has increased from ~ 280 ppm to ~ > 400 ppm recorded at Mauna Loa, Hawaii in May 2016 as shown in Figure 1.2 (Scripps, The Keeling curve) and by the year 2100 this is projected to rise to concentrations between 500 to 1000 ppm (Harley *et al.*, 2006; Hofmann *et al.*, 2010). The oceans have taken up around 30% of anthropogenically sourced CO_2 (IPCC, 2014) and predicted levels, based on existing trends, suggest that a lowering of pH of the oceans by approximately 0.2 units will happen over the next 50 years (Johnson *et al.*, 2013). In both the atmosphere and the oceans, the concentration of CO_2 is increasing at a rate of

approximately 3% per year (Johnson *et al.*, 2013) and the acidity of the surface of the oceans has increased by 26% since the introduction of anthropogenic industrial practices (IPCC, 2014). Historical and current CO_2 concentrations are shown in Figure 1.1.

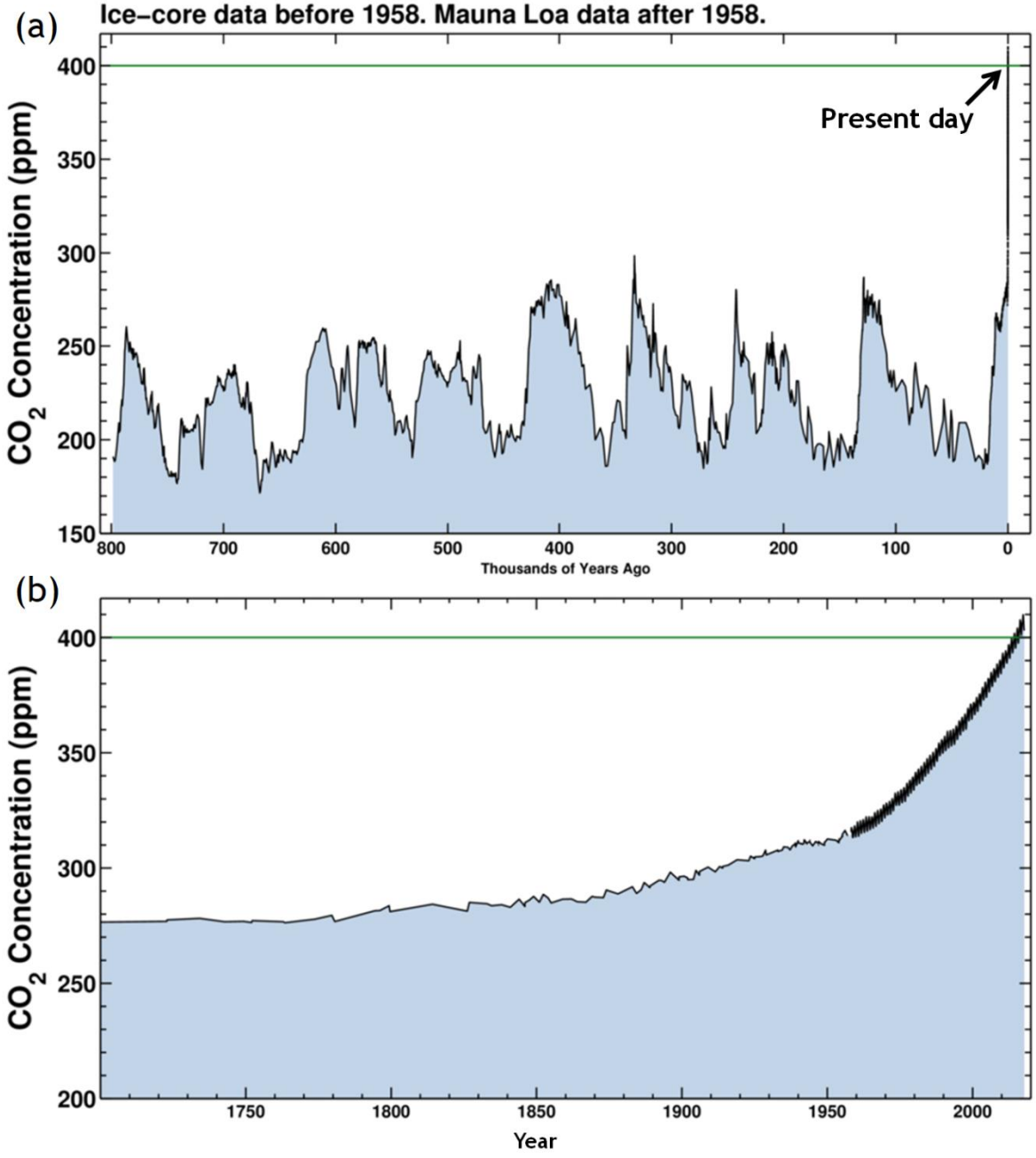

Figure 1.1: CO_2 concentrations from ice cores (pre-1958) and data from Mauna Loa (post-1958). (a) present day atmospheric CO_2 concentration has reached a record high over the past 800 000 years surpassing 400 ppm. (b) CO_2 data from 1700 – present. (Figure adapted from Scripps Institute of Oceanography https://scripps.ucsd.edu/programs/keelingcurve/)

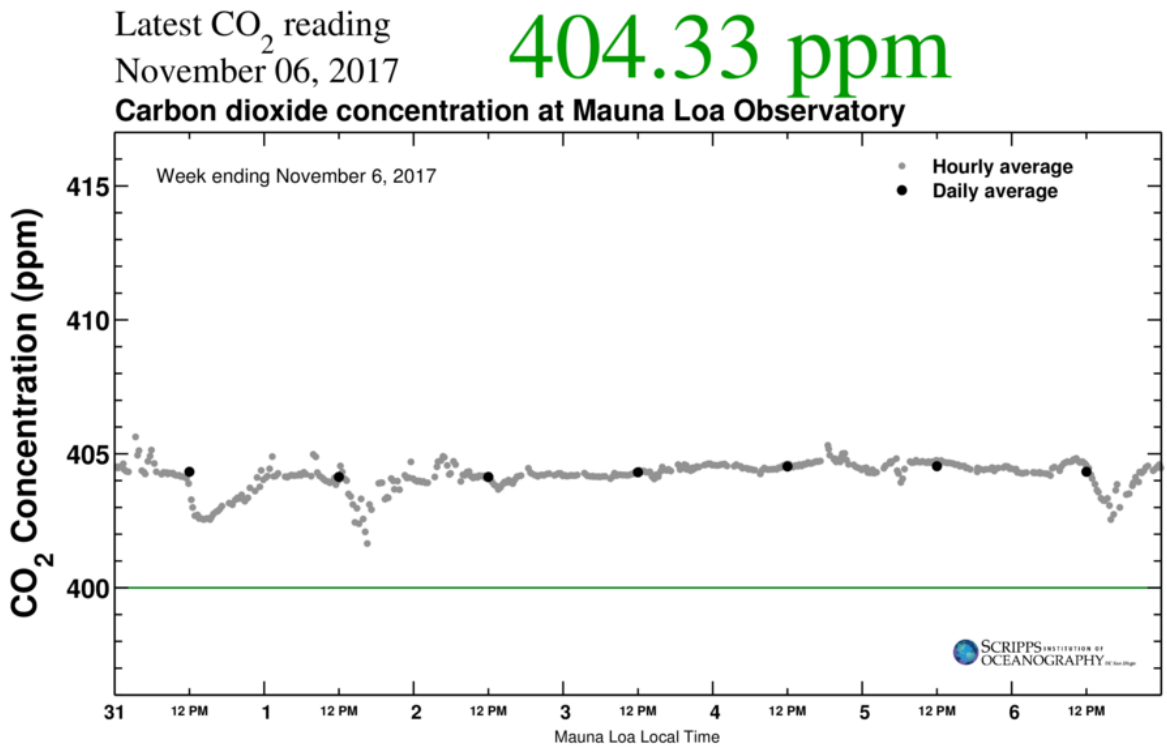

Figure 1.2: An example of daily readings of atmospheric CO_2 (on 6th November 2017) which are recorded at Mauna Loa Observatory, Hawaii. Atmospheric CO_2 has surpassed an average concentration of 400 ppm for the first time in human history and has done since 2016. (Figure adapted from Scripps Institute of Oceanography https://scripps.ucsd.edu/programs/keelingcurve).

As well as the high atmospheric concentration of CO_2, simultaneously the concentration is increasing so rapidly (faster than any natural change that has occurred over millions of years) that any adaptations that organisms can make may be negated by the rate of change occurring (Bell and Collins, 2008; Gienapp *et al.*, 2008; Visser, 2008). Climate models have predicted that a worst case scenario could arise around atmospheric levels of 550 ppm where there could be global net dissolution of coral reefs (Silverman *et al.*, 2009). With the current rise of CO_2 levels in the atmosphere left unmitigated, it is possible that this scenario will arise within this century (Veron *et al.*, 2009).

It has become increasingly important to monitor CO_2 concentrations in the marine environment in an easy and cost-effective manner because of the consequences of OA. For the purpose of this project, an inexpensive sensor was developed to monitor the natural variability of pCO_2 in marine coastal areas. This was also complimented by separate analyses of the wet chemistry of seawater samples and measurements of other variables from established

sensors, e.g. dissolved oxygen (DO), pH, chlorophyll, salinity and temperature. This high-temporal data encompassed both temperate and tropical coastal marine systems and has led to a clearer understanding of the various physical and biogeochemical processes influencing the fluxes of the marine carbonate coastal system and the main drivers behind this natural variability on varying time scales, e.g. diurnal, diel and seasonal cycles.

1.2 Ocean acidification

Ocean acidification describes the trend of increasing acidity within the world's oceans spanning long-term timeframes such as decades or longer (e.g., Orr *et al.*, 2005; Fabry *et al.*, 2008; Kroeker *et al.*, 2013). The main cause of this increasing acidity is the rising amount of CO_2 in the atmosphere from anthropogenic sources like the burning of fossil fuels (IPCC, 2014). This CO_2 sinks into the oceans and changes the existing chemical baseline of the marine environment (Orr *et al.*, 2005). The main driver of gas exchange is the difference in CO_2 concentration between the atmosphere and the sea. Along with the exchange coefficient, these physicochemical parameters dictate the exchange of gas from one medium to another. Temperature has a large influence on this exchange (gas is less soluble in warm water than in cold water) combined with salinity and wind strength (Takahashi *et al.*, 2002; Portner *et al.*, 2005). There is a discrepancy of CO_2 partial pressure between the atmosphere and the surface of the water and eventually equilibrium will be reached between the two mediums. Equilibrium is not immediate however, and can take approximately a year for the CO_2 content of the surface of the ocean and the CO_2 content of the atmosphere to equilibrate (Dickson and Millero, 1987; Leuker *et al.*, 2000). During this time, it is possible to have discrepancies in CO_2 content between the surface of the ocean and the atmosphere. Due to naturally forced events (as opposed to anthropogenic), the majority of these discrepancies on small temporal scales are driven by biological activity (See section 1.3.1, page 15) but also hydrographic and topographic factors which dictate ocean circulation (See section 1.3.2, page 16).

Molecules of CO_2 from the atmosphere dissolve into seawater which then forms a weak acid called carbonic acid (H_2CO_3). The acid dissociates into its constituent ions (hydrogen ion (H^+) and a bicarbonate ion (HCO_3^-)). Therefore,

there is a net increase in the concentration of hydrogen ions which will consequently decrease the pH and increase the acidity. The majority of the hydrogen ions (some will remain as hydrogen ions) will then combine with carbonate ions (CO_3^{2-}) to form additional bicarbonate ions (Leuker *et al.*, 2000). This therefore results in a decrease in the pool of carbonate ions (see Figure 1.3). This has potential consequences for calcifying organisms in the oceans because they will not be able to build their shells or tests as easily (See Section 1.2.1.1, page 9 for further information).

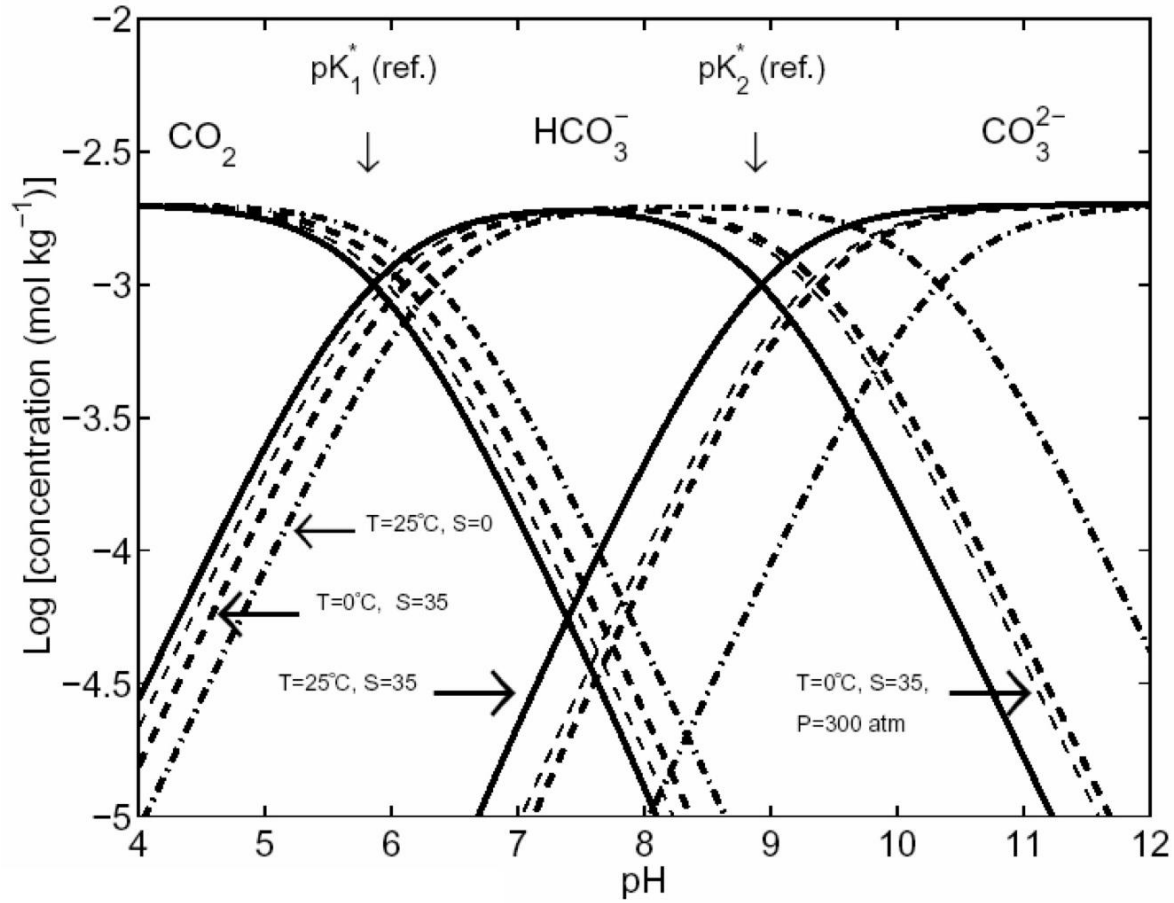

Figure 1.3: Bjerrum plot or the oceanic carbonate equilibrium curve which shows how ocean carbonate chemistry and pH are connected. Atmospheric CO_2 sinks into the ocean creating an acid which then dissociates into its constituent ions. (Zeebe and Wolf-Gladrow, 2001).

Equilibrium constants are used to describe the relationship between the chemical species shown in Figure 1.3 (Riebesell *et al.*, 2010):

$$K_O = \frac{[CO_2^*]}{f(CO_2)}; \quad (1)$$

$$K_1 = \frac{[H^+][HCO_3^-]}{[CO_2^*]}; \quad (2)$$

$$K_2 = \frac{[H^+][CO_3^{2-}]}{[HCO_3^-]}; \quad (3)$$

$$K_B = \frac{[H^+][B(OH)_4^-]}{[B(OH)_3]}; \quad (4)$$

$$K_w = [H^+][OH^-] \quad (5)$$

(K_o = equilibrium constant,

K_1 = 1st dissociation constant of carbonic acid,

K_2 = 2nd dissociation constant of carbonic acid,

K_B = stoichiometric equilibrium constant of boric acid,

K_W = stoichiometric equilibrium constant of water)

These equilibrium constants are all a function of temperature, pressure and salinity (Millero, 2007) and can be used in the calculation of CO_2 (see Chapter 3 for further information).

1.2.1 Consequences of OA

The decrease in pH (see Figure 1.4) and the change of carbonate chemistry of the oceans can potentially have far reaching consequences for the physical and biogeochemical constitution of marine ecosystems including changes in the physiology, growth and reproduction of marine organisms. Therefore, a thorough comprehension of the factors behind these fluxes is important for the understanding of the consequences of the global rise of CO_2 on ocean ecosystems.

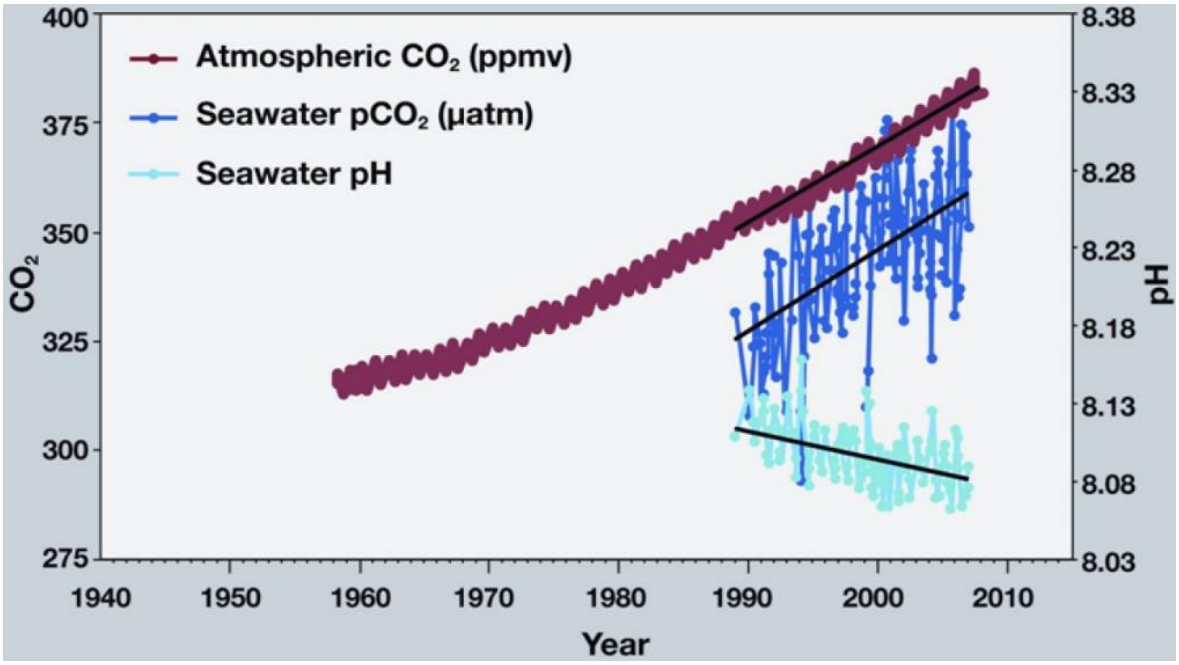

Figure 1.4: Data from Mauna Loa Observatory showing a rise in atmospheric CO_2 corresponding to a rise in seawater *p*CO_2 and seawater pH (NOAA, 2012). Purple line shows atmospheric CO_2 (ppmv), dark blue line shows seawater *p*CO_2 (µatm) and light blue line shows seawater pH.

Models predict that the future repercussions involved with increasing oceanic acidity will be large and varied. In particular, an increase of atmospheric CO_2 from current levels to a stabilised 450 ppm may result in just 8% of coral reefs inhabiting waters that can sustain calcification (Cao and Caldeira, 2008). The Arctic Ocean has been highlighted as an area that could be particularly affected by high concentrations of CO_2. Gas dissolves more efficiently in colder waters and therefore uptake of CO_2, compared to warmer waters, will be greater. Indeed, models suggest that if the concentrations reach a value above 450 ppm CO_2, then environments that are corrosive to aragonite (a polymorph of $CaCO_3$ which some organisms use for calcification along with or instead of calcite, another polymorph of $CaCO_3$) are likely to dominate (Steinacher *et al.*, 2009). Such conditions have already been documented in certain areas of the Arctic Ocean where there has been an increase in sea ice melt which has led to conditions where the undersaturation of aragonite prevails (Yamamoto-Kawai *et al.*, 2009). All areas are affected by ocean acidification and not just the equatorial, tropical areas which are regularly focussed on within this research area.

Most research to date has focused on calcifying organisms and the effects on calcification rates but there is also now an indication that ocean acidification can have other negative effects on fundamental physiological processes such as sexual function and growth (Kurihara, 2008), regulation of body pH (Portner, 2008), photosynthesis (Anthony *et al.*, 2008; Crawley *et al.*, 2010, Iglesias-Rodriguez *et al.*, 2008), respiration (Rosa and Seibel, 2008), behaviour (Munday *et al.*, 2009), and the ability to buffer other stressors in the marine environment (Hoegh-Guldberg *et al.*, 2007; Hutchins *et al.*, 2009; Portner *et al.*, 2005). Studies have shown that lower invertebrates may be particularly susceptible to increasing marine acidification especially during early stages of development and life-history (Portner, 2008). In laboratory perturbation experiments, when pCO_2 concentrations were raised from 360 to 10360 µatm, echinoderm fertilisation rates lowered (Kurihara, 2008). The relevance of using such a high concentration of µatm however is to be questioned as it is unlikely that any organism would survive these levels. A reconstruction of actual extreme concentrations that are predicted in the future would be of more use in OA research. When pH lowers by 0.4 units (this is the extreme limit of future predictions of acidification by 2100), there was a reduced success rate of fertilization of echinoderm eggs (Havenhand *et al.*, 2008). Larval deformities and irregularities occurred in bivalves and echinoderms grown in treatments of 1000 and 2000 µatm (Kurihara, 2008). This also occurred in brittle stars larvae exposed to three levels of pH between 8.1 and 7.7 (Dupont *et al.*, 2008). When the pH decreased by 0.2 units, brittle star larvae mortality increased from 30% to 100% (Dupont *et al.*, 2008). Mollusc larvae metamorphosis, growth and survival rate all decreased when exposed to pCO_2 levels of 650 ppm (Talmage and Gobler, 2009).

Ocean acidification has the potential to alter fundamental ecological factors like the abundance, composition or predation of certain species and therefore fundamentally changing marine ecosystems as well as producing a number of indirect effects. In dynamic areas like shelf and slope ecosystems, the carbon cycle is influenced by the amount of calcification by organisms. Therefore, with interruptions in the ability of organisms to calcify because of higher pCO_2 levels, the carbon cycle will be indirectly affected (Lebrato *et al.*, 2010). The rate of

microbial degradation will be altered and therefore affect nutrient cycling (Swanson and Fox, 2007).

However, some studies have shown that there may actually be some positive impacts from a higher pCO_2 concentration. Seagrass, a key primary producer forming the base for a highly diverse and productive ecosystem, can have an increase in growth under elevated pCO_2 conditions specifically from 477 to 2000 ppm (Hendriks *et al.*, 2010) possibly as a result of higher levels of DIC lowering carbon limitation. This could be an indication of the response from other fundamental primary producers in the coastal system like seaweeds and non-calcifying phytoplankton. It is clear that ocean acidification can cause additional feedbacks but whether they are stabilising or destabilising can depend on a number of factors and although it is a generalisation to say that non-calcifying biogenic habitat may thrive under elevated pCO_2 conditions and calcified structures may suffer, current research suggest that this may be the case. Nonetheless, what is implicitly evident is that more research needs to be undertaken and more data needs to be gathered within this study area.

1.2.1.1 Calcifying organisms

Organisms that form their shells, tests and skeletons from calcium carbonate are at risk from the decreasing pool of carbonate ions which is a direct effect of ocean acidification (Hofmann *et al.*, 2010). These organisms are dependent upon saturation states of the carbonate ion that enables biogenic calcification (e.g. aragonite and calcite) (Andersson *et al.*, 2008; Cohen and Holcomb, 2009). If there is carbonate saturation, then calcification of carbonate structures takes place. However, if there is carbonate undersaturation (which occurs under ocean acidification conditions), then dissolution is more likely to take place. Pacific oyster bivalves (*Crassostrea gigas*) and edible mussels (*Mytilus edulis*), key species important for the health of certain marine habitats, had lowered calcification rates as concentrations of pCO_2 were raised from approximately 600 to 2000 ppm (Gazeau *et al.*, 2007). Eastern oysters (*Crassostrea virginica*) reared at pCO_2 concentrations of 800 µatm had lower larvae growth and calcification compared with ones reared at 280 µatm (Miller *et al.*, 2009; Talmage and Gobler, 2009).

There are three planktonic groups that monopolise calcification within the ocean: pteropods, coccolithophores and foraminiferans (Boyd *et al.*, 2010). Coccolithophores have been the focus of early research into the consequences of changing concentrations of the carbonate ion due to ocean acidification. They are enveloped by calcite plates (coccoliths) and are ubiquitous over the global ocean. In temperate latitudes, they often generate large spring blooms. To produce calcareous structures, they convert two bicarbonate ions (HCO_3^-) to one CO_2 and one $CaCO_3$ so although they contribute to the sink of CO_2 through photosynthesis, conversely they can be a net source of CO_2 into the atmosphere (Boyd *et al.*, 2010). Studies have been extensively carried out on coccolithophores not only because of their abundance but also because of their ecological and biogeochemical importance to the ecosystem. Research has highlighted that with increasing concentrations of CO_2 predicted over the next century, calcification in the coccolithophore species *Emiliania huxleyi* may be reduced (Riebesell *et al.*, 2000; Zondervan, 2007). However, the complex CO_2 cycling involved with coccolithophores means that certain physiological processes could possibly thrive under high-CO_2 conditions. Currently the photosynthetic carbon fixation capacity in *E. huxleyi* is undersaturated so its abundance could increase in the future with the higher predicted CO_2 levels (Rost *et al.*, 2003). Although a complicated system, evidence suggests that the ratio of inorganic carbon to organic carbon will be displaced from the status quo with increasing concentrations of CO_2.

The differences in response to ocean acidification could point to the different pathways that organisms use to calcify (Ries *et al.*, 2009). Monitoring the adaptations of these organisms that usually reside in low-alkalinity areas may give indications to evolutionary and physiological tolerance.

1.2.1.1.1 Maerl and cold-water coral

Temperate field work conducted within this Ph.D. project focussed on an area with a large bed of red coralline algae (*Lithothamnion glaciale*) commonly known as maerl. This calcifying algae is found extensively in coastal areas within the photic zone from the polar regions to the equator. Usually maerl exist in high density populations and have long-life spans of over 100 years (Parry, 1981; Pianka, 1970). The limiting factor for maerl habitat is the

availability of light but they also need an environment which is relatively well flushed with a suitable current which will stop sedimentation (but not so large as to cause displacement or damage (Foster, 2001)). Maerl beds have been suggested to be a sink for atmospheric CO_2 (Bensoussan and Gattuso, 2007; Short *et al.*, 2007) and seem to be highly vulnerable to OA conditions in comparison to other calcifying organisms (Martin *et al.*, 2008).

A study by Findlay *et al.* (2013) focussed on *lophelia pertusa* (a cold water coral) in the Mingulay reef, Scotland. The variability in pH in the area directly above the reef was shown to be relatively large over one semi-diurnal tidal cycle of ~ 0.1 pH unit and a corresponding shift in the levels of pCO_2 concentration of ~ 60 µatm which is postulated to correspond to future levels in ~ 25 year time. In the seasonal cycles, the physical oceanographic drivers dictate the carbonate chemistry of the area. In the summer, surface waters reach the vicinity of the reef due to downwelling and consequently bring higher pH, warmer, oligotrophic waters to an area which would otherwise have waters characteristic to deeper areas in which these types of reefs reside. With these coral already experiencing a high natural variability, the ever encroaching ocean acidification and warming will be a pressing concern for areas like these (and also a useful area to study for information on how organisms survive over large fluxes).

The location focussed on within this research encompassed a vast maerl bed and displayed a notable natural variability of carbonate chemistry due to the presence of these organisms. Therefore this was a suitable site to test the effectiveness of the developed pCO_2 sensor.

1.2.1.1.2 Coral reefs

Tropical field work conducted within this Ph.D. project focussed on an area with extensive coral reefs. Warm water corals reefs inhabit waters that are between 20 – 38 ^{o}C (Nybakken and Bertness, 2005) and therefore are found mostly between 30 ^{o}N and 30 ^{o}S of the equator (See Figure 1.5).

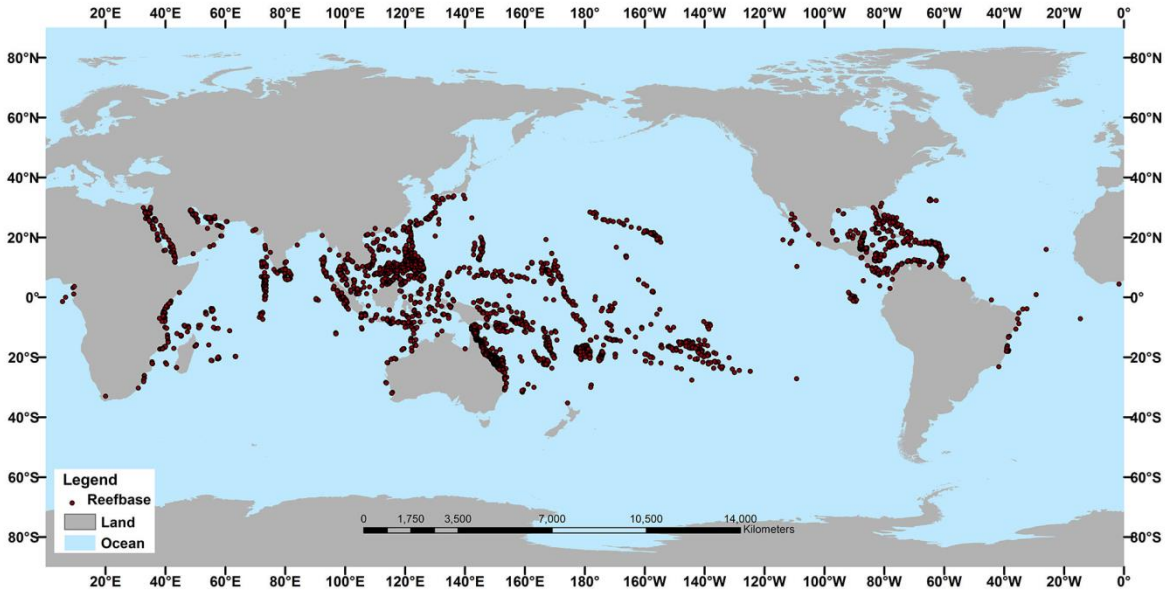

Figure 1.5: Distribution of warm water coral reefs (Adapted from NOAA, 2012).

Corals are calcifying organisms and the surrounding seawater they inhabit must facilitate adequate calcium carbonate production to build reef structures. As such, they are extremely vulnerable to a change in the carbonate chemistry of the water especially under conditions that support calcium carbonate dissolution, i.e. ocean acidification. It is vital that diverse research is undertaken to predict large-scale responses of coral reefs to increasing acidification of the oceans primarily focussing on the physiological response of these organisms to changing seawater carbonate chemistry (Hoegh-Guldberg *et al.*, 2007; Przeslawski *et al.*, 2008; McCulloch *et al.*, 2013; Hoegh-Guldberg *et al.*, 2017; Cornwall *et al.*, 2018; Langdon *et al.*, 2018).

Due to the formation of carbonate, it has been suggested that coral reefs may be a source of CO_2 to the atmosphere (Suzuki and Kawahata, 2003). During the day there is net calcification on coral reefs and conversely at night there is usually net dissolution (Yates and Halley, 2006; Zhang *et al.*, 2012) which will consequently drive the carbonate chemistry of the surrounding water (Bass *et al.*, 2012).

As with the temperate field work, the tropical site was chosen for the suitable test that would be presented to the sensor because of the predicted forcing of the natural carbonate chemistry caused by the reef. Both areas are also of

importance to a vast array of associated organisms that use either the coral reefs or the maerl beds as habitat. These areas need to be closely monitored for any environmental effects of increasing CO_2 in the atmosphere.

1.3 Natural variability of carbonate chemistry in coastal areas

Coastal areas often have a larger and more extreme natural variability in parameters such as pH and pCO_2 compared to the open ocean. Natural variability in fluxes of carbonate chemistry and the resulting natural acidification can be forced by numerous variables. Natural variability of carbonate chemistry also has various spatial and temporal cycles (Johnson *et al.*, 2013). These changes in pH occur over comparatively short periods of time and include a range of physical and biogeochemical influences like photosynthesis and respiration along with tidal mechanisms containing different concentrations of CO_2 (e.g. benthic, atmospheric, low biomass nutrient-deficient waters and high biomass nutrient-rich waters). Weather phenomena can also be a driver of more pronounced fluxes over and above the normal annual and daily cycles. Fresher water can be introduced into a coastal system and therefore can alter the carbonate chemistry of the area and lower the pH (fresh water input lowers the alkalinity content and thus the pH will lower along with A_T) after extreme weather events (Johnson *et al.*, 2013).

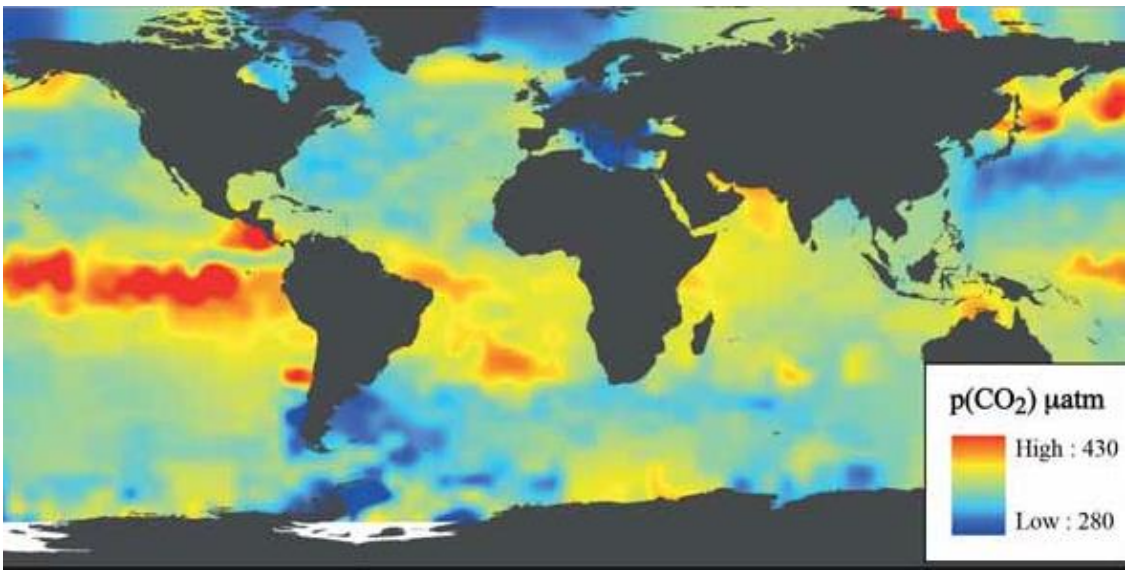

Figure 1.6: Variability of surface pCO_2 (µatm) over the Earth's oceans (Figure from Riebesell *et al.*, 2010)

CO_2 concentration in coastal waters will naturally increase or decrease in environments where:

- There is a differential between the concentration in the atmosphere and the concentration in the water. A higher concentration in the atmosphere will cause the ocean to act as a 'sink' for CO_2 (as it always has done historically) and therefore if there is a higher amount of CO_2 in the atmosphere compared to recent records then the CO_2 concentration in the oceans will consequently increase.

- The temperature of the water decreases (Copin-Montegut, 1988).

- There is a net break-down of organic matter through numerous biogeochemical actions including but not limited to oxygen, sulphate, manganese, iron or nitrate reduction.

- There is formation of calcium carbonate in which the reaction produces CO_2.

Conversely, the CO_2 content of the water column will decrease if there is the presence of the following:

- Transportation of CO_2 from the seawater to the atmosphere.

- CO_2 will be taken up by biological activity when photosynthesising and consequently the CO_2 content in the water column will decrease.

- When calcium carbonate dissolves, CO_2 is consumed in the process and the total CO_2 content will decrease.

- When the water temperature increases CO_2 content can decrease (Copin-Montegut, 1988).

Areas of naturally high CO_2, e.g. shallow CO_2-emitting vents, act as natural laboratories and can help researchers understand and evaluate ocean acidification both on a temporal and spatial level but also on a species/individual ecosystem level (Hall-Spencer *et al.*, 2008; Hall-Spencer and Rodolfo-Metalpa, 2009; Apostolaki *et al.*, 2014).

The natural variation in marine carbonate parameters must be taken into account when looking at current and future effects of ocean acidification on the marine environment. Historical variability in environmental parameters should also be considered when researching ocean acidification since these factors play a considerable part in forming the ecological physiology and natural tolerances of animals in the marine environment and can also be used to see how these animals will adapt to future global change (Riebesell *et al.*, 2010).

1.3.1 Biological processes

The seasonal cycle of DIC and pH is dictated heavily by primary productivity. Throughout the spring and summer months in temperate regions there is an increased amount of primary productivity and consequently there is a drawdown of CO_2 and a rise in the pH unit. The cycle is also alternate and during darkness there will generally be (although not in every case) increased respiration and remineralisation and the concentration of carbon in the water column will increase while the pH will decrease due to the release of CO_2 in these processes. These short-term dynamics combined with the long-term effects should therefore be considered an important factor in ocean acidification studies. Therefore, to adequately predict the future effects of climate change, it is important to understand the natural scope and dynamics of carbonate systems in the marine environment and the reasons behind the variability observed.

CO_2 is an important indicator of trophic activity in the water column and therefore the measuring and monitoring is important for the understanding of the biogeochemical status of the study site. Concentrations of CO_2 give an indication of the temporal and spatial balance between the production of CO_2 during the decomposition of organic matter in respiration and a sink for CO_2 during daily photosynthesis (Rost *et al.*, 2003). An area is described as 'net autotrophic' when there is a larger amount of CO_2 taken up (in processes like

photosynthesis) than given out (in processes like respiration) and likewise, an area is described as 'net heterotrophic' if more CO_2 is given out than taken up. The latter is a process that is more likely to happen under anthropogenic influence where organic matter has been artificially introduced through factors like sewage outflows or agriculture and creates a situation where there is a greater amount of pCO_2 in the seawater than in the atmosphere. Net-autotrophism leads to a situation where the pCO_2 in the seawater is less than that in the atmosphere and this is more likely to happen when there is little or no human influence introduced into the area. Depending on the amount of CO_2 present in a water column, there will be differing types of phytoplankton temporally and spatially over the earth's oceans (although it should be noted that CO_2 is not the only driving factor). Therefore the amount of CO_2 present directly affects the constituent make-up of water column phytoplankton according to their need for available CO_2 (Rost *et al.*, 2003).

1.3.2 Physical processes

Physical drivers like seasonal upwelling has been reported in the California Current System (CCS) (Feely *et al.*, 2008; Hauri *et al.*, 2009). In the North Pacific, there are areas of naturally high respiration which in turn means that the aragonite saturation states are relatively low and therefore especially vulnerable to continued anthropogenic acidification of the ocean. Upwelling and mesoscale eddy formation can force these lower pH water masses with pCO_2 levels of around 1100 µatm (Feely *et al.*, 2008) to the surface and therefore the CCS surface waters could become permanently undersaturated with respect to aragonite within a relatively small time scale in the future (Hauri *et al.*, 2009). Areas where there is similar physical oceanography by virtue of geography may also be at risk of these phenomena, for example, where eastern boundary currents exist (Wootton *et al.*, 2008). The Eastern North Pacific is already undergoing a decrease in pH and therefore increased ocean acidification beyond the projected 0.2 pH unit of average global ocean decrease (Johnson *et al.*, 2013).

1.3.3 Importance of coastal areas

Coastal areas show considerable temporal variability in pH and carbon system parameters and this consequently means that some of these regions will already be experiencing the change that surpasses the projected levels of future pH trends. Large fluxes in natural variability of carbonate chemistry in these areas means that there may be an added stress on these ecosystems combined with the higher pCO_2 concentrations (e.g., Ray *et al.*, 1992; Suchanek, 1994; Sejr, 2011; Wesslander *et al.*, 2011).

Coastal biogeochemistry is often a much more complex field to describe compared to open oligotrophic oceans due to the many different inputs both natural and anthropogenic near coastal areas. Fjordic, estuarine areas are influenced by factors such as fresh-water run-off, agricultural input and hydrographic and topographic physical dynamics which makes the characterisation of coastal areas an often complex and unique task.

The majority of benthic oceanic $CaCO_3$ production is within coastal areas (Borges and Gypens, 2010). Coastal areas contain 20% of surface pelagic oceanic $CaCO_3$ deposition (Gattuso *et al.*, 1998). All of this contributes to the importance of studying these areas with respect to the potential alteration of carbon feedback loops on the ecology of the coastal environment. Coastal areas are widely accepted as being some of the most important ecological and socio-economic areas on the globe (Harley *et al.*, 2006). 43% of the global total of ecosystem goods, e.g. food resources, raw materials and services come from the coastal environment (intertidal zones out to the continental shelf) (Costanza *et al.*, 1997; Martinez *et al.*, 2007). If current trends continue, there is a risk of irreparable damage to marine ecosystems which has a serious knock-on effect for human welfare.

Coastal areas can also be affected by different anthropogenic inputs other than dissolution of atmospheric CO_2 in seawater. Extra nutrients can be introduced into the coastal ocean, for example, deposition of reactive nitrogen and sulphur from the burning of fossil-fuels and agriculture can decrease the alkalinity (Doney *et al.*, 2007). This lowering of alkalinity can be further compounded by the introduction of river water into coastal systems containing a higher acidity

and also through the dynamics and interchange with the sediments on the seafloor (Salisbury *et al.*, 2008). Acidity can also be increased as the oxidation of organic matter from upland areas changes the concentration of carbonate ions in the chemistry of the seawater (Gattuso *et al.*, 1998).

The coastal system is a highly complex and dynamic place where many physical changes happen throughout a variety of timescales from diel to seasonal to annual cycles. Acidification is only one process in many. With global climate change, factors such as temperature, stratification and hypoxia are all being increased (Bograd *et al.*, 2008; Meehl *et al.*, 2007) and anthropogenic acidification will put added pressure on already fragile ecosystems. All these stressors combined will produce unpredictable reactions that cannot be accounted for in single-factor experiments, for example, a combination of higher pCO_2 plus higher temperatures will give a different reaction to the combination of higher pCO_2 and UV light (Swanson and Fox, 2007; Martin and Gattuso, 2009; Gao and Zheng, 2010; Connell and Russell, 2010). In terms of ocean acidification research, coastal regions are of great importance and the complexities of organism response to increasing acidity can give indications on how marine ecosystems can and will cope with future projected levels of CO_2.

1.4 Carbonate chemistry parameters

There are six carbonate chemistry variables which can be used to describe the whole oceanic carbonate system: Dissolved Inorganic Carbon (DIC), Total Alkalinity (A_T), pCO_2, pH along with bicarbonate and carbonate ion concentrations (Marion *et al.*, 2011). Two of these variables can be used along with ancillary data (i.e. salinity, temperature, pressure) to calculate any of the other four variables. DIC and A_T must be derived from analyses of seawater but both pH and pCO_2 can be measured *in-situ* (Clarke *et al.*, 2017).

1.4.1 Hydrogen ion concentration (pH)

pH is defined as the hydrogen ion concentration in a sample of water:

$$pH = -log_{10}(H^+) \quad (6)$$

The pH of a sample is highly dependent on the temperature and pressure, i.e. if the temperature or pressure of the sample is changed, then the pH of the sample will simultaneously change (Riebesell *et al.*, 2010). This is because ionization increases (or decreases) as the temperature of the water increases (or decreases) and therefore the H^+ ion concentration will also increase (or decrease). As a consequence, the pH will decrease (or increase).

1.4.2 Dissolved Inorganic Carbon (DIC)

The definition of total dissolved inorganic carbon (DIC) is as follows;

$$C_T = [CO_2^*] + [HCO_3^-] + [CO_3^{2-}] \ \ (Dickson, 2007) \tag{7}$$

It is the combined total of all of the three carbonate species (aq): carbon dioxide (CO_2^*), bicarbonate (HCO_3^-) and carbonate (CO_3^{2-}). DIC is not related to the temperature and pressure of a sample (Riebesell *et al.*, 2010).

1.4.3 Total Alkalinity (A_T)

The Total Alkalinity (A_T) of seawater can be defined as the seawaters capability to neutralise or buffer an acid, i.e. a resistance to a change in pH. It is the difference in protons in a seawater sample compared to a sample with "arbitrarily defined zero level protons" (Dickson, 1981).

$$A_T \approx [HCO_3^-] + 2[CO_3^{2-}] + [B(OH)_4^-] + [OH^-] - [H^+] \ \ (Dickson, 1981) \tag{8}$$

Because A_T is a neutralisation process it is usually measured by titration. Although with pressure and temperature changes, the individual species that constitute A_T will change, when they are put together linearly as shown in Equation 8, there will be no change to the overall A_T (Riebesell *et al.*, 2010).

1.4.4 *p*CO_2 and the carbonate system of seawater

The partial pressure of carbon dioxide (*p*CO_2) in equilibrium in air with a sample of water is the quantification of the gaseous part of CO_2 in solution. Henry's Law describes the relationship between *p*CO_2 and CO_2^*:

$$pCO_2 = \frac{CO_2^*}{K_0} \quad (9)$$

K_0 represents the solubility of the gas and in seawater this is always constant for CO_2.

Dissolved carbon dioxide (CO_2) exists in the ocean in three main inorganic forms: free aqueous carbon dioxide (CO_2 (aq)), bicarbonate ions (HCO_3^-) and carbonate ions (CO_3^{2-}). One small component of [CO_2 (aq)] is carbonic acid (H_2CO_3) which comprises less than 0.3% of the total. CO_2 is defined as the sum of [CO_2 (aq)] and [H_2CO_3]. Henry's Law connects gaseous carbon dioxide [$CO_{2(g)}$] and [CO_2] when in thermodynamic equilibrium:

$$CO_2\ (g) \overset{K0}{=} [CO_2] \quad (10)$$

where K_0 is the solubility coefficient of CO_2 in seawater which is temperature and salinity dependent (Weiss, 1974). It must be noted that partial pressure is not an expression for the concentration of a real gas but rather an ideal gas. Fugacity is the term used when referring to a concentration of a real gas within a sample of real gases. Ideal gases are used in the thermodynamic equation of state;

$$PV = nRT \quad (11)$$

where P represents pressure, V represents volume, n is the number of moles in a gas, R represents the gas constant and T is the absolute temperature.

When the carbonate components are dissolved in water, they react with water molecules, hydrogen ions and hydroxyl ions and are connected through these acid-base equilibria:

$$CO_2 + H_2O = HCO_3^- + H^+ \quad (12)$$

$$HCO_3^- = CO_3^{2-} + H^+ \quad (13)$$

The speciation of the carbonate components in seawater of a typical surface pH (8.2) is [CO_2] comprising of 0.5%, [HCO_3^-] being 89% and [CO_3^{2-}] being 10.5%. Therefore, this shows that the majority of the dissolved carbonate chemistry consists of bicarbonate ions rather than CO_2. Total dissolved inorganic carbon (DIC) is defined as the sum of the total of the dissolved carbonate species, i.e.,

$$DIC = [CO_2] + [HCO_3^-] + [CO_3^{2-}] \quad (14)$$

DIC, A_T, pCO_2 and pH are all linked and if two of these variables are known then a complete calculation of the carbonate system can be obtained (Zeebe and Wolf-Gladrow, 2001).

1.4.5 Using analytical parameters for calculation of pCO_2

Seawater samples are used to verify pCO_2 concentrations from sensors and this approach was used within this Ph.D. project. CO2SYS is a programme developed to calculate a certain variable from two out of the four carbonate parameters (i.e. pH, A_T, DIC, pCO_2) and supporting data (i.e. temperature and salinity) (Lewis and Wallace, 1998). It is written in compiled Microsoft QuickBASIC and is used in the format of a DOS based .EXE file. CO2SYS is open-source and can be downloaded for use by any interested parties. It is possible to use the program in a single-input mode or a batch-input mode. To calculate pCO_2 as in this research, DIC and A_T were input into the programme with temperature and salinity and pCO_2 was output. It was developed further for use in excel by Pierrot *et al*. (2006). This system allows the user to choose certain constants or scales like the pH scale and equilibrium constants. The user can then enter their two known CO_2 system variables which in this project, were A_T and DIC from laboratory analyses of seawater samples. The program then uses this information to calculate the other CO_2 system variables. For more details on the exact system used in this research please see Chapter 3, Section 3.3.6.3 (page 71).

1.4.5.1 Optimal parameters

Certain combinations of carbonate parameters will provide a better accuracy than others due to propagation of error in certain analyses (Millero, 2007). Riebesell *et al.* (2010) recommend using DIC and A_T for the calculation of pCO_2 due to the relative ease of collecting and preserving seawater samples (the labour involved is the same for both and can be collected at the same time). The samples can be analysed at a later date and the use of CRMs (Certified Reference Materials) ensures a level of accuracy required.

1.5 Development of low-cost pCO_2 sensor

With the increasing recognition of the need for research into ocean acidification over the last decade, there has also been a concurrent and concerted effort into the development of pCO_2 sensors and an emphasis on their use in high-temporal resolution research within the marine environment including the carbonate cycles in the ocean (e.g. Johnson *et al.*, 2007). High-frequency temporal and spatial *in-situ* measurements of pCO_2 can provide a comprehensive overview of the carbonate system of the marine environment including fluxes and net community production (Wayne, 2000; Luger *et al.*, 2006; Takahashi *et al.*, 2009; Bozec *et al.*, 2011). pCO_2 measurements, both on a large and small scale, in coastal areas, continental shelves, fjords, rivers etc. will provide information on the annual, seasonal and diel biogeochemical processes within these areas (Thomas and Schneider, 1999; Thomas *et al.*, 2004; Kaltin and Anderson., 2005; Wesslander *et al.*, 2011).

With this increased emphasis comes a rapid increase in the amount, type and quality of sensors within the field of differing sizes, power, precision, accuracy and stability. Some sensors are capable of deployment on moorings and drifters for over a year with a high-frequency of measurements (e.g. SAMI, PSI CO_2-Pro). Commercial pre-existing pCO_2 sensors are expensive ($25000 - $50000 (Riebesell *et al.*, 2010)) and can be inaccessible to many. pCO_2 sensors have been used in numerous studies (DeGrandpre *et al.*, 1995; Friedrich *et al.*, 1995; Hood *et al.*, 1999; Alvares *et al.*, 2002; Gago *et al.*, 2003; Carillo *et al.*, 2004; Kuss *et al.*, 2006; Kortzinger *et al.*, 2008a, b; Blackford *et al.*, 2014; Shitashima *et al.*, 2015). ACT (Alliance for Coastal Technologies) have also conducted thorough

reviews and testing of several of the advanced pCO_2 sensors that are commercially available.

Equilibration	Phase measurement	Measurement method	Sensor examples
Contact between water-gas	Gas	NDIR	Schar *et al.*, (2010c); Nemoto *et al.*, (2009)
Gas permeable interface	Gas	NDIR	Kayanne *et al.*, (2002); Fiedler *et al.*, (2012); Saderne *et al.*, (2013); this study
Gas permeable interface	Indicator solution	Electrode	Shitashima (2010)
Gas permeable interface	Indicator solution	Fluorescence	Goyet *et al.*, (1992); Tabacco *et al.*, (1999); Rubin and Ping Wu (2000)
Gas permeable interface	Indicator solution	Spectrophotometry	Degrandpre (1993); Lefevre *et al.* (1993); Degrandpre *et al.* (1995; 1999); Wang *et al.* (2002; 2003); Nakano *et al.* (2006); Lu *et al.* (2008)

Table 1.1: Examples of different pCO_2 sensors currently available and their different working methods. References have been provided for details of each of these sensors (adapted from Jiang, 2014).

There are a number of techniques used for *in-situ* measurement of marine pCO_2. One of the most efficient is a spectrophotometric approach. This involves measuring the optical absorbance ratios of samples to which indicators have been added. In this technique, calibration is of utmost importance due to the reliance of measurements based on absorbance ratios of the molecularly characterised indicators. Other techniques include ISFETs (Ion selective field effect transistors) which are deployed on ARGO floats and can provide high-resolution data of pH profiles of water columns. They are calibrated when they reach the deepest point in their descent which coincides with the point where the pH changes are minute. Mass spectrometry can profile DIC but also give concurrent high-resolution profiles of an assortment of dissolved gases. This technique, however, is relatively power-hungry. Ultraviolet spectroscopy is used for direct readings of concentrations of CO_3^{2-} in seawater. UV absorbances are measured at certain wavelengths after lead has been added to the sample. Conductimetry is used for obtaining DIC profiles by acidifying the seawater sample which is then equilibrated over a membrane from an alkaline standard solution. Conductimetry is not suitable for scenarios that need high-frequency measurements, e.g. hourly (Byrne 2014).

For the purposes of this project, non-dispersive infrared techniques were focussed on. The principles of NDIR are discussed in detail in Chapter 2, Section 2.1.1 (page 28).

The main objective of this project was to develop a low-cost, low power autonomous pCO_2 sensor which could be used singularly or in bulk by interested parties without incurring any financial risk. There are many important requirements to take into account that are expected from both industry and the scientific community when designing sensor systems, for example, accuracy and precision, stability of long-term measurements, high frequency of sampling, ease of use/maintenance, low power requirements and consumption.

1.5.1 Other applications

Carbon Capture and Storage (CCS) is being developed as a way to sequester CO_2 from large industrial sources within geological structures either terrestrially or in the ocean where it will not interact with the atmosphere. This method is being regarded as one of the most important ways to mitigate the effects of increasing atmospheric CO_2 and ocean acidification (Gough and Shackley, 2005; Haszeldine, 2009; Wilkinson *et al.*, 2013). The areas of storage must be deemed to be appropriate areas for climate change mitigation, i.e. they must have the ability to contain gases for long-term sequestration. The sites are usually depleted oil and gas reservoirs or saline formations underneath the seafloor (http://www.ccsassociation.org/). If a CCS site were to leak, the associated consequences of CO_2 dissolution in seawater would follow, i.e. increase in acidity, lowering of pH and lower saturation states for polymorphs of $CaCO_3$ to name but a few. Blackford *et al.* (2008) state that damage would only be extensive (>10 km scale) if leaks were persistent and also low in comparison to impacts of OA. This is an area where pCO_2 sensors can be applied in monitoring CO_2 levels in carbon capture and storage areas. In summer 2012, QICS (Quantifying and Monitoring Potential Ecosystem Impacts of Geological Carbon Storage) carried out an environmental experiment in Ardmucknish Bay, Oban whereby small-scale release of CO_2 was simulated as an example of leakage from a CCS site. It was concluded that pCO_2 sensors within this work were effective at detecting and monitoring the rate of emission and concentrations of pCO_2 but also the overall pattern in the area, i.e. the sensors detected that a large and varied pattern of pCO_2 was created by the leakages over the site (Shitashima *et al.*, 2015). A "network" of sensors was recommended by Blackford *et al.*, 2014 for early detection of CO_2 leaks. Therefore, it is vital to further promote,

develop and improve measurement capabilities for seawater pCO_2 and provide it in a manner that is easily accessible.

1.6 Summary and thesis aims

Understanding the drivers behind the regulation of carbonate chemistry variables in coastal systems is a complex one. Coastal areas are recognised as being of special importance in term of OA research as they may naturally already be undergoing the magnitude of future changes projected for overall OA. These environments are therefore important for research not only for the possible adaptations that organisms make to a rapidly changing low pH/high pCO_2 area but also for the added pressure that may be put on these systems from the direct influence of anthropogenic CO_2.

Thesis aims:

- underlining the possible potential of a low-cost *in-situ* pCO_2 sensor by showing the use and benefits in contrasting settings (mesocosms (see Chapter 3), temperate field (see Chapter 4) and tropical field (see Chapter 5));

- to augment knowledge and understanding of this rising technology in all areas of science and industry accountable for analysing coastal carbonate chemistry monitoring;

- to systematically trial the sensor in a scientifically defensible way at moderately small costs in terms of time, labour and money and;

- use this sensor and other supporting sensors to characterise the natural variability of marine parameters in two different field environments, i.e. a temperate and tropical area.

A flow diagram is shown in Figure 1.7 to further clarify the stages of progression throughout the duration of this research.

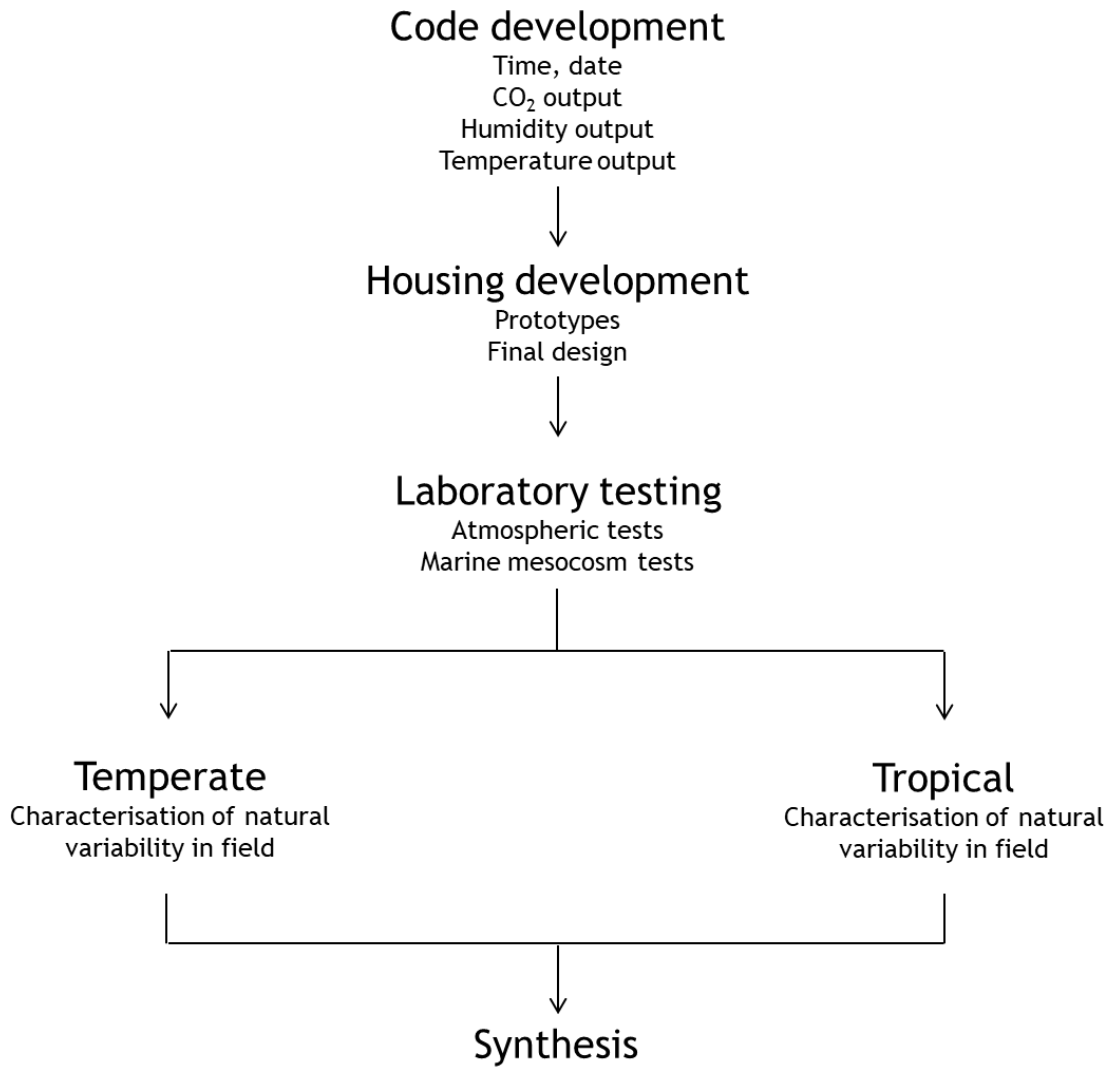

Figure 1.7: Links between stages of R&D and field work

1.7 Thesis organisation

The thesis contains 7 Chapters in the following order:

- Chapter 2: ***"Development of a low-cost pCO_2 marine sensor"*** provides a comprehensive overview of the development and manufacture of a marine-proof pCO_2 sensor complete with tests of electronic platforms, battery sources and housing.

- Chapter 3: ***"Laboratory performance evaluation of pCO_2 sensor"*** consists of performance tests of the sensor, battery pack and housing in a variety of environments both atmospheric and marine.

- Chapter 4: ***"Characterising natural variability of coastal carbonate systems and ancillary variables in a temperate marine environment"*** presents data from Loch Sween, Scotland using the developed pCO_2 sensor and ancillary sensors to construct a description of the drivers behind the natural variability of carbonate chemistry in the area.

- Chapter 5: ***"Characterising natural variability of coastal carbonate systems and ancillary variables in a tropical marine environment"*** presents data from the Red Sea, Egypt using the developed pCO_2 sensor and ancillary sensors to construct a description of the drivers behind the natural variability of carbonate chemistry in the area.

- Chapter 6: ***"General discussion"*** brings together all results including an evaluation of the development and performance of the pCO_2 sensor in the laboratory and an assessment of results from data collection in both temperate and tropical areas.

- Chapter 7: ***"Conclusions"*** presents a summary of the results and also suggestions for future development and uses of the pCO_2 sensor.

2 Research and development of pCO_2 sensor

2.1 Introduction

The operation and measurement principle of a pCO_2 sensor, as well as the manufacture of a hydrophobic, gas diffusive housing, is described in this chapter. The sensor is based on non-dispersive infrared (NDIR) principles and was developed to measure the partial pressure of CO_2 in the marine environment. Three electronic platforms were tested (Mega 2560 R3, Tinyduino and Arduino Uno) and software was developed with the aim of producing a stable, accurate and precise marine pCO_2 reading in a cost-effective manner.

In researching atmospheric CO_2 sensors, it was found that there were many existing sensors that were cheap and could be modified. It was crucial however, to pick the right sensor. The COZIR CO_2 sensor which is manufactured by Gas Sensing Solutions (GGS) fitted the specifications needed to use within this project for the design of the marine pCO_2 sensor. There are several principles on which carbon dioxide sensors work but the favoured industry method is NDIR and although not as cheap as other methods, preferred standards of stability, accuracy and low power consumption are achieved (Gibson and MacGregor, 2013).

2.1.1 Principles of non-dispersive infrared (NDIR) CO_2 sensors

NDIR operates on basic spectroscopic principles of wavelength absorption where different gases will absorb infrared light at different wavelengths, more specifically gas molecules will absorb packets of energy that are the same as their own discrete vibrating energy. Infrared radiation is absorbed by CO_2 molecules at numerous wavelengths (2.7, 4.25, 15μm (Skoog *et al.*, 2006)) but the optimum wavelength is at 4.25 μm where there is lower interference (Kaur *et al.*, 2015).

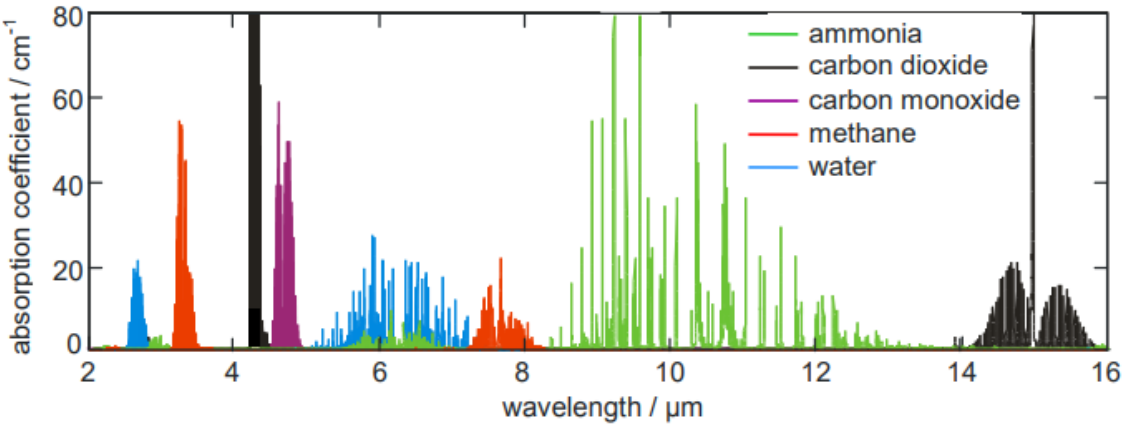

Figure 2.1: Absorption spectra in the mid-infrared range of 5 different gases. Gases can be identified by their individual wavelengths. In the infra-red range, the spectra are in the form of lines which represent molecular vibrations within discrete energy levels. (Figure adapted from Hodgkinson and Tatam, 2012).

The gas concentration is then determined because the gas-absorbing degree is directly proportional to this concentration. The radiation which is absorbed is connected to the CO_2 by the Lambert-Beer law (Equation 15) (Gopel *et al*, 1991; Kwon *et al*, 2009);

$$\frac{I_d}{I_o} = e^{-\alpha c l} \tag{15}$$

(where I_d = intensity transmitted through sample; I_o = reference intensity or intensity input into sample (standard); α = CO_2 absorption coefficient; c = concentration of CO_2; l = length of the optical path from source to detector).

The components of an NDIR CO_2 sensor include an IR (infrared) radiation source, detector, optical bandpass filter and an optical path between the source and the detector (see figure 2.2). The bandpass filter limits the IR intensity that is measured in a specific wavelength region. The detector measures the reduction in intensity of the signal. The CO_2 concentration is therefore given by Equation 16;

$$CO_2 \propto \ln \frac{I_d}{I_o} \tag{16}$$

IR light interacts with most molecules by exciting molecular vibrations and rotations. When the IR frequency matches a natural frequency of the molecule, some of the IR energy is absorbed.

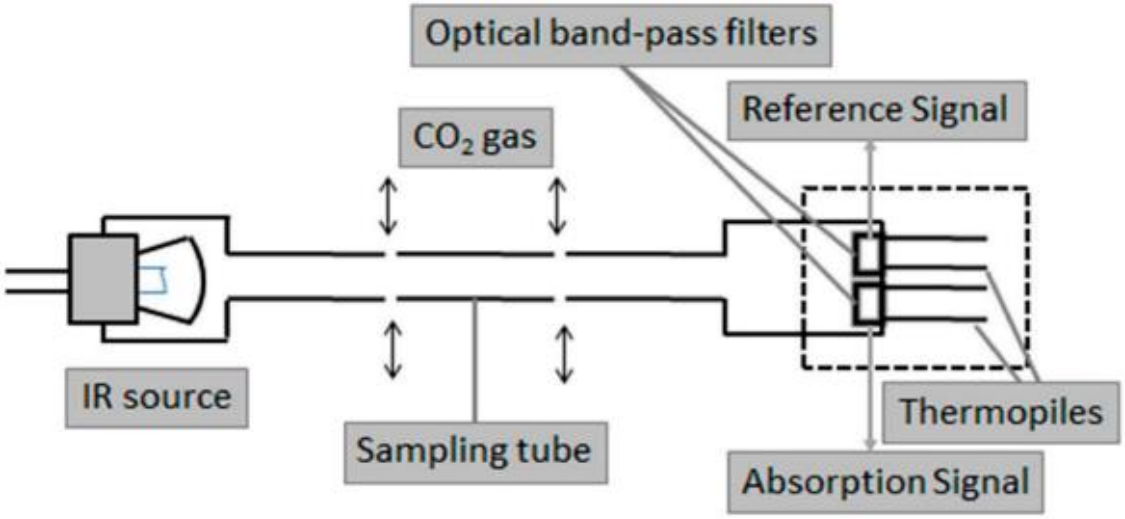

Figure 2.2: Basic structure of an NDIR CO_2 sensor including IR lamp, a chamber, optical filter x 2 and thermopiles (Figure adapted from Wang *et al*., 2005).

For gases, the molecular density is directly proportional to the pressure and inversely proportional to the temperature. Thus, temperature and pressure corrections must be applied when using IR absorption to determine CO_2 concentrations (Lee and Lee, 2001). Fundamentally, it is the density of the gas within the chamber that is measured (Mendes *et al*., 2015). Therefore, this technique is dependent on the ambient temperature and pressure so these variables must be taken into account to produce accurate measurements (Mendes *et al*., 2015). The difference in the amount of infrared input into the sensor at the source and the amount detected by the receiver in the final reading is measured. This will give the concentration of CO_2 molecules in the gas chamber using this proportional relationship (Lee and Lee, 2001). This whole process is achieved by diffusion over a PTFE membrane.

2.2 Motivation

2.2.1 Importance of pCO_2 measurement in the marine environment

To be able to understand the natural variables which drive the climate, effective monitoring of the environment and these variables is essential (DeGrandpre, 1993; Johnson *et al.*, 2007). There is a need to have comprehensive *in-situ* monitoring of these parameters in both high quantity and high quality (Johnson *et al.*, 2013). The reasons for continuous measurement of pCO_2 in the marine environment are numerous;

- Firstly, we can establish if a coastal area is acting as a source or sink of atmospheric CO_2 (Takahashi *et al.*, 1993; Raven and Falkowski, 1999; Takahashi *et al.*, 2002; Sabine *et al.*, 2004; Dore *et al.*, 2009; Capone and Hutchins, 2013; Garrard *et al.*, 2013). Dynamic physical and biogeochemical processes at the surface of the ocean govern the content of CO_2 dissolved at the surface. These processes can take place over different temporal and spatial patterns (Watson *et al.*, 1991). pCO_2 measurements, both on a large and small scale, in coastal areas, continental shelves, fjords, rivers etc. will provide information on the annual, seasonal and diel biogeochemical processes within these areas (Thomas and Schneider, 1999; Thomas *et al.*, 2004; Kaltin and Anderson, 2005; Wesslander *et al.*, 2011). The variability of coastal environmental parameters such as DO, pH, temperature, salinity and dissolved CO_2 is large and differs throughout each system on a regional (Steinacher *et al.*, 2009), seasonal (McNeil and Matear, 2008), latitudinal (Orr *et al.*, 2005) basis. It can also vary with depth (Caldeira and Wickett, 2003) or habitat (Striegl *et al.*, 2007). Coastal areas are projected to be of increased risk to global change compared to open areas of the ocean and it is therefore imperative to characterise the variables in these areas (Capone and Hutchins, 2013). Continuous, high-temporal and spatial measurements of *in-situ* pCO_2 will go some way in helping to provide that information easily and create an understanding of the drivers and the variability behind fluxes in different coastal areas (Johnson *et al.*, 2013).

- This type of monitoring is also useful for determining the effects of the changing water saturation states for calcifying organisms. The saturation states of calcite and aragonite can be calculated with these continuous pCO_2 measurements and one other parameter of the carbonate system (pH, T_A or total DIC) and can therefore aid in the monitoring of the ecosystems (Dickson *et al.*, 2007).

- Net Community Production (NCP) can be measured directly through this process. This is a highly variable process over several timescales and continuous measurements will help contribute to better records of how the carbon cycle changes and over what times scales it changes (Wayne, 2000; Luger et al., 2004; Bozec *et al.*, 2006; Johnson *et al.*, 2007; Takahashi *et al.*, 2009; Capone and Hutchins, 2013; Takeshita *et al.*, 2016). High-frequency temporal and spatial *in-situ* measurements of pCO_2 can provide a comprehensive overview of the carbonate system of the marine environment including fluxes and net community production (Wayne, 2000; Luger *et al.*, 2004; Bozec *et al.*, 2006; Takahashi *et al.*, 2009).

In the past, the most common method of monitoring ocean carbonate chemistry would have to be conducted on scientific cruises that were typically labour intensive, logistically complex and expensive to run (Degrandpre, 1993). Seawater samples are usually removed from the *in-situ* environment by means of recovering samples from depth where subsequently, analysis in a wet chemistry laboratory would take place to calculate a pCO_2 value. However, problems arise with such non-continuous sampling for a few of the carbonate parameters. pH cannot be directly transferrable when taken out of situ because this measurement is specific to the temperature and pressure conditions from which it was retrieved. This is also true of fugacity measurements of CO_2 (Dickson *et al.*, 2007). However, because samples of DIC and A_T do not change when the temperature or pressure of the sample changes, the laboratory and *in-situ* values are interchangeable. It is important to choose carbonate parameters carefully when quantifying a marine system. DIC and A_T measurements will ensure a certain level of accuracy for calculations of CO_2 (Byrne 2014) and therefore these two parameters have been chosen for the purpose of this

project enabling direct comparison to the developed sensors readings. This method of deriving a value for pCO_2 is however fraught with difficulty. Depending on topography, hydrography, climate conditions, equipment and budget, sampling can be an arduous task. While sensors can be programmed to log as needed, the retrieval of seawater from depth as often as desired to give a comprehensive picture of the carbonate chemistry of an area can often be an impossible task due to a variety of logistics. Traditional data collection (seawater samples without *in-situ* sensor measurement) would only provide a one-dimensional moment in time at one location and are subsequently limited in their extent of accurate extrapolation. Because of these restrictions in data collection, there is a growing demand for development of different techniques which are more likely to aid the gathering of important *in-situ*, long-term data (Petersen *et al.*, 2011). The subsequent analyses in the laboratory are also time consuming with possible error propagation throughout the process (Frank *et al.*, 2014). Seawater analyses is only useful if there is exacting and precise practice throughout numerous steps (Bockmon and Dickson, 2015), i.e. in collection, in storage and in each step of analyses. Obtaining better spatial and temporal resolution in measurements will mean a concerted effort on behalf of the scientific community towards development of sensors and this project goes some way to making the process easier and more accessible to all interested parties.

Samples of seawater can still be an important aspect of marine CO_2 calculation however. As mentioned, samples can be analysed and the subsequently calculated values can be used to corroborate *in-situ* readings made by sensors. It is a possibility that you can characterise the whole CO_2 system in a sample of seawater (Dickson, 2007). A sample of seawater can be analysed for dissolved inorganic carbon (DIC) which can be measured in the laboratory by acidifying the seawater and consequently measuring the resultant CO_2 gas that is produced:

$$C_T = [CO_2^*] + [HCO_3^-] + [CO_3^{2-}] \quad (17)$$

Total alkalinity (A_T) was the other parameter (for the purpose of this project) that was analysed within the seawater samples. Together with DIC, this parameter is used to calculate the CO_2 content of the specific seawater sample

using the computer programme CO2SYS. A_T is the total of the surplus proton acceptors over proton donors in 1kg of seawater sample:

$$A_T = [HCO_3^-] + 2[CO_3^{2-}] + [B(OH)_4^-] + [OH^-] + [HPO_4^{2-}] + 2[PO_4^{3-}] + [SiO(OH)_3^-] + [NH_3] + [HS^-] + \cdots - [H_F^+] - [HSO_4^-] - [HF] - [H_3PO_4] - \cdots; \quad (18)$$

Titration of the seawater sample with hydrochloric acid is the method of analysis for A_T. Both these techniques were utilised within this project to obtain a value of CO_2 for seawater samples which were subsequently compared with the readings on the developed pCO_2 sensor (see chapters 3, 4 and 5).

There are many crucial factors to take into account when developing these types of sensors, e.g. ideally they would be autonomously operated with only occasional servicing and calibration, they would have the ability to make high-frequency measurements with the desired accuracy and precision needed, they would be resistant to biofouling, easily utilised and functional with other sensors, have a compact size, a low power usage, a low cost and be simple to use.

The development of the autonomous pCO_2 sensor within this project has provided sustained *in-situ* data collection for different coastal sites, i.e. a temperate coastal site and a tropical coastal site (see Chapter 4 and Chapter 5 respectively). Ultimately, this pCO_2 sensor can be used to measure on a daily, weekly and, in future work, potentially seasonal and annual time scales.

2.3 Aims

The objective of this part of the project was to produce a coastal, marine pCO_2 sensor which fulfils the following criteria:

- it must be produced at a relatively low-cost;
- it must be operable on low-power;
- it must accurately measure marine pCO_2;

- it must be practical to use in a marine field environment, i.e. compact, lightweight and portable;

- it must be able to log data autonomously, i.e. data is downloaded and retrievable once recovered;

- it can be programmed for different measuring needs; and

- it must be suitable for the marine environment, i.e. durable and able to withstand saltwater submersion, corrosion and biofouling.

Thus the sensor needed to be able to characterise the natural variability of pCO_2 in marine coastal areas easily, efficiently and accurately at a relatively low-cost.

2.4 Materials and methods

Several stages were involved in the initial design of the marine pCO_2 sensor;

1. Software was developed using several codes which were used with several combinations.

2. Suitable housing was developed and several options were investigated.

Each stage is described in detail within this chapter.

2.4.1 Specifications of the sensor

Because this sensor was used to get patterns of hourly, daily, weekly and (for future work) annual carbonate chemistry patterns minute accuracy was not necessary. Due to the highly variable nature of carbonate chemistry in coastal areas compared to the very slight changes of parameters in open, pelagic areas, an accuracy such as ±1 μatm was not needed (for examples of coastal versus pelagic variability see, e.g. Ohde and van Woesik, 1999; Hales *et al.*, 2005; Wootton *et al.*, 2008; Hofmann *et al.*, 2011; Baumann *et al.*, 2015). pCO_2 in coastal areas regularly fluctuates by more than 50 μatm and therefore the

accuracy of the COZIR CO_2 sensor (COZIR-AH-2000) fulfils the needs of this project (see bullet point 3 below).

Further to this, the COZIR CO_2 sensor also met many more of the requirements for basing the marine pCO_2 sensor on (details in Table 2.1):

1. The sensor operates on NDIR technology by diffusion of CO_2 over a PTFE membrane;

2. It is one of the lowest power NDIR sensors manufactured for commercial use and is able to run on ultra-low power (3.5 mW);

3. The sensor measures from 0 – 2000 ppm and has an accuracy of ± 50 ppm (N.B. the correct units for atmospheric CO_2 is ppm and likewise, for CO_2 in water is µatm. This does not affect the numerical value which is interchangeable between media);

4. Runs on a supply voltage of 3.3 v and has a peak current of 33 mA;

5. The warm-up time is less than 10 seconds. There is 1.2 seconds to the first reading and the response time is 30 seconds to 3 minutes (this can be configured within software using coding). The reading is refreshed twice per second.

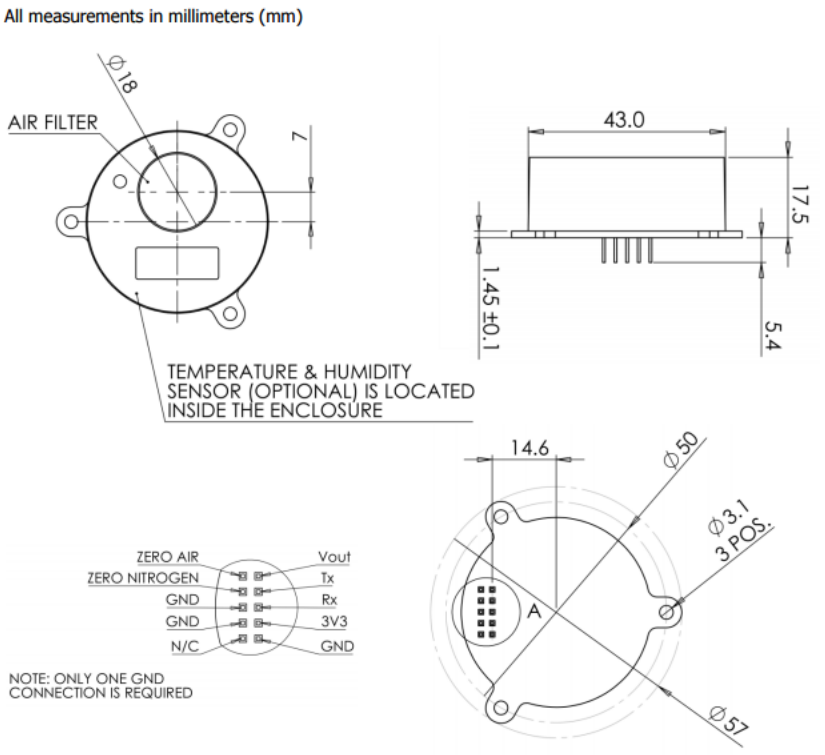

Figure 2.3: Dimension schematic of COZIR-AH-2000 Ambient CO_2 sensor (Courtesy of GSS Data Sheet http://www.gassensing.co.uk/media/1050/cozir_ambient_datasheet_gss.pdf). All measurements in mm.

Figure 2.4: COZIR-AH-2000 Ambient CO_2 sensor from GSS

General Performance	
Warm-up time	< 10s. 1.2s to first reading
Operating conditions	0^oC to 50^oC (standard), -25^oC to 55^oC (extended range) 0 to 95% RH, non-condensing
Recommended storage	-30^oC to $+70^oC$
CO2 Measurement	
Sensing method	Non-dispersive infrared (NDIR) absorption. Patented gold-plated optics, solid-state source and director
Sample method	Diffusion
Measurement range	0-2000ppm, 0-5000ppm, 0-1%
Accuracy	±50 ppm +/- 3% of reading
Calibration	Autocalibration
Non linearity	< 1% of FS
Pressure dependence	0.13% of reading per mm Hg in normal atmospheric conditions
Operating pressure range	950 mbar to 1050 mbar
Response time	30 secs to 3 mins (Configurable via filter type and application) Reading refreshed twice per second
Electrical/Mechanical	
Power input	3.25 to 5.5v (3.3v recommended), peak current 33 mA, average current < 1.5mA
Power consumption	3.5 mW

Table 2.1: Specifications of COZIR-AH-2000 ambient atmospheric CO_2 sensor (information courtesy of http://www.airtest.com/support/datasheet/COZIRSerialInterface.pdf).

2.4.2 Electronics platform development

The sensor required specific programming in order for it to meet the needs of this project. The preassembled sensor was only an atmospheric sensor and would not run in that form and needed to be adapted for marine use. For it to run autonomously and record the necessary data in the correct way, the sensor was required to be integrated into an electronics platform onto which code for the sensor could be uploaded. For this project, the open-source electronics prototyping platform Arduino was chosen.

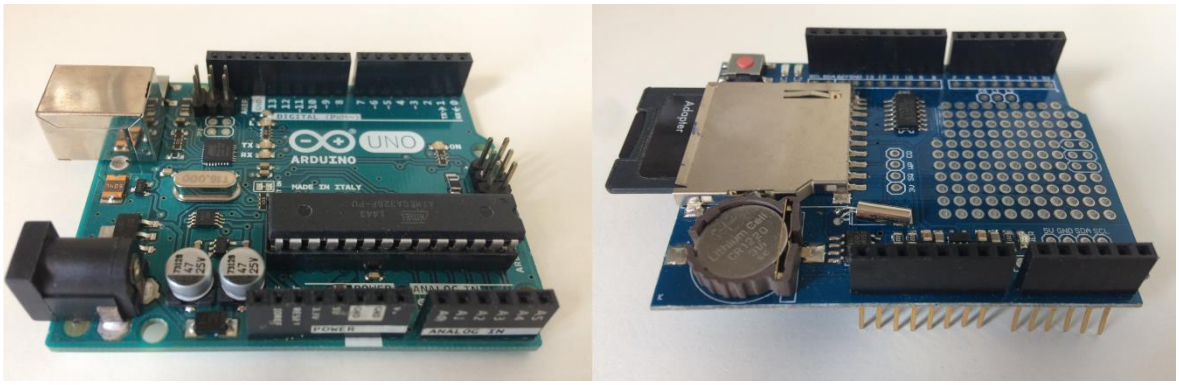

Figure 2.5: Left: Arduino UNO board including microcontroller and USB input. Right: RTC shield with SD card attachment. The RTC shield is stacked on top of the UNO. The shield fits into the pins on the UNO board without impeding the functionality of the main Arduino pins.

It has easily manipulated hardware and software for a large variety of uses and is a relatively cheap and low-power platform. There are many different forms of boards and extensions for different needs which can either come preassembled or in parts to suit the developer's needs. Arduino boards have a microcontroller which can be programmed using the coding language of C and can be run on a laptop or autonomously with battery power. Specifically, Arduino was useful for this project because it was cheap, enabled communication with the sensor (not easy to do on other platforms), enabled the sensor to be powered by batteries and also allowed for the 'dumping' of data onto an SD card on an extension board or 'shield' (see Figure 2.5).

Specifically, the Arduino Uno board was chosen as the best main platform upon which to programme the sensor for different sampling needs.

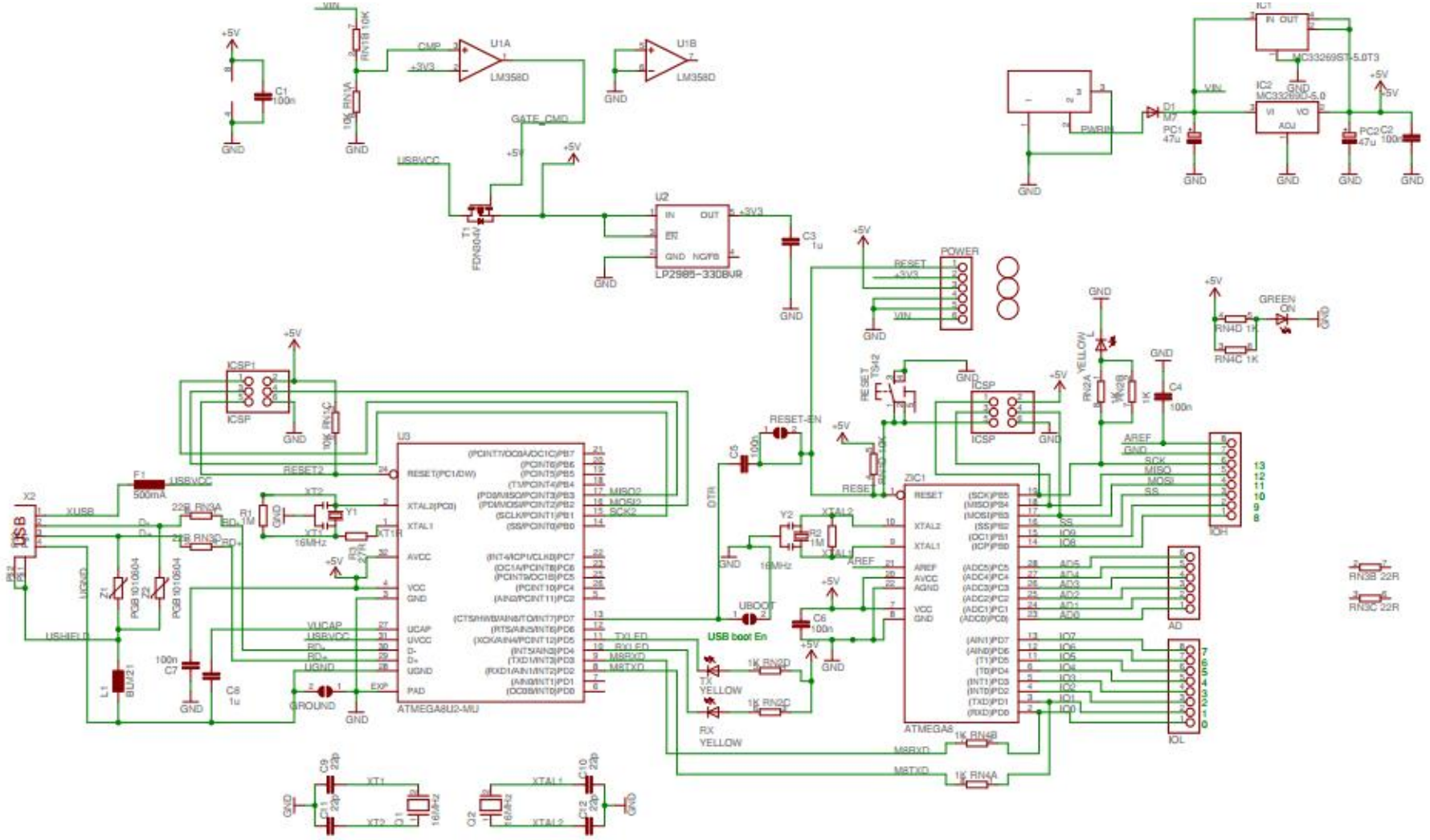

Figure 2.6: Schematic of Arduino Uno board (Courtesy of https://www.arduino.cc/en/uploads/Main/arduino-uno-schematic)

Technical specification	
Microcontroller	ATmega328
Operating voltage	5v
Input voltage (recommended)	7-12v
Input voltage (limits)	6-20v
Digital I/O pins	14 (of which 6 provide PWM output)
Analogue input pins	6
DC current per I/O pin	40 mA
DC current for 3.3v pin	50 mA
Flash memory	32 KB of which 0.5 KB used by bootloader
SRAM	2 KB
EEPROM	1 KB
Clock speed	16 MHz

Table 2.2: Technical specifications of Arduino Uno board (https://www.arduino.cc/en/Products/Compare)

2.4.2.1 Specific components of Uno

Transistor-transistor logic (TTL) serial data is received and transmitted via pins 0 (RX) and 1 (TX) (see Figure 2.7). The ATmega8U2 USB-to-TTL serial chip is linked to these pins. The ATmega328 will store code via a flash memory (see specifications in Table 2.2). It is possible to 'interrupt' signals via pins 2 and 3 whereby specified code can stop signal to these pins (this is relevant to future work in Chapter 6, Section 6.7 (page 292). This is useful if wanting to conserve power during deployment. Pins 3, 5, 6, 9, 10, and 11 supply pulse width modulation (PWM) which allows the digital pins to mimic analogue output, i.e. a simulation of values between both HIGH and LOW although still being output as a digital signal.

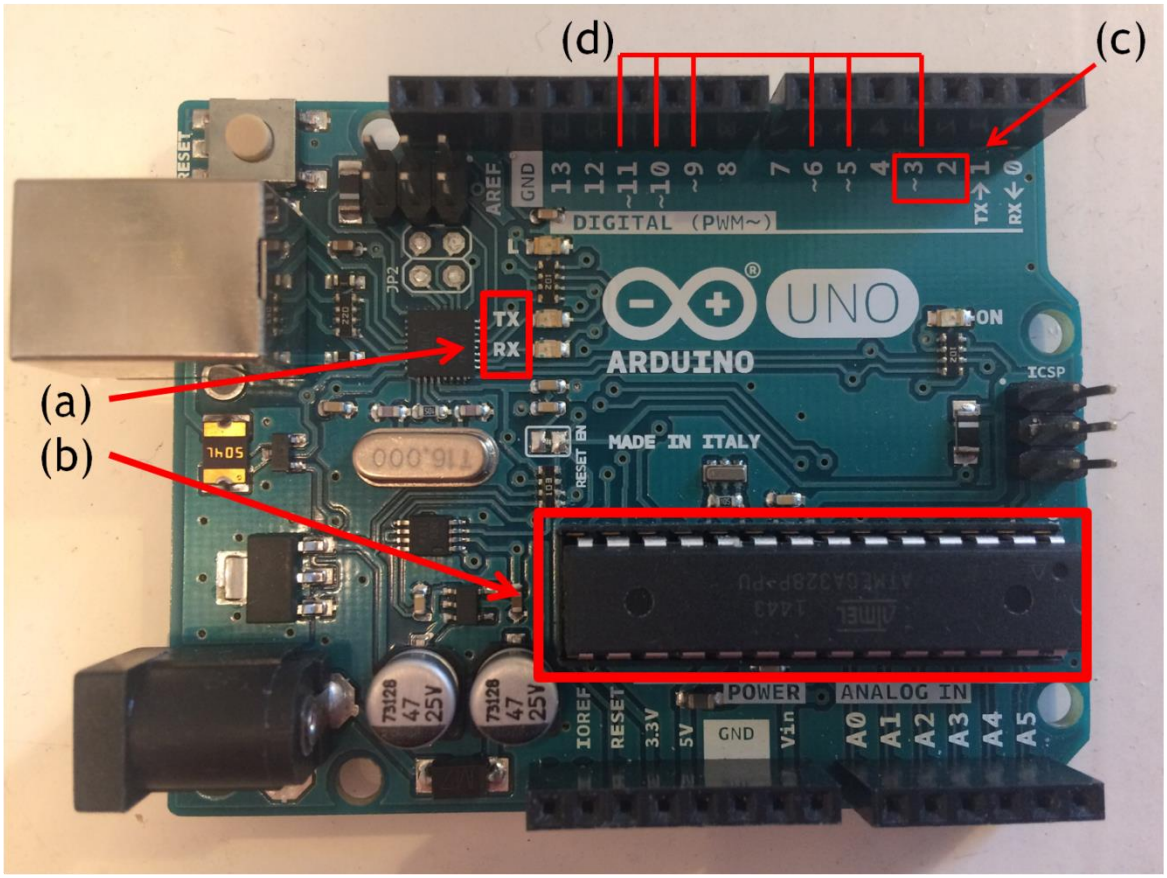

Figure 2.7: Specific components of the Arduino Uno (more information in the body of the text). (a) RX and TX. (b) ATmega8U2. (c) Pins 2 & 3. (d) PWM pins.

There is very low power loss (supplies full voltage but for varying durations of time) in this arrangement which is highly advantageous for the purpose of this project. Not only do these methods save power but they also produce a superior signal. There is also the choice of a serial peripheral interface (SPI) which will link data from the microcontroller and SD card on this set-up. SPI can be used instead of the serial ports (TX and RX) which has the advantage of more control over when data is sent and also the synchronicity of that data. Instead of TX and RX, that may have slightly different synchronicity with the internal clock, SPI will ensure individual lines for sending data and an internal 'clock' that will ensure both lines stay in sync. A similar arrangement that Arduino also caters for is I^2C communication. I^2C is like SPI but instead of one 'master' and multiple 'slaves', I^2C can also have multiple 'masters' ('master' is usually the part of the circuit that generates the clock signal and the 'slave' usually receives this signal).

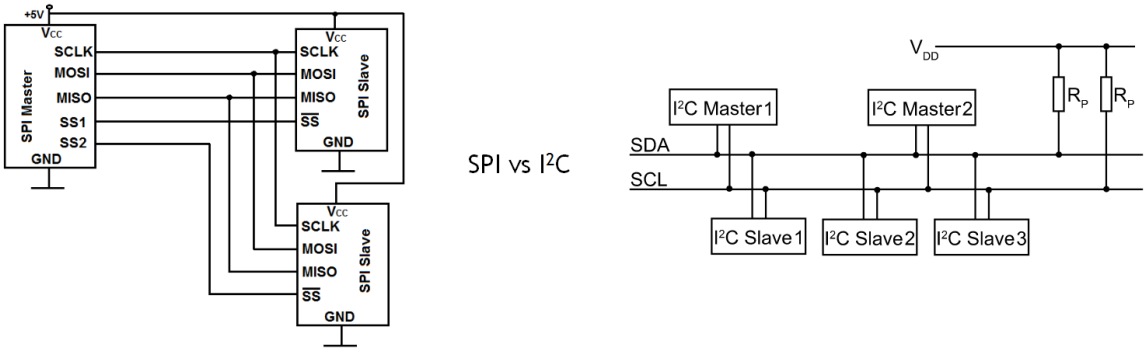

Figure 2.8: SPI with multiple slaves and one master vs I^2C with multiple slaves and multiple masters. The master is usually the microcontroller on a circuit. In SPI, to communicate with a particular slave, that line is made 'High'. There can be multiple SS (slave select) lines to communicate with the slaves or a 'daisy-chain' can be used to amalgamate one SS line to communicate to all slaves. In I^2C, data is sent over the same line but avoiding clashes by using an 'open drain' with a pull-up resistor. SCLK; Serial clock (output from master), MOSI; Master output Slave input, MISO; Master input Slave output, GND; Ground, SDA; Serial data line, SCL; Serial clock line. (Figures adapted from; http://www.learningaboutelectronics.com/Articles/Multiple-SPI-devices-to-an-arduino-microcontroller.php & http://dlnware.com/i2c)

Both SPI and I^2C are supported by Arduino. Another advantage of Arduino Uno is that communication between the board and other devices is easily facilitated, e.g. a computer, other shields and, pertinent in this case, sensors could all be connected to Arduino Uno easily. The "shields" or printed circuit expansion boards could be used to personalise the board according to the needs of the project. Included in the design was an RTC (Real Time Clock) shield (see Figure 2.5). An RTC was required for the recording of time along with the 'dumping' of the CO_2 data onto an SD card (which is included in the RTC). Accurate recording of time was imperative so that a proper assessment of the data on an hourly, diurnal, seasonal and yearly scale could be ascertained.

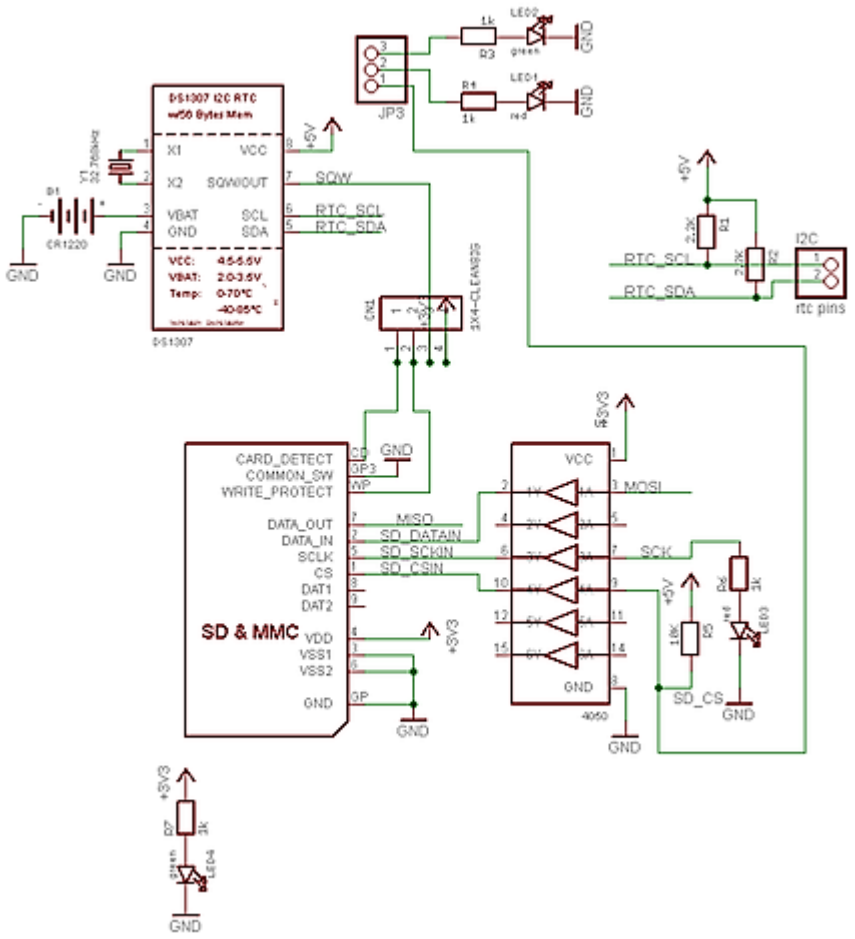

Figure 2.9: Schematic of components in RTC shield (figure adapted from https://learn.adafruit.com/assets/35519)

2.4.3 Software design & development

The Arduino and pCO_2 sensor could now be programmed to perform the tasks desired for this project. The COZIR sensor (from GSS) comes with ready-made software which provides the user with an output of CO_2, temperature and humidity via a USB cable into a laptop or computer. However, because this sensor was being developed to run autonomously and also underwater, it was necessary to develop new software from scratch for these needs. The code that is compatible with Arduino is in the language of C and several different types of code needed to be developed for the running of the sensor. The software that was developed for this project included code to:

- output the detected CO_2 concentration;
- output the measured temperature;

- output the measured humidity;
- output the measured voltage from the sensor;
- output the date and time; and
- write to the SD card

The following sections detail the important steps involved in this and full code is available in the appendix. The main functions within the code are included here (Section 2.4.3.1) for clarification.

2.4.3.1 CO_2, Temperature (or humidity) and SD code development

It was necessary to include libraries that enabled the time to be returned correctly. It was also imperative to include libraries that would enable connection with the SPI on the Arduino and also the SD card. A software serial port was set up.

```
#include <Time.h>

#include <SPI.h>

#include <SoftwareSerial.h>
#include <SD.h>
#include <Time.h>
#include <Wire.h>
#pragma GCC diagnostic ignored "-Wwrite-strings"
#include <DS1307RTC.h>

SoftwareSerial mySerial(2,3);
```

(N.B. RX →sensor TX line and TX → sensor RX line)

The string value was declared with each range being different (up to 2% = 1; up to 65% = 10; up to 100% = 100).

```
String val="";
double co2=0;

double multiplier=10;
```

Serial communication was started with the computer and text was printed to the serial monitor including the function to get the time from the RTC.

```
Serial.begin(9600);
delay(3000);

Serial.println(F("CO2meter.com Cozir example"));
Serial.println(F("Setup"));


setSyncProvider(RTC.get);
 if(timeStatus()!= timeSet)
    Serial.println("Unable to sync with the RTC");
 else
    Serial.println("RTC has set the system time");
```

The serial connection with the sensor was started.

```
mySerial.begin(9600);


sprintf(cmd, "K %u", 0);
Serial.println(cmd);
Command(cmd);
delay(600);
Serial.println(mySerial.available());
Serial.print(F("Response from K 0 "));
while (mySerial.available() > 0) {
  output = mySerial.read();
  Serial.print(output);
}
Serial.println(" ");
```

Firmware version and sensor serial number along with delays (to stop a conflict of signal) were added.

```
Command("Y");
delay(600);
Serial.println(mySerial.available());
Serial.print(F("Response from Y "));
while (mySerial.available() > 0) {
  output = mySerial.read();
  Serial.print(output);
}
Serial.println(" ");
```

The sensor was switched to polling mode whereby the sensor only reports readings when requested rather than a constant stream of data. The measurements will remain in the background with the output being dormant.

```
sprintf(cmd, "K %u", 2);
Serial.println(cmd);
Command(cmd);
delay(600);
Serial.print(F("Response from K 2 "));
while (mySerial.available() > 0) {
  output = mySerial.read();
  Serial.print(output);
```

The output fields were then determined. In the following case, humidity and CO_2 were chosen and the code was set to 4100 (CO_2 value = 4 and H value = 4096) but if temperature and CO_2 were required the code could be changed to 68 (CO_2 value = 4 and T value = 64) (See Appendix for additional information on this). This was sourced from the COZIR ambient sensor specification sheet.

```
Serial.println(" ");
  sprintf(cmd, "M %u", 4100);
Serial.println(cmd);
Command(cmd);
delay(600);
Serial.print(F("Response from M"));
while (mySerial.available() > 0) {
  output = mySerial.read();
 Serial.print(output);
```

The SD card activation loop was initialised. It must be noted that the CS (chip select) pin 4 is set as an output by default. Even if it is not used as the CS pin, the hardware SS (slave select) pin (pin 10 on Arduino) must be left as an output or the SD library functions will not work.

```
Serial.print(F("Initializing SD card..."));

if (!SD.begin(10)) {
  Serial.println(F("initialization failed!"));
  return;
}
Serial.println(F("initialization done."));
```

The RTC was then prompted for output.

```
  if (timeStatus() == timeSet) {
    digitalClockDisplay();
  } else {
    Serial.println("The time has not been set.  Please run the Time");
    Serial.println("TimeRTCSet example, or DS1307RTC SetTime example.");
    Serial.println();
    delay(1000);
  }
  delay(600);
}

void digitalClockDisplay(){
  // digital clock display of the time
  Serial.print(hour());
  printDigits(minute());
  printDigits(second());
  Serial.print(" ");
  Serial.print(day());
  Serial.print(" ");
  Serial.print(month());
  Serial.print(" ");
  Serial.print(year());
  Serial.println();
```

CO_2 and humidity (or temperature depending on need) was then requested with the frequency of readings also set at this point, e.g. for a reading every five minutes the delay was set to 300000, for a reading every 2 minutes the delay was set to 120000, for a reading every minute, the delay was set to 60000, etc.

```
  Command("Q");

delay(300000);

ind=0;
Serial.print(F("ind and buffer value "));
Serial.print(ind);
Serial.print(" ");
Serial.println(buffer[ind]);

Serial.println(F("reading line"));

Serial.println(mySerial.available());
while(mySerial.available() > 0)
  {
    buffer[ind]=mySerial.peek();
    output = mySerial.read();
    Serial.print(output);
    ind++;
```

2.4.3.2 Additional Real Time Clock (RTC) code

As well as the main body of code, additional code was needed to initially set the time on the RTC. This was then incorporated into the main code.

```
#include <Wire.h>
const int DS1307 = 0x68;
const char* days[] =
{"Sunday", "Monday", "Tuesday", "Wednesday", "Thursday", "Friday", "Saturday"};
const char* months[] =
{"January", "February", "March", "April", "May", "June", "July", "August","September", "October", "November", "December"};
```

All values were initialised;

```
byte second = 0;
byte minute = 0;
byte hour = 0;
byte weekday = 0;
byte monthday = 0;
byte month = 0;
byte year = 0;
```

A delay allows the MCU (microcontroller) to read the current date and time and an option for the user to change the date and time was also added.

```
void setup() {
  Wire.begin();
  Serial.begin(9600);
  delay(2000);

  Serial.print("The current date and time is: ");
  printTime();
  Serial.println("Please change to newline ending the settings on the lower right of the Serial Monitor");
  Serial.println("Would you like to set the date and time now? Y/N");

  while (!Serial.available()) delay(10);
  if (Serial.read() == 'y' || Serial.read() == 'Y')
```

There was a continuous function for converting bytes to decimals and vice versa.

```
void loop() {
}
byte decToBcd(byte val) {
  return ((val/10*16) + (val%10));
}
byte bcdToDec(byte val) {
  return ((val/16*10) + (val%16));
}
```

The next set of code allows the input of data.

```
void setTime() {
  Serial.print("Please enter the current year, 00-99. - ");
  year = readByte();
  Serial.println(year);
  Serial.print("Please enter the current month, 1-12. - ");
  month = readByte();
  Serial.println(months[month-1]);
  Serial.print("Please enter the current day of the month, 1-31. - ");
  monthday = readByte();
  Serial.println(monthday);
  Serial.println("Please enter the current day of the week, 1-7.");
  Serial.print("1 Sun | 2 Mon | 3 Tues | 4 Weds | 5 Thu | 6 Fri | 7 Sat - ");
  weekday = readByte();
  Serial.println(days[weekday-1]);
  Serial.print("Please enter the current hour in 24hr format, 0-23. - ");
  hour = readByte();
  Serial.println(hour);
  Serial.print("Please enter the current minute, 0-59. - ");
  minute = readByte();
  Serial.println(minute);
  second = 0;
  Serial.println("The data has been entered.");
```

For data to be sent to the RTC, the following code was added;

```
Wire.beginTransmission(DS1307);
Wire.write(byte(0));
Wire.write(decToBcd(second));
Wire.write(decToBcd(minute));
Wire.write(decToBcd(hour));
Wire.write(decToBcd(weekday));
Wire.write(decToBcd(monthday));
Wire.write(decToBcd(month));
Wire.write(decToBcd(year));
Wire.write(byte(0));
Wire.endTransmission();
```

```
byte readByte() {
  while (!Serial.available()) delay(10);
  byte reading = 0;
  byte incomingByte = Serial.read();
  while (incomingByte != '\n') {
    if (incomingByte >= '0' && incomingByte <= '9')
      reading = reading * 10 + (incomingByte - '0');
    else;
    incomingByte = Serial.read();
  }
  Serial.flush();
  return reading;


void printTime() {
  char buffer[3];
  const char* AMPM = 0;
  readTime();
  Serial.print(days[weekday-1]);
  Serial.print(" ");
  Serial.print(months[month-1]);
  Serial.print(" ");
  Serial.print(monthday);
  Serial.print(", 20");
  Serial.print(year);
  Serial.print(" ");
  if (hour > 12) {
    hour -= 12;
    AMPM = " PM";
  }
  else AMPM = " AM";
  Serial.print(hour);
  Serial.print(":");
  sprintf(buffer, "%02d", minute);
  Serial.print(buffer);
  Serial.println(AMPM);
}


void readTime() {
  Wire.beginTransmission(DS1307);
  Wire.write(byte(0));
  Wire.endTransmission();
  Wire.requestFrom(DS1307, 7);
  second = bcdToDec(Wire.read());
  minute = bcdToDec(Wire.read());  hour = bcdToDec(Wire.read());
  weekday = bcdToDec(Wire.read());
  monthday = bcdToDec(Wire.read());
  month = bcdToDec(Wire.read());
  year = bcdToDec(Wire.read());
}
```

2.4.3.3 Voltage output code development

It is possible to have a special voltage output option on the COZIR sensor which is proportional to the averaged CO_2 concentration. If this option is required a factory modified sensor needs to be specially ordered from GSS. A formula provided by the COZIR data sheet can then convert this voltage output into μatm (marine)/ppm (atmospheric). This output was used in the temperate field deployment of the sensor (see Chapter 4, page 182). It was compared with a second sensor which was set to output the conventional CO_2 also deployed at the same time to see if there was any advantage to either output. The output voltage and CO_2 measured by the sensor have a linear relationship as stated in the COZIR specification data sheet. The output voltage is provided by Pulse Width Modulation (PWM) of the sensor supply voltage. The supply voltage was therefore important when producing the code because it is directly related to the output voltage. Depending on the supply voltage, this could be changed within the code easily to account for how the sensor was powered for different runs, i.e. AC or DC.

Using the voltage, a CO_2 concentration can be calculated as follows from Equation 19:

$$CO_{2\ \mu atm/ppm} = \frac{full\ scale\ concentration\ \times V_o}{V_s} \qquad (19)$$

(Where Vo = voltage output (at pin 9), Vs = supply voltage (at pin 3))

The developed code is able to give input voltages between 0 and 5v into integer values between 0 and 1023 (see Figure 2.10). Using a linear equation, i.e. $m = \frac{y_2 - y_1}{x_2 - x_1}$ with x = read value & y = voltage, this can be converted into a meaningful value for μatm/ppm output.

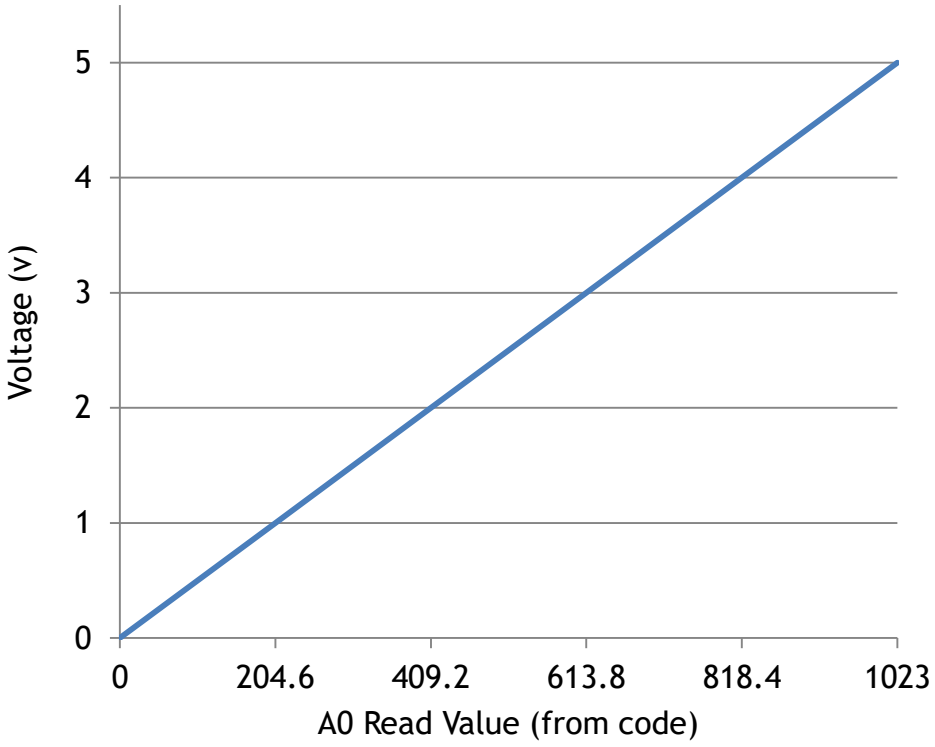

Figure 2.10: Linear relationship between output and voltage. This relationship was used to create code which would output voltage from the CO_2 sensor.

The sensor and electronics were programmed to output voltage as such;

```
#include <SD.h>
#include <SPI.h>

int analogPin = A0;
int readValue;
float Voltage;

int chipSelect=4;
File mySensorData;

void setup() {

  pinMode(analogPin,INPUT);
  Serial.begin(9600);

  pinMode(10, OUTPUT);
  SD.begin(chipSelect);

}

void loop() {

  mySensorData= SD.open("VData.txt", FILE_WRITE);

  if (mySensorData) {

  readValue = analogRead(analogPin);
  Voltage = (3.3/675.)*readValue;
```

2.4.4 Power

A key aspect of the development and design of the sensor was how to adequately power it. The whole design included many different components all of which would draw and use a certain amount of power. Each component had to be taken into consideration. The specifications of the pCO_2 sensor design meant that the batteries could not be too expensive, heavy or large which also imposed restrictions on the power options.

The main Arduino board had a jack connector allowing batteries to be easily incorporated into the system making it able to run autonomously. Arduino boards draw ~42mA of current and with A/C supply have a minimum draw of 3.3v. Even when the board is not taking a reading, it will still be using a basic current of 10mA. Power consumption of the board in normal working mode would be around 0.14W and even when not in use the power consumption would still be 0.03W.

Batteries were tested and generic rechargeable AA batteries were chosen to run the system on. These batteries would generally provide 2.5 Watt-hours of energy and four of these provided 10 Watt-hours of energy. This typically supplied power to the system for approximately 72 hours (longer in warmer waters).

Figure 2.11: Battery set-up of holder with jack connection and four rechargeable AA batteries.

2.4.5 Housing design

The requirement of the sensor to record data underwater meant a significant amount of R&D had to be lent to the production of a proprietary housing which could contain the sensor and electronics securely, protect the system from moisture, biofouling and erosion and also allow the permeation of CO_2 through the walls to reach the internal sensor. The unit had to be suitable for shallow (< 20 m), dynamic marine waters and have the capability to remain *in-situ* for a prolonged amount of time.

The precise requirements for the housing of the sensor included;

- the ability to keep the electronics and sensor dry whilst underwater,
- ease of permeation of CO_2 through the housing walls,
- it must be retrievable,
- the ability to be easily opened and closed for reuse and reprogramming and
- construction with relatively inexpensive materials.

2.4.5.1 Initial housing design

The initial prototypes were made from simple, mass-produced Tupperware made from polyethylene and/or polypropylene. Tupperware was chosen because it was easily sourced, affordable and came in a variety of sizes for initial starting-point testing. This also meant there was room for experimentation without the commitment to expensive materials. The plastic boxes were modified to allow CO_2 to reach the sensor (polyethylene and polypropylene are not permeable to CO_2). PTFE (polytetrafluoroethylene) is a material that is hydrophobic but permeable to CO_2 and filters in this material were used as a way in which the gas could transfer from the surrounding waters into the container to reach the sensor without enabling the ingress of water. Although PTFE is an expensive material, when the small filters (see Figure 2.12a) were bought in bulk the unit price was made relatively low. It was through this

small filter in the plastic box that CO_2 was able to reach the sensor. The fragile filter was made more durable by being placed between sintered glass diffusers, placed in a hole in the plastic container and secured with aquarium-standard silicon (see Figure 2.12b).

11 prototypes in total (different materials and designs) were made and the housing then underwent waterproofing testing in the Marine Mesocosm Facility at The University of Glasgow without the sensor inside. They were tested over different timescales from 6 hours to 48 hours. Once the tests deemed the set-up waterproof, the pre-programmed sensor with the electronics and the battery pack was placed inside the box and tested underwater (see Chapter 3 for experimental details).

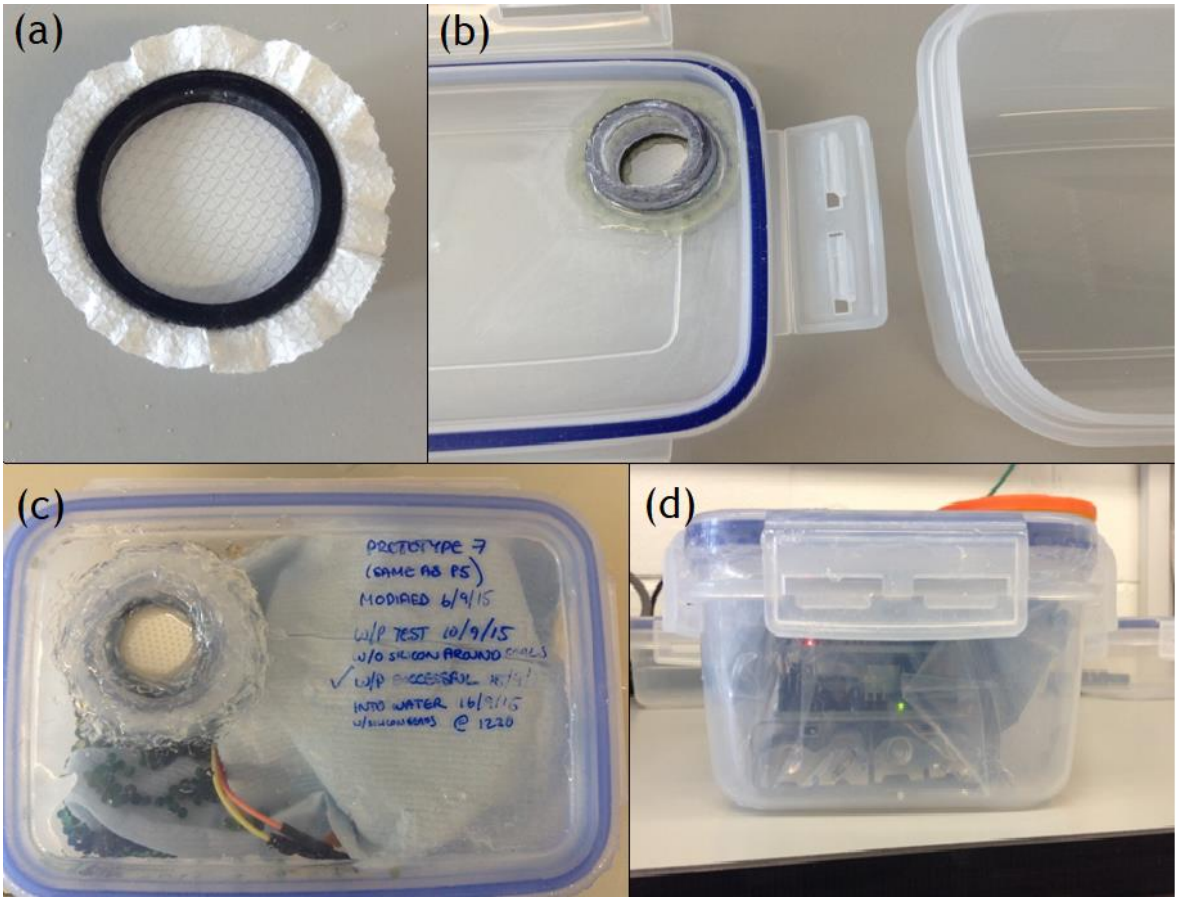

Figure 2.12: (a) PTFE filter held in place by rubber ring and sintered diffuser. (b) Underside of PTFE filter fixed in place with silicone in lid of plastic container. (c) PTFE filter inserted into lid of plastic container and secured to rest of container with silicone. (d) Electronics, sensor and battery pack secured inside housing.

This design however, was deemed unsuitable as too much human error was introduced when trying to replicate the set-up. Drilling a hole in the containers meant an increased likelihood of human error in waterproofing or damaging the container as a whole. The PTFE filters were very fragile and again, fitting these increased the likelihood of error when constructing the housing. Drilling into the container was preferably to be avoided which meant finding a housing that was entirely permeable to CO_2. In addition, there was an air flow issue in that CO_2 was not consistently being read by the sensor (see Chapter 3, section 3.4.3.3, page 90).

2.4.5.2 Final housing design

Hollow PTFE tubing was chosen as a replacement for the initial design to enable CO_2 to reach the sensor inside the housing due to the higher surface area which would be permeable to the gas. Although an expensive material, again, if bought in bulk it would reduce the price to approximately £24 per unit of PTFE tubing. Experience of PTFE in the form of filters had shown that this was an effective material in keeping humidity out of the housing but allowing CO_2 to reach the sensor. Although this form of housing was much more expensive than Tupperware boxes, the set-up would lend itself more favourably to the needs of the project. PTFE tubing provided a compact, heavy-duty casing in which the sensor and electronics were more adequately protected. In the intermediate, 2 temporary designs were used for the collection of data:

1. PTFE tube with plastic ends sealed with silicone as shown in Figure 2.13b (later in the design process, silicone was deemed unsuitable for use in this project (see Chapter 3, Section 3.4.5, page 101 for experimental details)).

2. Bungs on the end of PTFE tube (see Figure 2.13c)

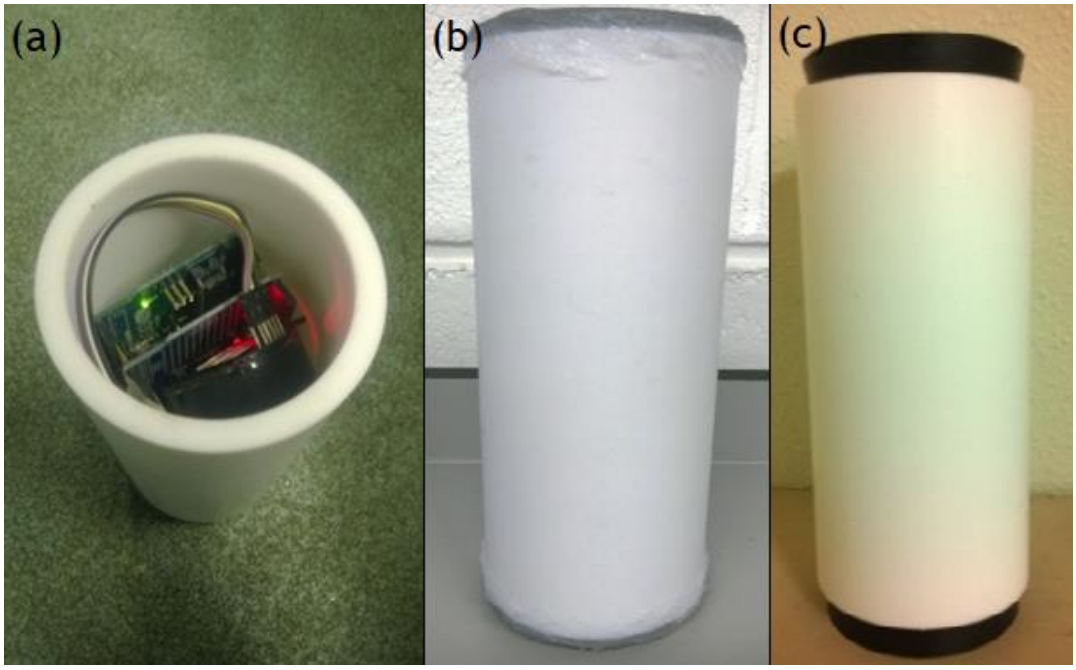

Figure 2.13: Left: Electronics and sensor inside PTFE tube; Middle: PTFE tube with plastic inserts secured with silicon; Right: PTFE tube with bung inserts mitigating the need for silicon

The final design was engineered to a high standard with PTFE screw lids being manufactured from PTFE rod (see Figure 2.14). A solid PTFE rod was purchased and lids were made from this. Threading was put on the existing hollow PTFE tube and this enabled the lids to be taken on and off without material modification. Differential pressure needed to be lower than the pressure on all sealing surfaces and it was deemed that the best way to achieve this was to incorporate O-rings into the housing design. There must be a pressure exerted (force per unit area) that is larger than the difference in pressure between the inside and outside. An O-ring works by changing shape according to the pressure and creates more pressure on the surfaces that need to be sealed than the existing pressure differential. It was essential that this part of the design was well engineered and considerations such as materials used and dimensions needed were given special attention. O-rings were incorporated into the main body of the tube to add a firm safety precaution against water leaking into the system.

Figure 2.14: Final PTFE housing design with PTFE threaded lids

	Dimensions (cm)
Length of tube	19.7
Outside diameter	9
Inside diameter	6.7

Table 2.3: Dimensions of one unit; PTFE tube plus PTFE lids

2.5 Results

The research and development of the marine pCO_2 sensor was a significant component of the Ph.D. The software and housing underwent several tests all of which are detailed in Chapter 3, the results of which show the successful development and design of a marine-proof pCO_2 sensor.

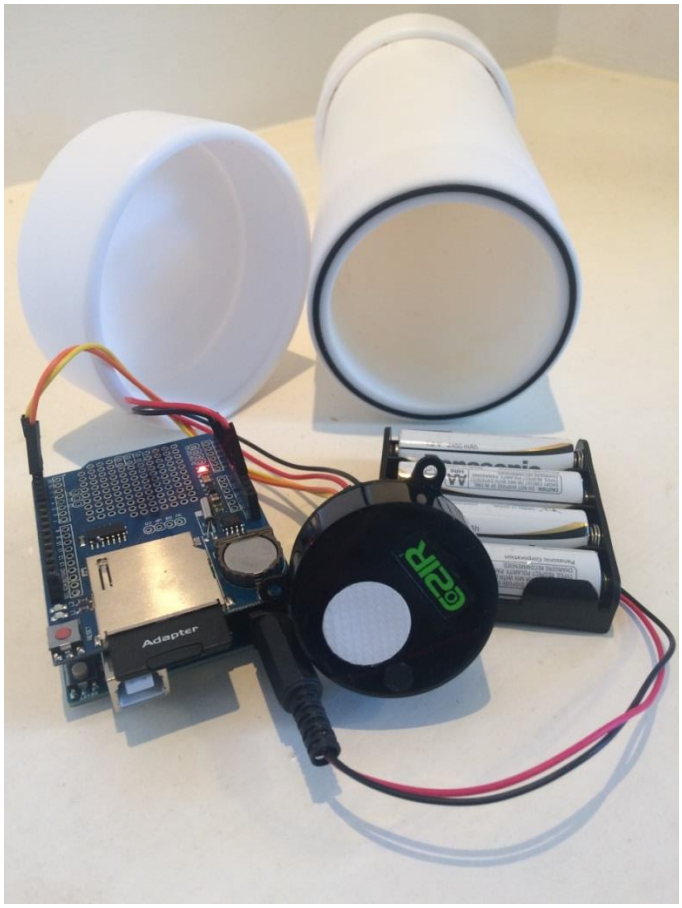

Figure 2.15: The final design of the housing plus sensor. Pictured is the PTFE tubing with threaded lid and o-ring system, battery pack, sensor and electronics.

2.6 Discussion

One of the main objectives in developing a marine pCO_2 sensor was that it had to be low-cost. Marine pCO_2 sensors range in price from approximately $12000 to $50000 (Ge *et al.*, 2014) with prices varying depending on method of measurement and deployment, source of power and any available accessories. An approximate breakdown of parts and their cost is given below (see table 2.4).

	Cost (£)
Arduino Uno Board	19.99
Batteries (4 x AA Rechargable NiMH)	15.00
Battery holder with Arduino jack	2.00
COZIR CO_2 sensor	128.00
Jumper wires	1.00
Nitrile O-rings	0.60
PTFE rod	71.81
PTFE tube	23.88
RTC shield	12.00
SD card	5.00
TOTAL	**279.28**

Table 2.4: Cost of materials for one unit of a pCO_2 sensor

The total cost of one unit of the developed pCO_2 sensor is approximately £280 which, compared to pCO_2 sensors currently on the market, is a remarkably low price.

The sensor was able to be manufactured to meet the requirement of low-power operation. Both the electronics platform and the sensor were chosen so as to meet this criterion. The development of even lower power through both the software and hardware is discussed as part of further work in Chapter 6, Section 6.7, page 292.

The sensor developed was both practical and suitable for the marine environment. The housing plus sensor was small and, in both laboratory and in the field, the unit was able to withstand sustained immersion (<20m) whilst

recording data autonomously (see chapter 3, 4 and 5). It was also able to be programmed according to different sampling needs.

2.7 Conclusion

Chapter 2 dealt with the development of a pCO_2 sensor. The pCO_2 sensor produced was low-cost, low-power, durable and able to run autonomously in a marine environment. The use of the sensor in experimental laboratory and field environments is further discussed in Chapters 3, 4 and 5.

3 Laboratory performance evaluation of pCO_2 sensor

3.1 Introduction

The accuracy and abundance of field data is crucial for calculating both coastal and oceanic CO_2 fluxes (Pierrot *et al.*, 2009). The development of accessible (i.e. low-cost and practical) sensors is an important step in bridging the gaps that exist in regional and global data. There is a wide range of diversity in design and use with currently available pCO_2 sensors (Pierrot *et al.*, 2009). Some of these systems have been comprehensively reviewed (see Kortzinger *et al.*, 2000; Schar *et al.*, 2009; 2010a; 2010b; 2010c) and most are at the high-end scale of pricing, i.e. £15 – 50k. This project introduces a novel approach to producing a low-cost marine pCO_2 sensor which can contribute to the collection of *in-situ* pCO_2 data in coastal regions.

This chapter presents the initial testing of the pCO_2 sensor developed at The University of Glasgow (see Chapter 2). It is a small, low-cost unit developed to continuously measure *in-situ* pCO_2. To test the effectiveness of the sensor, experimental tests (both atmospheric and marine) were conducted. The performance of the sensor was first tested in atmospheric conditions under both ambient and known-gas concentrations and temperature incubations. Calibration of the sensor was also carried out using known-gas concentrations. For marine testing, waterproof housing was developed and the sensor was then tested in mesocosms at The University of Glasgow. These mesocosms simulated shallow field environments both with known (supplied by gas mixes) concentrations of pCO_2 in seawater and ambient concentrations of pCO_2 in seawater. Concurrent to the sensor testing was discrete seawater sampling. The seawater samples were analysed for A_T and DIC which was consequently used (along with other ancillary parameters) to calculate the concentrations of pCO_2 of the seawater in the mesocosms. This aided sensor calibration and validation.

Results confirm the potential for this sensor to be used in the field to characterise the natural variation of pCO_2 in marine coastal areas leading to an improved understanding of the physical and biological environmental drivers in

these areas. The sensor was successfully applied to both an atmospheric and marine environment and details of sensor testing are described in following sections.

3.2 General aims

The aim of this chapter was to assess and evaluate the effectiveness of a pCO_2 sensor in 1) an atmospheric environment and 2) a marine environment. The electronics, responsiveness and housing were all rigorously tested in controlled laboratory environments. Instrument performance verification was necessary to ensure that the technology was effective and that it could be a valuable tool to support coastal marine biogeochemical science. Not only was this evaluation to demonstrate the performance and feasibility of this instrument but also to help with identifying and addressing the limitations of the sensor.

A brief summary of the laboratory experiments conducted include:

- Atmospheric tests in a variety of set-ups including within chambers of known-gas concentration and temperature incubations. This was to test the response of the sensor (and the constructed housing) in different conditions, i.e. the reaction of the sensor to different ppm CO_2 concentrations and different temperatures.

- Marine mesocosm tests in a variety of set-ups including in seawater of ambient, CO_2 spiked and natural CO_2 variation by coralline algae to test the response of the sensor (and housing) underwater.

Each individual experiment is commented on in greater detail throughout the chapter.

3.3 General methods

Because there are varied types of experiments included within this chapter, the following general methods section will describe recurring methods and experimental set-ups but the subsequent sections will give more detail on each individual tests which are dealt with chronologically.

3.3.1 Mesocosm apparatus

The underwater deployments were at The University of Glasgow Marine Mesocosm Facility. The mesocosms contained re-circulating seawater tanks of dimensions 800 x 400 x 350 mm (210L). Natural seawater was continually pumped around each system and the mesocosms were able to mimic diel cycles with a timed UV light (see Figure 3.1).

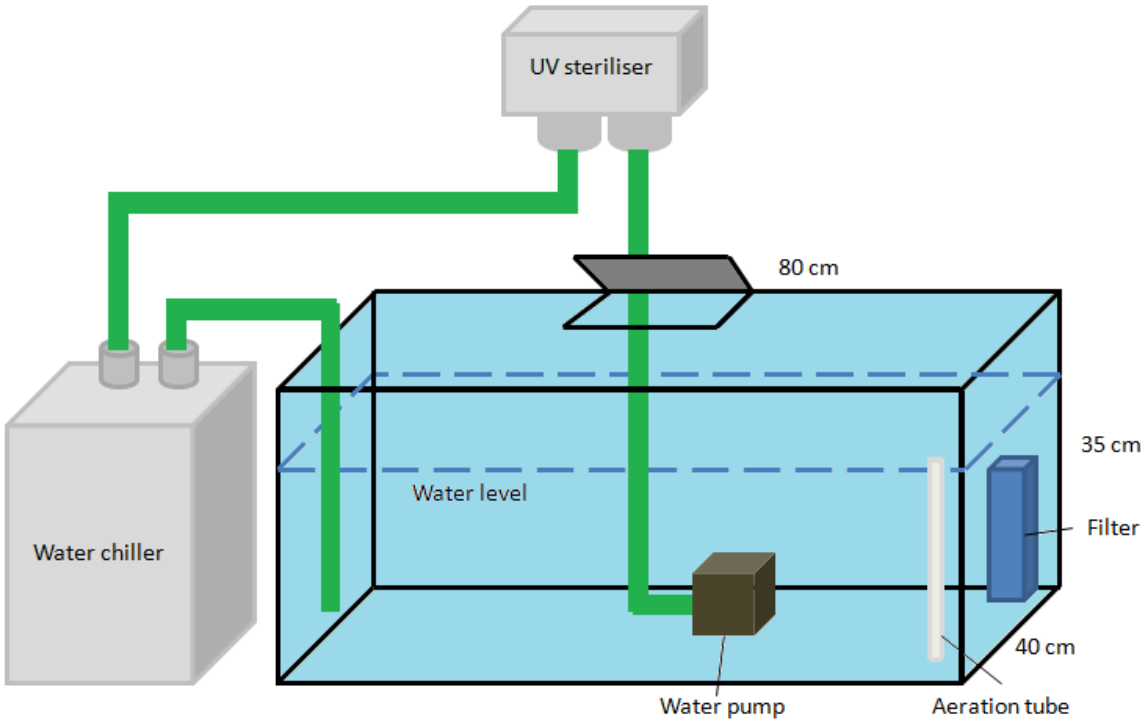

Figure 3.1: Mesocosm set-up at The University of Glasgow. The natural seawater tank had recirculating water with an internal pump.

3.3.2 Sensor calibration

The sensor underwent a 2-point calibration with gases of known concentration (400 and 1000 ppm) from a commercially available gas-mixing system supplied by BOC. The calibration gases were CO_2 in a nitrogen (N) mixture. A gas mixture is used for calibration gases because the carrier gas of nitrogen will help keep the CO_2 concentration stable over time (Inoue *et al.*, 1995). According to specification, the certified values have an uncertainty of < = 5%. An atmospheric test chamber was constructed (see Section 3.3.3, page 67 for details) which was used to house the sensor during calibration. Gas was pumped

into the chamber and the sensor was allowed to equilibrate to the specific gas concentration. Software (COZIR Sensor 2.0) from GSS was used to zero the sensor and input the specific concentration. This was done with calibration gases of CO_2 concentrations 400 ppm and 1000 ppm. This was a 'span' calibration which was determined using Equation 20;

$$Span\ calibration\ factor = \frac{known\ gas\ concentration\ \times existing\ span\ calibration}{sensor\ reading} \quad (20)$$

The correct command was entered into the software (information from COZIR datasheet) to program the span calibration factor into the sensor.

3.3.3 Construction of chambers

Test chambers were constructed for this experiment (see Figure 3.2). Several different sized chambers were used but all had the same operation and construction principles. The sealed chambers were made of plastic (polyethylene and/or polypropylene) and modified to include 'IN' and 'OUT' valves so that known-concentration gas could be injected into the chamber and also allowing the system to then be closed thus mimicking an environment with a certain concentration of CO_2. Some of the experiments were conducted in a temperature controlled incubator (LMS) to keep the temperature constant at 8^oC. The incubator temperature is accurate to ± 1^oC. A gas mixture of CO_2 and N_2 was supplied to the test chamber. In this case, 400 ppm and 1000 ppm CO_2 concentration were used. These specific concentrations were used because they span the pCO_2 range between the current day and that expected in 2100 by the IPCC.

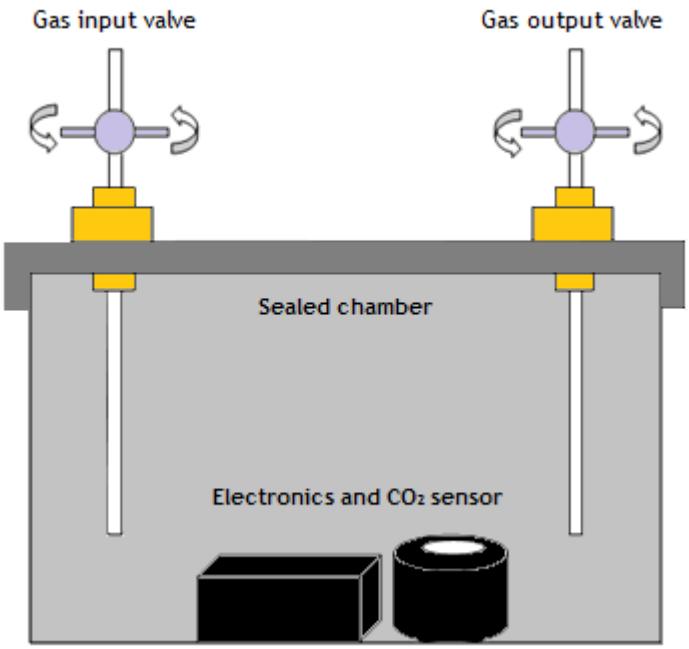

Figure 3.2: Example of sealed chamber set-up to test response of sensor to known gas concentrations

3.3.4 Seawater sample collection

In some mesocosm experiments, seawater samples were taken during sensor deployment. This was to analyse the seawater for A_T and DIC concentrations. Discrete water samples were collected in accordance with standard protocols (Dickson *et al.*, 2007). Specific details for the separate collections are given in the individual descriptions of experimental methods in the relevant sections. The general protocol was as follows. Seawater samples for A_T and DIC were collected in triplicate using borosilicate glass syringes and transferred to 12 ml borosilicate vials (Labco). Borosilicate glass was used due to its excellent thermal properties, high chemical resistance and its non-porous nature. The water sample therefore was unlikely to be affected by any outside inputs like oxygen which would change the chemical composition of the sample. Minimal gas exchange with the atmosphere was ensured by transferring the seawater slowly and smoothly into the vials directly from the syringe. This meant that no air bubbles were introduced into the sample. A slight overflow of water was left to form a meniscus which would further ensure no trapping of air bubbles when the lid was screwed onto the vial. They were then poisoned with 10 µL of

mercuric chloride ($HgCl_2$) to prevent any further biological activity inside the vial which would alter the carbonate chemistry in the sample. The lids were carefully placed on the vials, again ensuring no air bubbles were present in the sample. The vials were stored in a refrigerator before being analysed.

3.3.5 Data processing

3.3.5.1 Background noise

Background and baseline noise is a regular feature of all sensors (Miecznikowski and Sellers, 2002). Background noise was reduced by smoothing with a moving average (order = 15). A moving average was obtained by taking the most recent data point and adding it to the summation. Sequentially the oldest data point was then removed and the end total was divided by the number of data points. This produced an average but an average that 'moves' sequentially through the time that data is being recorded by the sensor. This had the effect of 'smoothing' the data and reducing noise.

3.3.5.2 Drift

Occasionally, the noise-filtered data would reveal a drift in the sensor data which would then require correction. Normalisation was used to remove this drift. The data was normalised within Excel using linear regression. Drift did not always happen throughout data collection. Drift was characterised within the data by a constant upward trend irrespective of the actual pCO_2 concentration. This drift was corrected by finding y with respect to x from a graph of the data and subtracting from the moving average. The minimum of these new values was subtracted from the drift correction values. This was then divided by the difference in the maximum and minimum of the moving average. Finally this was used in Equation 21 to produce data without drift.

$$data \times (\max(MA) - \min(MA)) + \min(MA) \quad (21)$$

MA = moving average

3.3.6 Seawater analyses

3.3.6.1 A_T analysis

The method used for quantifying A_T is by titration as per the methods of Yao and Byrne (1998). Certified Reference Material (CRM) from Scripps Institution of Oceanography was used to calibrate the measurements before samples were run and also between every 10 samples. They were analysed in triplicate with an average taken and were kept at a constant temperature (25°C) using a water bath (Julabo ED-19 Open Heating Bath Circulator). In this case, 0.01 mol hydrochloric acid (HCl) (background of 0.6 mol of sodium chloride (NaCl)) was added into 10 ml of seawater sample until the pH reached an approximate value of 4. The acid was made with a NaCl background so as to mimic the ionic characteristics of the seawater (Zeebe and Wolf-Gladrow, 2001). After acidification, absorbance was measured by spectrophotometry with the DR 5000 bench-top spectrophotometer with Bromocresol green indicator ($C_{12}H_{14}Br_4O_5S$) at 616 nm and 444 nm wavelengths. The absorbance ratio along with temperature and pH were used to determine total alkalinity (Yao and Byrne, 1998). This calculation is based on mass-balance and equilibrium equations and is processed using an excel spreadsheet program. The equivalence point of values of the pH region of 3 to 3.5 is established using a non-linear least-squares fit of the results. For total alkalinity, the following equation describes the circumstance in which the protons correspond to the equivalence point (Zeebe and Wolf-Gladrow, 2001);

$$[H^+]_F + [HSO_4^-] + [HF] + [H_3PO_4] = \quad (22)$$

$$[HCO_3^-] + 2[CO_3^{2-}] + [B(OH)_4^-] + [OH^-] + [HPO_4^{2-}] + 2[PO_4^{3-}] +$$

$$[SiO(OHO_3^-] + [NH_3] + [HS^-]$$

The hydrogen ion, with respect to the above proton condition, has an analytical total concentration (C_H) of;

$$C_H = [H^+]_F + [HSO_4^-] + [HF] + [H_3PO_4] \quad (23)$$

$$- [HCO_3^-] - 2[CO_3^{2-}] - [B(OH)_4^-] - [OH]$$

$$- [HPO_4^{2-}] - 2[PO_4^{3-}] - [SiO(OH)_3^-] - [NH_3] - [HS^-]$$

The consequence of this is that the total alkalinity is the negative of the initial analytical concentration of the hydrogen ion and vice versa (Zeebe and Wolf-Gladrow, 2001).

After acid has been added in the titration process the following equation applies;

$$C_H = \frac{mC - m_o A_T}{m_o + m} \quad (24)$$

(m = mass of acid with concentration C (mol kh-soln^{-1}),

m_o = mass of sample)

This can then be substituted into the hydrogen ion concentration equation;

$$\frac{mC - m_o A_T}{m_o + m} \quad (25)$$

$$= [H^+]_F + [HSO_4^-] + [HF] + [H_3PO_4]$$

$$- [HCO_3^-] - 2[CO_3^{2-}] - [B(OH)_4^-] - [OH]$$

$$- [HPO_4^{2-}] - 2[PO_4^{3-}] - [SiO(OH)_3^-] - [NH_3] - [HS^-]$$

For this process, this equation is the foundation of all the calculations within the spreadsheet program (Zeebe and Wolf-Gladrow, 2001).

3.3.6.2 DIC analysis

DIC was analysed by quantifying the extracted CO_2 by NDIR analysis (Goyet and Snover, 1993; O' Sullivan and Millero, 1998; Kaltin *et al.*, 2005). The samples were analysed using AIRICA (Automated Infra-Red Inorganic Carbon Analyser)

Version 2.4, Marianda. This used infra-red detection of the CO_2 extracted from an acidified sample. AIRICA gives a DIC which is within ±1.5 to 2 µmol kg^{-1} (0.1%) (Call *et al.*, 2017). The operational procedure of this instrumentation is as follows. A syringe pump was used to inject the seawater sample into a stripper which introduced acid (phosphoric acid (H_3PO_4)) into the sample until the pH reached below 4.5 and in doing so, CO_2 was then released. The acidified sample was then stripped of the CO_2 by a carrier gas containing nitrogen. Water content was removed as much as possible by a Peltier-element and a Nafion dryer and then the gas was measured by the LI-COR 820 (an NDIR analyser). The AIRICA analysed DIC by integration of the CO_2 ratio. CRMs were used to calibrate the measurements before samples were run and also between every 10 samples (as with A_T). The samples were analysed in triplicate with an average taken. Each sample was an average of four integral peaks (see example of peaks in Figure 3.3).

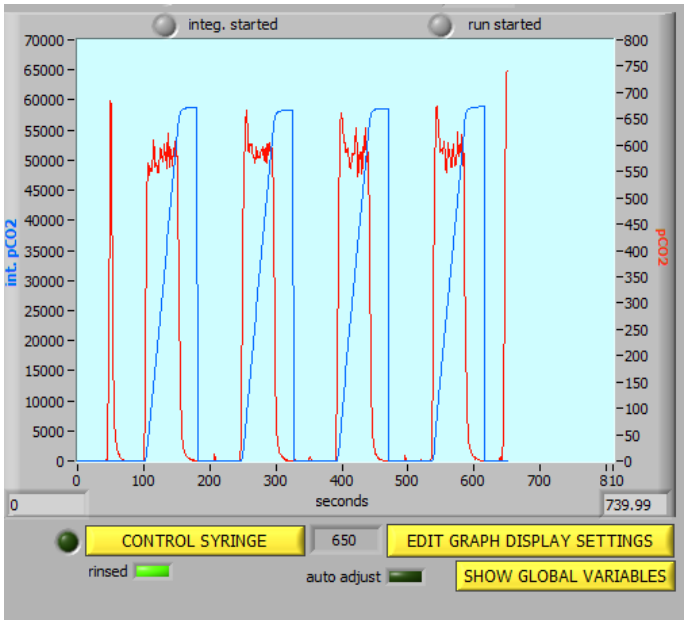

Figure 3.3: Four integral peaks shown within software of AIRICA.

3.3.6.3 pCO_2 calculation from water chemistry

Once A_T and DIC were determined, CO2SYS (Pierrot *et al.*, 2006) was used to calculate pCO_2 concentrations from A_T, DIC, temperature and salinity. The equilibrium constants (K_1 and K_2) used were from Mehrbach *et al.* (1973) refit by Dickson and Millero (1987), KSO_4 from Dickson and the pH seawater scale

(mol/kg^{-}SW). Ancillary data of pH, HCO_3^-, CO_3^{2-} concentrations and calcite (Ω_{Ca}) and aragonite (Ω_{Ar}) saturation states were also calculated within CO2SYS.

3.3.7 Programming the sensor

Before any deployment (atmospheric or marine) each sensor was programmed with the developed code (see Appendix for full code). This was conducted by connecting the electronics and sensor via USB cable to a laptop. The code was pre-loaded onto Arduino Web Editor and once the Arduino Uno board was connected to the software, the code was uploaded onto the board. The batteries were connected to the electronics and subsequently, the set-up was disconnected from the laptop making autonomous deployment possible. A Standard Operating Procedure (SOP) for the sensor is included in the Appendix.

3.4 Individual experimental methods, results & discussion

The following sections provide information on each individual experimental set-up in a chronological order. For clarity, the results and discussions are included within each corresponding section.

3.4.1 Initial sensor performance

The atmospheric base sensor purchased from GSS was assessed (See information on sensor in Chapter 2, Section 2.4.1, page 36). The sensor was not yet able to be immersed into a marine environment as waterproof housings were still being tested so alternative tests involving CO_2 spiked seawater were used. These tests were a first step in seeing how sensitive the sensor was to different environments. This was a categorical-type approach to investigate if the sensor was able to register large changes in pCO_2 before more detailed analyses were performed.

3.4.1.1 Aims

The aims were to;

- Assess the performance of the sensor in an atmospheric headspace of a seawater tank of known CO_2 concentration.

- Assess the performance of the sensor when the PFTE membrane on the sensor is directly exposed to the same concentration of seawater, i.e. a drop of seawater is directly placed on the PTFE membrane.

- Compare the two sets of data.

3.4.1.2 Methods

The performance of the sensor was tested in the headspace of an aquarium tank of known concentration versus the performance of the sensor with CO_2 spiked water droplets. In lieu of a waterproof housing which was yet to be designed, the safest way to expose the sensor to seawater at this point was with a small water droplet on the PTFE membrane on the outside of the sensor ensuring no saturation of the delicate electronics.

The sensor was attached to a computer by a USB cable. The software running with the sensor was COZIR 2.0 which is the standard software provided by the manufacturer. The sensor was placed in the headspace above the mesocosm (just above the level of the seawater) and left to continually record the CO_2 concentrations venting from the water (see Figure 3.4).

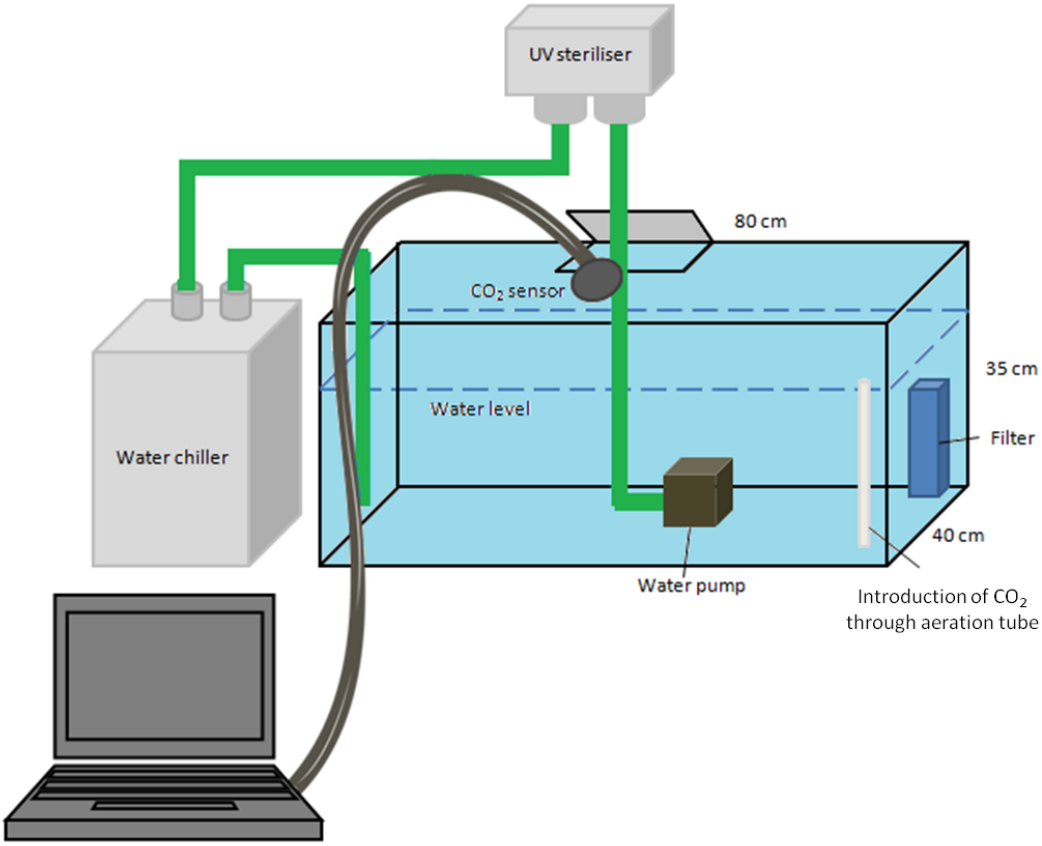

Figure 3.4: Mesocosm set-up with CO_2 sensor in headspace above the seawater. Different tanks contained different CO_2 concentrations

The concentrations received by the sensor in the headspace were then compared with the output of the sensor when a drop of the same seawater was directly placed on the PTFE membrane (see Figure 3.5). This was to assess whether there was a corresponding or different reaction to the specific ppm concentration and to gauge a general first impression of how the sensor would react to these different situations. This was done with tanks of pCO_2 seawater concentration of 380 µatm, 750 µatm and 1000 µatm. The sensor was set to record two readings every second for a total of 7 minutes each.

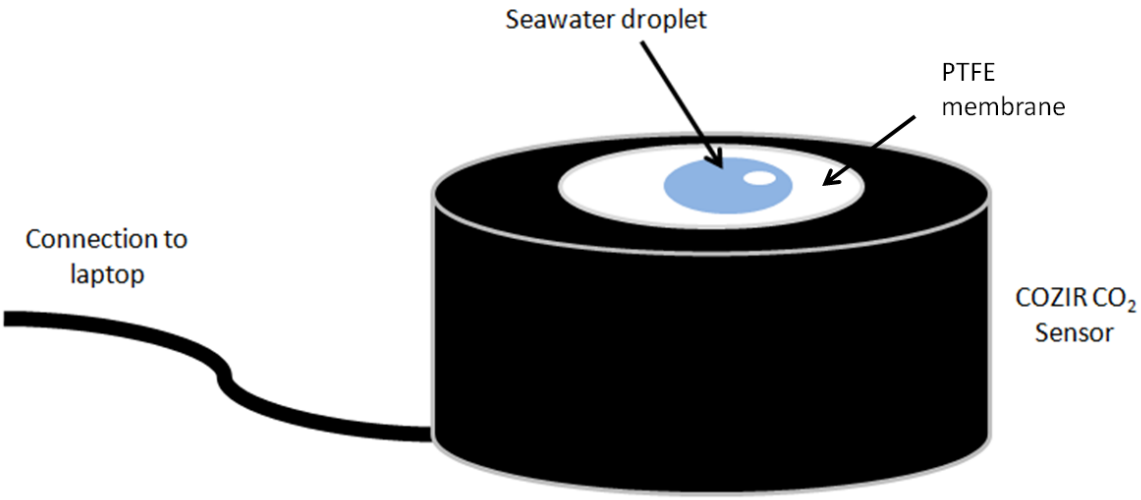

Figure 3.5: COZIR atmospheric CO_2 sensor with seawater droplet of specific concentration placed on the PTFE membrane. The sensor was continually connected to a laptop with GSS software which was outputting the CO_2 data. Note that the membrane was not fully covered with seawater as to prevent damage to the sensor. Therefore atmospheric CO_2 will still be influential in the CO_2 concentrations that the sensor outputs.

3.4.1.3 Results

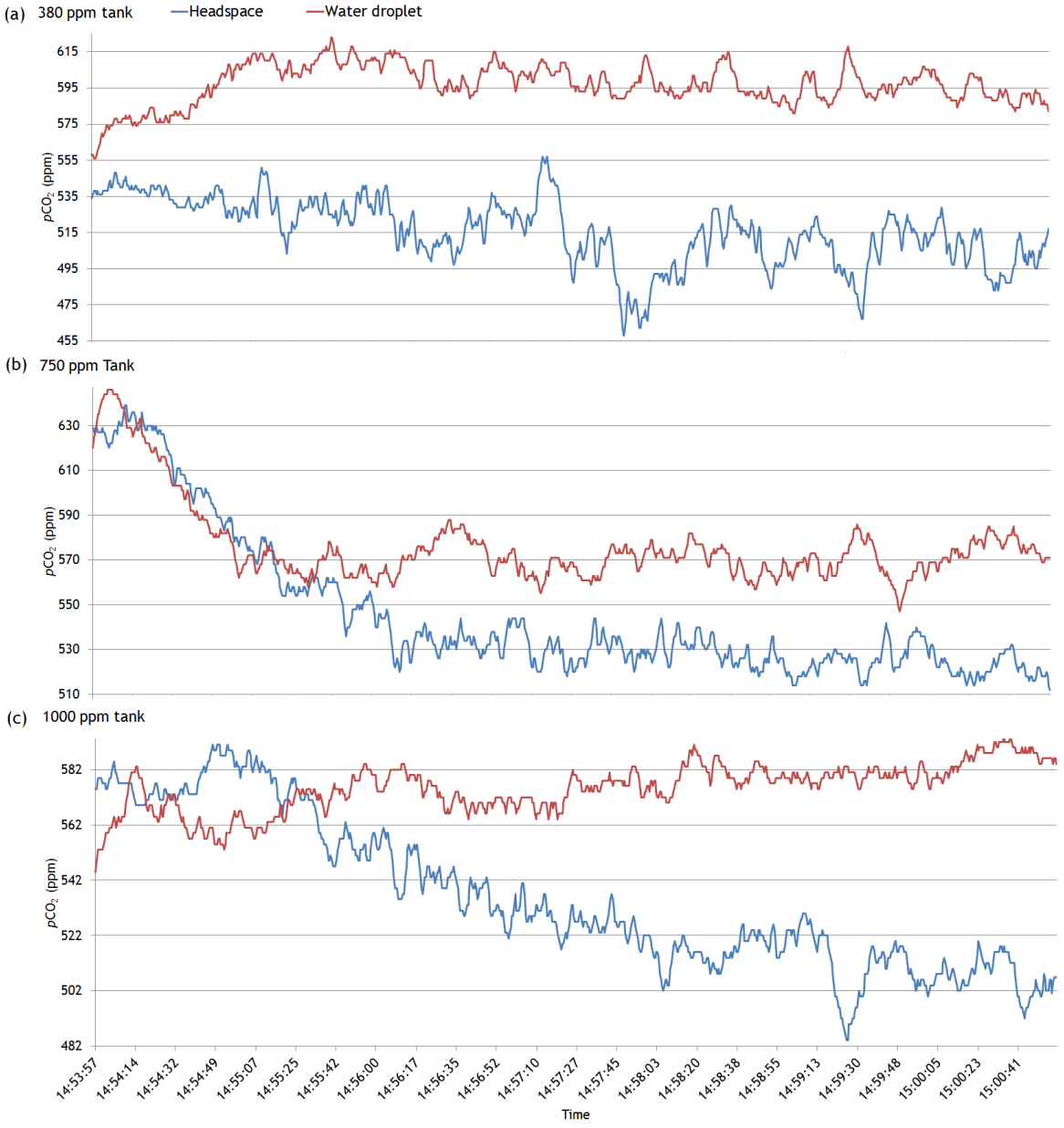

Figure 3.6: Headspace against water droplet for three mesocosms with different CO_2 concentrations. Two readings per second were recorded for 7 minutes each. (a) 380 ppm seawater. The 'headspace' run had an average concentration of 511 ± 17 ppm and the 'water droplet' run had an average concentration of 599 ± 9 ppm. (b) 750 ppm seawater. The headspace run had an average concentration of 528 ± 7 ppm and the 'water droplet' run had an average concentration of 571 ± 7 ppm. (c) 1000 ppm seawater. The 'headspace' run had an average concentration of 521 ± 15 and the 'water droplet' run had an average concentration of 579 ± 6 ppm.

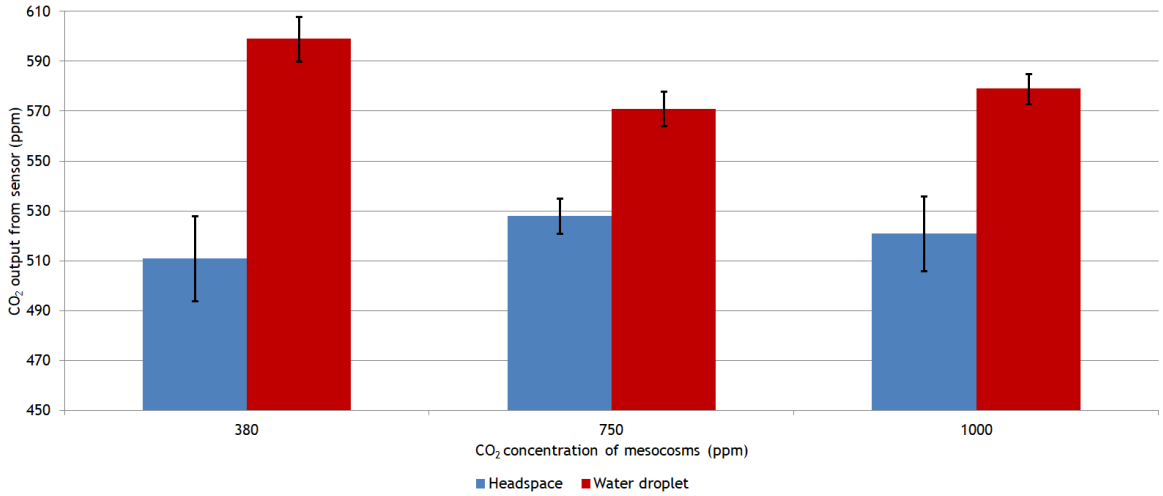

Figure 3.7: Bar chart of average CO_2 sensor concentration from different mesocosms when in headspace and directly exposed to seawater. 380 ppm tank; Headspace 511 ± 17 ppm, Water droplet 599 ± 9. 750 ppm tank; Headspace 528 ± 7 ppm, Water droplet 571 ± 7 ppm. 1000 ppm tank; Headspace 521 ± 15 ppm, Water droplet 579 ± 6 ppm.

3.4.1.4 Discussion

The sensor takes 1 – 2 minutes to equilibrate with the environment (see Figure 3.6). The three tanks that were used in the experiment were artificially manipulated with CO_2 concentrations of 380, 750 and 1000 ppm. With all three comparisons, the CO_2 concentration of direct exposure to the seawater droplet was higher than the concentration of the CO_2 when the sensor was in the headspace of the mesocosm (see Figure 3.7). The assumption was that the CO_2 off-gassing from seawater in the tank filled the headspace above the tank. However, this may not be the case and the headspace may not be filled with the same concentration as the tank because it is still effectively surrounded by atmospheric conditions. It would be reasonable to suggest that readings would perhaps be higher than normal atmospheric concentrations due to the close proximity of the sensor to an environment that has an artificially inflated concentration.

Tank CO_2 ppm seawater concentration	Average headspace ppm	Average water droplet ppm	Δ ppm
380	511	599	88
750	528	571	43
1000	521	579	58

Table 3.1: Comparison of headspace vs. water droplet CO_2 concentrations. Water droplet concentrations were higher than headspace concentrations,

The headspace data from the sensor for each of the tanks were very similar (511, 528 and 521ppm) as were the water droplet data (599, 571 and 578 ppm). This experiment provided a gauge in the reactivity of the sensor. The water droplet would not induce a change in the sensor readings to the correct concentration of the tanks because it is still effectively an atmospheric run. It was not expected that the sensor would read the absolute CO_2 concentration of the tanks but it was expected that the sensor would present the correct hierarchy of results. For the purpose of these experiments, the sensor was deemed to be sensitive enough to proceed with further experimentation.

3.4.2 Known gas concentration tests

Known gas concentration tests were used to assess the output of the sensor when in a closed CO_2 concentration-specific environment. These were atmospheric tests with the sensor autonomously run in a chamber which was injected with CO_2 gas (for details of chamber see Section 3.3.3, page 66). These tests doubled up as testing the newly developed code and also battery life testing for the autonomous set-up. These were the first autonomous tests whereby the sensor was programmed and put in a chamber to run until the batteries failed. This experimental run was also the first time the sensor was calibrated in the laboratory (for details of calibration see Section 3.3.2, page 65).

3.4.2.1 Aims

1. Develop code to output CO_2 and temperature (see Chapter 2, Section 2.4.3.1, page 45)

2. Develop code to output humidity (see Chapter 2, Section 2.4.3.1, page 45)

3. Design battery set-up to run sensor autonomously (see Chapter 2, Section 2.4.4, page 54)

4. Test power consumption

5. Assess sensor accuracy and precision in known gas concentrations

6. Familiarity with procedure of calibration of sensor

3.4.2.2 Methods

3.4.2.2.1 Power evaluation

A power evaluation test with 4 x AA Nickel Metal Hydride 2450 mAh batteries was conducted. The sensor was programmed and recorded atmospheric data in the laboratory. When the running time for these batteries had been established, known-gas concentration tests were run firstly with 1000 ppm CO_2 and then with 400 ppm CO_2. The sensor and electronics were placed inside the constructed chamber which was filled at a constant rate with either 1000 ppm CO_2 or 400 ppm CO_2 depending on the individual experiment. The same methodology was used regardless of the gas concentration. The sensor was left to record pCO_2 data once every five minutes and the accuracy and precision of the sensor was evaluated.

3.4.2.3 Results

3.4.2.3.1 Power evaluation and 1000 ppm tests

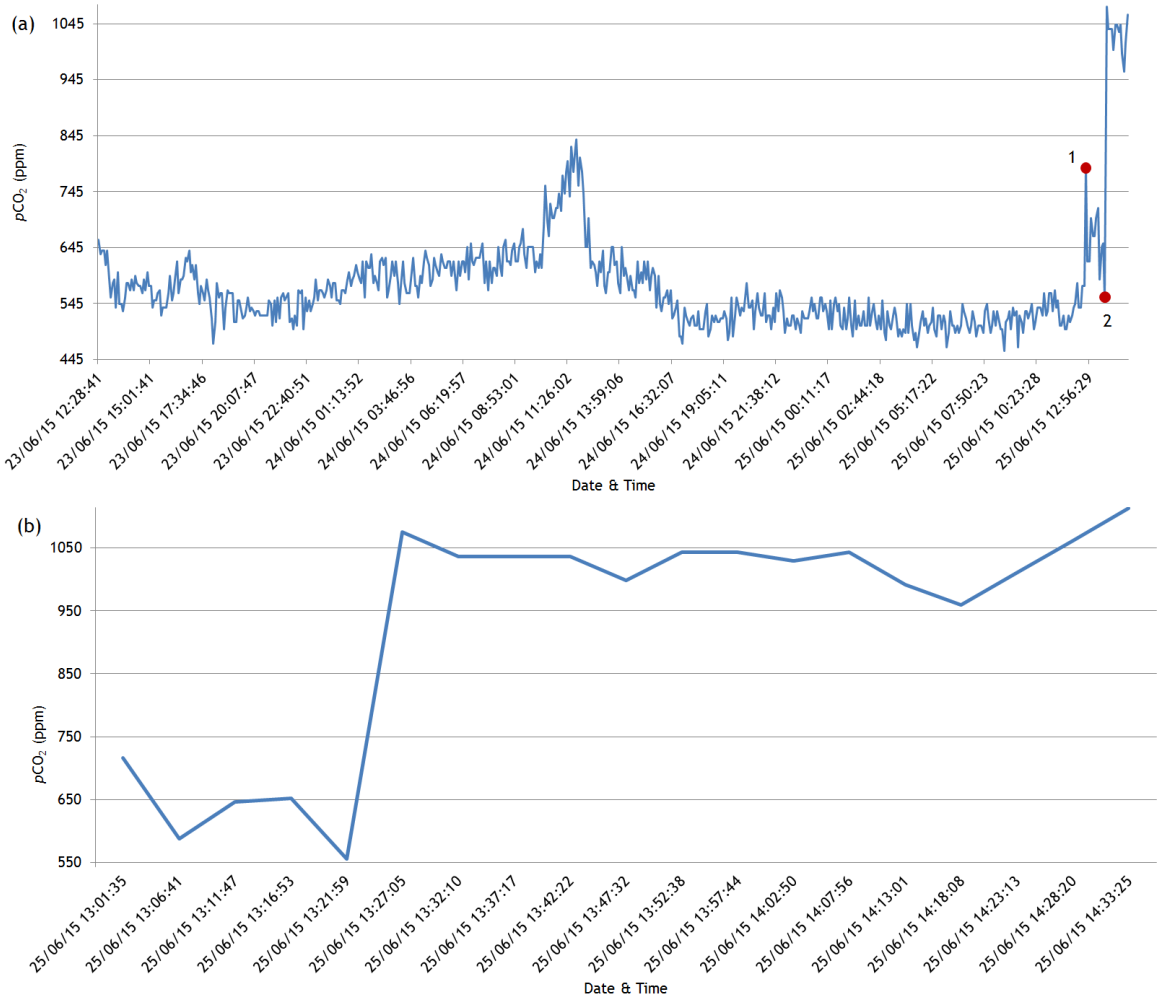

Figure 3.8: (a) 53h 47m sensor performance and power evaluation at ambient ppm and 1000 ppm on 23rd – 25th June 2015. Battery power 4 x AA NiMH 1.2v 2450mAh. (1) Sensor placed in closed chamber (2) and input of 1000 ppm @ 1320 hours. There was power failure 1 hour after this injection. (b) Closer inspection of the sensor CO_2 readings during only the gas injection of 1000 ppm CO_2 near the end of the run. Mean = 1028 ± 37 ppm during the 1000 ppm CO_2 gas injection.

This was first and foremost a battery test but because the batteries were running longer than expected (i.e. after two days they were still powering the sensor), the sensor was put into the chamber of known gas concentration to also test the sensor output as well as the battery power. 1000 ppm CO_2 gas was injected into the chamber. The data collected show ambient CO_2 concentrations for a busy laboratory (see Figure 3.8a). When the sensor was exposed to 1000 ppm, the resulting readings were very close to expected. The batteries ran out

not long after the injection of 1000 ppm. A closer inspection of the time when the gas was injected into the chamber is shown in Figure 3.8b. Further tests were subsequently conducted based on this set-up.

A shorter run with a 9v Nickel Metal Hydride 200 mAh battery in a 1000 ppm chamber was undertaken to assess the longevity of this battery. The battery lasted for approximately 3 ½ hours. When 1000 ppm CO_2 was injected into the chamber, the sensor read an average concentration of 982 ± 25 ppm over the duration of the run. A longer test was needed however to test if the sensor had any significant drift (see Figure 3.9).

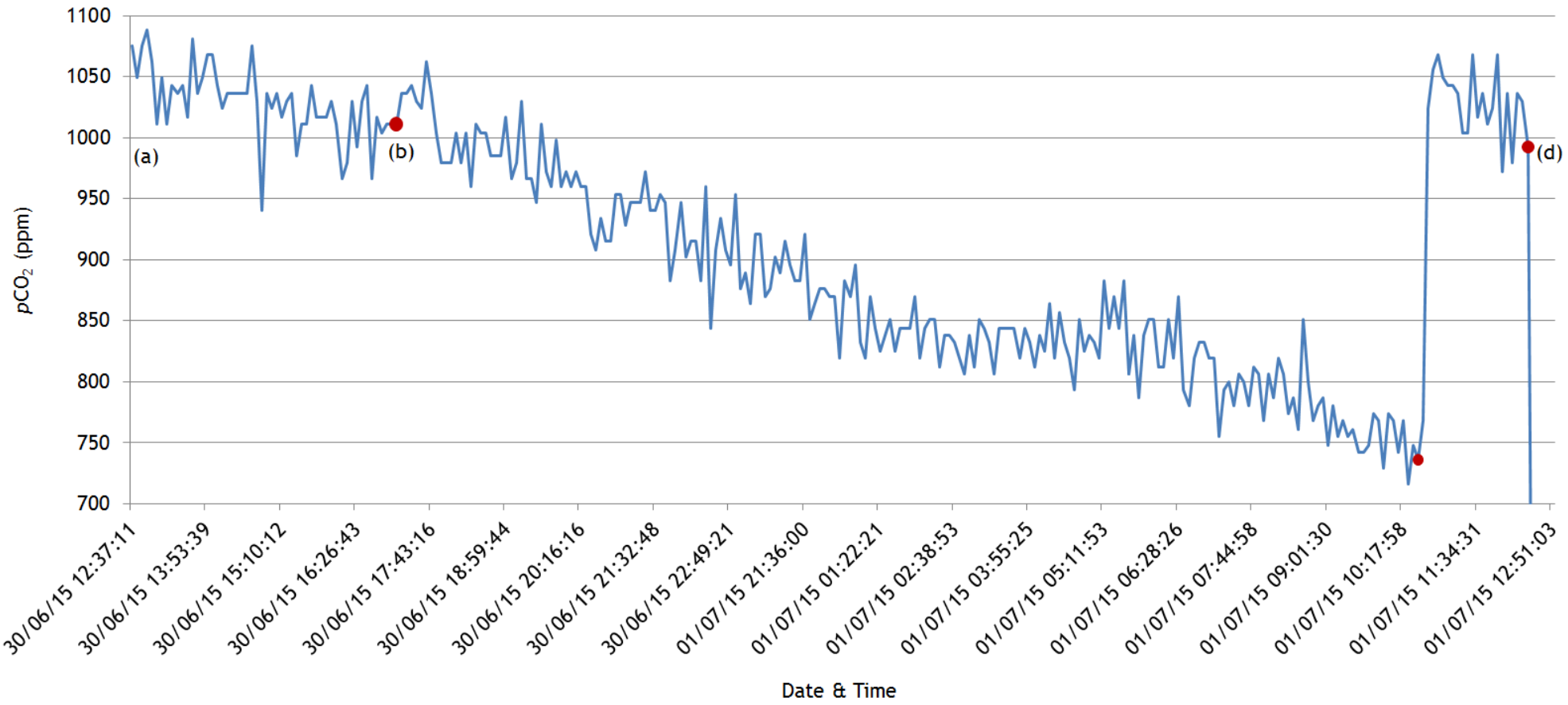

Figure 3.9: 24 hour run in gas chamber with 1000 ppm to test for sensor drift (Battery power 4 x AA NiMH 1.2v 2450mAh). (a) initial 'flushing' of 1000 ppm gas and closing of valves at 14:50, 30/06/15 (b) additional input of 1000 ppm gas at 1710, 30/06/15 (c) additional input of 1000 ppm gas at 1038, 01/07/15 (d) Sensor taken out of the chamber at 1230, 01/07/15. Overall mean 912 ± 98 ppm.

To test for drift in the sensor, a 24 hour run in a gas chamber with 1000 ppm CO_2 was undertaken as shown in Figure 3.9. There was a gradual downward trajectory in the CO_2 concentration until there was an injection of 1000 ppm. The sensor then read what would be expected of approximately 1000 ppm until power failure. Another similar run was undertaken to further investigate the performance of the sensor. This run suggested that there may have been a leak in the experimental chamber rather than confirming any drift in the sensor.

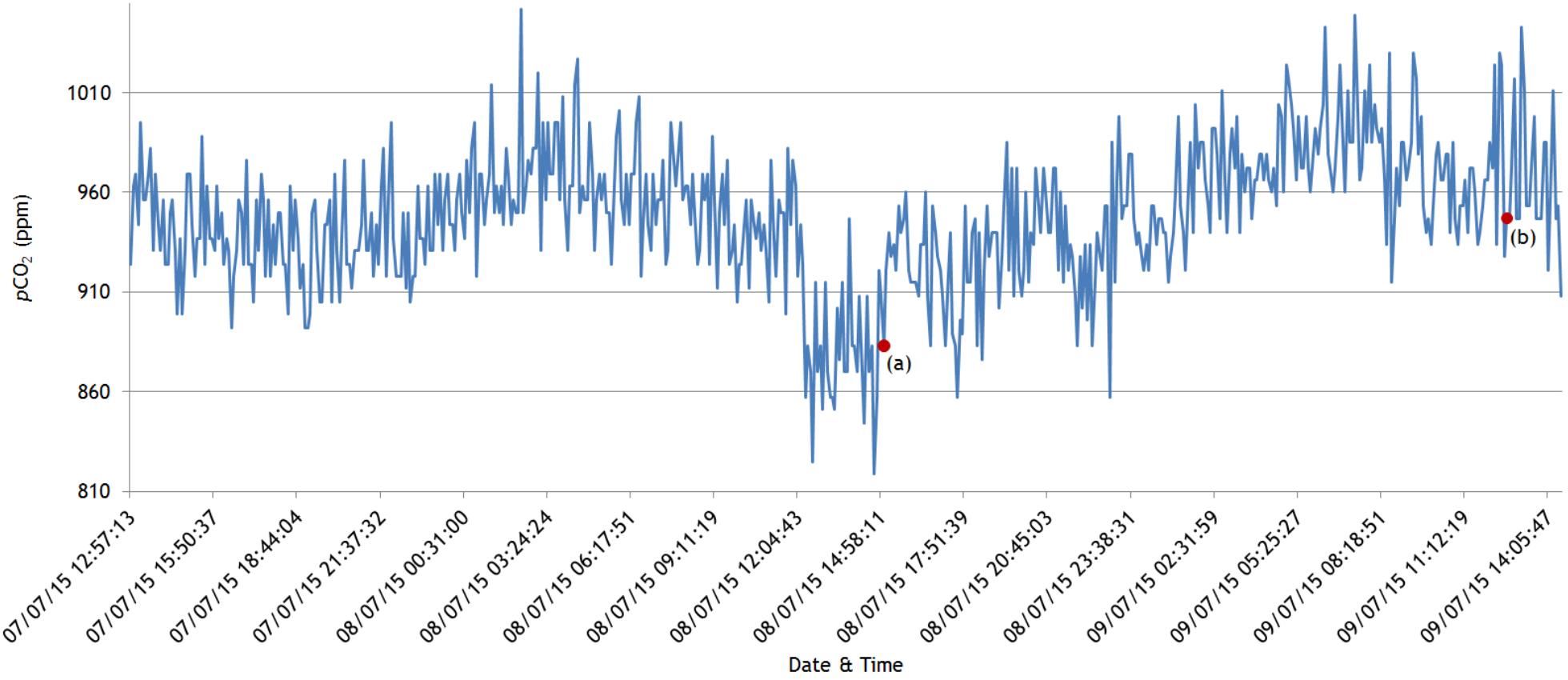

Figure 3.10: 50 hour run 7th to 9th July 2015 in gas chamber with 1000 ppm (Battery power 4 x AA 1.2v 2450mAh NiMH). Overall mean = 948 ± 35 ppm. (a) Spiked with 1000 ppm gas at 1450, 08/07/15. (b) Spiked with 1000 ppm gas at 1220, 09/07/15.

A 50 hour run of the sensor in the chamber injected with 1000 ppm is shown in Figure 3.10. Again, with the injection of gas, the sensor was reading approximately as would be expected. There was a gradual drop in the concentration that the CO_2 sensor was recording half way through the run until it was injected again with 1000 ppm gas. Subsequently the reading began to rise again towards a 1000 ppm concentration. The sensor would be calibrated before the next run in the gas chamber which would this time contain 400 ppm CO_2 gas.

3.4.2.3.2 400 ppm

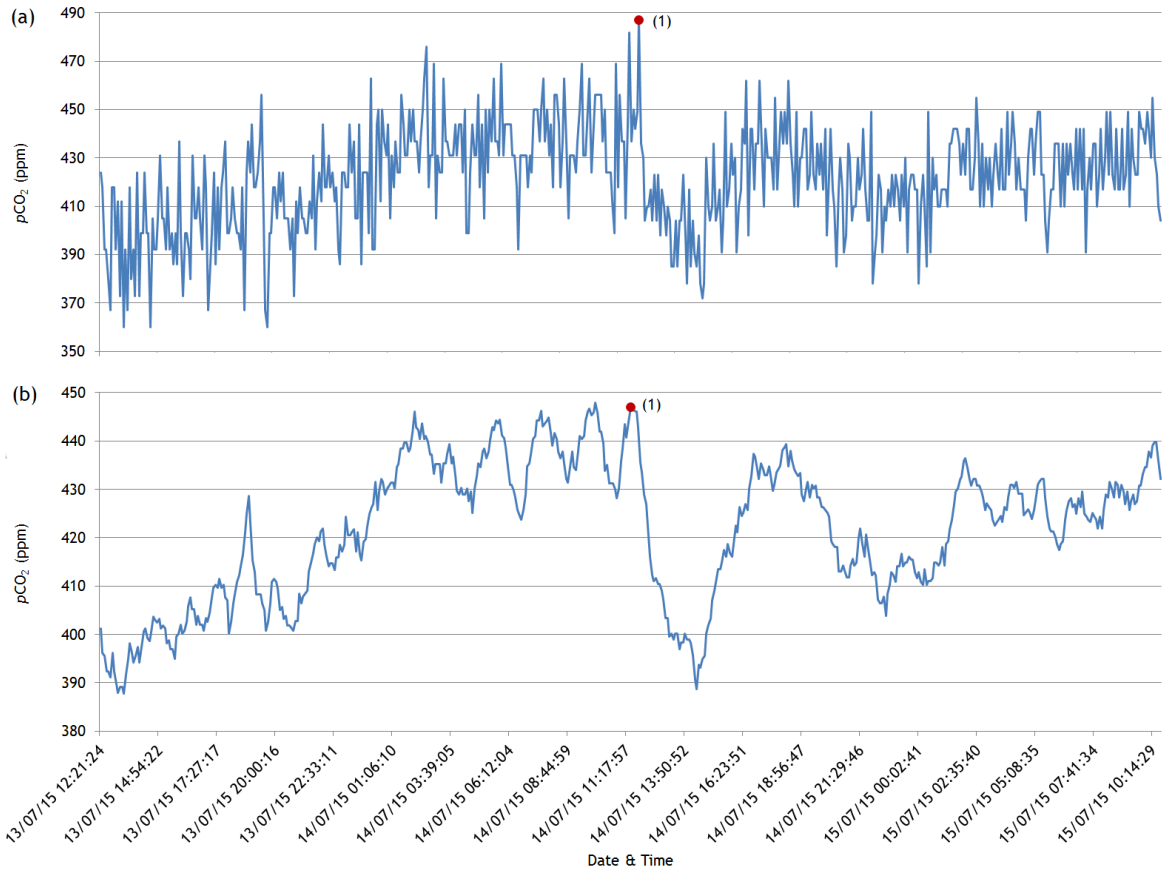

Figure 3.11: 47 hour run inside 400 ppm chamber (Battery power 1.2v 2450mAh NiMH). (1) Input of 400 ppm into the chamber. (a) Raw data mean 422 ± 21 ppm (b) Noise-filtered (MA 10) data mean 422 ± 14 ppm.

The sensor, when initially put into the 400 ppm gas chamber was reading as expected. The concentration gradually increased over time until injected once more with 400 ppm gas. The concentration then decreased to the expected value but rose again which perhaps reflected ambient CO_2 in the laboratory, i.e. higher than 400ppm.

3.4.2.3.3 1000ppm and humidity

Figure 3.12: 4.5 hour run outputting both CO_2 and humidity in 1000 ppm chamber. Humidity mean = 38 ± 0.1 %. (a) Raw data which shows a drift in the sensor. Mean = 990 ± 6 ppm. (b) Drift-corrected CO_2 data. Mean = 984 ± 3 ppm.

This was a short 4.5 hour run for initial observations and testing of the code to output humidity. Humidity was approximately 38%. The raw data (Figure 3.12a) appeared to show a drift in the sensor readings. The drift-corrected CO_2 output is shown in Figure 3.12b. The CO_2 data from the sensor produced a value as would be expected when situated in a chamber of 1000 ppm CO_2 (drift-corrected data having a mean of 984 ppm).

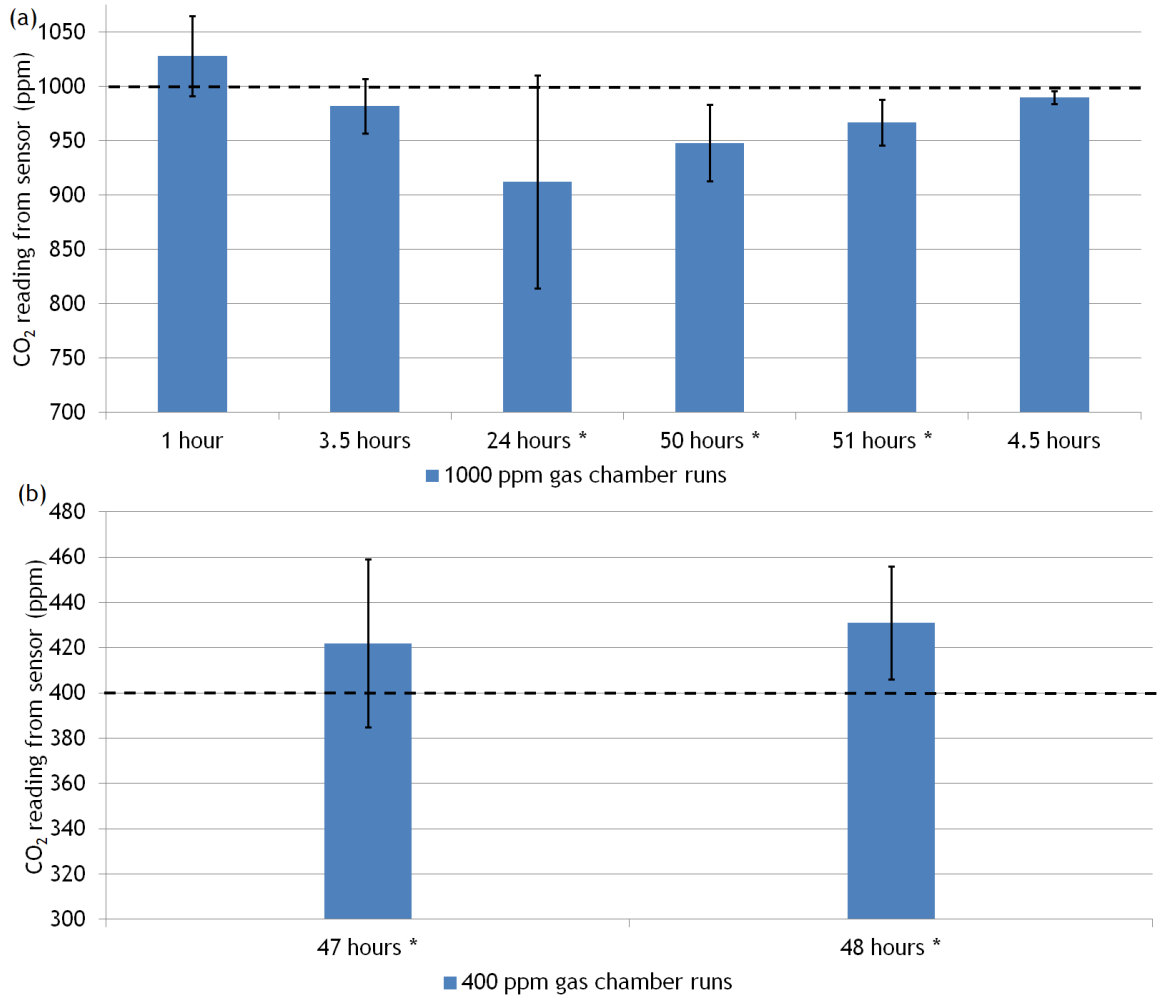

Figure 3.13: Summary of all known-gas concentration tests. *runs where more gas of the same concentration was put into the chamber during the test. Dotted line is the concentration of gas that was input into the chamber. N. B. tests were of different durations so result will vary accordingly. (a) Average concentration of 1000 ppm tests. 1 hour mean = 1028 ± 37 ppm; 3.5 hour mean = 982 ± 25 ppm; 24 hours mean = 912 ± 98 ppm; 50 hours mean = 948 ± 35 ppm; 51 hours mean = 967 ± 21 ppm; 4.5 hours mean = 990 ± 6 ppm. (b) Average of 400 ppm tests. 47 hours mean = 422 ± 14 ppm; 48 hours mean = 431 ± 8 ppm.

3.4.2.4 Discussion

Overall, in the known-gas concentration tests there were a number of conclusions made. The sensor reacted immediately to an input of 1000 ppm CO_2 gas and reached concentrations with an average of 1028 ppm. The COZIR data sheet states that the sensor has an accuracy of ± 50 ppm and the results show that the sensor has performed well in this specific run. A longer test was needed however to adequately gauge the output of the sensor. Overall, in the known-gas concentration tests the sensor would almost always have a mean within ± 50 ppm of the known concentration. In the longer runs that it did not get within this number there was a clear explanation for this. It became obvious

that the chamber used was not completely air tight. The plastic was also a porous material. When left for a longer run, the CO_2 concentration would gradually fall downwards but immediately change when another injection of gas was input into the chamber. The gas chamber was constructed with cost-effective materials under a time constraint but was deemed suitable for the purpose of this project. The initial drift test within this section showed that it was the chamber that was causing the downward drift due to it not being airtight. In future tests, it will become clear that there actually *is* a drift in the sensor but always in an upward direction. When the data were filtered of noise, it became apparent that the sensor was drifting. When drift was evident from the noise-filtered data then it was necessary to normalise the data to correct this

3.4.3 Underwater tests (initial design)

This section deals with the very first underwater trial of the sensor. This was using the initial housing design of Tupperware and a PTFE filter attached to the lid with aquarium silicone (see Chapter 2, Section 2.4.5.1, page 55). The lid was also secured with more silicone.

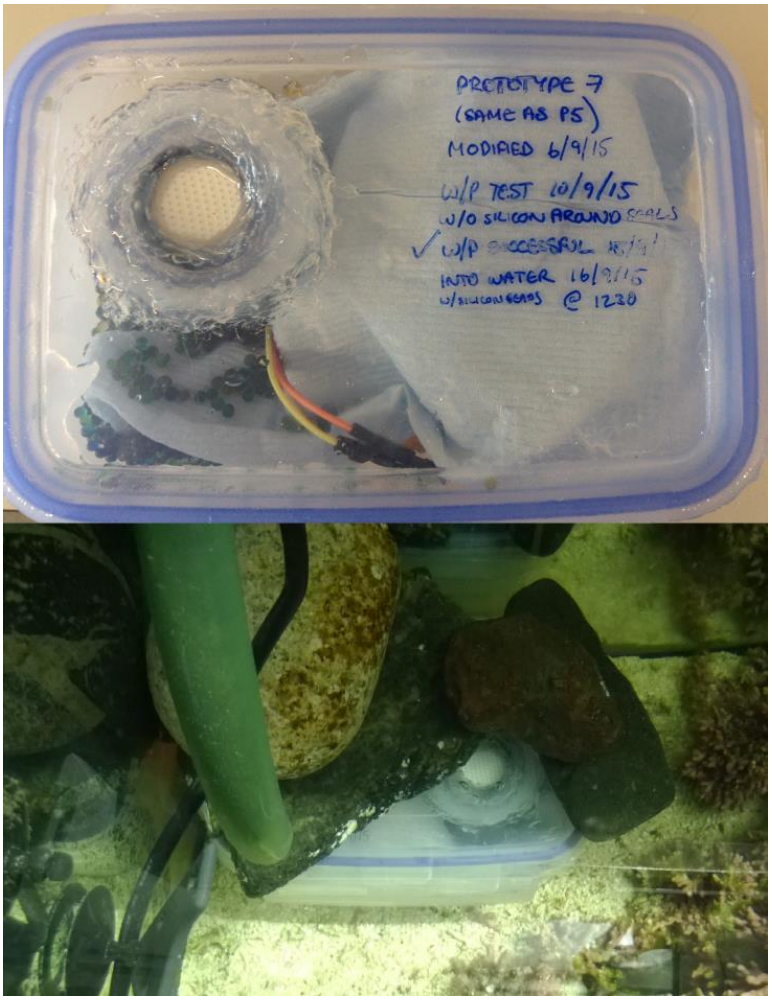

Figure 3.14: Initial prototype of pCO_2 sensor. Top: Electronics and sensor inside plastic box with a PTFE filter allowing gas to pass through. Bottom: Initial prototype underwater in ambient mesocosm. Due to a high buoyancy, the prototype had to be weighed down initially.

3.4.3.1 Aims

1. Test effectiveness of housing underwater, i.e. evidence that pCO_2 could reach the sensor through the housing in seawater, the durability of the housing and also the effectiveness in keeping the sensor and electronics dry.

2. Have an accurate pCO_2 output from the sensor whilst autonomous and underwater.

3.4.3.2 Methods

Structured underwater tests were carried out with the initial design of housing (see Figure 3.14). The programmed sensor was put into the housing and then sealed with silicone to withstand being submerged into the mesocosm. The mesocosm was not manipulated with any gas. The housed sensor was then left for 48 hours and retrieved. This method was repeated twice.

3.4.3.3 Results

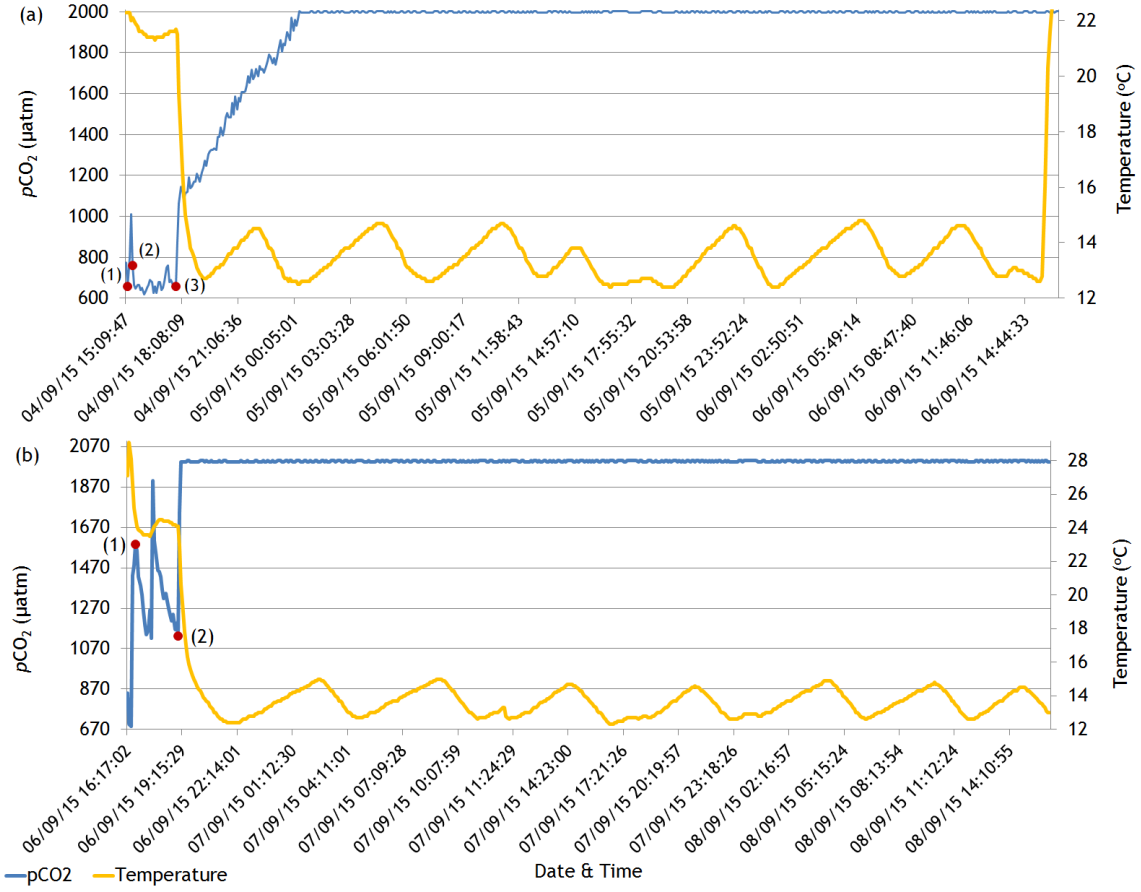

Figure 3.15: Underwater trial with initial housing set-up outputting seawater pCO_2 and seawater temperature. (a) 4th to 6th September 2015 for 49 hours (1) sensor placed under PFTE filter in housing and secured with silicone (2) housing sealed with silicone (3) placed underwater in the ambient mesocosm. (b) 6th September to 8th September 2015 48 hour run (1) sensor placed in housing and sealed. (2) placed underwater in the ambient mesocosm

For the duration of the run, the CO_2 readings reached and then stayed at the concentration of 2000 µatm (the maximum that the sensor can record) (see Figure 3.15a). This is likely to be an erroneous value rather than a true concentration of CO_2. The shallow, ambient tank should have been reading

around 400 μatm as it equilibrates with the atmosphere. The temperature sensor did however show a cycle with peaks every 6.5 hours. The temperature in the mesocosm varies due to heating of the water by the UV lamps which are on a timer to simulate day and night cycles. Because the temperature sensor (which is integrated into the body of the COZIR sensor) appeared to work, it was therefore notable that the sensor overall was working underwater but something was affecting the CO_2 signal. Figure 3.15b was a repeat of the previous experiment. The same pattern as before was seen and therefore the erroneous CO_2 readings would have to be addressed before the next run. The sensor was set to run within the housing in an atmospheric environment and the results are shown in Figure 3.16 which alludes to no housing problem.

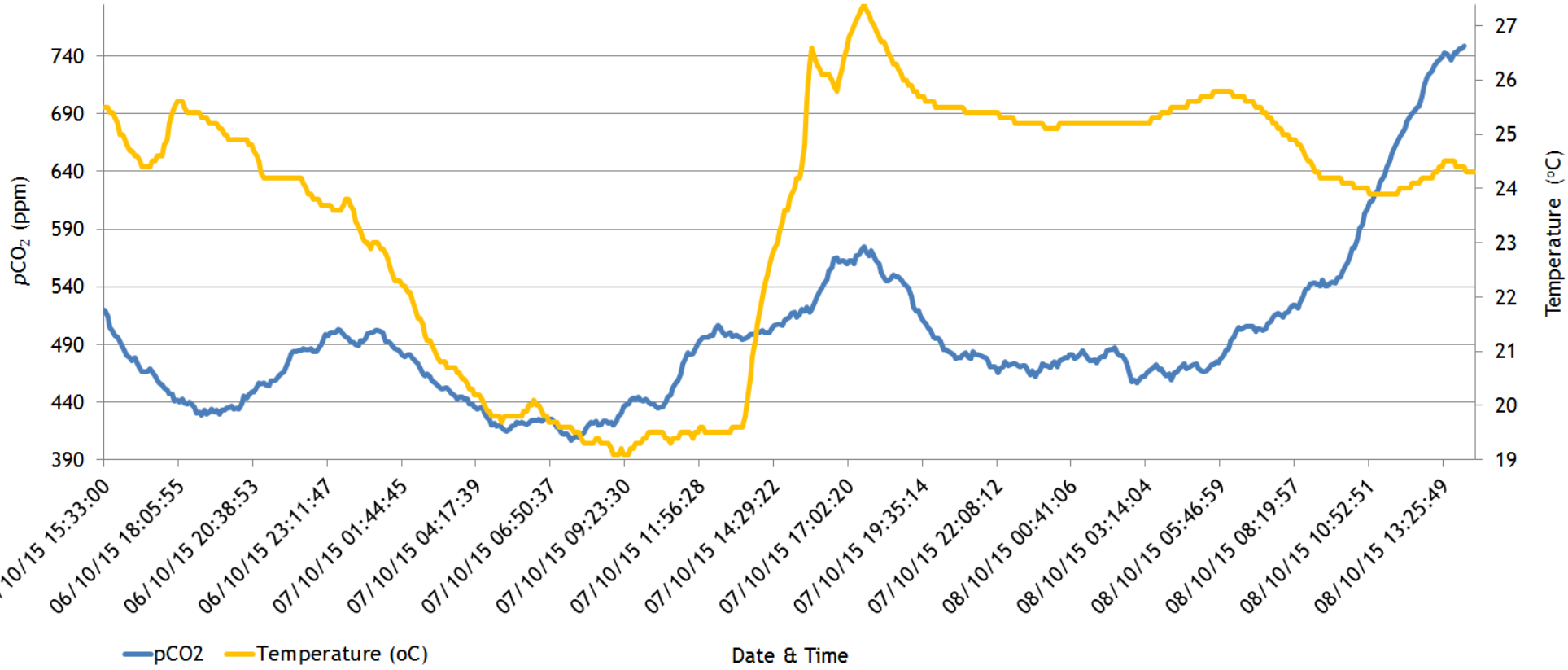

Figure 3.16: The sensor was started and placed within the housing and set to run in a busy office. The output was CO_2 and temperature. Silicone was not used in this process because there was no need to waterproof the housing.

3.4.3.4 Discussion - Issue with sensor or housing?

CO_2 gas, when the sensor was situated in the office (still in the housing), was able to be recorded by the sensor and both the CO_2 and temperature output gave values that were to be expected. The problem was only apparent when the housing and sensor was underwater. Although there didn't appear to be a problem with the CO_2 gas reaching the sensor through the housing in atmospheric conditions, to attempt to address the underwater problems, a design rethink of the housing that held the sensor was conducted. These tests confirmed that the initial prototype was not suitable underwater. Subsequent tests would reveal the problem and this is addressed in Section 3.4.5, page 101.

3.4.4 PTFE tube design

As described in Section 2.4.5.2, page 57, a new design of housing was manufactured. This design consisted of a hollow PTFE tube and two lids at the end. The lids initially were plastic inserts secured with aquarium silicone and lastly (which would be the final design), two screw-on PTFE caps which eliminated the need for silicone. Several experiments were carried out with the PTFE tube which will be detailed in the next section.

3.4.4.1 Initial Underwater runs

This section presents the experiments conducted with the PTFE tube set-up and the different lids used will be detailed within each section. This encompassed many different runs which over the course of experiments were fluid in aims.

3.4.4.1.1 Aims

1. Assess the performance of the new housing and sensor underwater by conducting similar tests as previous, i.e. in marine mesocosms both in ambient and CO_2 concentration specific environments.

3.4.4.1.2 Methods

The PTFE tube was used to house the electronics and sensor. Plastic inserts were placed at each end of the tube and secured with aquarium silicone (see Figure 3.17).

Figure 3.17: PTFE tube with plastic inserts sealed with silicone. The sensor and electronics were housed inside and put underwater in the mesocosm

This set-up was immersed underwater in a mesocosm for several different time scales and the performance of the housing, sensor and also the data produced were analysed.

3.4.4.1.3 Results

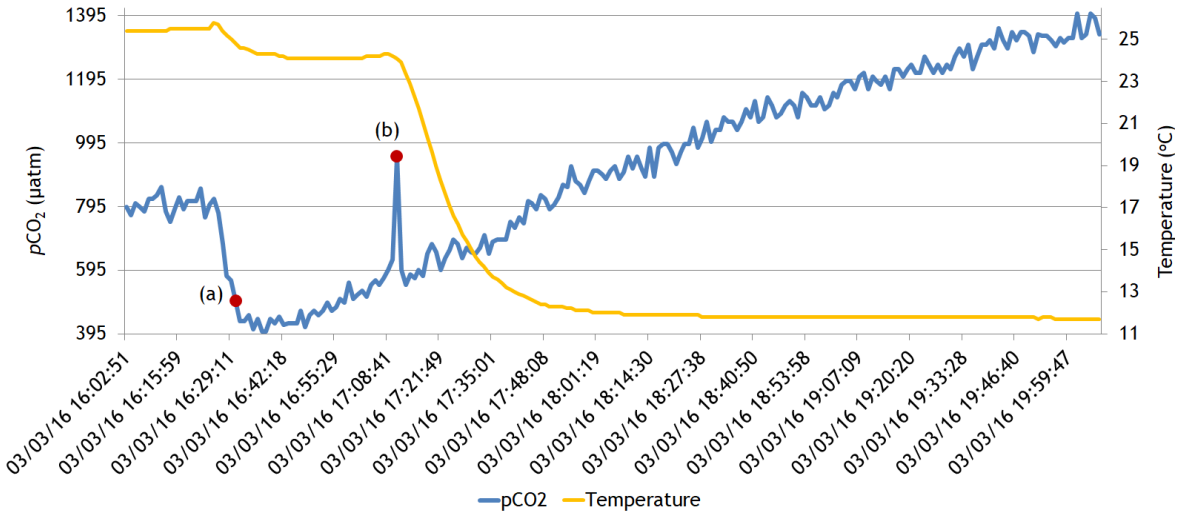

Figure 3.18: First immersion of PTFE tube design underwater (3 hours with 9v battery). (a) sealed in tube with silicone (b) placed underwater in a mesocosm.

Although only a short run, Figure 3.18 shows data that again produced a continual upwards drift that could mean that the CO_2 signal would possibly reach the maximum sensor value again, i,e, give an erroneous value. A longer run was then tried to see further evidence of this.

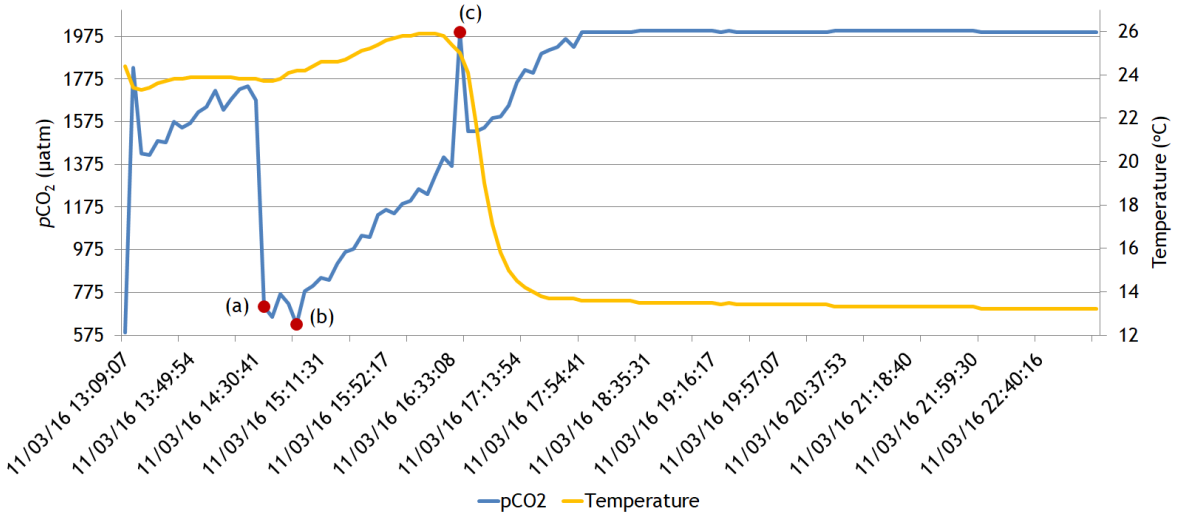

Figure 3.19: 2 day run from 11th to 13th of March 2016 of CO_2 and temperature output in PTFE tube with 1000 ppm (initially an atmospheric run (at 1312) then an underwater run (1640). Shown is only the data up to 2310 on 11th. (a) housing flushed through with 400 ppm gas then aborted because of too much pressure (b) back in tube and waterproofed with silicone and left to dry for 2 hours. (c) placed underwater.

Once the sensor was allowed to settle underwater, the sensor outputted the maximum reading of 2000 µatm again. The next run was to check any problems with the housing and the ability of the sensor to receive CO_2.

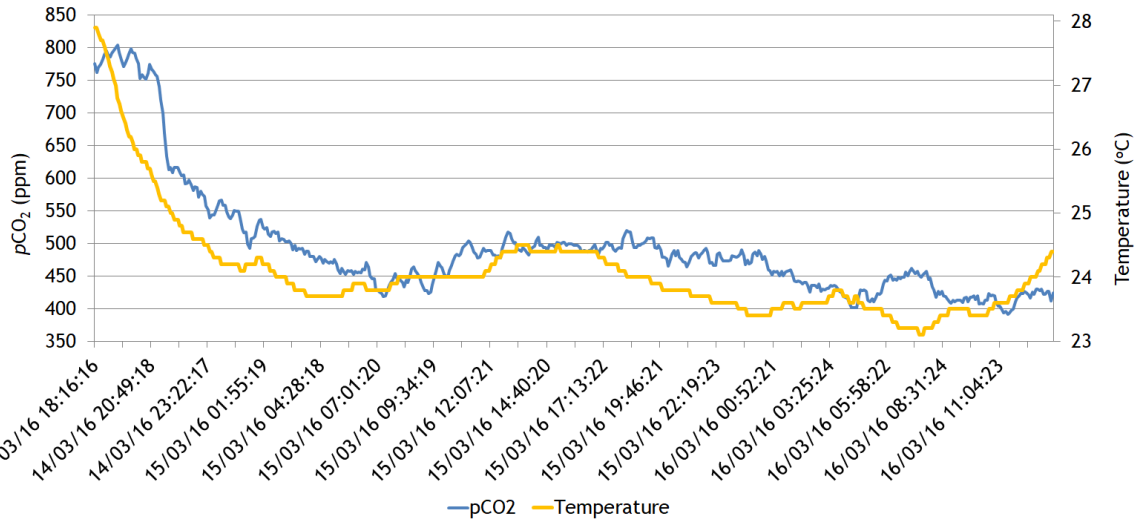

Figure 3.20: Atmospheric, autonomous run in PTFE tube. The sensor was programmed to output CO_2 and temperature and placed in the PTFE tube housing. The housing was then left to record in an office.

The atmospheric run in Figure 3.20 shows the senor within the PTFE housing which was situated in a busy office for 42 hours. The sensor performs well inside the tube. It was therefore necessary to investigate why the sensor and housing was not working as expected underwater.

3.4.4.2 Humidity

Initially it was though that perhaps the humidity was having an effect on the CO_2 readings. The humidity levels and CO_2 values in a mesocosm tank were tested.

3.4.4.2.1 Aims

1. Develop code to output humidity from the sensor in conjunction with CO_2 readings.

2. Assess whether humidity was affecting the CO_2 values read by the sensor with the addition of a molecular sieve in the housing.

3.4.4.2.2 Methods

Incorporated within the COZIR CO_2 Ambient sensor there is an inbuilt humidity sensor; the Sensirion SHT21 chip. Code to check the humidity output was developed to see if humidity was affecting the CO_2 readings from the sensor (see section 2.4.3.1, page 45). The concentration of water vapour present may cause erroneous measurements of CO_2 by changing the density of the air that is being measured (Pearman and Leuning, 1980). CO_2 readings by the sensor are essentially density readings by NDIR. In some runs, a molecular sieve was used inside the housing; the molecular sieve consisted of desiccant beads made of porous crystalline metal-alumino silicates in the size range 1.6 - 2.5 mm (classification 4Å (Angstroms)). Moisture dessicant absorption happens with molecules under 4Å in diameter. Anything bigger than this, absorption will not take place. It was expected that smaller molecules, i.e. water molecules would be absorbed but larger molecules, i.e. CO_2 would not. Therefore if water molecules were causing the readings on the CO_2 sensor to reach a maximum, i.e. confusing the density measurements, the inclusion of a molecular sieve within the housing may prevent this.

The seawater in the mesocosm was kept at a fixed temperature of 8^{o}C via a chiller and CO_2 concentrations were manipulated naturally by coralline algae which force a 24 hour cycle, i.e. respiration at night increasing the CO_2 levels and photosynthesis during the day decreasing the CO_2 levels.

3.4.4.2.3 Results

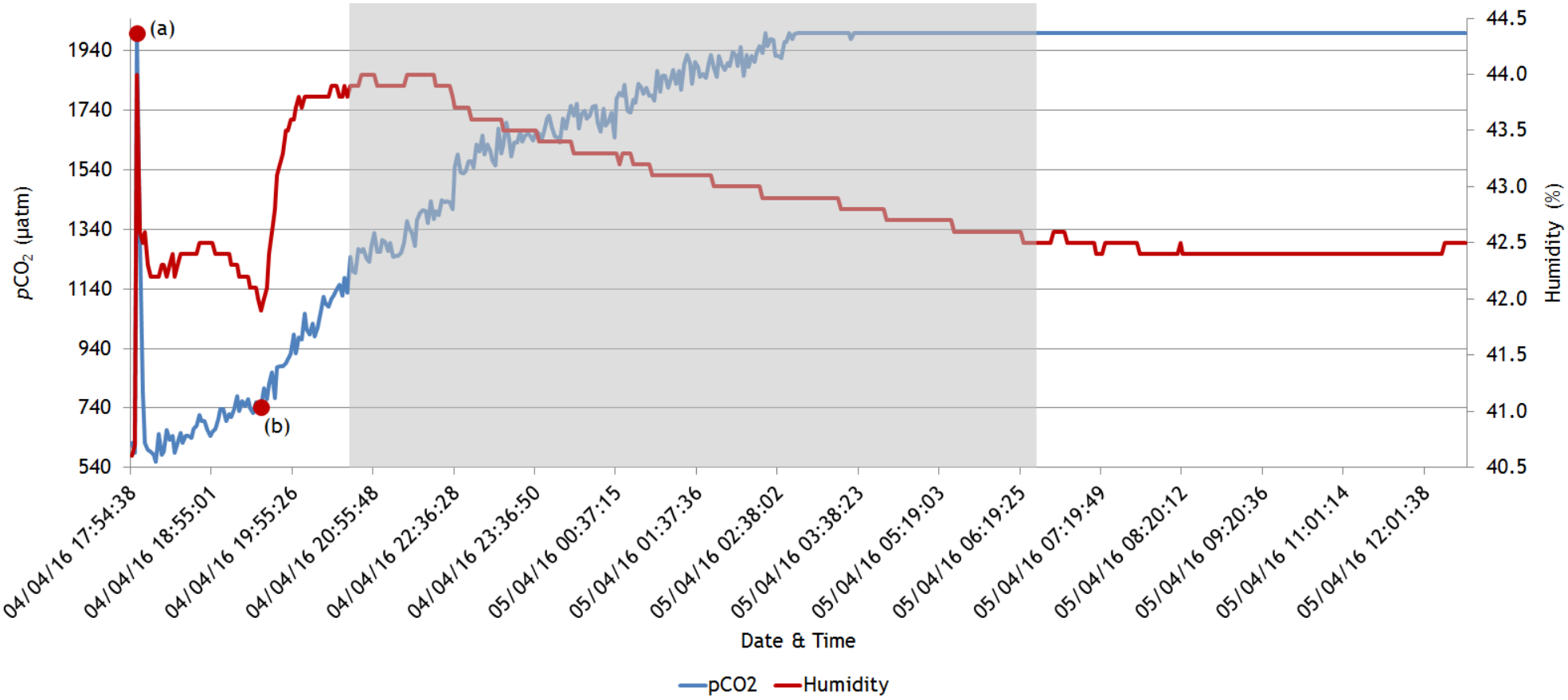

Figure 3.21: 18h 35m run of pCO_2 and humidity output in mesocosm kept at 8°C which contained coralline algae. Shaded area signifies the dark hours. (a) Sensor placed in tube with silicone seal (b) Sensor placed underwater

The pCO_2 and humidity output from the sensor is shown in Figure 3.21. This was an 18.5 hour run in the mesocosm. The humidity makes a predictable rise when the sensor is first placed into the mesocosm but does not rise to a significant level where there would be concern that it would affect the CO_2 signal. Again, the sensor reaches a value of 2000 μatm. This set-up was repeated. Although the test results show that the COZIR sensor is not significantly affected by humidity, more tests were done with the addition of a molecular sieve for further clarity.

3.4.4.3 Discussion

The Sensirion measures humidity by capacitive means. The sensor consists of a capacitor which has a humidity sensitive polymer as a dielectric. This polymer will take up water molecules according to the ambient humidity. This results in a change of the capacitance which is what is measured by the sensor. When pCO_2 concentration data were not reading as expected, i.e., the sensor was reaching a maximum pCO_2 concentration of 2000 ppm consistently, it was hypothesised that perhaps humidity was affecting the measurement of CO_2. Because CO_2 measurement is essentially a measurement of density, if there are excessive water droplets in the air then this may affect the components of gases in the mixture. However, when humidity was measured concurrently with pCO_2, levels of humidity were consistently less than 50% and it was deemed that CO_2 concentration was not erroneous because of humidity levels.

3.4.4.4 Molecular sieve beads

To investigate the possibility that humidity was affecting the CO_2 output of the sensor further, there was an addition of molecular sieve beads into the main body of the housing. Molecular sieve beads were used due to their unique water vapour adsorbing qualities and ability to remove excess moisture from the surrounding air.

3.4.4.4.1 Aims

1. Assess whether the addition of a molecular sieve in the main body of the housing will improve the quality of data produced from the CO_2 sensor.

3.4.4.4.2 Results

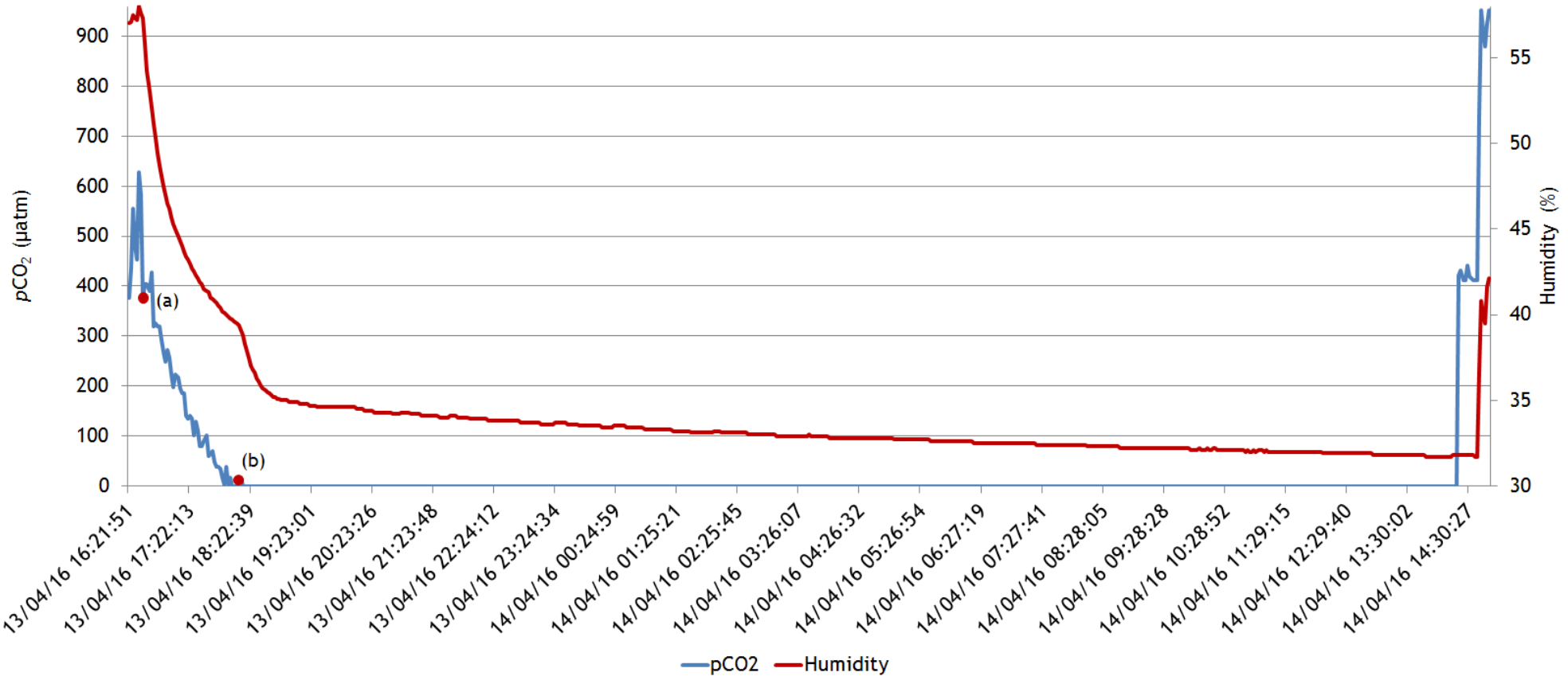

Figure 3.22: 21.5 hour run in PTFE set-up with molecular sieve outputting CO_2 and humidity in mesocosm at 8°C (a) placed into housing with silicone (b) placed underwater

An underwater run is shown in figure 3.22. The pCO_2 signal gradually reduced to 0 μatm for the duration of the run. The housing was taken out of the water. CO_2 signal returns when the sensor was taken out of the housing.

3.4.4.5 Discussion

When a molecular sieve was included in the deployment, the pCO_2 signal gradually reduced to 0 μatm. The CO_2 signal would return and gradually increase above 0 μatm when the sensor was taken out of the housing. Further investigation suggested that certain drying agents (i.e. molecular sieves) can absorb CO_2 and this would account for a value of 0 μatm being read by the sensor. With this particular molecular sieve, any molecules smaller than 4Å would be absorbed by the beads. H_2O molecules have an approximate diameter of 2.75Å. CO_2 molecules are smaller than H_2O molecules with a diameter of approximately 2.32Å. Therefore, a molecular sieve would not be used any further within this study. It was assumed that humidity did not affect the readings because at the specified wavelength (4.2 μm), water has no absorption bands and would therefore not affect the CO_2 readings (Hodgkinson and Tatam, 2012 (see Figure 2.1, page 29).

3.4.5 Silicone incubator tests

Tests were run on the use of the silicone in the design because of concerns of possible silicone degassing interfering with the CO_2 reading of the sensor.

3.4.5.1 Aims

1. To ascertain whether silicone was affecting the readings of CO_2 concentration by conducting tests ***with and without*** silicone in the set-up.

3.4.5.2 Methods

Silicone was used in the initial housing design for waterproofing purposes, e.g. securing lids. Because silicone could not be used for half of the experimental runs, the tests were conducted only in atmospheric conditions to ensure uniformity. The tests were performed in a temperature controlled incubator

kept at 8^{o}C (typical temperate winter seawater temperatures in Scotland). The programmed sensor was placed in the housing and shut and 400 ppm was pumped into the housing. The housing was then put into the incubator. In the tests which required silicone, it was used as for underwater tests to seal the housing. Conversely, silicone was not used in the other tests but all other protocol was exactly the same. Both results were then compared.

3.4.5.2.1 Results

3.4.5.2.1.1 Without silicone

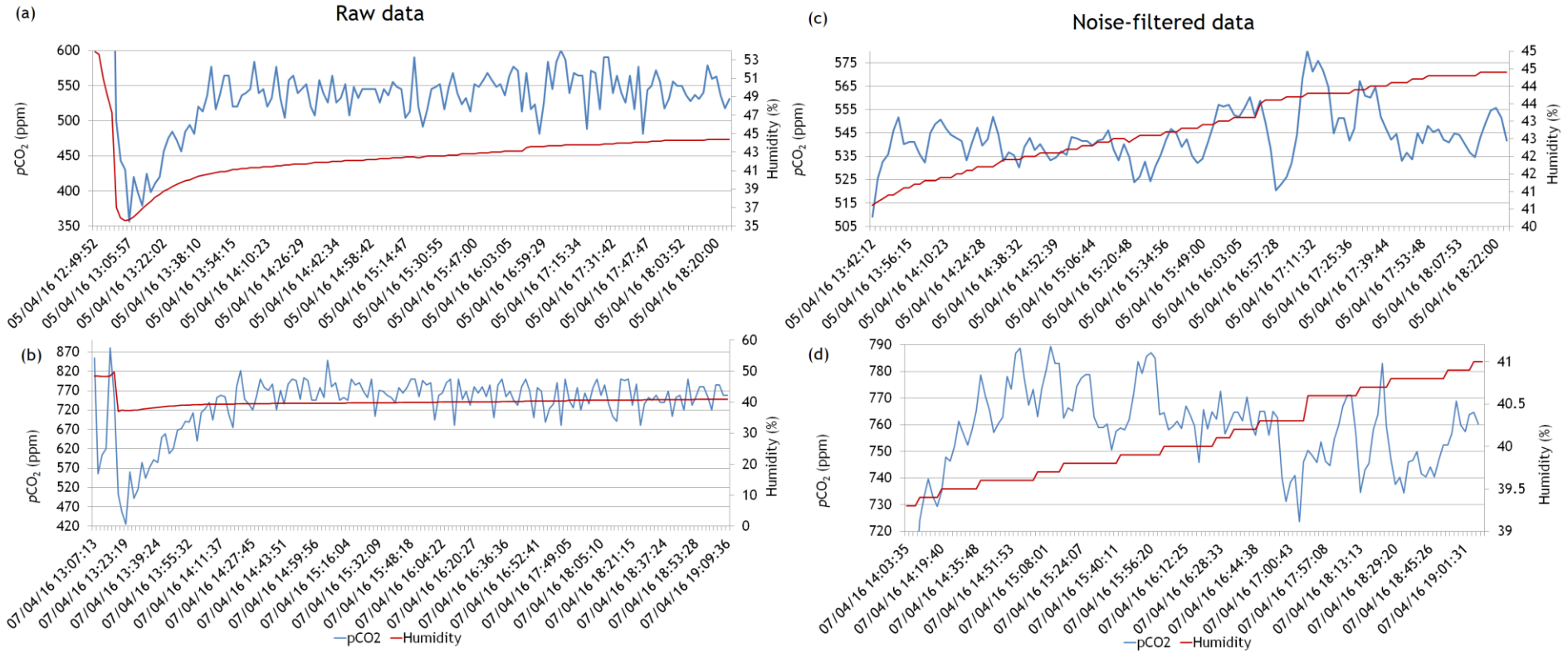

Figure 3.23: 6 hour runs of pCO_2 and humidity with injection of 400 ppm gas in housing with no silicone and placed in an atmospheric incubator set at 8°C. (a) 5th April 2016 raw pCO_2 and humidity data. Mean pCO_2 = 544 ± 24 ppm. (b) 7th April 2016 raw pCO_2 and humidity data. Mean pCO_2 = 760 ± 33 ppm. (c) Noise filtered version of 3.22a with a moving average of 5. Mean pCO_2 = 544 ± 11 ppm. (d) Noise filtered version of 3.22b with a moving average of 5. Mean pCO_2 = 759 ± 17 ppm.

In both 6 hour atmospheric runs without silicone, the sensor records a CO_2 concentration without any rise to beyond range (see Figure 3.23). The sensor however did show some drift in the data so this was corrected. These were positive findings as there was no obstruction to the output of either pCO_2 or humidity from the sensor. Another identical run was completed (see Figure 3.24). More detail is shown on the processing of the data. This was a longer run than the previous two to ensure there were no problems for longer deployments.

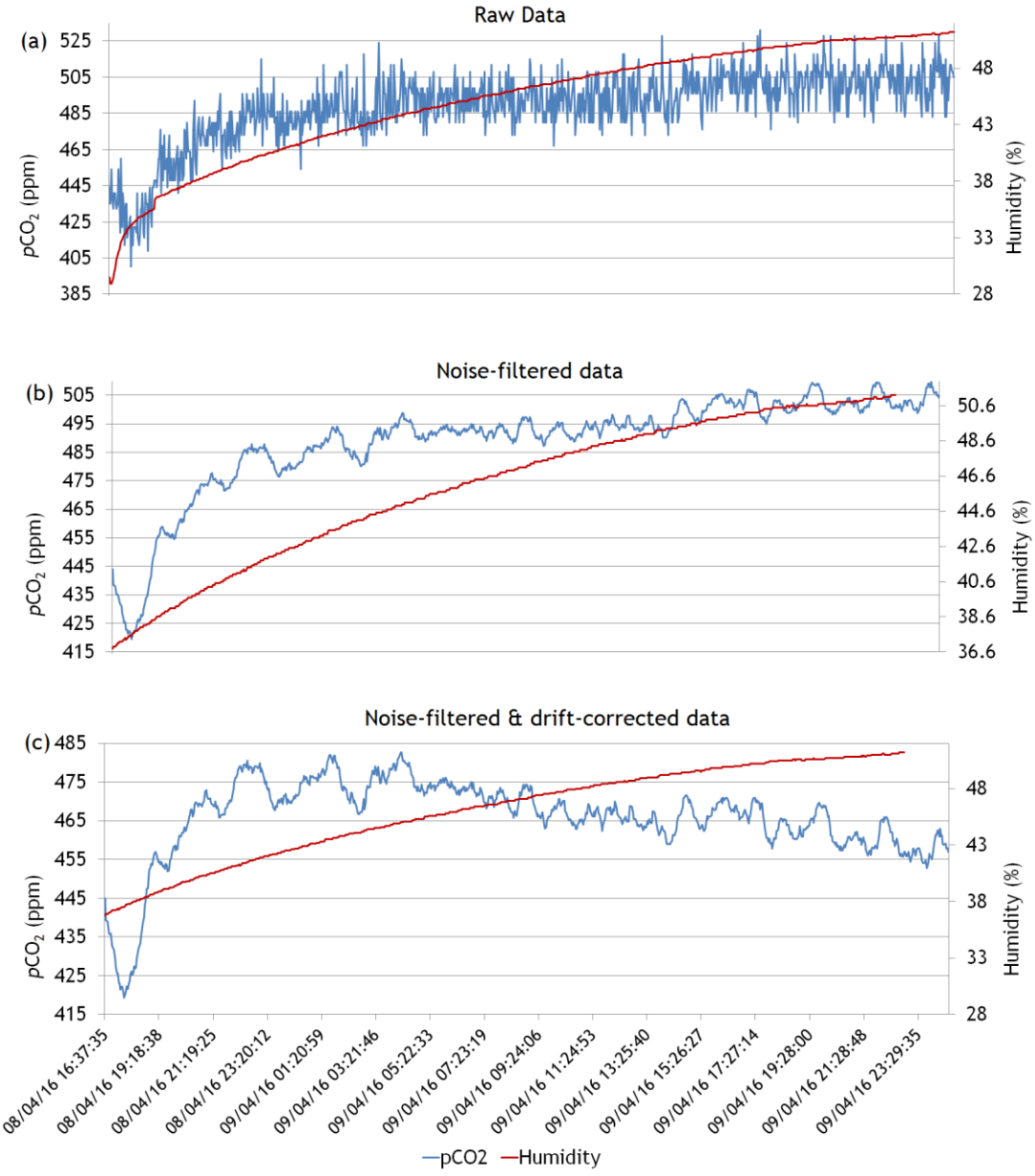

Figure 3.24: 8th to 10th April 2016 32.5 hour run of sensor in housing placed in an incubator at 8°C without using silicone with 400 ppm gas injected. (a) Humidity and raw pCO_2 and humidity data. pCO_2 mean = 489 ± 21 ppm. (b) Humidity and noise-filtered pCO_2 data. pCO_2 mean = 492 ± 11 ppm. (c) Humidity and noise-filtered and drift-corrected data. pCO_2 mean = 467 ± 7 ppm.

3.4.5.2.1.2 With silicone

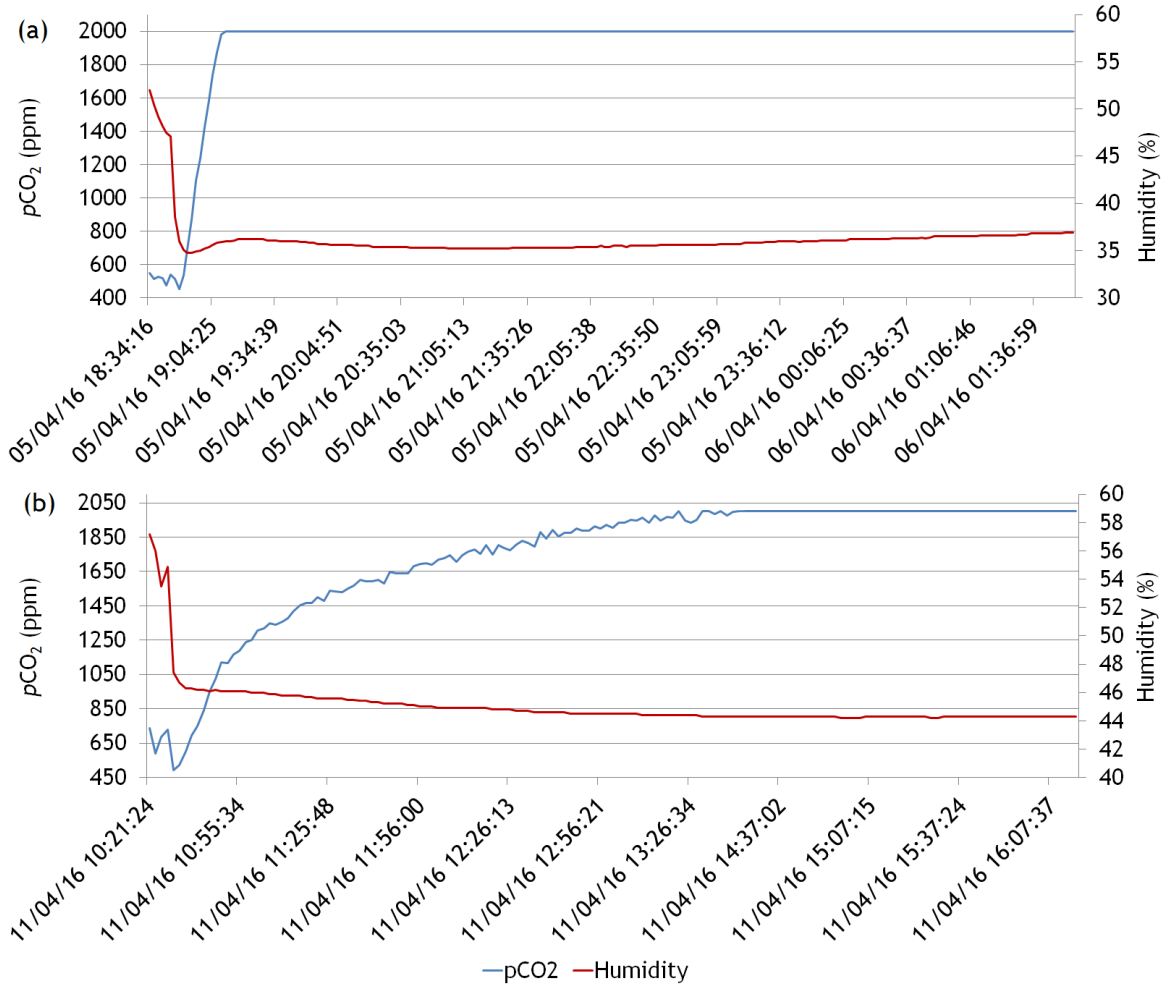

Figure 3.25: 6 hour runs of sensor in housing placed in an incubator at 8°C using silicone with 400 ppm gas injected. (a) 5th April 2016. Raw pCO_2 and humidity data. (b) 11th April. Raw pCO_2 and humidity data.

The humidity read as expected but the CO_2 readings reached a maximum of 2000 ppm on both runs as shown in Figure 3.25. These experimental runs suggested that silicone was having an effect on the sensor CO_2 output.

3.4.5.3 Discussion

When silicone was eradicated from the set-up, there appeared to be no problems with the CO_2 concentration being output by the sensor. In comparison, when silicone was introduced to the set-up again, the signal was corrupted. When silicone cures it releases acetic acid (ethanoic acid) (Penichon *et al.*, 2002).

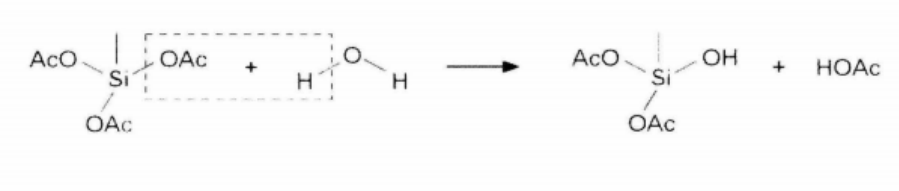

Acetic acid is given off after a hydroxyl group is formed when there is an addition of atmospheric water (Penichon *et al.*, 2002).

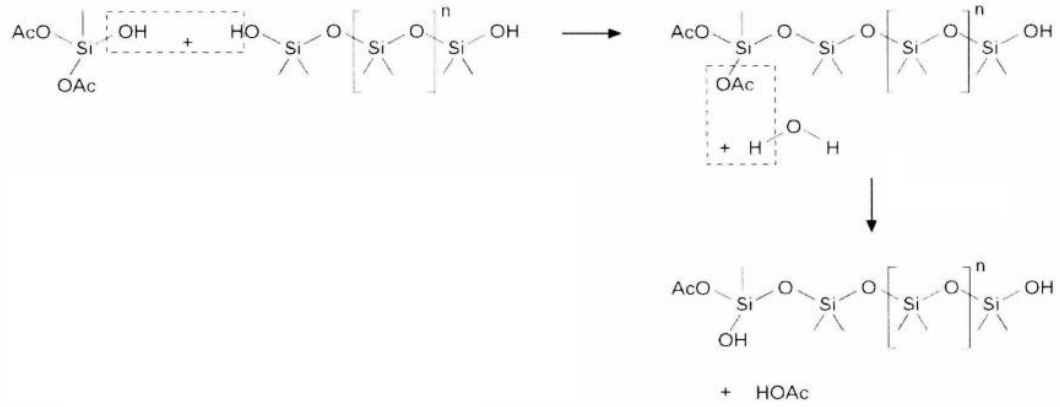

Siloxane is produced and water is released which consequently combines with another acetyl group and produces acetic acid (Penichon *et al.*, 2002). Acetic acid vapour may have a possible effect on CO_2 measurements as some absorption interferences can occur in NDIR gas analysers (You-Wen *et al.*, 2012). This was happening on the occasions that silicone was used so organic solvents were then avoided when waterproofing the housing

3.4.6 Comparison of two sensors (atmospheric)

This section deals with the comparison of two separate sensors which are running at the same time in an atmospheric environment. This experiment was carried out with new PTFE screw-on lids. This was to test the final housing set-up and the ability of CO_2 to reach the sensor through the newly modified housing.

3.4.6.1 Aims

1. Compare pCO_2 data of two sensors running simultaneously.

3.4.6.2 Methods

Another larger gas chamber was constructed with 'IN' and 'OUT' valves which could be opened and closed for the purpose of injecting specific concentration gas into the chamber (the chamber was the same as previously seen in Figure 3.2 but larger to accommodate all the apparatus). One sensor and its corresponding electronics were placed inside the PTFE tube housing while the other sensor and electronics were not placed inside the housing. Both, as described, were placed in the large gas chamber and 1000 ppm CO_2 was injected into the chamber.

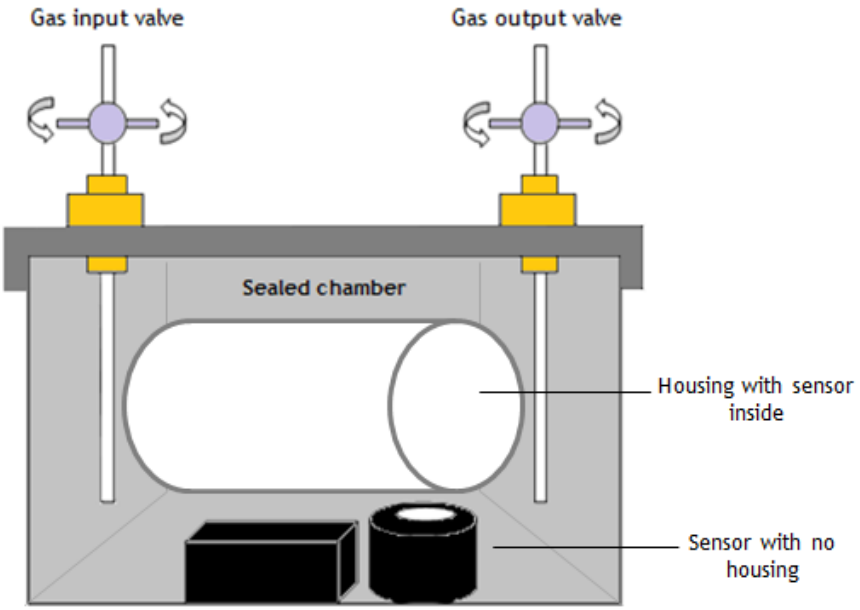

Figure 3.26: Atmospheric experimental set-up schematic. Sensor inside housing compared to sensor with no housing. Gas of concentration of 1000 ppm was injected into the chamber.

3.4.6.3 Results

3.4.6.3.1 Comparison of two sensors in known gas concentration in atmospheric conditions

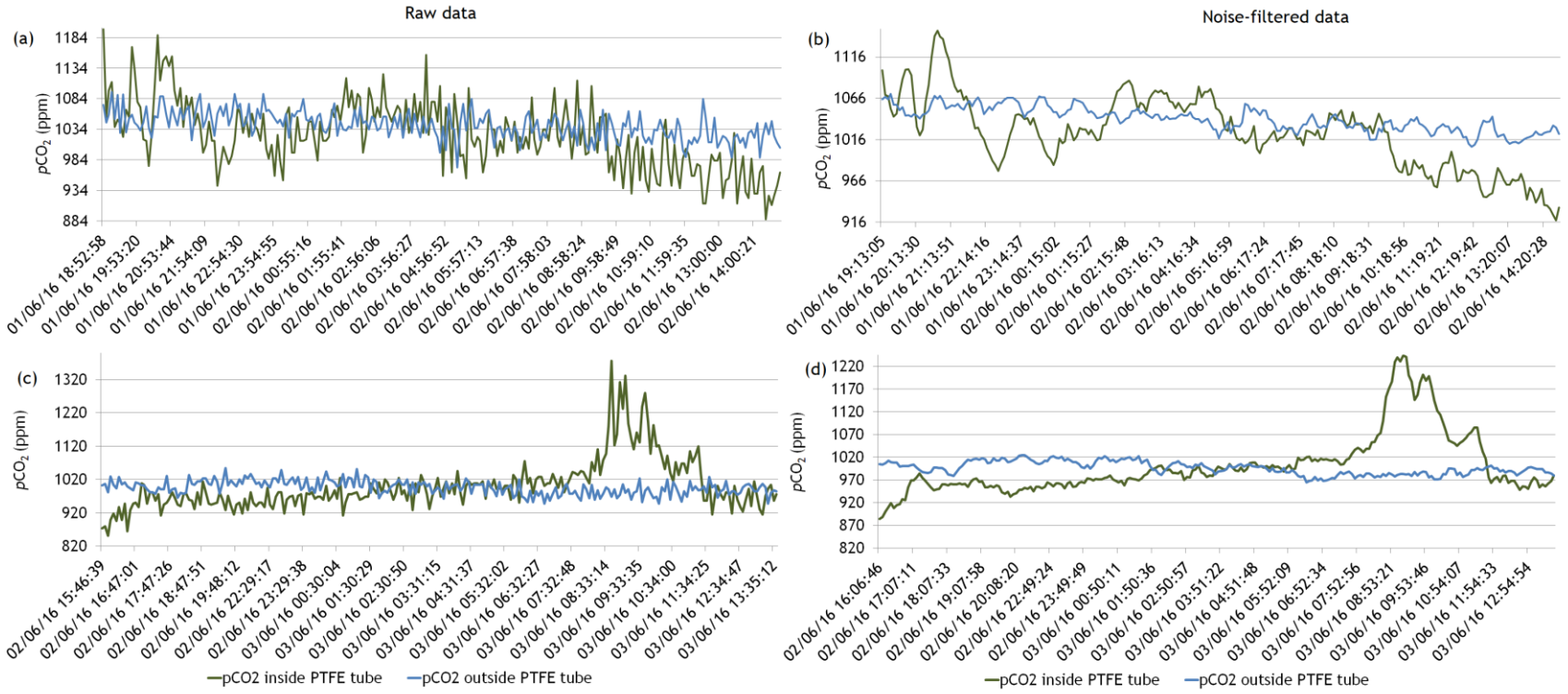

Figure 3.27: Comparison of one sensor inside PTFE tube with sensor outside of PTFE tube. Both placed in a gas chamber with a CO_2 concentration of 1000 ppm. (a) Raw data for 1st to 2nd June 2016 for 20.5 hours. Inside PTFE tube, CO_2 mean = 1024 ± 56 ppm, Outside PTFE tube CO_2 mean = 1041 ± 23 ppm. (b) Noise filtered version of (a) MA 5. (c) Raw data for 2nd to 3rd June 2016 for 22 hours. Inside PTFE tube, CO_2 mean = 999 ± 75 ppm. Outside PTFE tube, CO_2 mean = 996 ± 21 ppm. (d) Noise filtered version of (c) MA 5.

The CO_2 concentrations are very similar as shown in Figure 3.27. The result is a positive one as there is nothing impeding the CO_2 signals on either run. For both runs, the sensors show similar CO_2 concentrations (#1- 1024 and 1041 ppm; #2 – 999 and 996 ppm). In the first run, the sensor outside of the PTFE tube had a higher standard deviation but in the second run this was not the case. In the first run (Figure 3.27a and b) there appears however to be a comparatively large standard deviation with the sensor inside the tube as compared to the sensor outside of the tube. The comparison of the sensor pCO_2 concentration readings are favourable with only slight mean deviations from one another and also slight deviation from the concentration of 1000 ppm. The second run produced a similar signal from both sensors with similar standard deviations although there was a large spike with the sensor inside the PTFE tube. The reason behind this is unclear but is remarked on further in the discussion.

3.4.6.4 Discussion

Direct comparisons of two of the developed pCO_2 sensors running at the same time produced positive results and also confirmed no problem with the permeability of the PTFE tube with CO_2 gas getting from the atmosphere (or seawater) into the sensor within the housing.

There was only one occasion of a spike in the data over all the deployments. There could be numerous reasons for this and it is not an unusual occurrence in marine sensors (Timms *et al.*, 2011). This could be real data but it is more likely an erroneous peak caused by several possible reasons. The power component may have created a surge with the constantly oscillating voltage (although this would be unlikely to be as strong as shown as it was connected by DC power), it could be a radiated noise issue, a conducted noise issue or multiple impedance grounds. Puton *et al.* (2002) suggests that these spikes can happen in NDIR devices because of 'additional radiation'. However, because this phenomenon only happened once in the whole experimental process, it was not cause for concern and did not need further investigation. The sensors were calibrated before each run.

3.4.7 Known gas concentration tests with final design

Further tests were conducted in known gas concentrations with the final design of the housing and sensor (See Section 2.4.5.2, page 57).

3.4.7.1 Aims

1. To determine the reactivity of the sensor and final housing design when the environmental concentration of CO_2 is rapidly changed.

3.4.7.2 Methods

The programmed sensor and housing were placed in a large gas chamber where 1000 ppm and 400 ppm were alternately introduced to the chamber. In this run, the sensor was programmed to output a CO_2 reading every two minutes and was left to record for 48 hours. The sensor was placed in the chamber and the first flush of gas was of concentration 1000 ppm. The sensor was then left to record for 24 hours. After this time period, 400 ppm gas was flushed into the chamber and again, the sensor was left to record for 24 hours.

3.4.7.3 Results

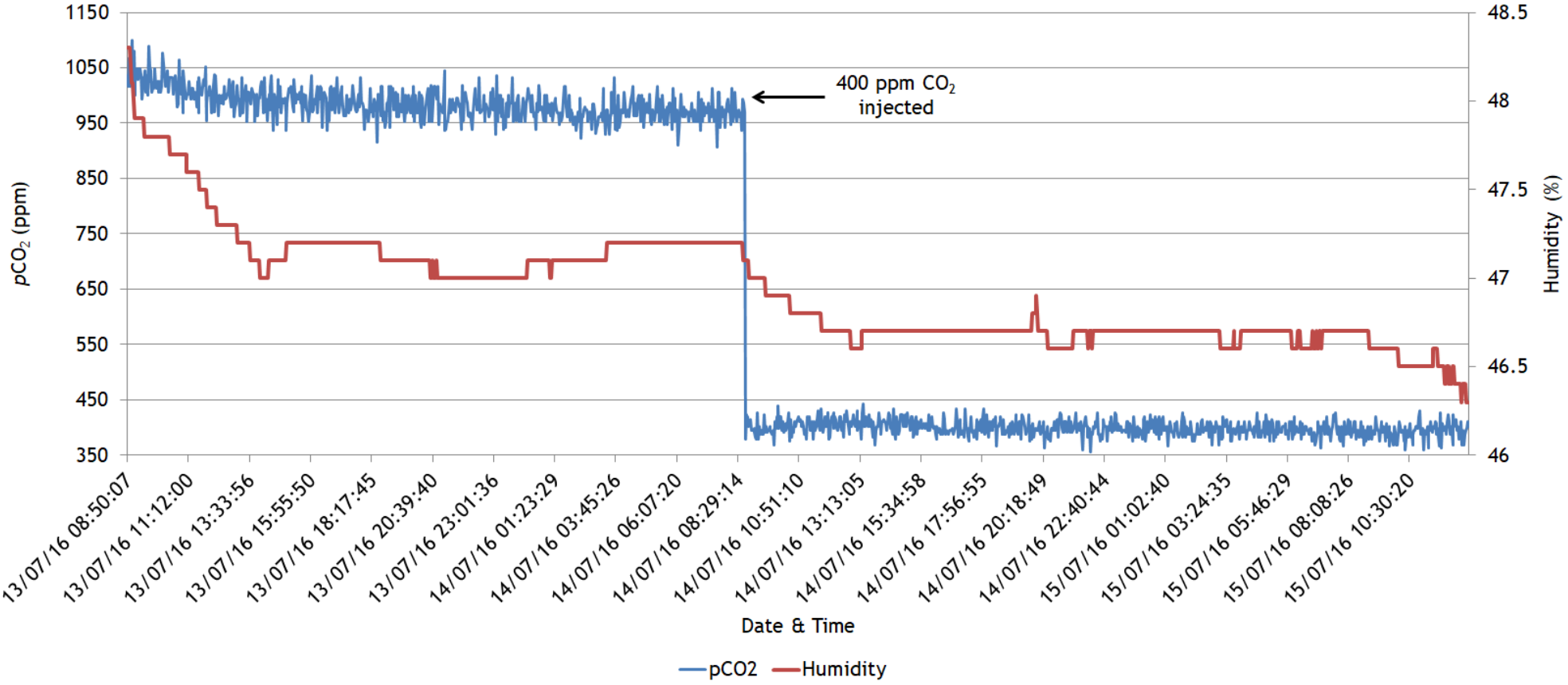

Figure 3.28: Assessment of CO_2 sensor in known concentration of alternate gases on 13th to 15th July 2016 for 48 hours. Sensor placed inside housing which was then placed inside gas chamber which was injected with alternate gasses (1000 ppm and 400 ppm). 1000 ppm injected into chamber at commencement of experiment (pCO_2 mean of this section = 985 ± 27 ppm). 400 ppm was injected into the chamber for the second half of the run (pCO_2 mean of this section = 399 ± 14 ppm). Sensor was set to produce a reading every two minutes.

This run successfully demonstrated that the sensor recognised a change in CO_2 concentration. When the concentration of gas injected into the chamber was changed from 1000 ppm to 400 ppm, there was a < 2 minute delay until the sensor reached approximately 400 ppm. The sensor was recording every two minutes so this is an approximation. From Figure 3.28, there appears to be an immediate reading by the sensor of a different concentration of gas. This is a fast enough response for most monitoring applications.

3.4.8 Mesocosm performance evaluations

The previous atmospheric experiment was replicated in a marine environment. Experiments to assess the reaction of the sensor when changed to different underwater CO_2 concentrations throughout approximately 48 hours were undertaken.

3.4.8.1 Aims

1. To determine the reactivity of the sensor and the final housing design when seawater concentration of CO_2 is alternately changed.

3.4.8.2 Methods

The tanks of seawater were manipulated by bubbling gases of predetermined CO_2 concentrations. The tanks were left for at least 24 hours to equilibrate (during bubbling) before undertaking the experimental process. Bubbling was run continuously throughout the experiment. The tanks only contained the manipulated seawater. There was no biological activity present that would additionally force the carbonate chemistry.

Discrete seawater samples were also taken to calculate the concentration of pCO_2 in the mesocosms (see General Methods 3.3.6, page 69). A sample was taken in each tank at the start and end of each deployment. This was conducted each time the sensor was put in and taken out of each mesocosm.

3.4.8.3 Results

3.4.8.3.1 Sensor pCO_2

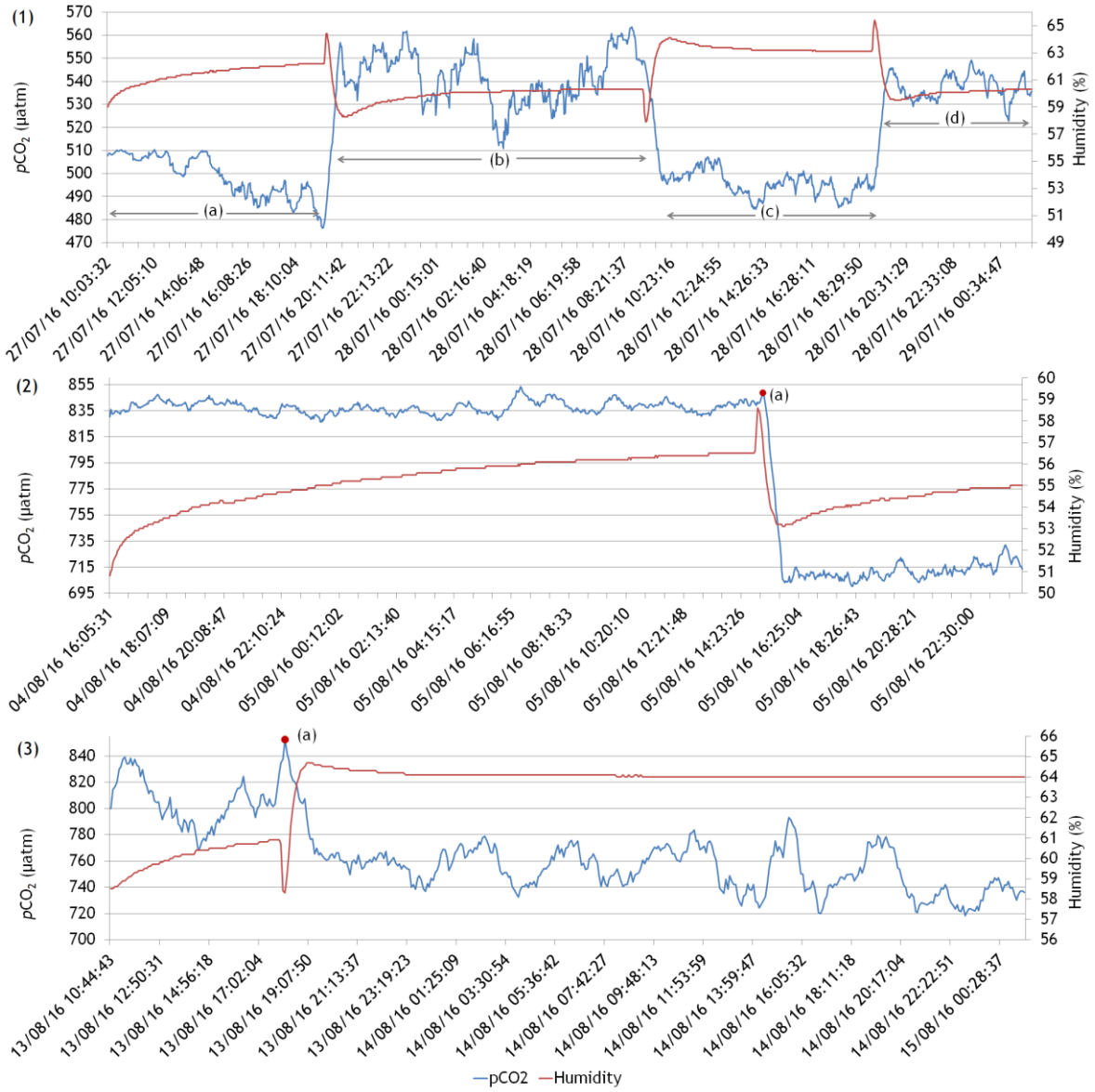

Figure 3.29: Sensor deployments in alternating mesocosms of differing pCO_2 concentrations showing sensor pCO_2 and humidity. (1) 40 hour run of sensor in two alternating mesocosms (Tank 1 = 'ambient' and Tank 2 = '1000' µatm) on 27th July to 29th July 2016. (a) Tank 1 pCO_2 mean = 499 ± 9 µatm. (b) Tank 2 pCO_2 mean = 541 ± 12 µatm. (c) Tank 1 pCO_2 mean = 496 ± 5 µatm. (d) Tank 2 pCO_2 mean = 538 ± 7 µatm. (2) 22 hour run of sensor in two alternating mesocosms (Tank 1 = '500' µatm and Tank 2 = '1000' µatm) on 4th to 5th August 2016. Mean pCO_2 for tank 1 = 838 ± 5 µatm. (a) sensor changed to tank 2 mean pCO2 = 718 ± 26 µatm. (3) 39 hour run of sensor in two alternating mesocosms (Tank 1 = '1000' µatm and Tank 2 = '500' µatm) on 13th to 15th August 2016. (a) Sensor changed to tank 2. Tank 1 pCO_2 mean = 807 ± 18 µatm. Tank 2 pCO_2 mean = 753 ± 16 µatm.

This run saw a definite register of a change in pCO_2 concentration from one tank to the other (see also the corresponding change in humidity). The pCO_2

concentration of the tanks was calculated from the seawater samples that were taken.

3.4.8.3.2 A_T and DIC

Seawater samples were analysed for A_T and DIC (see Figure 3.30)

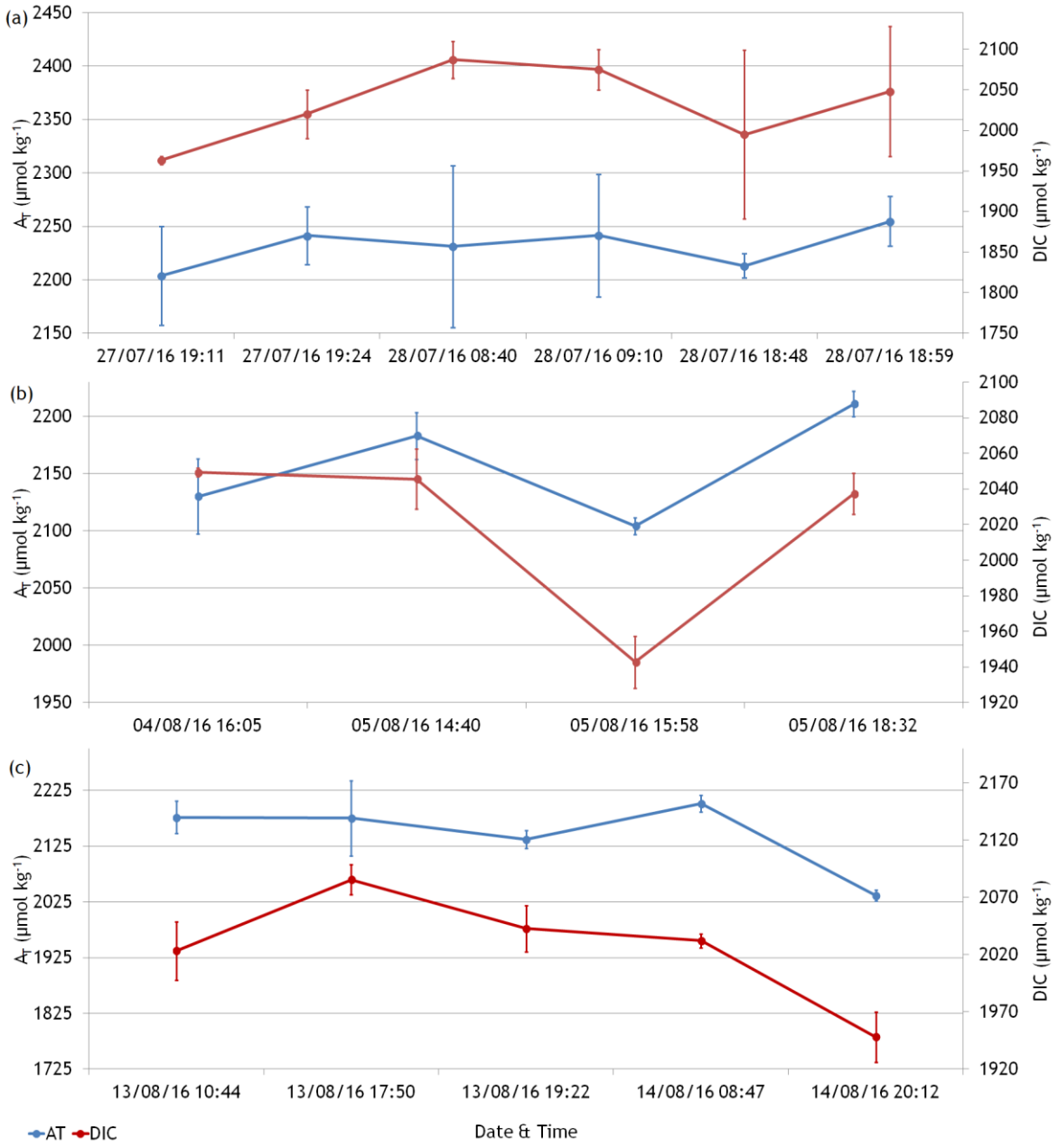

Figure 3.30: A_T and DIC for mesocosm deployments from seawater samples. A sample was taken when the sensor was first placed in a tank and a corresponding sample was taken in the same tank at the end of the run before the sensor was moved into the next tank. This was the sampling protocol for each experiment. (a) 27th to 29th July 2016. (b) 4th to 6th August 2016. (c) 13th to 15th August 2016.

3.4.8.3.3 Sensor pCO_2 and seawater pCO_2

From both A_T and DIC (and salinity and temperature), the pCO_2 of the mesocosm water was calculated (see Figure 3.31).

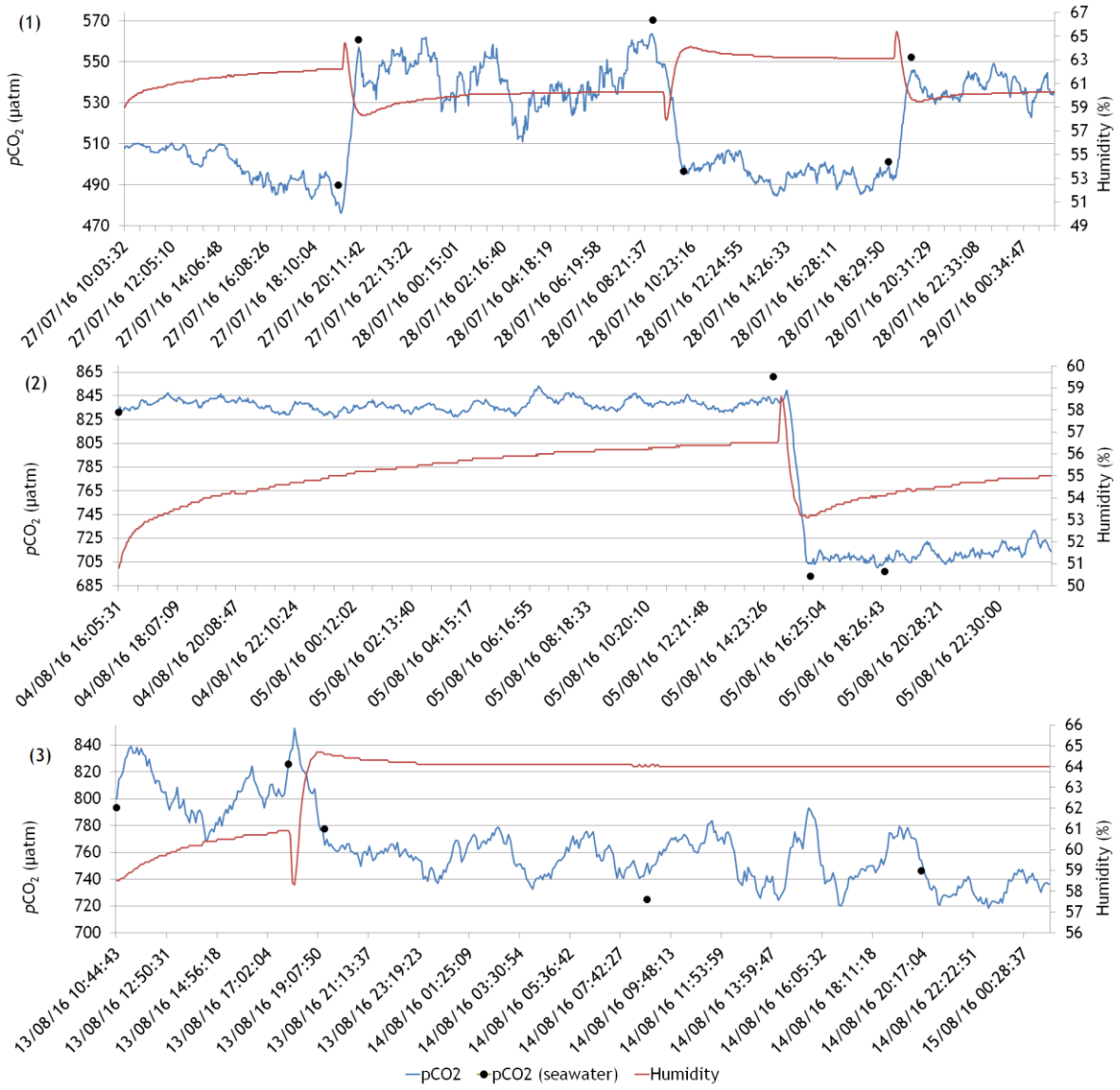

Figure 3.31: pCO_2 seawater concentrations (black dots) shown with pCO_2 sensor time series values (blue line) and time series of humidity (red line) in each alternating mesocosm. (1) 40 hour run of sensor in two alternating mesocosms showing seawater analysis concentration of pCO_2 and the corresponding concentration of pCO_2 from the sensor. Tank 1; seawater concentration 489.7, 496.5, 501 and corresponding sensor concentration 481.1, 498.8, 499.7. Tank 2; seawater concentration 560.5, 570.2, 552.1 and corresponding sensor concentration 556.9, 561.95, 545.5. (2) 22 hour run of sensor in two alternating mesocosms on 4th to 5th August 2016. Tank 1; seawater concentration 831.1, 861 and corresponding sensor concentration 830, 841. Tank 2; seawater concentration 693, 697 and corresponding sensor concentration 704, 705. (3) 39 hour run of sensor in two alternating mesocosms on 13th to 15th August 2016. Tank 1; seawater concentration 793, 825.5 and sensor concentration 800, 815. Tank 2; seawater concentration 777.1, 724.5, 746 and respective sensor concentration 765, 751.87, 753.4. The error on the sensor reading in terms of the seawater reading over these three deployments is on average ± 1.07% (see Figure 3.33a).

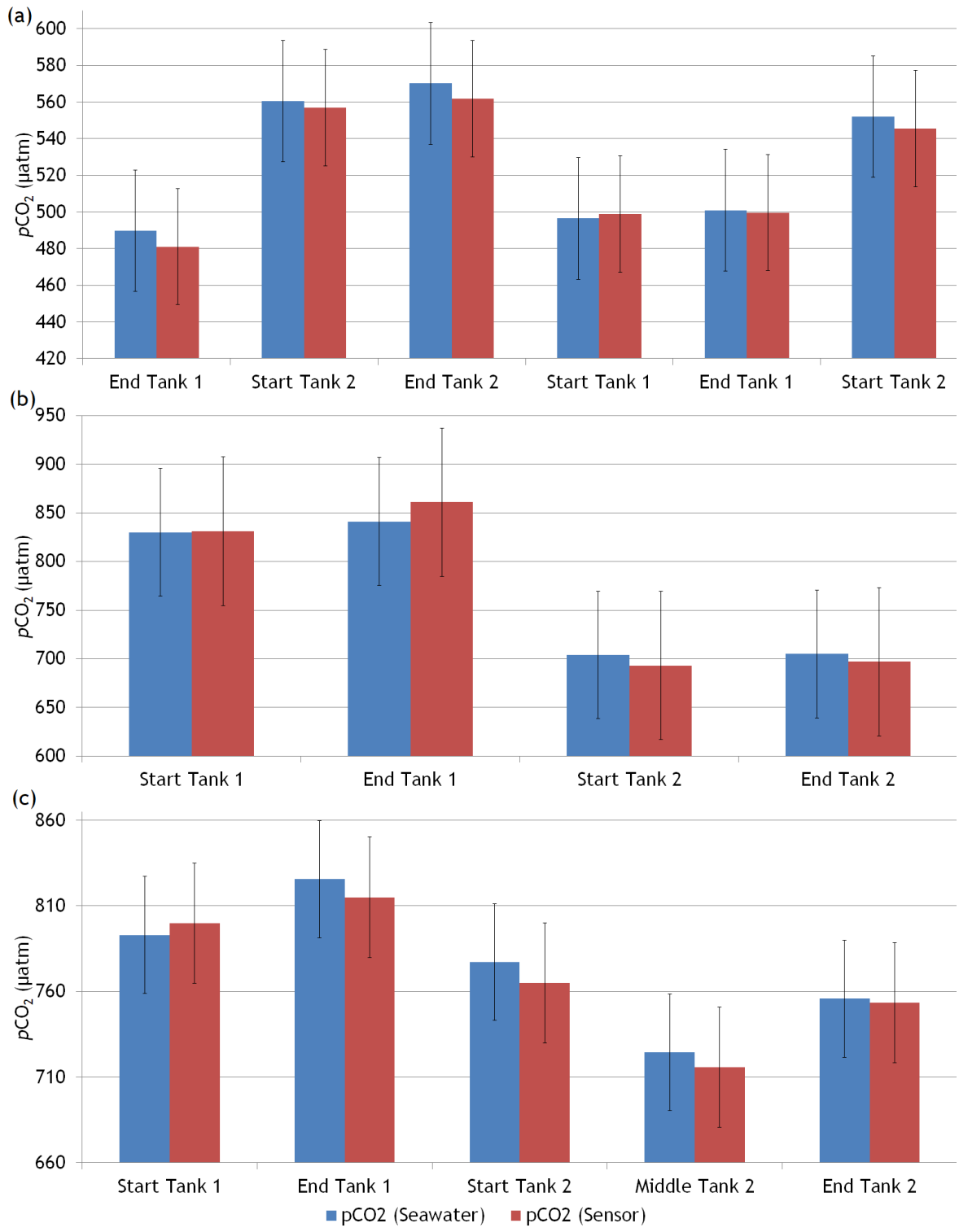

Figure 3.32: Comparison of seawater analysis concentrations of pCO_2 and sensor readings of pCO_2. (a) 27th – 29th July 2016. (b) 4th – 5th August 2016. (c) 13th – 15th August 2016.

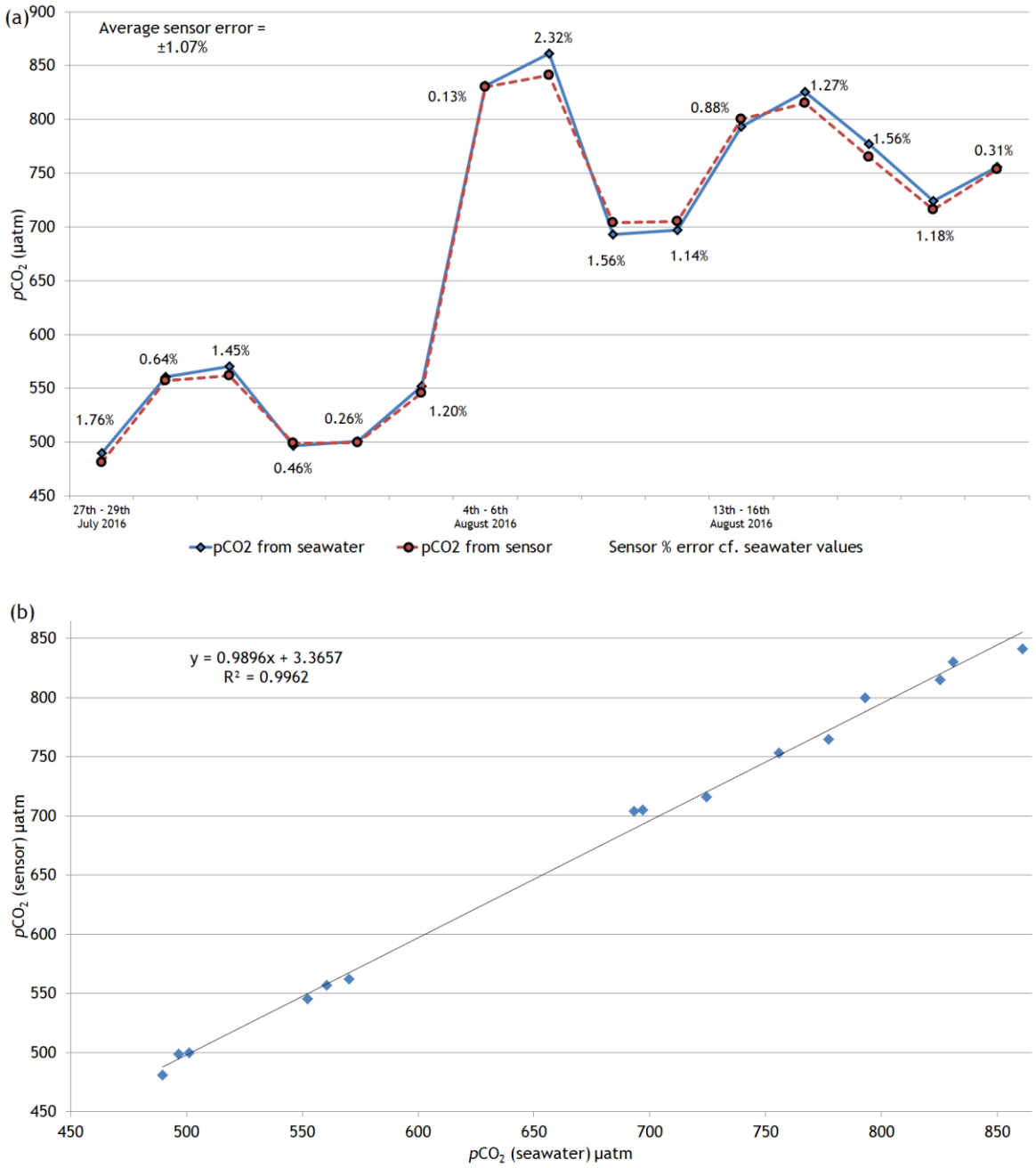

Figure 3.33: (a) The percentage error in the sensor pCO_2 readings compared to the seawater pCO_2 calculated concentrations. The average sensor error over these deployments was 1.07%. (b) scatter plot showing the correlation between sensor pCO_2 concentration and seawater pCO_2 concentration. Coefficient of determination; R^2 = 0.996. Pearson correlation coefficient; r = 0.997.

3.4.8.4 Discussion

Once suitable lids were researched and developed, the sensor performed well when alternating between mesocosms of different pCO_2 concentrations. The tanks were bubbled with air containing certain concentrations of CO_2 but it became evident from the seawater analyses (also backed up by the sensor data)

that the tanks did not contain the specific concentration. There were issues with the LICOR accuracy for the duration of the experiments. However, in the bigger picture this was not an issue as the discrete water sampling was used to corroborate the sensor readings. The important factor was that the sensor reacted immediately to an alternation of tanks and the sensor concentration was very similar to the seawater analyses concentration (see Figure 3.33a). The sensor would quickly recognise a change in CO_2 concentration with an uncertainty of ±1.07% (when compared with the seawater sample pCO_2 concentrations). Pearson correlation coefficient (and the coefficient of determination) for the two sets of data ($pCO_2[_{SW}]$ c.f. $pCO_2[_{SENSOR}]$) are 1 (see Figure 3.33b) and therefore assuming the seawater pCO_2 concentrations are the absolute correct value, this accuracy proved that the sensor was now ready for the field and had the ability to provide reliable results.

3.5 Conclusion

Overall after laboratory trials, the developed pCO_2 sensor was deemed to be suitable to be taken into the field for characterisation of the natural variability of the pCO_2 in contrasting coastal areas. The ability of the sensor to recognise and record differences in pCO_2 accurately was demonstrated over the course of this chapter. Potential drift was recognised and data processing procedures were familiarised with and carried out when necessary. Quality control of the sensor output was done with discrete seawater sampling to compare with the sensor output. The results show that the sensor CO_2 concentrations compare favourably with the CO_2 concentrations calculated from the seawater samples and the sensor had only a ± 1.07% error when compared with these samples. There was a shorter sensor response time in atmosphere (~ < 10s) and a slightly longer one underwater (~ < 2 mins). The successful laboratory performance evaluations proved that the sensor had an excellent accuracy and response time and therefore was deemed suitable for deployment in the field.

4 Characterising natural variability of coastal carbonate systems and ancillary variables in a temperate marine environment

4.1 Introduction

Marine coastal areas are dynamic and changeable compared to the open, pelagic ocean; coastal carbonate chemistry (and other ancillary parameters) have a temporal variability that will usually fluctuate to a greater extent than those in the open ocean over hourly, diurnal, seasonal and annual time scales (Caldeira and Wickett, 2003; Hoffman *et al.*, 2011). This is caused by a variety of drivers including: greater biological activity, temperature variability and more complicated hydrographic or topographic physical parameters where there may be increased freshwater runoff or the introduction of new water bodies with tides (Marra, 1997; Dickey, 2004; Johnson *et al.*, 2013). Coastal areas can be affected by anthropogenic activity like run-off from agriculture or industry which can cause eutrophication, i.e. an enrichment of nutrients in seawater which leads to enhanced primary production which can cause algae blooms and anoxia (Anderson *et al.*, 2008; Gowen *et al.*, 2012; Davidson *et al.*, 2014). A host of simultaneous processes can combine to force patterns of carbonate chemistry and therefore it can be a complicated task if trying to determine the cause of variability in each parameter (Rerolle *et al.*, 2014). There is increased need for the spatial variability of carbonate chemistry in coastal areas to be observed on a diurnal scale as opposed to seasonal cycles which are often the norm for ship-based observations (Inoue and Sugimura, 1988; Bates *et al.*, 1998; Fransson *et al.*, 2005; Dai *et al.*, 2009). Such diurnal scale records will help to deduce diel ecological stressors such as temperature and salinity which will vary according to aspects such as tides and weather and also identify any adaptation to these. It will also give a general environmental baseline from which different ecological communities function i.e. information on daily biogeochemical processes like primary productivity (Kinkade *et al.*, 1999).

Temperate marine areas are important to focus on in the context of their carbonate chemistry because of their relatively high productivity (compared to

say, the low productivity in tropics and subtropics) (Suchanek, 1994). These areas undergo large changes in variables such as light and temperature over the course of a year compared to tropical areas and this can have significant effects on marine ecosystems (Baggini *et al.*, 2014). The need to understand these complex environments is therefore vital to effective management which is, in turn, vital to the marine organisms inhabiting these areas. Temperate areas are defined as locations which are subject to neither high nor low climatic extremes (Wiedemann and Pickart, 2004). Temperate areas can equal or even surpass the biodiversity of tropical or terrestrial areas (Suchanek, 1994). Leigh *et al.* (1987) showed that the algae *Postelsia palmaeformis* which resides in a temperate coastal area has a higher primary productivity compared with terrestrial forests or even tropical rainforests. Temperate areas around the world are highly populated and coastal zones are under increasing threat from anthropogenic activities such as pollution from industry, development leading to habitat loss and exploitation of marine stocks (Suchanek, 1994). Therefore, coastal temperate environments are thought to be at a greater threat from the effects of global change (Ray *et al.*, 1992; Suchanek, 1994; Feely *et al.*, 2010) and being affected just as quickly as tropical areas (Beatley, 1991). Temperate environments encompass approximately half of the coastal areas over the surface of the Earth (Wiedemann and Pickart, 2004) and host large biodiverse marine communities which are often dependant on one another. For instance, kelp beds can host diverse ecosystems within their own ecosystem (Suchanek, 1994). The carbonate system of coastal areas remains poorly studied and comparisons of these can illuminate the different controls that force or inhibit the diurnal variability (Dai *et al.*, 2009). Over the course of this research, two very different coastal systems were compared – a temperate coastal area and a tropical coastal area. This chapter will quantify the variables determining the drivers of the carbonate system in a temperate coastal area. Sensors can provide *in-situ*, long-term and high-resolution data collection which can help in the monitoring and understanding of the complicated relationship between all parameters in a coastal area. This chapter will characterise the temperate coastal vegetated system in Caol Scotnish, Loch Sween, Scotland and quantify the forcing behind and relationship between marine parameters in the area using *in-situ* sensors (one being the marine pCO_2 sensor developed at The University of Glasgow during this thesis).

4.1.1 Marine parameters and their natural variability and interrelations in a coastal environment

Most carbonate chemistry within coastal seawaters and other marine variables are intrinsically linked. CO_2 enters the marine environment in numerous ways and has several controls and drivers. This makes for a complicated web of interrelated relationships and reactions (Zeebe and Wolf-Gladrow, 2001). There is permanent flux between the atmosphere and surface waters and the oceans are well known for being a sink for CO_2 (Sarmiento *et al.*, 2002; Caldeira and Wickett, 2003; Sabine *et al.*, 2004). Biological activity in the water also plays a large role in the temporal and spatial CO_2 content of the water as does temperature and tide control. These factors will all be addressed in the following subsections.

4.1.1.1 pH, *p*CO_2 and temperature in coastal areas

pH is an important parameter for determining the health of surface water of coastal oceans because it can be a gauge of the physical and biological activity taking place (Nakano and Watanabe, 2005). pH and *p*CO_2 have an inverse association, e.g. as *p*CO_2 concentration increases, pH will lower. Dissociation factors between *p*CO_2 and pH accord for the way other carbonate parameters are governed when there is an increase (or decrease) of *p*CO_2 (Zeebe and Wolf-Gladrow, 2001), i.e. a shift of ions to maintain equilibrium of carbonates. Most notably, there will be a decrease in the concentration of carbonate ions (CO_3^{2-}) (Kurihara *et al.*, 2007). A decrease in CO_3^{2-} will consequently lower the calcium carbonate saturation state (Ω) (Kurihara *et al.*, 2007) (see Equation 26) ;

$$\Omega = \frac{[Ca^{2+}]\,[CO_3^{2-}]}{K_{sp}^*} \tag{26}$$

(Where K_{sp}^* = stoichiometric solubility product for calcium carbonate)

The most common reason for a flux in the acidity content of seawater is *p*CO_2 where the addition of CO_2 to seawater will increase the acidity (Bialkowski, 2006). This happens when *p*CO_2 dissociates in seawater creating a weak acid called carbonic acid (H_2CO_3) which then itself dissociates to hydrogen ions and bicarbonate ions thereby decreasing the pH of the water (see Figure 4.1).

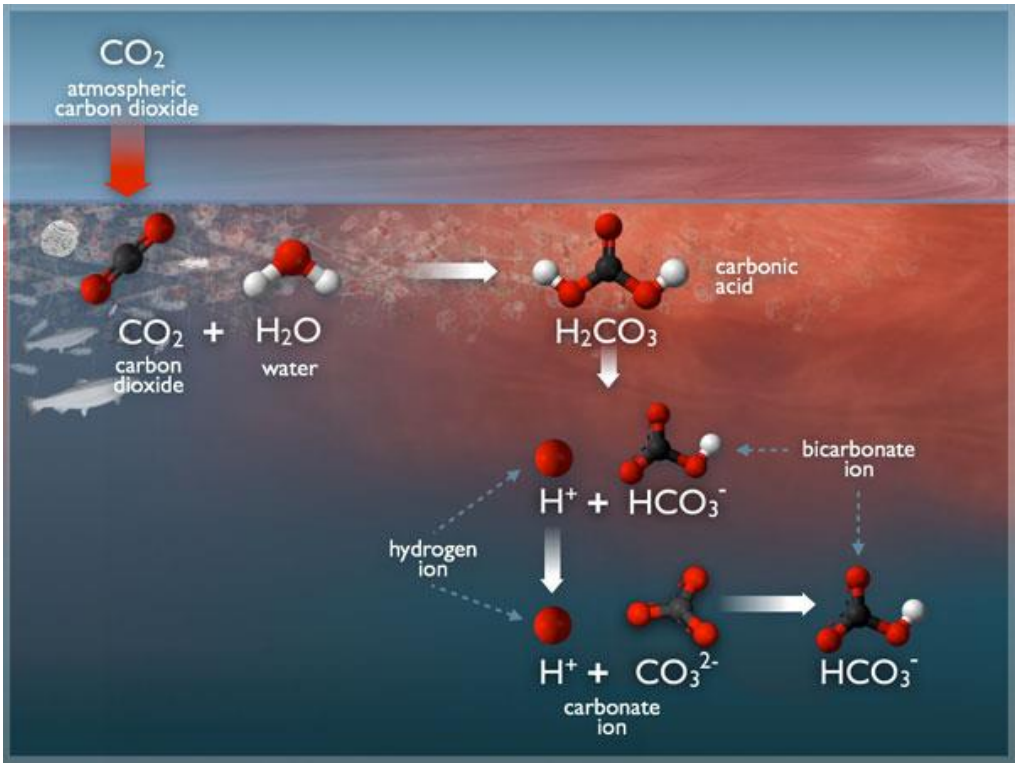

Figure 4.1: Molecules of CO_2 dissolved in seawater combine with molecules of water to form carbonic acid. Carbonic acid dissociates into hydrogen and bicarbonate ions. Some hydrogen ions will remain in this form and therefore increase acidity and lower the pH of the water. Most hydrogen ions however will combine with carbonate ions to form more bicarbonate ions (Graphic modified from WHOI)

Biological activity by marine organisms can influence the concentration of pCO_2 in a body of water by respiration, photosynthesis and decomposition and therefore increase or decrease the pH (Falkowski *et al.*, 1998; Gattuso *et al.*, 1998; Zeebe and Wolf-Gladrow, 2001; Sigman and Hain, 2012; Johnson *et al.*, 2013). Over a 24-hour cycle, there is usually a clear pH pattern (see Figure 4.2).

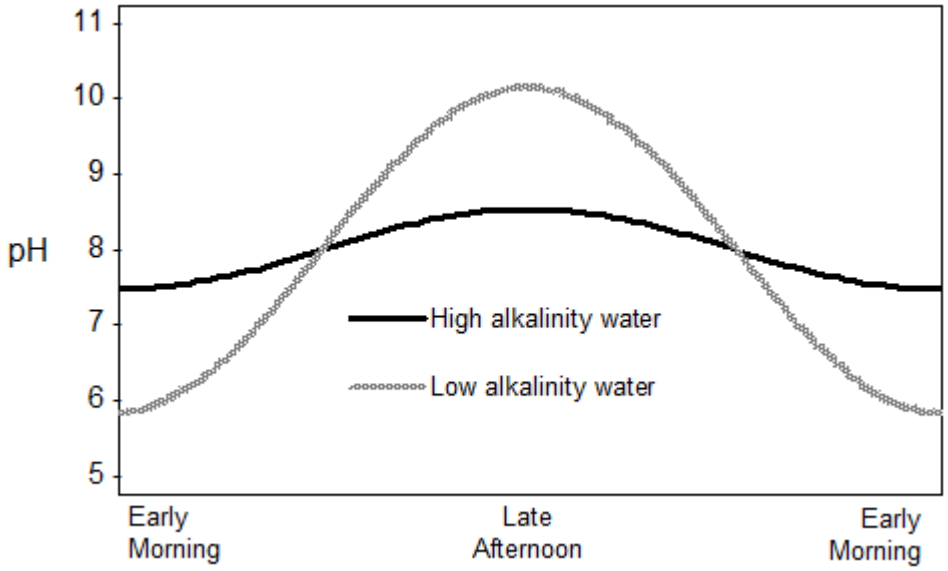

Figure 4.2: Diurnal fluctuation of pH in surface waters over 24-hours in high and low alkalinity waters (Figure modified from Wurts and Durborow, 1992)

The pH fluctuation is primarily driven by CO_2 which is drawn down by organisms during photosynthesis over the course of the day which results in a lowering of CO_2 concentrations and a consequent rise in the pH (with oxygen also being released). Conversely, CO_2 is given out by organisms during the respiration process at night (but it should be noted that this process is not restricted only to darkness hours) during which oxygen is consumed which raises the concentrations of CO_2 and lowers the pH, i.e. the seawater becomes less alkaline (Ware *et al.*, 1992; Wolf-Gladrow *et al.*, 2007).

Temperature has an influence on almost every marine parameter. It can affect metabolic and photosynthetic rates of organisms, salinity, pH, density and the concentrations of dissolved gases (Litt *et al.*, 2010). In general, the solubility of gases will decrease as the temperature increases (Litt *et al.*, 2010). As temperature increases or decreases, ion concentration will also change accordingly. If the temperature of the water changes, equilibrium must be reached according to Le Chatelier's Principle (Equation 27);

$$H_2O \leftrightarrow H^+(aq) + OH^-(aq) \quad (27)$$

Therefore, if there is an increase in the water temperature, a movement of ions to the left with that increase will ultimately lower the number of ions in the water. The consequence of this is an increase in the pH. Conversely, the same applies to a drop in temperature resulting in a lowering of pH (Wolf and Clark, 2014). It must be noted however, that a change in the water temperature will not make the water more acidic or basic. This will not change due to the ratio of hydrogen and hydroxyl ions remaining the same. Alternatively, the whole pH scale shifts to accommodate pure water being neutral, i.e. at 0°C pure water will have a pH of 7.47, at 25°C pure water will have a pH of 7.00 and at 100°C pure water will have a pH of 6.14 (Wolf and Clark, 2014) (See Figure 4.3).

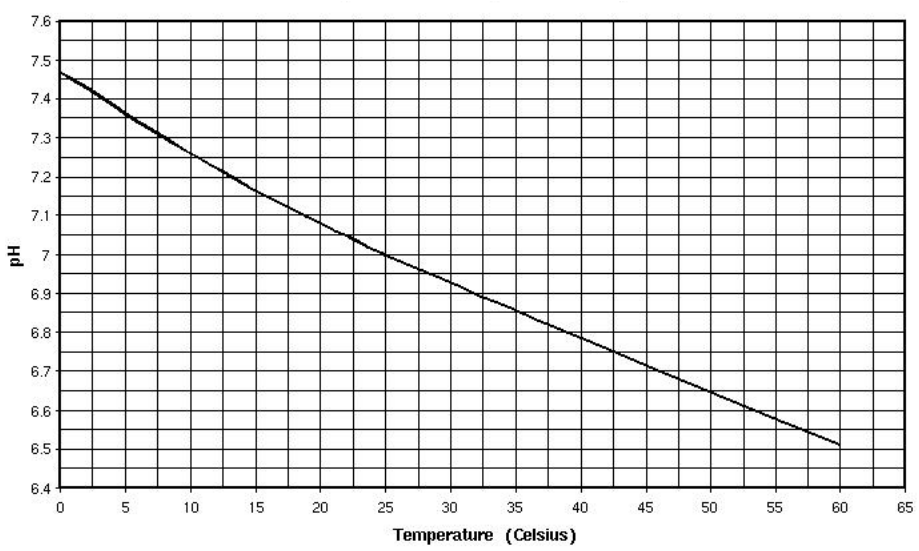

Figure 4.3: Relationship between pH and temperature (Figure courtesy of Wolf and Clark, 2014). pH of water varies with temperature, i.e. the pH of water at 0 degrees is 7.47 while at 45 degrees, the pH will be 6.7.

Complexity arises from the concurrent effects of several processes happening simultaneously. A temperature rise will often increase the stratification of the water column and also increase biological activity. Stratification of the water column will enhance the removal of particulate organic matter from the top layers of the water column and will therefore facilitate an overall increase in the pH of the surface water (Rerolle *et al.*, 2014). Temperature plays a significant role in governing concentrations of pCO_2 in surface waters (Inoue *et al.*, 1995). This is shown in areas of higher latitudes where more CO_2 is taken up

by the oceans because of low temperature (and high biological activity) (Mu *et al.*, 2014). Temperature can vary with the ebb and flow of the tide and therefore water movements can also be responsible for fluctuating biological processes and sea surface temperature (SST) which can then have a knock-on effect for pCO_2 concentrations in seawater.

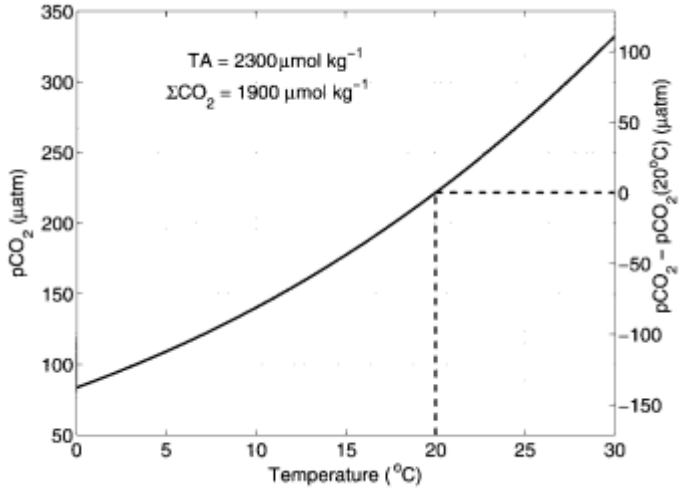

Figure 4.4: Relationship between pCO_2 and temperature. (Figure courtesy of Zeebe and Gladrow, 2001)

4.1.1.2 Dissolved Oxygen (DO)

DO is the amount of free oxygen that is not bound to any other element in a water body (Libes, 1992). DO is often used to characterise water quality because of the direct impact that the amount of DO has on the health of the organisms present in the water column. It is essential, depending on their individual needs, that organisms can utilise the right amount of DO where concentrations are not too high or not too low. It is an important parameter in vital physiological functions in organisms, e.g. photosynthesis and respiration (Spietz *et al.*, 2015).

4.1.1.2.1 Sources of DO

During photosynthesis, phytoplankton is the main source of the DO present at the top of the photic zone. There is also a natural flux from the atmosphere into surface waters (and vice versa) when there is a differential between the

concentration in the atmosphere and the concentration in the water (Guadayol *et al.*, 2014). The concentration of DO generally decreases with depth so organisms that need more oxygen for physiological processes usually reside at the top of the water column to receive higher concentrations of DO and ones that require less DO will remain lower down the water column (Fenchel *et al.*, 1990; Spietz *et al.*, 2015). DO is also utilised by microbes that break-down organic matter at depth which is a vital part of nutrient cycling in the marine system (Buchan *et al.*, 2014; Oni *et al.*, 2015). In stratified areas however, if there is an accumulation of decomposing organic matter on the seabed, DO can quickly be used up and therefore create an uninhabitable area for organisms (Litt *et al.*, 2010). DO mainly reaches surface coastal marine areas from the surrounding atmosphere and photosynthesis by phytoplankton (Upstill-Goddard, 2006; Wanninkhof, 1992; Davis, 1975).

4.1.1.2.2 DO and pCO_2

pCO_2 and DO are also strongly linked. Just as pH has an inverse relationship with pCO_2, DO also has the same inverse relationship with pCO_2. All three parameters (pH, DO and pCO_2) are closely connected with biological activity in the water column (Zeebe and Wolf-Gladrow, 2001; Kim *et al.*, 2006; Findlay *et al.*, 2013; Hendricks *et al.*, 2014). During photosynthesis, pCO_2 is consumed by organisms which, within this process, creates oxygen and therefore the oxygen content of the water increases over the course of the day with a corresponding decrease in pCO_2. Conversely, during the night cycle, pCO_2 is released during respiration and oxygen is used up. The night cycle should therefore show an increasing pCO_2 concentration with a decreasing concentration of DO (Morris and Taylor, 1983; Zeebe *et al.*, 1999; Bates *et al.*, 2009; Dai *et al.*, 2009; Anthony *et al.*, 2011; Smith *et al.*, 2013).

In the upper photic zone, phytoplankton drive photosynthesis and this is where DO concentrations are usually highest. The amount of photosynthesis that takes place is dependent on the amount that light can penetrate the water column. DO increases during sunlight hours as CO_2 and water are utilised by phytoplankton to make energy and oxygen (Equation 28). The amount of DO available will conversely decrease at night (Equation 29).

$$6CO_2 + 6H_2O \rightarrow C_6H_{12}O_6 + 6O_2\ (Photosynthesis\ utilising\ sunlight) \quad (28)$$

$$C_6H_{12}O_6 + O_2 \rightarrow CO_2 + H_2O + ATP \quad (Respiration\ during\ night) \quad (29)$$

(ATP = adenosine triphosphate)

However, this diel pattern is not a strict rule in coastal areas (see later in chapter). pCO_2 is low if there is strong primary productivity but it can also vary with other factors. Figure 4.5 shows the different processes which affect the concentrations of DO in surface coastal waters. Other factors will also have an influence on the solubility of oxygen in the marine environment, e.g. temperature and salinity which is commented on further in Section 4.1.1.2.3 below.

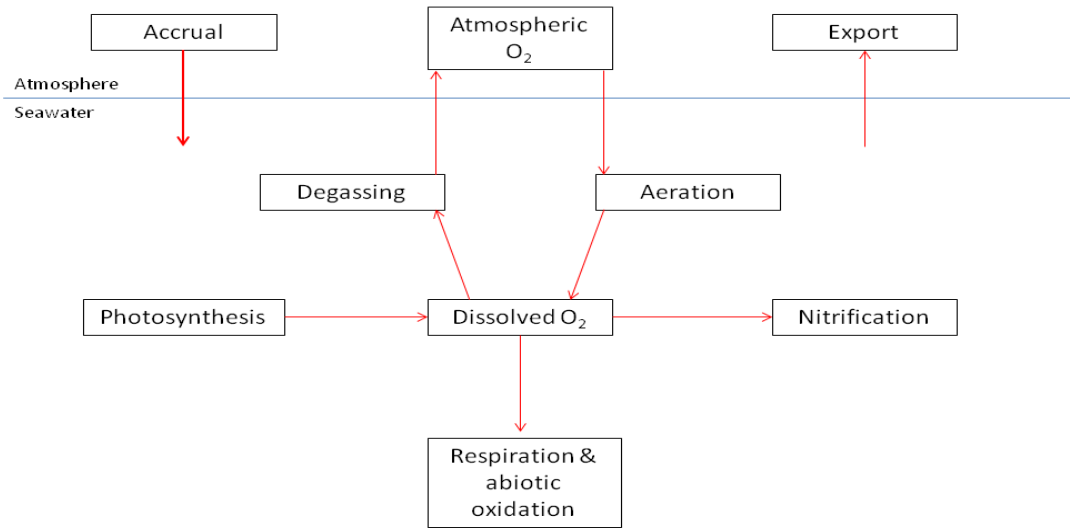

Figure 4.5: Factors affecting the dissolved oxygen concentration in surface waters. Oxygen is introduced to or removed from the sea surface because of concentration gradients between the atmosphere and the surface of the sea. This flux affects the concentration of oxygen as well as biological processes like photosynthesis and respiration also raising or lowering the immediate concentration of DO (modified from Connell and Miller, 1984).

4.1.1.2.3 Factors that influence the solubility of oxygen

Temperature, pressure and salinity will affect the concentration of dissolved oxygen in a body of water (Litt *et al.*, 2010). Dissolved Oxygen is affected non-

linearly by salinity and temperature. With higher temperatures, the solubility of oxygen will decrease (Wetzel, 2001). Therefore, surface water that is warmer than deeper waters will reach 100% air saturation with lower concentrations of dissolved oxygen than deeper waters. Similarly, as salinity decreases, DO concentrations will increase but gas solubility will also decrease as the temperature increases regardless of salinity concentration (Wetzel, 2001). Higher salinity water has less capacity to take up oxygen because of the salvation complex where the water molecules are attracted to dissolved ions from the salt. The non-polar oxygen molecules therefore have an even weaker attraction to water with the result of less oxygen dissolving into the water (Raven *et al.*, 2014).

Therefore, in lower salinity waters at the same temperature and pressure there will be a higher capacity to hold DO. At higher pressures, the DO concentration will be greater. Because of hydrostatic pressure, with every meter increase in depth the saturation of gas will lower by approximately 10% (Wetzel, 2001). Consequently, this means that warmer, shallower, higher salinity waters have less capacity to contain DO. Other factors that affect DO concentration must be taken into consideration however, i.e. microbial decomposition, biological metabolic processes and physical factors like tidal action, runoff and rainfall to get an accurate description of overall net DO content of waters (Smith *et al.*, 2013).

4.1.1.3 Chlorophyll

Chlorophyll is a photoreceptic molecule found in all phytoplankton which is used during photosynthesis when absorbing energy from the sun. Chlorophyll is often used as a proxy for the amount of phytoplankton present in the water column (Nakano and Watanabe, 2005; Behrenfeld *et al.*, 2009; Hallegraeff, 2010). Phytoplankton use photosynthetic pigments like chlorophyll which react with sunlight to create organic matter (Feldman *et al.*, 1984; Yoder and Kennelly, 2003; Richard and Schoeman, 2004).

4.1.1.3.1 Factors that influence chlorophyll content of surface waters

Chlorophyll content of waters can be governed by several factors. Physical aspects including surface winds which can affect mixing in the water column can often come hand-in-hand with the availability of nutrients and therefore the presence of phytoplankton (and therefore chlorophyll content) (Litt *et al.*, 2010). Light intensity and the amount of time cells were exposed to this light is one of the key factors dictating the diel cycle of chlorophyll (Glooschenko *et al.*, 1972). Temperature can also influence chlorophyll concentration (see Section 4.1.1.3.3). Chlorophyll-*a* can represent the amount of phytoplankton biomass and therefore an increase in chlorophyll concentrations should coincide with an increase of DO and a decrease of pCO_2 (Carrillo *et al.*, 2004).

4.1.1.3.2 Chlorophyll and pCO_2

If there are minimal concentrations of Chl-*a* in the water column, there will be less uptake of atmospheric CO_2 by photosynthetic processes (Litt *et al.*, 2010). High concentrations of Chl-*a* usually occur in conditions where there is high primary productivity (P.P.), i.e. photosynthetic processes which use energy to create organic matter, which itself is as a consequence of abundant light (high irradiance), stratified water bodies and high nutrient concentrations (essential elements including nitrogen, phosphorus, silicon and iron) (Litt *et al.*, 2010). Furthermore, under these conditions there will be increased uptake of pCO_2 by phytoplankton and therefore pCO_2 concentrations will decrease (see Equation 30).

$$\uparrow Chl-a \quad \uparrow P.P. \quad \uparrow irradiance \quad \uparrow nutrients \quad \downarrow pCO_2 \tag{30}$$

High Chl-*a* concentration can be seen in algal blooms which are also accompanied by very low daytime pCO_2 due to uptake by phytoplankton. Conversely, low Chl-*a* concentrations will occur in conditions of simultaneously low primary production, lower light concentrations and lower nutrients. pCO_2 will increase in these circumstances as it outgases into the surrounding waters during respiration (see Equation 31).

$$\downarrow Chl-a \quad \downarrow P.P. \quad \downarrow irradiance \quad \downarrow nutrients \quad \uparrow pCO_2 \tag{31}$$

4.1.1.3.3 Temperature and Chlorophyll

Temperature, sunlight and nutrient concentrations all dictate where phytoplankton proliferate. Since phytoplankton use chlorophyll when photosynthesising, chlorophyll can be used as a proxy for the concentration of phytoplankton present in a body of water (Riebesell *et al.*, 2010). For example, phytoplankton tend to be more plentiful in higher latitude, colder waters as these waters contain more nutrients (although this will vary during winter) (Riebesell *et al.*, 2010).

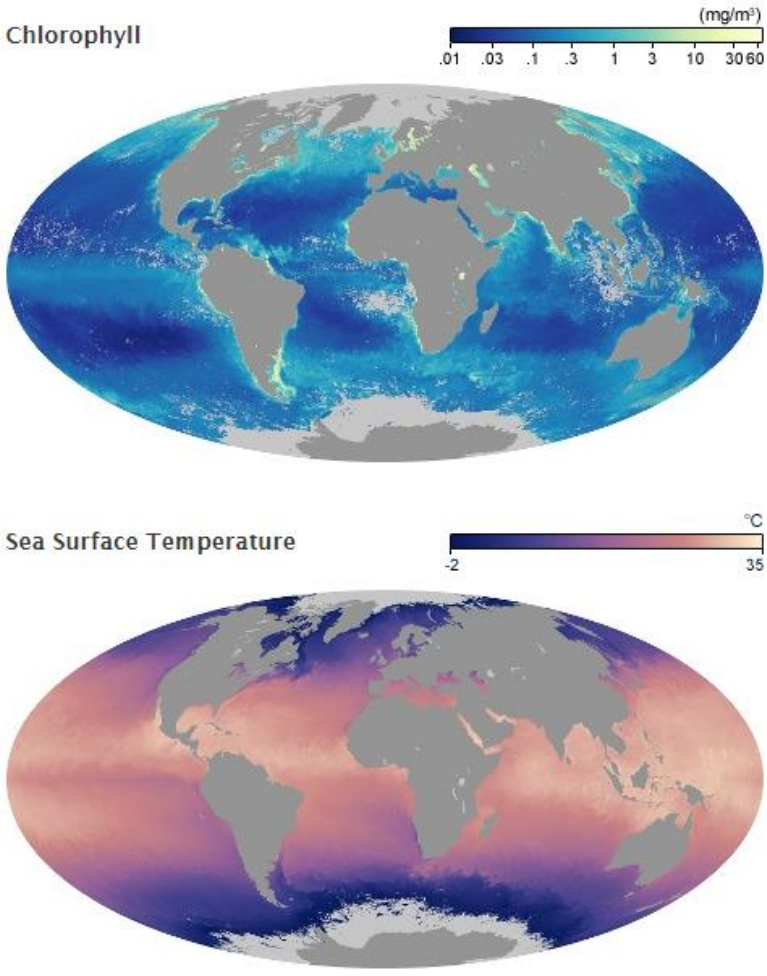

Figure 4.6: A comparison of chlorophyll content (mg/m^3 per month) and temperature (^{o}C) over the surface of earth (October 2016). In colder, higher latitude waters, there is a greater concentration of chlorophyll. Warmer waters have lower concentrations of chlorophyll in comparison. Also shown is the greater productivity of coastal waters in comparison to the open ocean (Figure courtesy of earthobservatory.nasa.gov).

Figure 4.6 shows that low chlorophyll content (low numbers of phytoplankton) coincides with higher sea surface temperatures and conversely, higher chlorophyll content coincides with lower temperature waters. This spatial variation shows we should expect relatively high concentrations of chlorophyll in the temperate, coastal site compared to tropical sites.

4.1.1.4 Salinity

In coastal regions, salinity can have a higher hourly, daily or seasonal differential compared to the open ocean. Open ocean salinity stays relatively constant due to the natural balances between evaporation and precipitation (Libes, 1992). Salinity is manipulated in coastal areas by freshwater input from runoff and also net evaporation leads to higher salinity waters whilst net precipitation will result in lower salinity waters (Libes, 1992; Wetzel, 2001).

4.1.1.4.1 Salinity and DO

The solubility of DO is affected by the salinity. The characteristics of saline water makes DO approximately 20% less soluble compared to fresh water at the same temperature (Miller *et al.*, 1988). Coastal areas can have unique halocline properties in that they can be either vertical or horizontal. Usually when strong tides are present in the area and are able to sufficiently mix the water, vertical haloclines can be produced between the difference salinities (see Figure 4.7) with an increasing vertical salinity towards the open ocean (Litt *et al.*, 2010; Talley and Pickard, 2011).

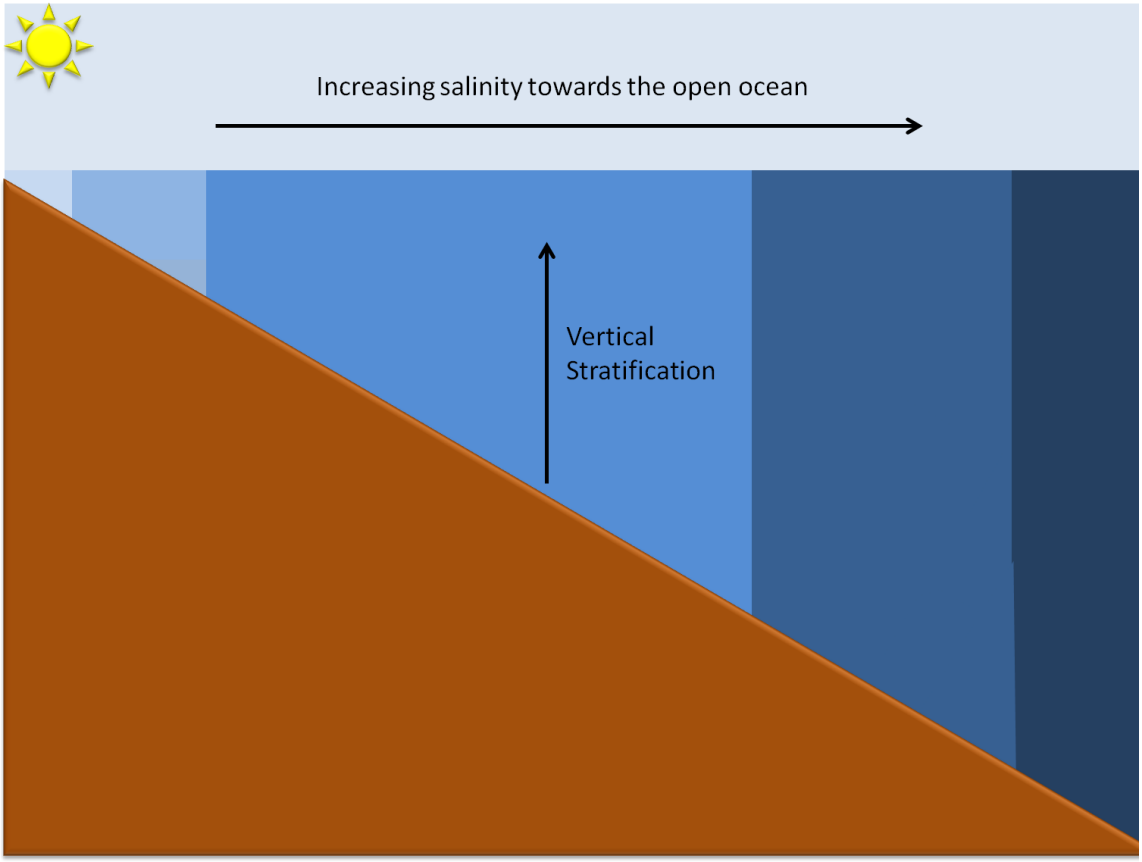

Figure 4.7: In an area with sufficient tidal mixing, a vertical stratification scenario with increasing salinity towards the open ocean may occur caused by the different densities between water bodies. In reality, there will not be a totally uniform vertical stratification. Salinity will generally increase towards the open ocean (Figure adapted from Perlman, 2014).

In areas where there may be insufficient tidal energy, horizontal haloclines can occur. Coastal areas have many differing inputs that affect the salinity of the water, e.g. freshwater runoff can rest on top of the higher density seawater and create an 'overflow'. Similarly, if higher salinity water enters a coastal area, this can then sink underneath the fresher water and create an 'underflow'. If there is an inflow with a similar concentration of salinity then there can be an 'interflow' where the original body of water can be intersected by the similar salinity water coming into the area (Libes, 1992).

4.1.1.4.2 Salinity and pCO_2

As with DO, salinity affects the solubility of pCO_2. Therefore, as with temperature (low temperature waters being more soluble to gases), water with a lower salinity will take up more pCO_2. Seawater with low salinity and low temperature will therefore have more capacity to hold dissolved gases than

seawater with a high temperature and high salinity (this can be compared to the characterisation of the tropical Red Sea in Chapter 5 where the sea was higher in salinity and temperature).

4.2 Motivation

The site chosen was a biogenic reef in a temperate coastal area. This area was chosen for several reasons;

(1) The extensive maerl reef means that there should be fluctuating carbonate chemistry over the diurnal cycle and a corresponding variation of pCO_2 concentrations (this may not be differentiated from general pelagic algal effects for which measuring is beyond the scope of this project). These differentials will be measured over small spatial but larger temporal scales (between 2 to 5 day/night cycles).

(2) This site would be a significant test for the developed sensor. The area contains a large biogenic reef with associated organisms which will result in constantly changing carbonate chemistry from biological activity (net community metabolism (NCM)). It is also a well-flushed area with changing water masses. Therefore, compared to an area with little biological activity and little mixing, there should be considerable and noteworthy pCO_2 patterns produced by the sensor.

(3) If an already existing natural baseline is established, then such data can be used to determine how much of a stressor changing atmospheric pCO_2 concentrations will be in the future (i.e. ocean acidification caused by climate change) for temperate, coastal biogenic reefs. Or indeed, if and how the reef is able to cope and adapt to large fluxes in concentrations over small temporal scales already.

4.3 Aims

The objectives of this field work were to characterise the natural variability of carbonate chemistry and other ancillary parameters in a coastal temperate area characterised by autotrophic biota and to evaluate the performance of pCO_2

sensors in a temperate field environment. This was conducted with the developed pCO_2 sensors, supporting sensors and with collection and analyses of discrete seawater samples.

The aims of this chapter were to:

(1) Test the *in-situ* functionality and performance of the newly developed pCO_2 sensor(s) in a temperate field environment over multiple day/night cycles in Loch Sween.

(2) Characterise the natural variability in a temperate environment of pCO_2 in Loch Sween in two different seasons (summer and autumn) using the newly developed sensor.

(3) Characterise the natural variability of other marine parameters in Caol Scotnish (pH, dissolved oxygen, chlorophyll, salinity, temperature, tidal action, A_T and DIC) to create a comprehensive record of the area.

It was hypothesised that (1) the developed pCO_2 sensor would be a valuable supporting tool in the characterisation of the natural variation in carbonate chemistry in temperate vegetated systems, (2) the seawater samples and other sensor readings would corroborate and also contribute to the creation of characterisations of marine parameters in the area, (3) the results would show Caol Scotnish to be a heavily tidal area and this will be the primary influence in driving other variables in the area.

4.4 Site description

Field work was conducted in Caol Scotnish, an arm of Loch Sween, Argyll, Scotland (56°01.99'N, 05°36.13'W) in July and September 2016. Loch Sween is situated on the west coast of Scotland approximately 164 km from Glasgow.

Figure 4.8: (a) Location of Caol Scotnish, Loch Sween situated in Scotland. (b) close-up of Caol Scotnish (Google Maps, 2018).

Figure 4.9: Caol Scotnish, temperate coastal field site. Caol Scotnish is a narrow arm of well-flushed water connected to the main body of Loch Sween.

Loch Sween is a sea loch with typical fjordic characteristics. It has several inlets making it somewhat complex in terms of physical oceanography. The arms all have their own unique hydrography and also contain varying fauna (Edwards and Sharples, 1986). Caol Scotnish (~7 m deep) is a narrow branch of water stretching NE from the main body of Loch Sween and contains an extensive maerl bed (*Lithothamnion glaciale*). Maerl is a photosynthesising calcifying algae which forms a hard skeleton of calcium carbonate ($CaCO_3$). Maerl beds, compared with other habitats, are the main depositor of carbonate (BIOMAERL *et al.*, 2003). They create long-lived beds that provide habitat for a wide variety of biota (Kamenos *et al.*, 2004a, b). Maerl photosynthesise and therefore influence the seawater chemistry themselves but because they also host a diverse associated ecosystem which in turn will also influence the seawater chemistry, they are a key player in driving the carbonate chemistry of this small fjord. Their skeleton is formed primarily during the day with the incorporation of both organic and inorganic carbon. Therefore, maerl beds can also be considered an important sink for carbon (Bensoussan and Gattuso, 2007; Short *et al.*, 2007). Their role in the carbon cycle of coastal areas is a significant factor when considering the patterns of carbonate chemistry in the Caol Scotnish area and will be commented on later in this chapter.

There were two characterisations of Caol Scotnish, one which ran for approximately 2.5 days from the 7th to the 9th of July 2016 (this was the first trial of the sensor so was a short deployment before the longer field work) and another running for approximately 4.5 days from the 19th to the 23st September 2016. The cycles encompassed a minimum of 2 day/night cycles and a maximum of 5 day/4 night cycles in the loch.

4.5 Methods: temperate deployment

4.5.1 Sensor measurements

The deployed sensors included a YSI EXO2 Sonde (to measure pH, DO, chlorophyll (only September deployment), salinity, temperature and depth) and the pCO_2 sensor(s) which were set to continuously record whilst in the field (for separate details of each deployment see the following sections 4.5.5.1 and 4.5.5.2, both page 139.). The sensors were deployed in Caol Scotnish using

SCUBA. Due to essential maintenance, i.e. changing batteries and operational checks, there are small, inconsequential gaps in the data when the sensors were recovered.

4.5.2 Data processing

For avoidance of repetition, please see Chapter 3, Section 3.3.5, page 68 on information on how the data were processed.

4.5.2.1 Statistical analyses

Correlation analysis was performed to determine the presence of relationships between measured variables and drivers (Microsoft Excel Correlation analysis was within a bigger regression analysis to find both the Pearson's correlation coefficient and the corresponding p-value). This was conducted on data from both the July and September deployments. Principal Correlation Analysis (PCA) was also undertaken to verify the previous analyses.

4.5.3 Calibration of sensors

Before deployment, the YSI EXO2 Sonde was calibrated at The University of Glasgow. For the 3-point pH calibration, the software used was KorEXO. A 3-point calibration was chosen to ensure the highest accuracy from the continual data collection. The pH probe was immersed into a calibration buffer (pH 4 buffer, pH 7 buffer and pH 10 buffer). The software was started (noting the temperature as the exact value of the pH buffers depend on this) and once the reading was stable, the calibration point was accepted on the software. This was repeated for each buffer after rinsing the probe with deionised water between each calibration point. The probe for DO was also calibrated by placing it in air-saturated water where the temperature and oxygen was allowed to equilibrate and using the same software. This works in much the same way as previously described but with a standard air-saturated value input into the software and stable data point being found from this. These were the only necessary calibrations needed with the YSI EXO2 Sonde.

The pCO_2 sensors were also calibrated before deployment at The University of Glasgow. The sensors underwent a 2-point calibration with gases of known

concentration from a commercially available gas-mixing system (BOC). The calibration gases were CO_2 in a nitrogen (N) mixture. A gas mixture is usually used for calibration gases because, in this case, the carrier gas of nitrogen will help keep the CO_2 concentration stable over time (Inoue *et al.*, 1995). The certified CO_2 concentrations have an uncertainty of < = 5%. A test chamber was constructed (See Chapter 3, Section 3.3.3, page 66 for details) which was used to house the sensor during calibration. Gas was pumped into the chamber and the sensor was allowed to equilibrate to the specific gas concentration. Software (COZIR Sensor 2.0) from GSS was used to zero the sensor and input the specific concentration. This was done with calibration gases of CO_2 concentrations 400 ppm and 1000 ppm. This was a 'span' calibration which was determined using Equation 32;

$$Span\ calibration\ factor = \frac{known\ gas\ concentration\ \times\ exisiting\ span\ calibration\ factor}{sensor\ reading} \quad (32)$$

The correct command was entered into the software (information from COZIR datasheet) to program the span calibration factor into the sensor.

4.5.4 Water masses

T-S (temperature – salinity) diagrams can be used as a water mass tracer (Helland-Hansen and Nansen, 1926). This method was employed in this project. Although more difficult to pinpoint the exact origin of water masses with surface water (because of constant flux with the atmosphere and other influences which change the properties) in comparison to deep water (conservative water masses), it can still be useful to plot both variables in the mixed layer against each other to see any patterns and changes in the two properties during the deployment. Different water masses enter Caol Scotnish by physical processes like the tides, significant weather influences like rainfall and strong winds and terrestrial runoff.

4.5.5 Sensor deployment

4.5.5.1 7th – 9th July 2016

This was the first run of the sensor in a field environment. One sensor was deployed in Caol Scotnish by SCUBA between the 7th & 9th of July 2016. The sensor was programmed to record 4 readings per minute. pH, DO, salinity, temperature and depth measurements were made using YSI EXO2 Sonde which was set to record measurements once every two minutes. The sensor was placed at a depth of 5 m tied to a frame above the maerl.

4.5.5.2 19th – 23rd September 2016

Two pCO_2 sensors were deployed using SCUBA on Monday 19th September and then retrieved again by SCUBA on Wednesday 21st September for maintenance. They were then re-deployed until finally being retrieved on 23rd September. One sensor was programmed to output volts (from which the pCO_2 could later be calculated) every five minutes and the other was programmed to output the pCO_2 in μatm every five minutes. Both outputs were then compared to assess if one output was better than the other whilst underwater. The advantages and disadvantages of this strategy are presented later in this chapter. Again, like the July deployment, the YSI EXO2 Sonde was also deployed at the same time to measure pH, DO, chlorophyll, salinity, temperature and depth and the sensors were placed at a depth of 5 m.

4.5.6 Wet chemistry

Seawater samples were used to validate the sensor pCO_2 readings against the analysed seawater wet chemistry. Samples were taken directly adjacent to the sensors to ensure the same body of water that passes over the sensors was collected. The samples were also used to characterise two carbonate chemistry parameters, A_T and DIC in the loch which will be mentioned in detail later. Laboratory instruments used for the analyses of the seawater samples is shown in Figure 4.10.

Figure 4.10: Laboratory instruments used to analyse seawater samples (Left: 848 Titrino Plus automated titrator; Top right: DR 5000 Lange spectrophotometer; bottom right: Automated Infra-Red Inorganic Carbon Analyser, Marianda).

4.5.6.1 Water sample collection

Discrete water samples were collected for both deployments in Caol Scotnish in accordance with standard protocols (Dickson *et al.*, 2007). Specific details for the separate deployments are given in the following sections.

4.5.6.1.1 7th to 9th July 2016

Water samples were collected at the start when first deploying the sensor (7th July) and then at the end when retrieving the sensor (9th July). Water was sampled using SCUBA. Seawater samples for A_T and DIC were collected in triplicate using glass syringes and transferred to 12 ml borosilicate vials. Minimal gas exchange with the atmosphere was ensured by transferring the seawater slowly and smoothly into the vials directly from the syringe. This meant that no air bubbles were introduced into the sample. A slight overflow of water was left to further ensure this. They were then poisoned with 10 µL of

mercuric chloride ($HgCl_2$) to prevent any further biological activity inside the vial which would alter the carbonate chemistry in the sample. The lids were carefully placed on the vials, again ensuring no air bubbles were present in the sample. The vials were then stored in a cool dark location before being taken back to the laboratory for analysis.

4.5.6.1.2 19th to 23rd September 2016

In this deployment, water samples were taken a minimum of twice a day and a maximum of four times a day (half way through the deployment when the sensor was momentarily retrieved for maintenance). Again, samples were collected using SCUBA adjacent to the sensors using the same methods and materials applied in Section 4.5.5.2, page 139.

4.5.6.2 A_T analysis

A_T remains constant in spite of CO_2 draw-down or outgassing (Zeebe & Wolf-Gladrow, 2001). However, A_T does vary with the release of nutrients and subsequent use of these nutrients by organisms. Precipitation of $CaCO_3$ will also affect the A_T (Zeebe & Wolf-Gladrow, 2001). For more details on analysis of A_T, please see Chapter 3, Section 3.3.6.1, page 69.

4.5.6.3 DIC analysis

DIC is depleted during calcification of organisms which is important to note in Loch Sween. For more details on analysis of DIC, please see Chapter 3, Section 3.3.6.2, page 70.

4.5.6.4 *p*CO_2 calculation from water chemistry

For details on *p*CO_2 calculation from water chemistry, please see Chapter 3, Section 3.3.6.3, page 71.

4.6 Results & Discussion 7th - 9th July 2016

4.6.1 Seawater wet chemistry

The developed pCO_2 sensor was initially only supposed to be submerged for half a day and retrieved on the same day. However, due to logistical issues, it could not be retrieved on the same day and subsequently was collected two days later. As the sensor was not set-up to record for this length of time, the final water sample coincided to a time when the batteries had discharged. This means a direct comparison of the sensor and seawater chemistry analysis could not be made but is still useful to be used as an indication of pCO_2 concentrations in the loch. Samples were only collected at the start and the end of the run so it is difficult to comment on 24-hour trends with either A_T or DIC.

4.6.1.1 Water chemistry

Time of sample	Salinity (psu)	T(°C)	A_T (µmol/kg⁻SW)	DIC (µmol/kg⁻SW)
Thursday 7/7/16				
1200	33.37	15.284	2261 (σ = 233; CV = 10%)	2103 (σ = 78; CV = 4.5%)
Saturday 9/7/16				
~ 1400	32.44	15.344	2248 (σ = 376; CV = 17%)	2051 (σ = 35; CV = 1.9%)

Table 4.1: Analysis of A_T and DIC from water samples taken from Caol Scotnish 7th to 9th July 2016. Date and time of samples with accompanying measurements of temperature and salinity from YSI EXO2 Sonde and the resultant A_T and DIC concentrations from analyses in the laboratory. σ = standard deviation of the reading while CV is the coefficient of variation, i.e. if CV = 4.5% then the SD is 4.5% of the mean.

The A_T in Caol Scotnish displays very similar concentrations at similar times of the day between the two sampling points. There is a slight difference in DIC between the two sampling points as shown on Figure 4.11.

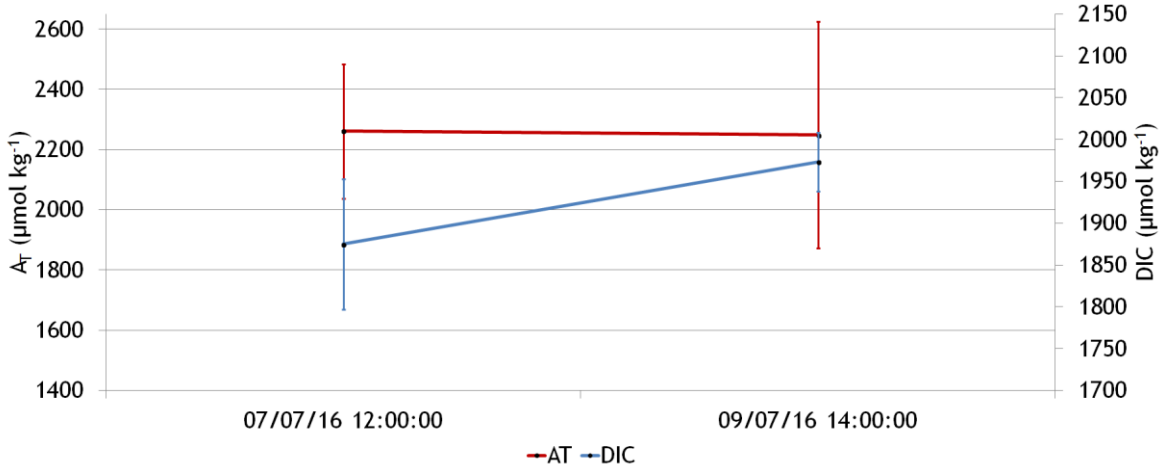

Figure 4.11: A_T and DIC in Caol Scotnish on 7th and 9th July 2016. Data presented as a mean with error bars showing the standard deviation.

A_T did not show a strong variation from sample 1 (7th July) to sample 2 (9th July). There was a slight increase in DIC from sample 1 to sample 2.

4.6.2 Comparison of pCO_2 data from sensor and pCO_2 data calculated from CO2SYS

DIC, A_T and ancillary data was used to calculate the pCO_2 concentrations from the water samples with CO2SYS as shown in Table 4.2.

Input Conditions				Output Conditions					
Salinity	T(°C)	A_T	DIC	pH	pCO_2	HCO_3^-	CO_3^{2-}	Ω_{Ca}	Ω_{Ar}
33.37	15.284	2261	2103	7.921	**541.3**	1961.6	121.2	2.92	1.81
32.44	15.344	2248	2051	8.024	**413.0**	1890.4	145.1	3.52	2.25

Table 4.2: *In-situ* parameters (input conditions) used to calculate ancillary data (output conditions) from seawater samples in Caol Scotnish in July. Salinity, temperature, A_T and DIC were used in CO2SYS to calculate concentrations of pH, pCO_2 (µatm), bicarbonate (HCO_3^-), carbonate (CO_3^{2-}), calcite saturation state (Ω_{Ca}) and aragonite saturation state (Ω_{Ar}). pCO_2 values are highlighted in yellow

The pCO_2 values from CO2SYS were then compared to the pCO_2 values from the sensor as shown in Figure 4.12.

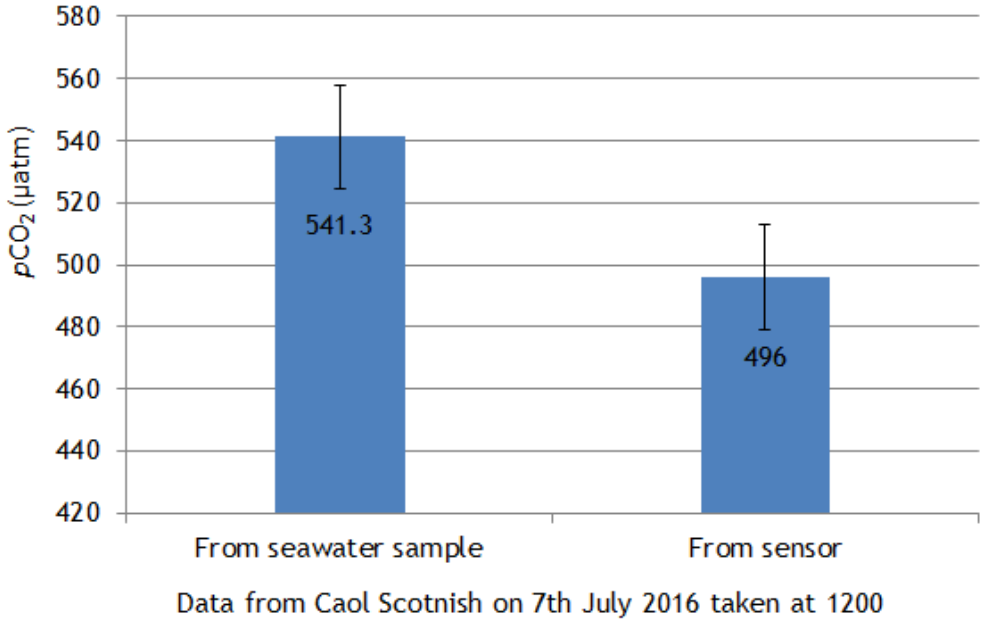

Figure 4.12: A comparison of CO2SYS pCO_2 concentration from seawater analyses and sensor pCO_2 concentration. ΔpCO_2 from seawater analysis and direct sensor reading = 45.3 µatm. Although a second seawater sample was taken at the end of the deployment, a comparison cannot be made with a sensor reading as it was not recording at this point (due to logistics, the sensor was deployed for longer than originally programmed)

4.6.3 Characterisation of carbonate parameters in Caol Scotnish (7th – 9th July 2016) with sensor measurements

In-situ field measurements of the following parameters were made; pCO_2 (with the developed sensor), pH, DO, salinity, temperature and depth. This was the first in-situ testing of the newly developed pCO_2 sensor.

4.6.3.1 Natural variability of carbonate chemistry and other physicochemical variables in Caol Scotnish 7th to 9th July 2016

A comparison of the time series of all variables recorded in Caol Scotnish is shown in Figure 4.13. More detail is given in individual analyses in the following sections.

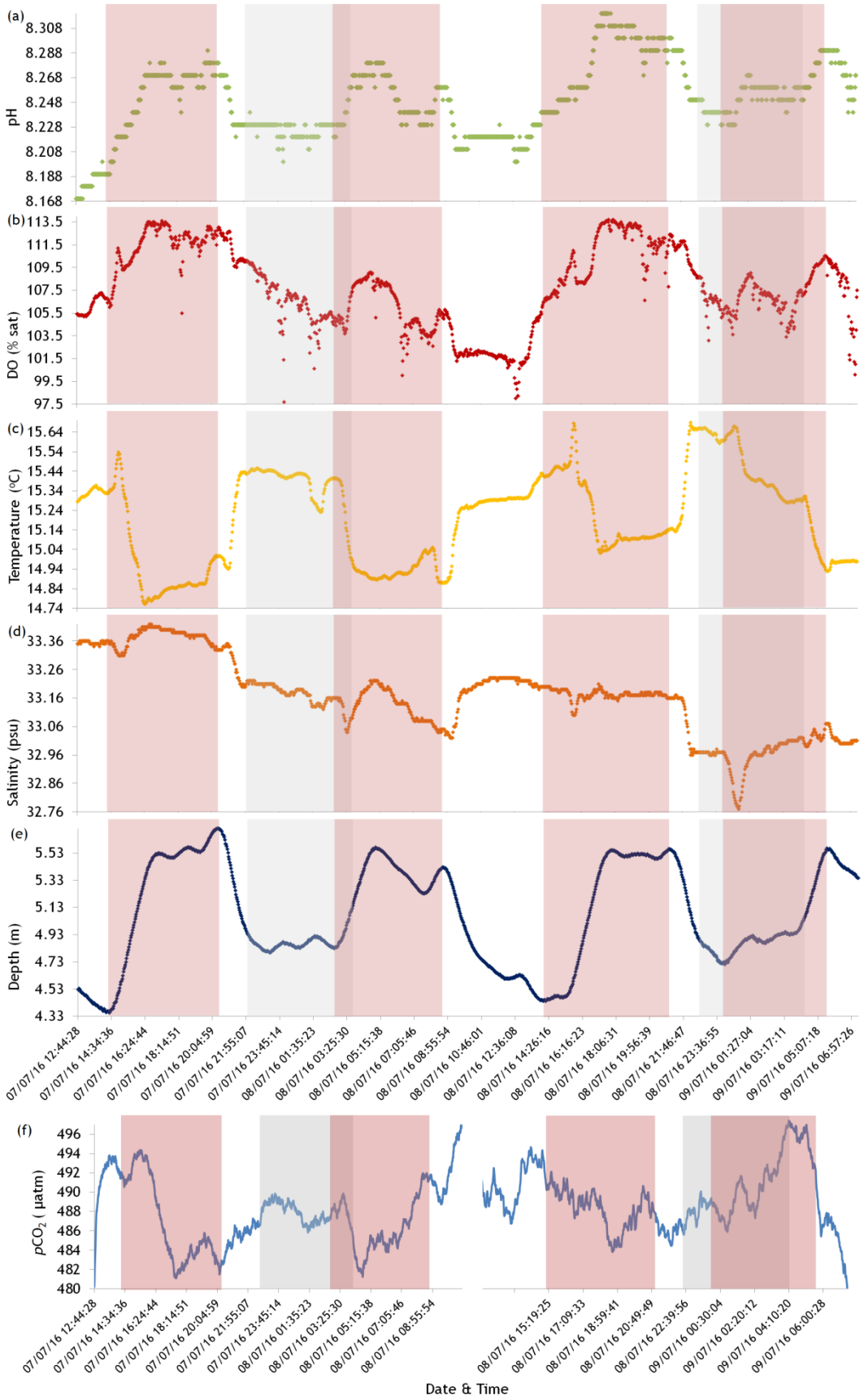

Figure 4.13: Summary plot and comparison of all variables in Caol Scotnish .YSI EXO2 Sonde (a, b, c, d, e) and pCO_2 sensor (f) time series data from 7th to 9th July 2016. (a) pH (b) DO (c) Temperature (d) Salinity (e) Depth of water above sensor (f) pCO_2 time series from developed sensor which has a gap in the data (57 min) due to sensor maintenance. Deployment was for 42h 35m in total. Pink shade shows incoming flood tide. Grey shade shows hours of darkness.

The diel period in July in Caol Scotnish encompassed approximately 18 hours of daylight and approximately 6 hours of darkness. In this cycle, sunset was at 22:07 on the first night and 22:06 on the second night. Dusk was at 23:06 and 23:04. Dawn was at 03:50 on the first night and 03:52 on the second night. Sunrise was at 04:49 and 04:50. It can therefore follow that there would be a longer amount of time available for primary productivity to occur during the long daylight hours in the summer months.

From the time series shown in Figure 4.13, it is clear that there is a significant tidal influence in Caol Scotnish and subsequent analysis found it to be the dominant driver of each variable. The very nature of the area which is narrow and surrounded by close banks mean that tides are a significant driving force behind fluctuations of most parameters as compared to open areas in the sea (for comparison see Chapter 5 where tides have little influence in the dynamically different tropical deployment). In this area, the tide is reasonably large with a total difference from low to high tide on average being 1.35m. The tidal pattern is semi-diurnal. The depth of water above the sensor ranged from 4.36m (minimum low tide) to 5.71m (maximum high tide).

The pH in Caol Scotnish is highly influenced by tidal activity but also to a lesser extent has some superimposition with diel signals. The pH cyclical fluctuation in Caol Scotnish was from 8.17 to 8.32 (ΔpH = 0.15) with a daily mean of 8.25 and a nightly mean of 8.24. pH started to increase 2 – 3 hours before sunrise which is expected as it gradually becomes lighter at dawn and the light energy begins to be utilised in photosynthesis. The pH is highest towards the latter hours of the daylight period (at dusk, 2 -3 hours before sunset) when there will be a peak of photosynthetic activity. Coralline algae can photosynthesise at different times of the day using "photoinhibition strategies" in which they adapt to high or low light levels to enable them to keep photosynthesising (Burdett *et al.*, 2014). This would suggest that 2-3 hours before dusk in Caol Scotnish is the optimum time for the algae to photosynthesis, i.e. not too light and not too dark. After sunset, photosynthesis and associated CO_2 uptake will gradually cease and correspondingly the pH will fall and the pCO_2 content of the seawater will increase. Although biological processes have an influence on pH, the tide has arguably a larger influence with the pH increasing everytime there is a flood tide

in the area. Overnight on the last night of deployment when a low pH would be expected due to biological respiration, the flood tide enters the area and increases the pH. There were also pH lows during daylight hours (when highs should be expected if solely governed by biological factors due to photosynthesis) but higher pH waters were then introduced with the flood tide. It can be concluded therefore that the pH pattern was predominantly driven by the tides in the area and diel cycles were mostly concealed when looking at the time series (biological processes can still be seen but in a secondary capacity).

DO fluctuation in Caol Scotnish was from 97.7% to 113.7% (ΔDO = 16%) with a daily mean of 108.03% and a nightly mean of 106.31%. Like the pH, the DO in July in Caol Scotnish would start to increase 2 – 3 hours before sunrise which is as standard in most diel cycles when it gradually becomes lighter at dawn and photosynthesis begins. The DO is highest towards the latter hours of the daylight period (at dusk, 2 -3 hours before sunset) when there will be an accumulation of photosynthetic activity. After sunset, photosynthesis will cease and DO will be drawn down and utilised by organisms with CO_2 being released into the seawater. Again like the pH, although these biological processes can be seen in places in the time series and are important to note, the diel cycles were mostly superseded by tidal action. The DO has a very similar pattern to pH where DO peaks and troughs are mostly governed by the tidal action, with DO increasing with each flood tide.

The temperature in Caol Scotnish fluctuated from 14.76^{o}C to 15.69^{o}C (ΔT = 0.93^{o}C) with a daily mean of 15.13^{o}C and a nightly mean of 15.41^{o}C. The temperature is strongly correlated with the tides and is dictated by changes in the water masses that flow into and out of the area rather than being dictated by insolation. The flood tide brings water masses of a lower temperature into Caol Scotnish.

The salinity in Caol Scotnish varied from 32.77 psu to 33.42 psu (Δsal = 0.65 psu) with a daily mean of 33.20 and a nightly mean of 33.06 psu. Although correlation analysis does not point to a strong relationship between salinity and tides in July, there is a subtle salinity change with the tides (a slight increase with each flood tide) but this may have been buffered by the increasing rainfall

over the duration of the deployment. Salinity is further discussed in Section 4.7.4, page 215.

The pCO_2 cyclical fluctuation in Caol Scotnish was from 481.21 µatm to 496.99 µatm (ΔpCO_2 = 0.15) with a daily mean of 487.61 µatm and a nightly mean of 487.76 µatm. The pCO_2 is mainly governed by the tides but simultaneously has patterns of biological activity. At night there is an increase in pCO_2 but also during the day there is an increase in pCO_2 with the flood tide that enters the area.

All variables, their correlations and drivers are further discussed in detail throughout this chapter.

4.6.3.1.1 Drivers of variation in Caol Scotnish 7th to 9th July 2016

Over the course of this deployment, the tides were the principal driving force behind the patterns in pCO_2 and most variables in Caol Scotnish. Caol Scotnish displayed strong tidal influences and any diel patterns were usually superseded by this (with a few exceptions). The tides introduced different bodies of water into Caol Scotnish. Depth was recorded for the duration of the deployment, i.e. the height of water above the sensor was measured and this provided a proxy for tidal action. Loch Sween in July does not exhibit two regular tidal cycles. Overnight in July in Caol Scotnish, the tide was out. During the day, there were two high tides and one low tide. This corresponds with two low tides and two high tides over 24 hours. Paired variables were analysed and the most correlated are shown overleaf. The strongest correlations are visibly seen with the parallel time series and quantified through Pearson's correlation coefficient (and simultaneously with equations of a straight line). Analyses was centred around tidal (flood tide is represented in pink) and diel (night is represented in grey) patterns over the course of the deployment of the sensors. Principal Component Analysis (PCA) was also undertaken to support the previous analyses.

4.6.3.1.1.1 Variables driven by the tide

4.6.3.1.1.1.1 Depth and Temperature

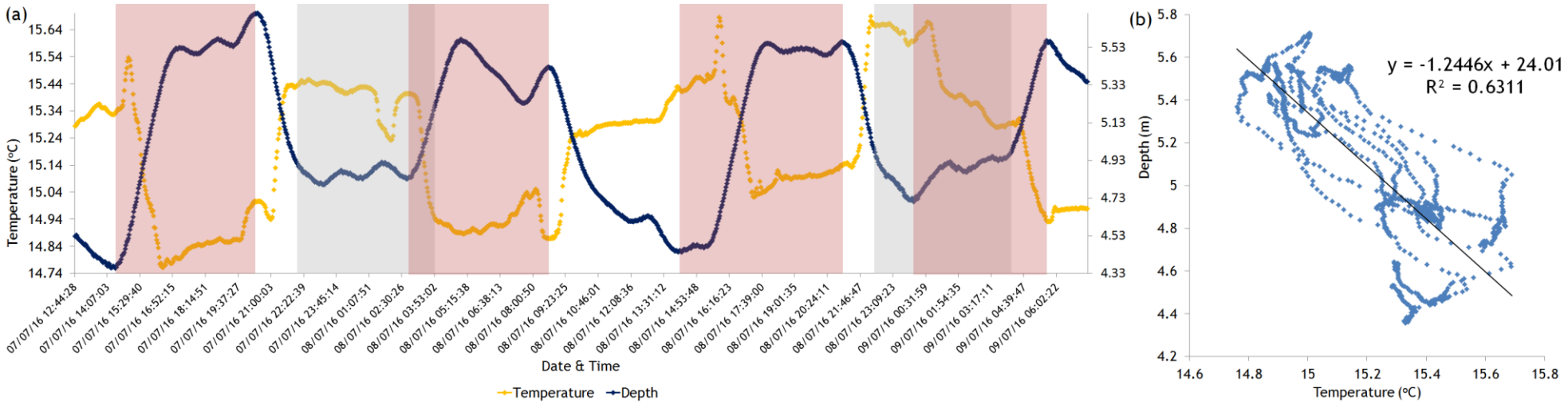

Figure 4.14: (a) Parallel time series of temperature and tidal action in Caol Scotnish from 7th to 9th July 2016 encompassing day (no shade), night (grey shade) and flood tide (pink shade). Temperature; Mean = 15.20 ± 0.24 °C. Depth; Mean = 5.09 ± 0.38 m. (b) Scatter graph of temperature and depth of water with linear trendline. Coefficient of determination; R^2 = 0.63. Pearson correlation coefficient; r = -0.79. p < 0.001.

The parallel time series of temperature and tidal action is shown in Figure 4.14a. There is a significant negative correlation ($r = -0.79$, $p < 0.001$) between temperature and tidal action in Caol Scotnish (Figure 4.14b). Overall, the temperature in Caol Scotnish in July was most highly correlated with the tides. When a flood tide entered the area, there was a decrease in the temperature which suggests colder water masses were being introduced with the incoming tide.

4.6.3.1.1.1.2 Depth and pH

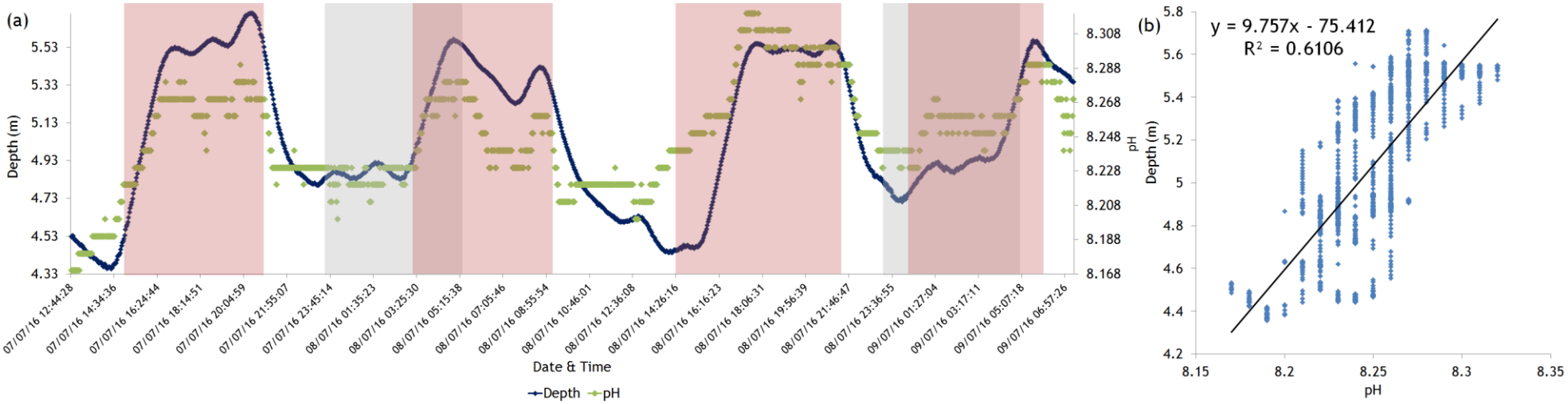

Figure 4.15: (a) parallel time series of pH and tidal action in Caol Scotnish from 7th to 9th July 2016 encompassing day (no shade), night (grey shade) and flood tide (pink shade). pH; Mean = 8.25 ± 0.03. Depth; Mean = 5.09 ± 0.38m. (b) scatter graph of temperature and depth of water with linear trendline. Coefficient of determination; R^2 = 0.61. Pearson correlation coefficient; r = 0.78. p < 0.001.

The parallel time series of tidal action and pH in Caol Scotnish is shown in Figure 4.15a. There is a significant positive correlation ($r = 0.78$, $p < 0.001$) between tidal action and pH in Caol Scotnish (Figure 4.15b). Overall, the pH in Caol Scotnish in July was highly correlated with the tides. When a flood tide entered the area, there was an increase in the pH which suggests higher pH water masses were being introduced with the incoming tide. It is shown that biological processes/diel patterns are swamped by tidal processes. During the night cycle where pH would be expected to remain low due to the release of CO_2 in respiration processes, the incoming flood tide raises the pH within the hours of darkness.

4.6.3.1.1.1.3 DO and pH

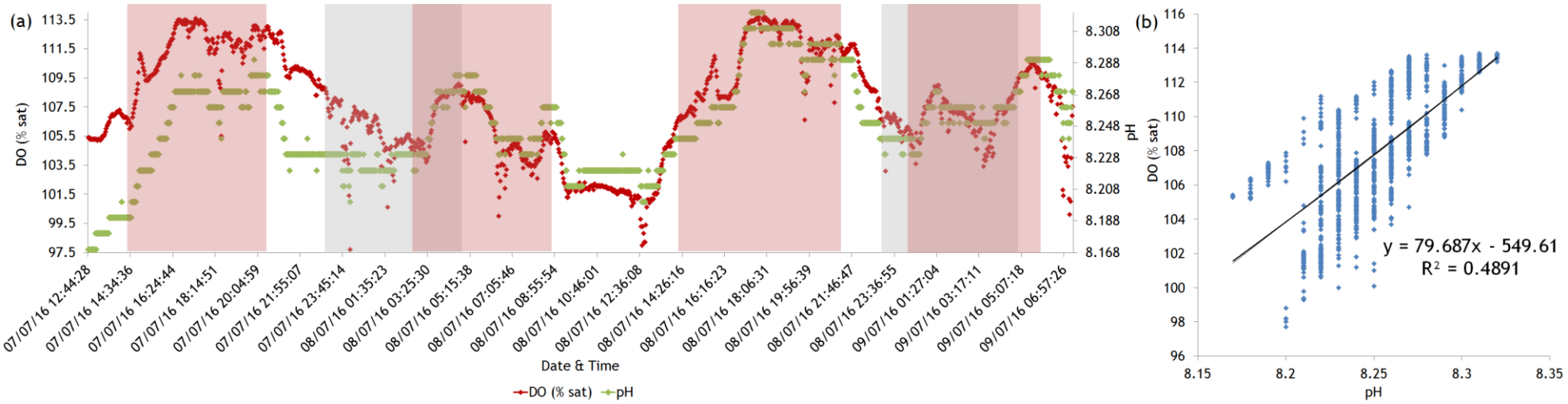

Figure 4.16: (a) parallel time series of DO and pH in Caol Scotnish from 7th to 9th July 2016 encompassing day (no shade), night (grey shade) and flood tide (pink shade). pH; Mean = 8.25 ± 0.03. DO; Mean = 107.84 ± 3.43 %sat. (b) scatter graph of DO and pH with linear trendline. Coefficient of determination; R^2 = 0.49. Pearson correlation coefficient; r = 0.70. p < 0.001

pH and DO in Caol Scotnish in July is shown in Figure 4.16a. The pH and DO in Caol Scotnish exhibited a significant positive correlation ($r = 0.70$, $p < 0.001$) as shown in Figure 4.16b. This pattern, as previously mentioned, is mainly governed by the tidal influence in the area with both variables increasing in concentration with the flood tide. When the flood tide is not influential, the two parameters may be driven by photosynthesis and respiration where during the day, both pH and DO increase according to photosynthesis. Conversely, pH and DO decrease during respiration at night time when pCO_2 is given out by organisms. This pattern however is superseded by tidal influences on numerous occasions.

4.6.3.1.1.1.4 pCO_2 and pH

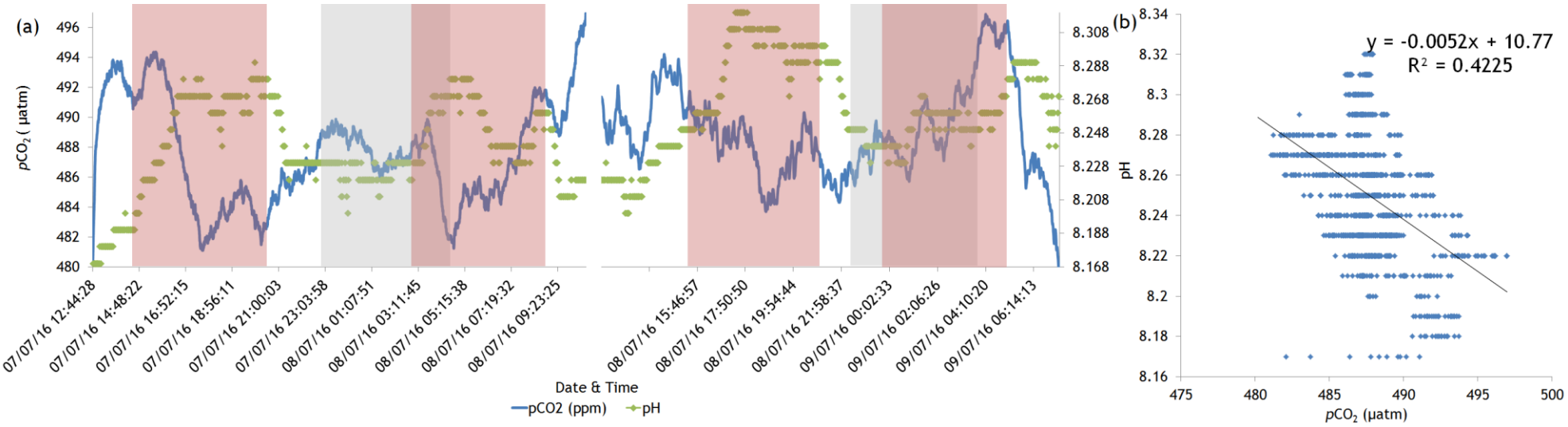

Figure 4.17: (a) parallel time series of pCO_2 and pH in Caol Scotnish from 7th to 9th July 2016 encompassing day (no shade), night (grey shade) and flood tide (pink shade). pCO_2; Mean = 488 ± 2.36 µatm. pH; Mean = 8.25 ± 0.03. There is a 57 minute gap in the pCO_2 data because of sensor maintenance during deployment. (b) scatter graph of pH and pCO_2 with linear trendline. Coefficient of determination; R^2 = 0.42. Pearson correlation coefficient; r = -0.65. p < 0.001.

The parallel time series of pH and pCO_2 in Caol Scotnish in July is shown in Figure 4.17a. There is a significant inverse correlation between pH and pCO_2 in Caol Scotnish ($r = -0.65$, $p < 0.001$) as shown in Figure 4.17b. Again, both these variables show diel patterns but only when not superseded by the main influence of the flood tide. pCO_2 tends to decrease with the introduction of the flood tide although there may also be biological micro-influences.

4.6.3.1.1.1.5 Depth and DO

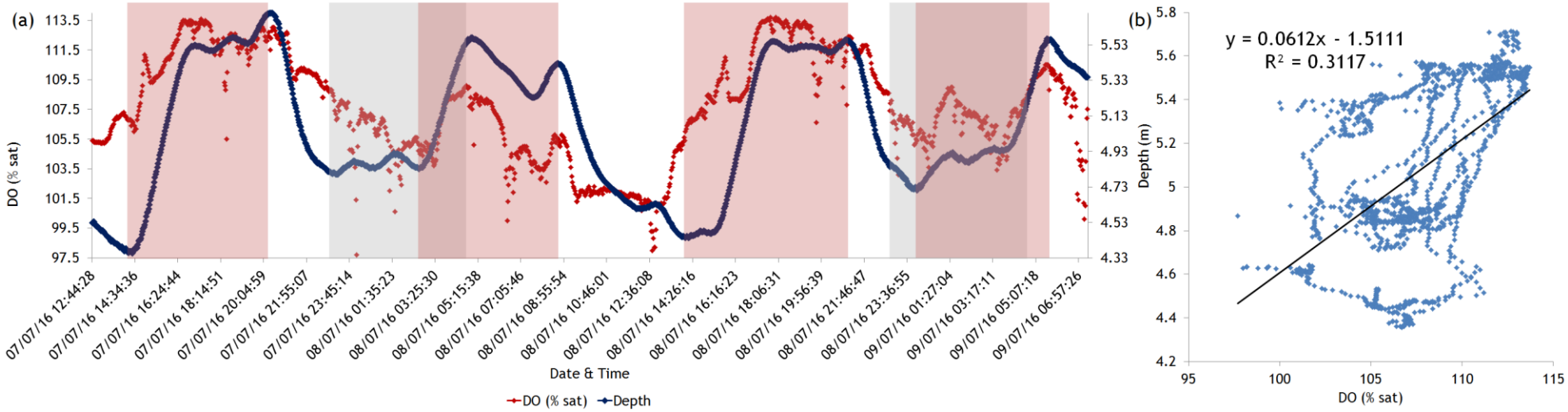

Figure 4.18: (a) parallel time series of tidal action and DO in Caol Scotnish from 7th to 9th July 2016 encompassing day (no shade), night (grey shade) and flood tide (pink shade). Depth; Mean = 5.09 ± 0.38 m. DO; Mean = 107.84 ± 3.43 %sat. (b) scatter graph of DO and depth of water with trendline. Coefficient of determination; R^2 = 0.31. Pearson correlation coefficient; r = 0.56. p < 0.001.

The parallel time series of tidal action and DO in Caol Scotnish is shown in Figure 4.18a. There is a significant positive relationship between the two variables ($r = 0.56$, $p < 0.001$) shown in Figure 4.18b. DO is mainly goverened by the tides and will generally increase with the incoming flood tide (although the time series also includes micro-patterns as previously mentioned).

4.6.3.1.1.1.6 Depth and pCO_2

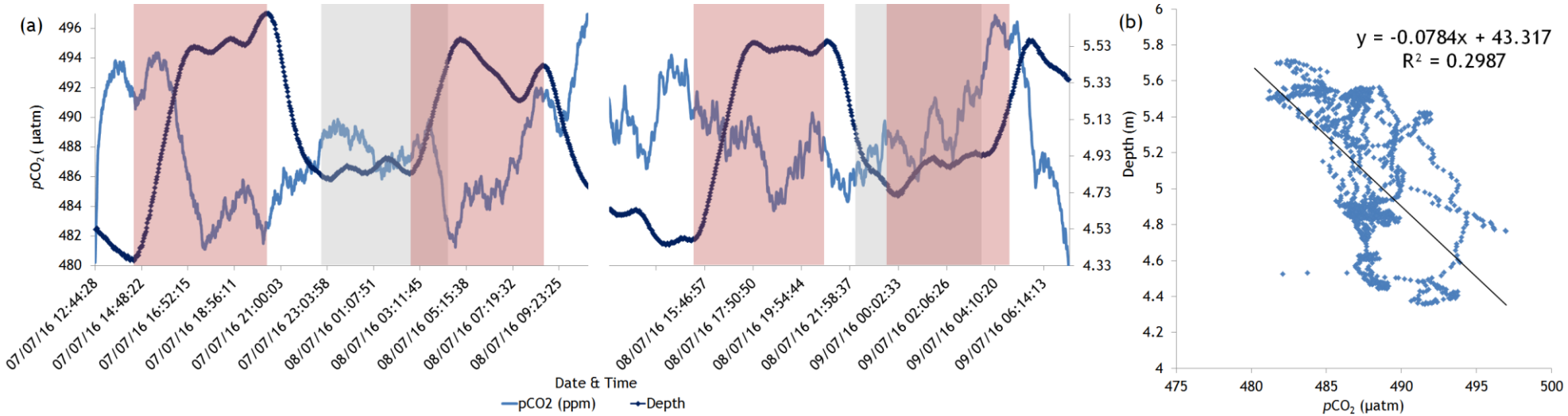

Figure 4.19: (a) parallel time series of tidal action and pCO_2 cycle in Caol Scotnish from 7th to 9th July 2016 encompassing day (no shade), night (grey shade) and flood tide (pink shade). Depth; Mean = 5.09 ± 0.38m. pCO_2; Mean = 488 ± 2.63 µatm. (b) scatter graph of depth and pCO_2 with linear trendline. Coefficient of determination; R^2 = 0.30. Pearson correlation coefficient; r = -0.55. p < 0.001.

The parallel time series of tidal action and pCO_2 in Caol Scotnish in July is shown in Figure 4.19a. There is a significant inverse correlation between the tidal action and pCO_2 ($r = -0.55$, $p < 0.001$) as shown with the trend line in Figure 4.19b. The pCO_2 was evidently governed by the tide and generally increased with the flood tide.

4.6.3.1.1.1.7 pH and Temperature

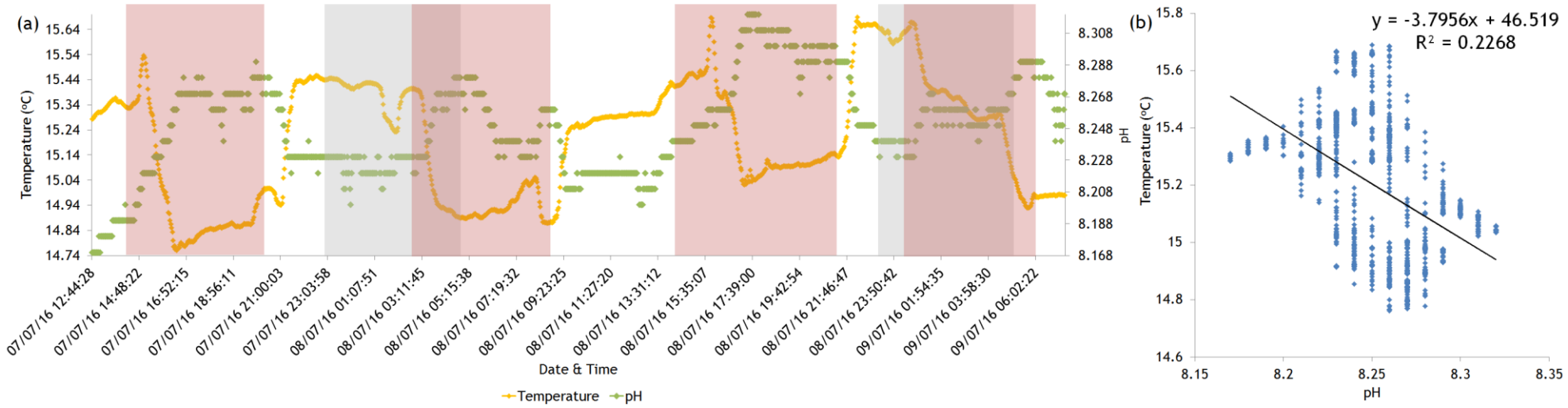

Figure 4.20: (a) parallel time series of pH and temperature in Caol Scotnish from 7th to 9th July 2016 encompassing day (no shade), night (grey shade) and flood tide (pink shade). Temperature; Mean = 15.20 ± 0.24 °C. pH; Mean = 8.25 ± 0.03. (b) scatter graph of temperature and pH with linear trendline. Coefficient of determination; R^2 = 0.27. Pearson correlation coefficient; r = -0.48. p < 0.001.

The parallel time series of pH and temperature in Caol Scotnish in July is shown in Figure 4.20a. There is a significant inverse correlation between the two variables ($r = -0.48$, $p < 0.001$) as shown in Figure 4.20b. Again, as previously mentioned both pH and temperature were mainly governed by tidal action in the area.

T-S (temperature – salinity) diagrams can be used as a water mass tracer and this method is employed in the next section.

4.6.3.1.1.1.8 Temperature and Salinity

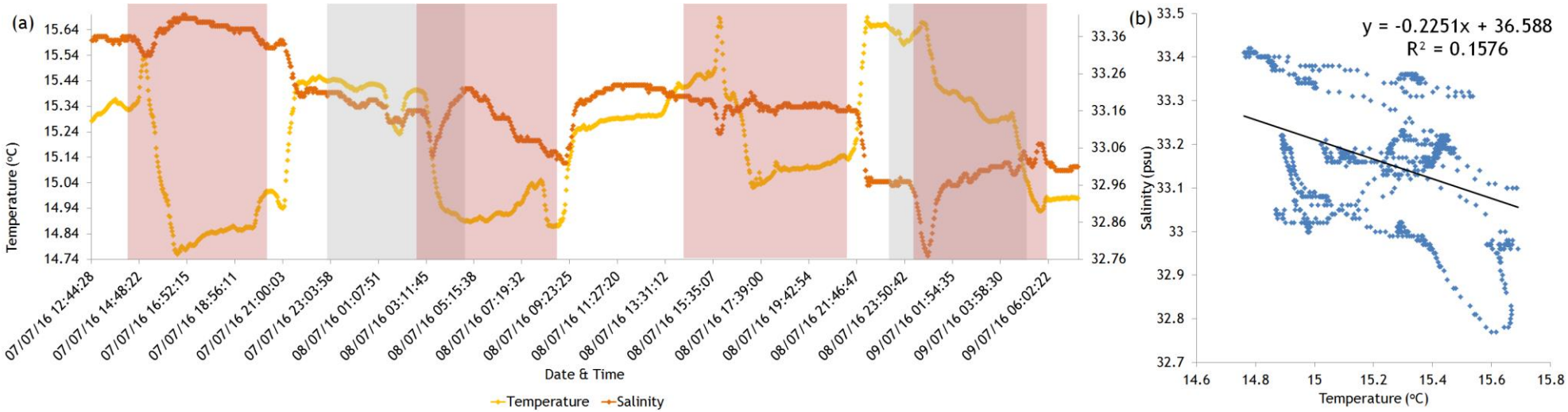

Figure 4.21: (a) parallel time series of temperature and salinity cycle in Caol Scotnish from 7th to 9th July 2016 encompassing day (no shade), night (grey shaded) and flood tide (pink shade). Temperature; Mean = 15.20 ± 0.24 °C. Salinity; Mean = 33.17 ± 0.14 psu. (b) scatter graph of temperature and salinity with linear trendline. Coefficient of determination; R^2 = 0.16. Pearson correlation coefficient; r = -0.40. p < 0.001.

The parallel time series of temperature and salinity is shown in Figure 4.21a. There was a significant inverse correlation between temperature and salinity ($r = -0.40$, $p < 0.001$) as shown in Figure 4.21b, both mostly governed by the tidal action in the area.

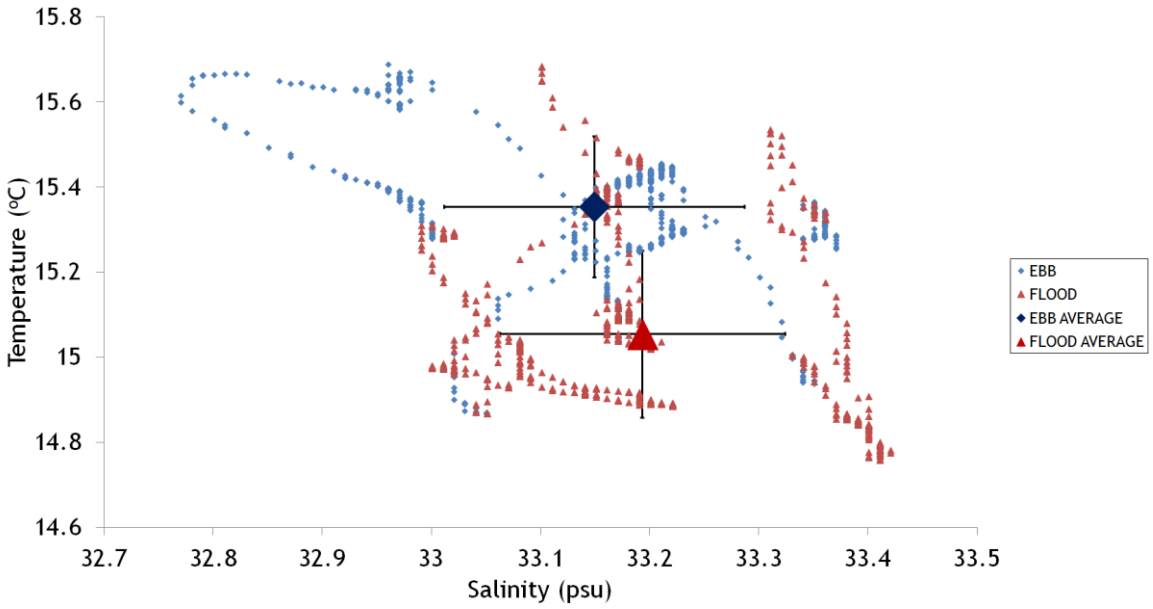

Figure 4.22: T-S diagram showing flood tide and ebb tide according to their temperature and salinity properties in Caol Scotnish on 7th – 9th July 2016. Average ebb tide: Salinity = 33.149 ± 0.138 psu, Temperature = 15.35 ± 0.17 °C, Average flood tide: Salinity = 33.193 ± 0.131 psu, Temperature = 15.06 ± 0.20 °C.

Looking closely at the T-S diagram, it is possible to separate out flood and ebb tides by their temperature and salinity properties (see Figure 4.22). This shows higher salinity and colder temperatures are brought in by the flood tide but higher salinities also span the ebb tide.

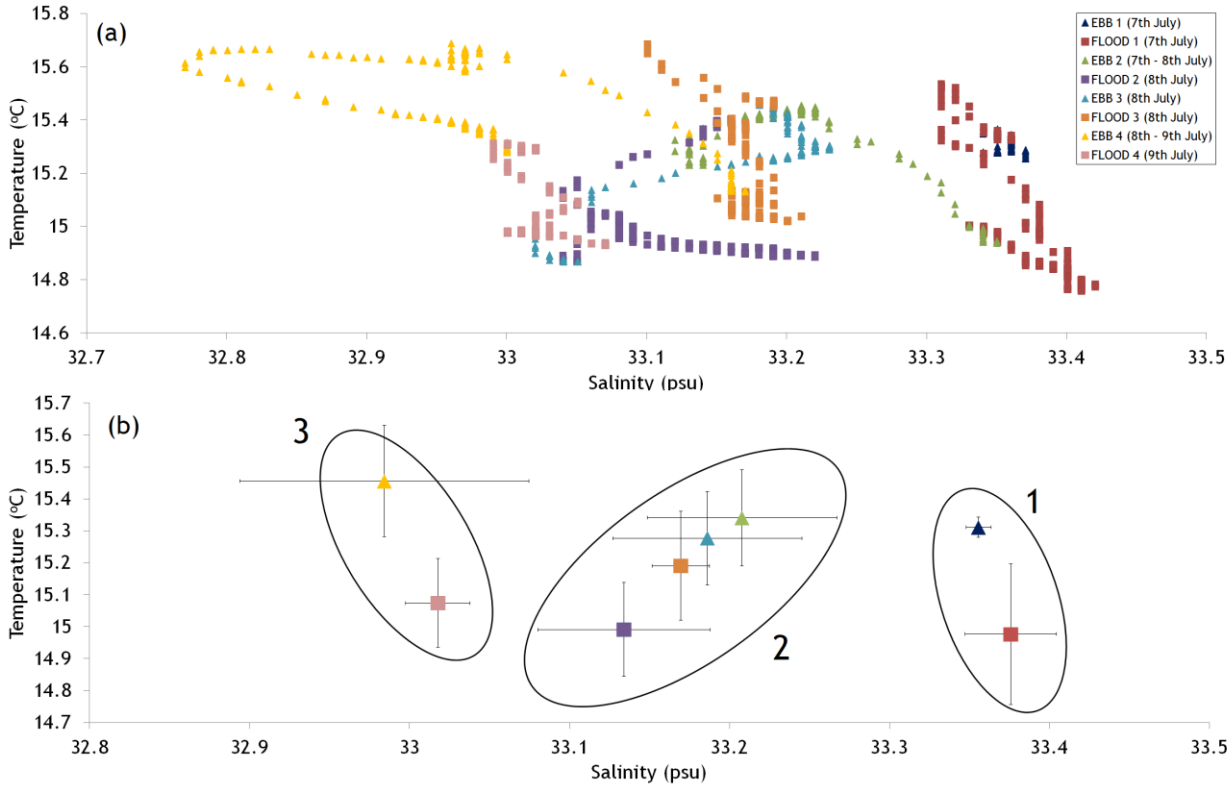

Figure 4.23: (a) T-S diagram showing each flood and ebb tide over the deployment in Caol Scotnish 7th – 9th July 2016 according to their temperature and salinity properties. (b) Average; Ebb 1: Salinity = 33.355 ± 0.008 psu, Temperature = 15.31 ± 0.03 °C. Flood 1: Salinity = 33.376 ± 0.029 psu, Temperature = 14.98 ± 0.22 °C. Ebb 2: Salinity = 33.208 ± 0.059 psu, Temperature = 15.34 ± 0.15 °C. Flood 2: Salinity = 33.134 ± 0.05 psu, Temperature = 14.99 ± 0.15 °C. Ebb 3: Salinity = 33.186 ± 0.059 psu, Temperature = 15.28 ± 0.15 °C. Flood 3: Salinity = 33.169 ± 0.018 psu, Temperature = 15.19 ± 0.17 °C. Ebb 4: Salinity = 32.984 ± 0.090 psu, Temperature = 15.46 ± 0.17 °C. Flood 4: Salinity = 33.018 ± 0.020 psu, Temperature = 15.07 ± 0.14 °C. Separate water masses are shown in individual circles.

Going further, as shown in Figure 4.23a, each colour represents each different flood and ebb tide in the deployment. The first flood tide water mass is different from the second flood water mass. It is likely that the second and third flood tide however, is the same water mass as they share similar T-S properties. The flood tides are generally colder than the ebb tides. Figure 4.23b shows that there are three separate water masses in this deployment according to their T-S properties.

Water mass	Salinity (psu)	Temperature (°C)	Water Type
1 (Ebb & Flood 1)	33.31 - 33.42 (μ = 33.370)	14.76 - 15.54 (μ = 15.07)	highest salinity, lowest temperature
2 (Ebb 2 & 3; Flood 2 & 3)	33.02 - 33.35 (μ = 33.175)	14.871 - 15.686 (μ = 15.21)	middling salinity, middling temperature
3 (Ebb & Flood 4)	32.77 - 33.07 (μ = 32.996)	14.93 - 15.69 (μ = 15.32)	lowest salinity, highest temperature

Table 4.3: Different water mass properties in Caol Scotnish on 7th – 9th July 2016.

Flood tide 1 had high salinity waters and as ebb tide 2 is in process, there was a lowering of salinity which may be due to precipitation and/or run-off. The second flood tide was an even lower salinity than the second ebb tide which again could be due to precipitation and/or run-off. It was also a lower temperature. As the tide ebbs from this (ebb tide 3), the salinity and temperature rise which may mean that evaporation was the net process compared to precipitation on this part of the deployment as the weather was dry. As the third flood tide came in, there was a slight lowering of salinity and temperature. The fourth ebb had the lowest salinity of the deployment but the highest temperature which could mean there was added precipitation and/or runoff but the water was also being warmed. The fourth flood tide brought in lower temperatures but higher salinity waters. In general water mass 1 had the properties of highest salinity and the lowest temperature. Water mass 2 had the properties of middling salinity and middling temperature and water mass 3 had properties of the lowest salinity and the highest temperature (all shown on Figure 4.23b).

4.6.3.1.1.1.9 pCO_2 and DO

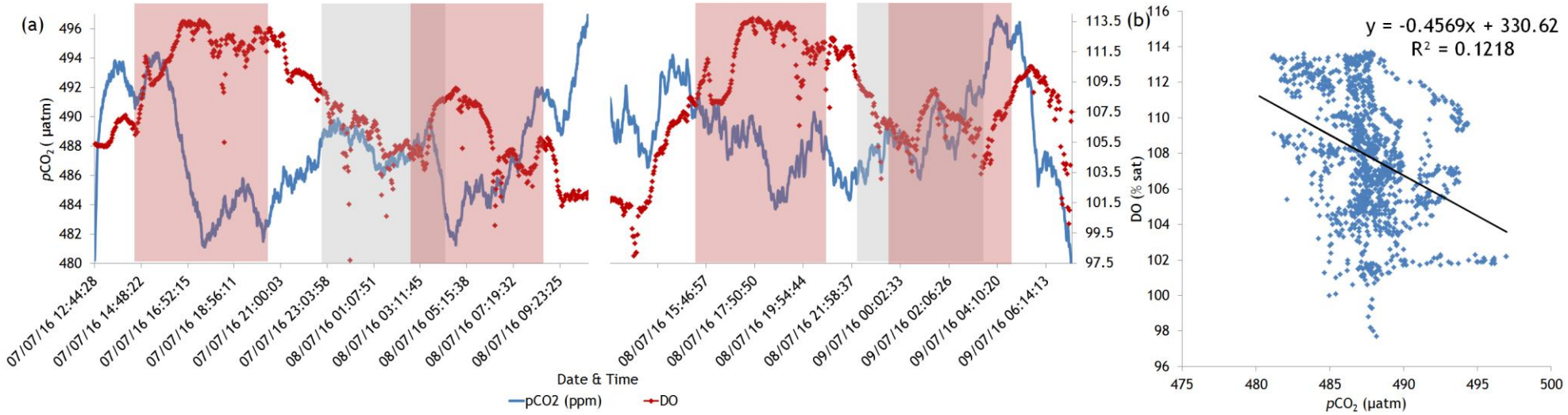

Figure 4.24: (a) parallel time series of pCO_2 and DO in Caol Scotnish from 7th to 9th July 2016 encompassing day (no shade), night (grey shade) and flood tide (pink shade). pCO_2; Mean = 488 ± 2.63 µatm. DO; Mean = 107.84 ± 3.43 %sat. (b) scatter graph of DO and pCO_2 with linear trendline. Coefficient of determination; R^2 = 0.12. Pearsons correlation coefficient; r = -0.35. p < 0.001.

The parallel time series of pCO_2 and DO in Caol Scotnish is shown in Figure 4.24a. There is a significant negative correlation between pCO_2 and DO ($r = -0.35$, $p < 0.001$) as shown in Figure 4.24b. Both variables are significantly driven by tidal action with secondary micro-patterns of biological activity.

4.6.3.1.1.1.10 pCO_2 and Temperature

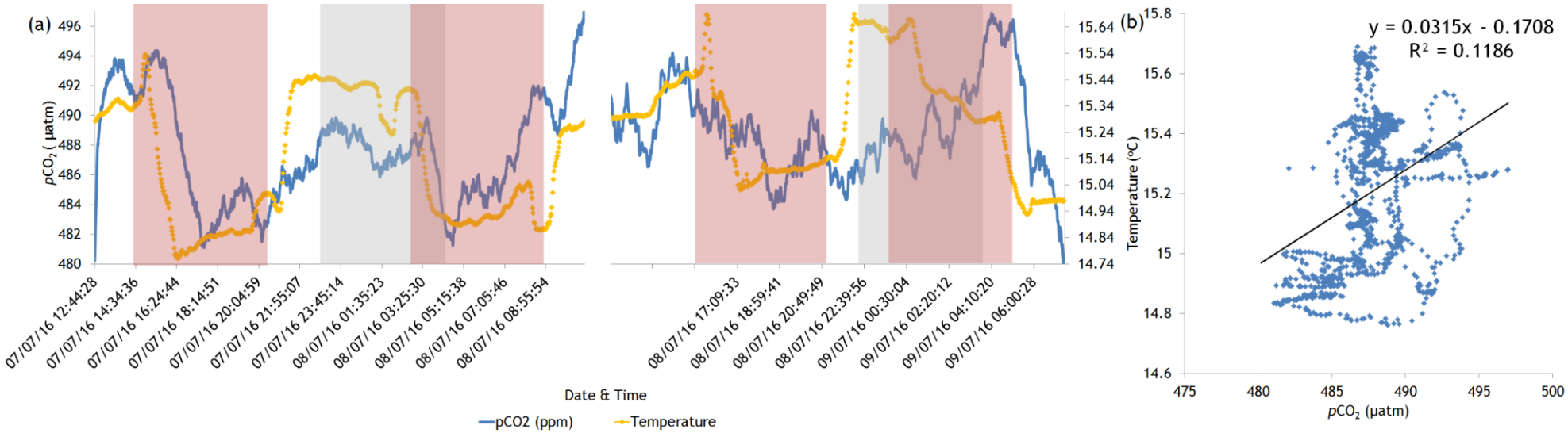

Figure 4.25: (a) parallel time series of pCO_2 and temperature in Caol Scotnish from 7th to 9th July 2016 encompassing day (no shade), night (grey shade) and flood tide (pink shade). pCO_2; Mean = 488 ± 2.36 µatm. Temperature; Mean = 15.20 ± 0.24 °C. (b) scatter graph of pCO_2 and temperature with linear trendline. Coefficient of determination; R^2 = 0.12. Pearson correlation coefficient; r = 0.34. p < 0.001.

The parallel time series of pCO_2 and temperature in Caol Scotnish is shown in Figure 4.25a. There is a significant positive correlation between pCO_2 and temperature ($r = 0.34$, $p < 0.001$) as shown in Figure 4.25b.

Temperature can alter pCO_2 in seawater because of a shift in the thermodynamic balance of the carbonate chemistry (Dai *et al.*, 2009). However, it was more than likely that the temperature was being driven to a greater extent by the tides in Caol Scotnish (which is also correlated strongly with the pCO_2). Different water masses which ebb or flood with the tides can affect the concentration of pCO_2 in the body of water (Chen and Hsing, 2005; Dai *et al.*, 2009).

4.6.3.1.1.1.11 DO and Salinity

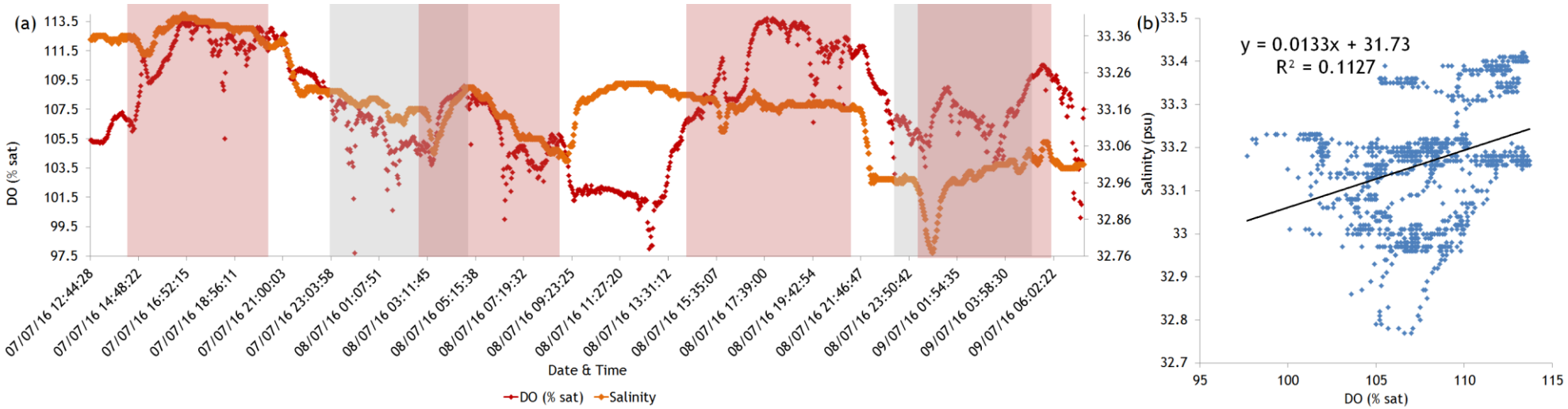

Figure 4.26: (a) parallel time series of DO and salinity in Caol Scotnish from 7th to 9th July 2016 encompassing day (no shade), night (grey shade) and flood tide (pink shade). DO; Mean = 107.84 ± 3.43 %sat. Salinity; Mean = 33.17 ± 0.14 psu. (b) scatter graph of salinity and DO with linear trendline. Coefficient of determination; R^2 = 0.11. Pearson correlation coefficient; r = 0.34. p < 0.001.

The parallel time series of DO and salinity in Caol Scotnish is shown in Figure 4.26a. There is a significant positive correlation between DO and salinity in Caol Scotnish ($r = 0.34$, $p < 0.001$) as shown in Figure 4.26b. Again, both are governed by the tides.

4.6.3.1.1.1.12 DO and Temperature

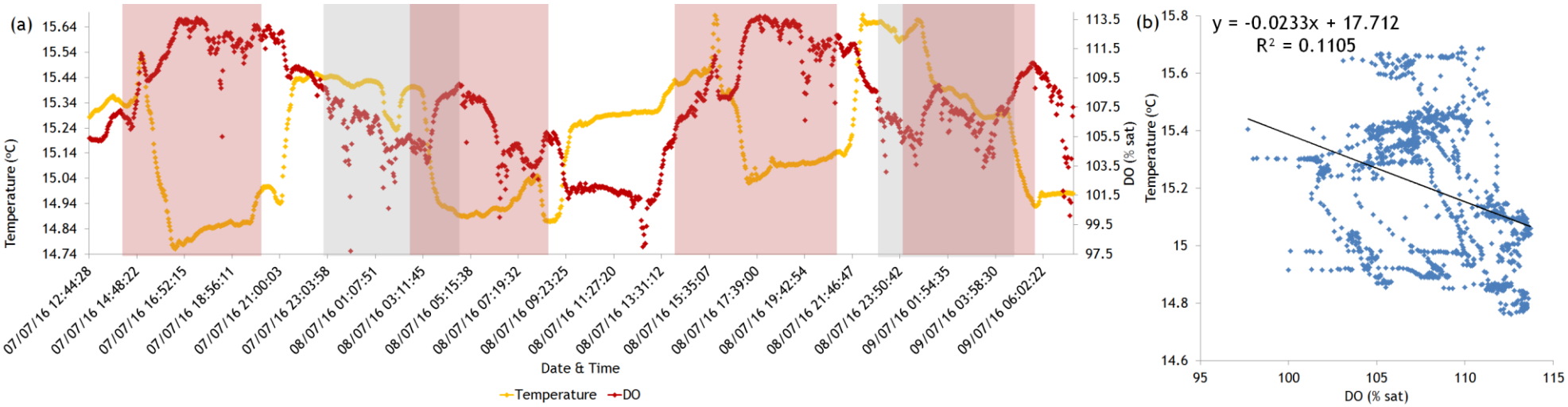

Figure 4.27: (a) parallel time series of DO and temperature in Caol Scotnish from 7th to 9th July 2016 encompassing day (no shade), night (grey shade) and flood tide (pink shade). DO; Mean = 107.84 ± 3.43 %sat. Temperature; Mean = 15.20 ± 0.24 °C. (b) scatter graph of temperature and DO with linear trendline. Coefficient of determination; R^2 = 0.11. Pearson correlation coefficient; r = -0.33. p < 0.001.

The parallel time series of DO and temperature in Caol Scotnish is shown in Figure 4.27a. There is a significant negative correlation between DO and temperature in Caol Scotnish ($r = -0.33$, $p < 0.001$) and both are governed by the tides.

4.6.3.1.2 Principal component analysis (PCA)

As a further statistical investigation, PCA was run on the data from Caol Scotnish in July. The resulting correlation circle is shown in Figure 4.28.

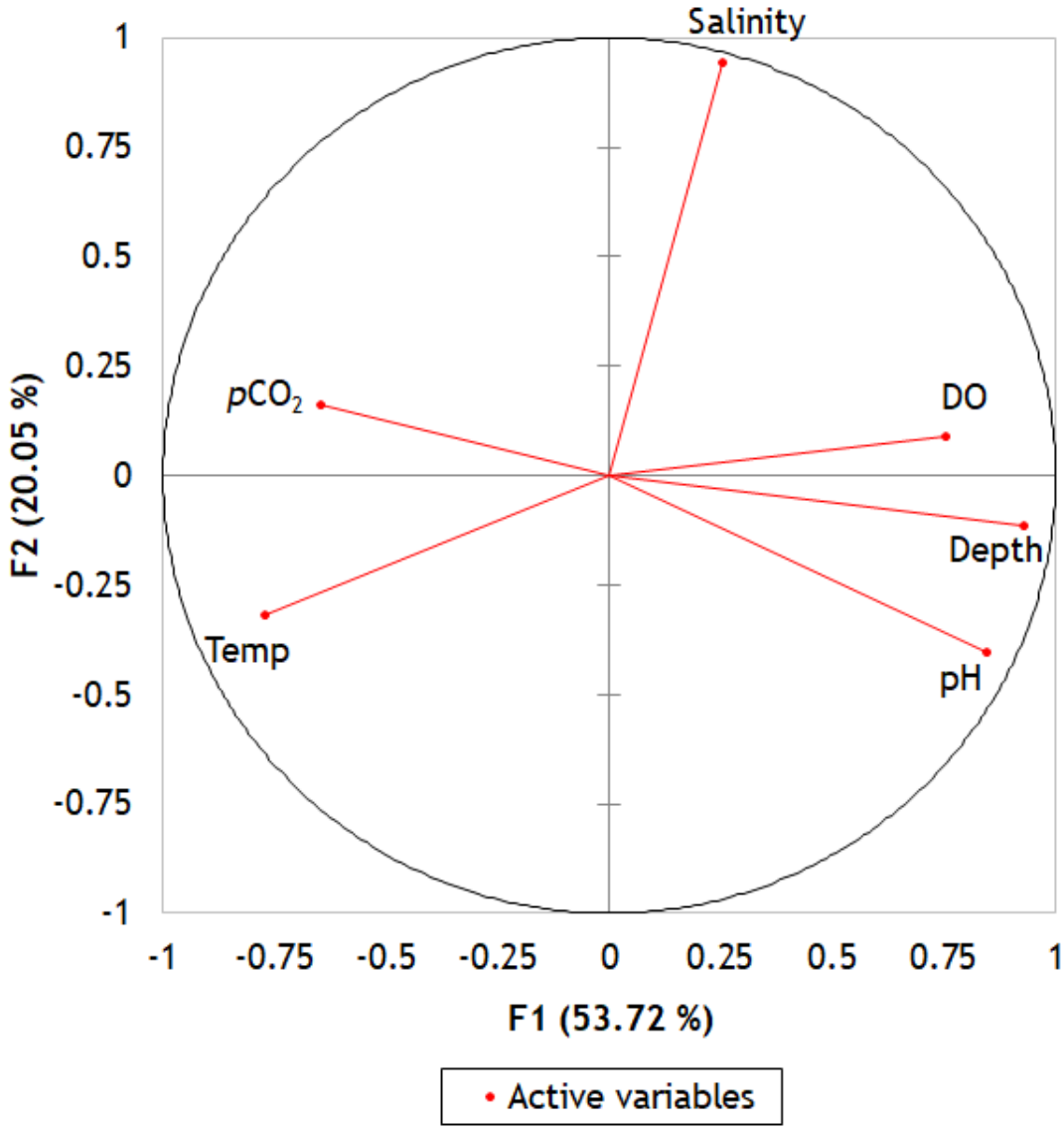

Figure 4.28: PCA showing the correlation circle from Caol Scotnish in July. If two variables are far from the centre and close to one another then they are positively significantly correlated. If two variables are orthogonal to one another then they are not related (in this case primarily salinity with pH, pCO_2 and depth). If two variables are on opposite sides of the centre then they are negatively significantly correlated.

PCA confirms the previous analyses and Figure 4.28 can be summarised as follows in Table 4.4 (which also acts as a summary of the previous analyses of the variables in Caol Scotnish and their correlations).

Positively significantly correlated	Not correlated	Negatively significantly correlated
Depth & pH (r = 0.78)	Salinity & pH (-0.14)	Depth & Temperature (-0.79)
DO & pH (r = 0.70)	Salinity & pCO_2 (-0.08)	pCO_2 & pH (-0.65)
Depth & DO (r = 0.56)	Salinity & Depth (0.08)	Depth & pCO_2 (-0.55)
pCO_2 & Temperature (0.34)		pH & Temperature (-0.48)
DO & Salinity (0.34)		Temperature & Salinity (-0.40)
		pCO_2 & DO (-0.35)
		DO & Temperature (-0.33)

Table 4.4: Correlated and non-correlated variables in Caol Scotnish in July according to PCA.

4.7 Results & Discussion 19th – 23rd September 2016

4.7.1 Seawater wet chemistry

In the September deployment, samples were taken throughout the day and evening over the space of five days (see Table 4.5 for exact sample times). The samples were analysed in triplicates with an overall average taken.

4.7.1.1 Water chemistry

Time of sample	Salinity (psu)	T(°C)	A_T (µmol/kg⁻SW)	DIC (µmol/kg⁻SW)
Monday 19/9/16				
1500	32.85	15.436	1615* (σ = 188; CV = 11.7%)	2089 (σ = 5.4; CV = 0.26%)
2115	32.67	15.587	1693* (σ = 33; CV = 2%)	1827* (σ = 30; CV = 1.6%)
Tuesday 20/9/16				
0900	33	15.057	2196* (σ = 321; CV = 14.6%)	2074 (σ = 22.6; CV = 1.09%)
2130	32.69	15.075	2003 (σ = 28; CV = 1.4%)	2082 (σ = 25; CV = 1.2%)
Wednesday 21/9/16				
0900	32.81	14.836	2389* (σ = 337; CV = 14%)	1977 (σ = 104; CV = 5.3%)
1020	32.61	15.242	1950* (σ = 309; CV = 15.8%)	1875 (σ = 80; CV = 4.2%)
1555	32.61	15.165	2038 (σ = 37; CV = 1.8%)	1896 (σ = 141; CV = 7.5%)
2120	32.74	14.933	2027* (σ = 81; CV = 4%)	1871 (σ = 135; CV = 6.6%)
Thursday 22/9/16				
0910	32.8	14.819	1991* (σ = 32; CV = 1.6%)	2054 (σ = 25; CV = 1.2%)
1510	32.46	15.238	2002* (σ = 31; CV = 1.5%)	1973 (σ = 37; CV = 1.8%)
2115	32.71	15.015	2010 (σ = 8.8; CV = 0.4%)	1991* (σ = 33; CV = 1.7%)
Friday 23/9/16				
0910	32.79	14.687	1716* (σ = 172; CV = 10%)	1908 (σ = 121; CV = 6.3%)

Table 4.5: A_T and DIC from water samples taken from Caol Scotnish 19th to 23rd September 2016. Shown is date and time of samples with accompanying measurements of temperature and salinity from YSI EXO2 Sonde and the resultant A_T and DIC concentrations from analyses in the laboratory. *samples frozen in storage where the error is expected to be large because of the resultant change in carbonate chemistry due to introduction of oxygen. σ represents the standard deviation of the reading while C.V. is the coefficient of variation.

A_T does not show a significant diel trend over the course of the deployment in Caol Scotnish (see Figure 4.29). There is some variation in the first half of the deployment but uncertainty is large with these measurements. The second half of the week shows little fluctuation in A_T. There is no clear pattern with DIC with a variation of concentrations during both the day and night cycles.

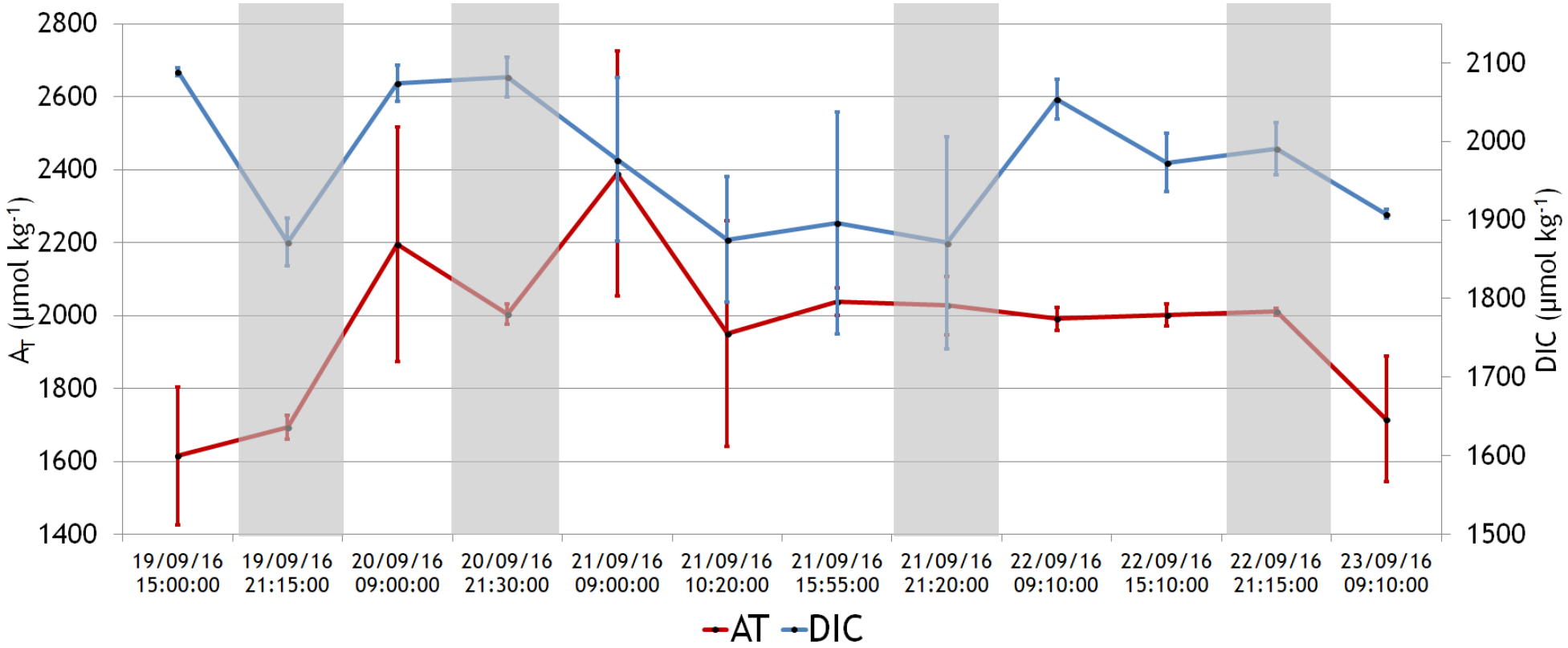

Figure 4.29: Concentrations of A_T and DIC in Caol Scotnish 19th to 23rd September 2016. Samples taken at night are within the grey shaded areas.

4.7.2 Comparison of pCO_2 data from sensor and pCO_2 data calculated from CO2SYS

DIC, A_T and ancillary data were used to calculate the pCO_2 concentrations from the water samples with CO2SYS as shown in Table 4.6.

Input Conditions				Output Conditions					
Salinity (psu)	T(°C)	A_T (µmol/kg$^-$SW)	DIC (µmol/kg$^-$SW)	pH	pCO_2 (µatm)	HCO_3^- (µmol/kgSW)	CO_3^{2-} (µmol/kgSW)	Ω_{Ca}	Ω_{Ar}
32.85	15.436	1615	2089	6.641	12856	1606	3.4	0.08	0.05
32.67	15.587	1693	1827	7.161	4105	1663	11.5	0.28	0.18
33	15.057	2196	2074	8.080	646	1951	98.7	2.38	1.53
32.69	15.075	2003	2082	7.374	2958	1949	21.4	0.52	0.33
32.81	14.836	2389	1977	8.630	161	1680	290.5	7.03	4.49
32.61	15.242	1950	1875	7.954	781	1778	67.8	1.64	1.05
32.610	15.17	2038	1896	8.159	495	1771	106.0	2.57	1.64
32.740	14.93	2027	1871	8.197	442	1741	113.6	2.75	1.76
32.800	14.82	1991	2054	7.423	2608	1931	23.6	0.57	0.36
32.460	15.238	2002	1973	7.778	1207	1879	48.8	1.18	0.76
32.710	15.015	2010	1991	7.735	1321	1896	45.2	1.09	0.70
32.790	14.687	1716	1908	7.035	5399	1693	8.7	0.21	0.13

Table 4.6: *In-situ* parameters (input conditions) used to calculate ancillary data (output conditions) from seawater samples in Caol Scotnish in September. Salinity, temperature, A_T and DIC were used in CO2SYS to calculate concentrations of pH, *p*CO2 (µatm), bicarbonate (HCO_3^-), carbonate (CO_3^{2-}), calcite saturation state (Ω_{Ca}) and aragonite saturation state (Ω_{Ar}). pCO_2 values are highlighted in yellow.

The pCO_2 values from CO2SYS were then compared to the pCO_2 values from the sensor as shown in Figure 4.30.

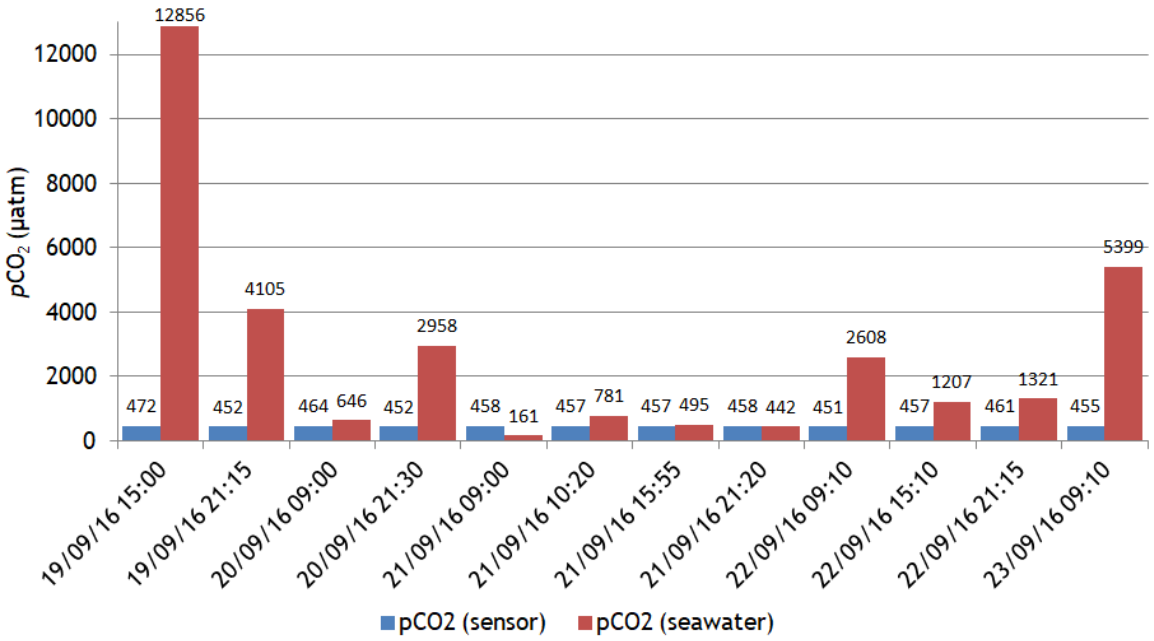

Figure 4.30: A comparison of CO2SYS pCO_2 concentration from seawater analyses and *in-situ* sensor pCO_2 concentration. The concentration of pCO_2 in µatm is shown above each data point.

When the pCO_2 concentration of the sensor was compared with analyses of the pCO_2 concentration of the seawater samples, the majority of readings did not match up. It must be noted that during storage some of the samples were unfortunately frozen in a faulty fridge and therefore the quality of the samples for analyses was compromised. Looking at Figure 4.30, the seawater analyses produced pCO_2 concentrations that were either erroneously high or vice versa, e.g., a sample collected at 15:00 contained a concentration of 12856 µatm and such a high value would be unlikely in any area. A concentration of 161 µatm could be feasible in the middle of the day where photosynthesis outperforms respiration but this is unlikely for a sample which was collected at 09:00. Additionally, a sample 1 hour later at 10:20 produced a concentration of 781 µatm and this quick increase seems implausible. Such a large increase would suggest a massive amount of calcification occurring in the space of an hour which again, is highly unlikely. This highlights the difficulties in multiple step sample analyses with collection, storage, individual analysis and subsequent error propagation throughout

4.7.3 Characterisation of carbonate parameters in Caol Scotnish (19th – 23rd September 2016) with sensor measurements

In-situ field measurements of the following parameters were made; pCO_2 (direct CO_2 output measured in μatm, pCO_2 (derived from voltage output), pH, DO, chlorophyll, salinity, temperature and depth.

Two of the developed pCO_2 sensors were deployed in Caol Scotnish for this run. They were both exactly the same with the exception that one was programmed to directly output pCO_2 in ppm and the other was programmed to output voltage in volts which would then be converted into a pCO_2 output afterwards using a specified formula (See Chapter 2, Section 2.4.3.3, page 52). This was to see if there were any benefits to choosing a different measurement output in the software that was previously developed (See Chapter 2).

4.7.3.1 Natural variability of parameters in Caol Scotnish 19th to 23rd September 2016

Overleaf is a comparison of the time series of all variables recorded in Caol Scotnish (see Figure 4.31). More detail is given in individual analysis in the following sections.

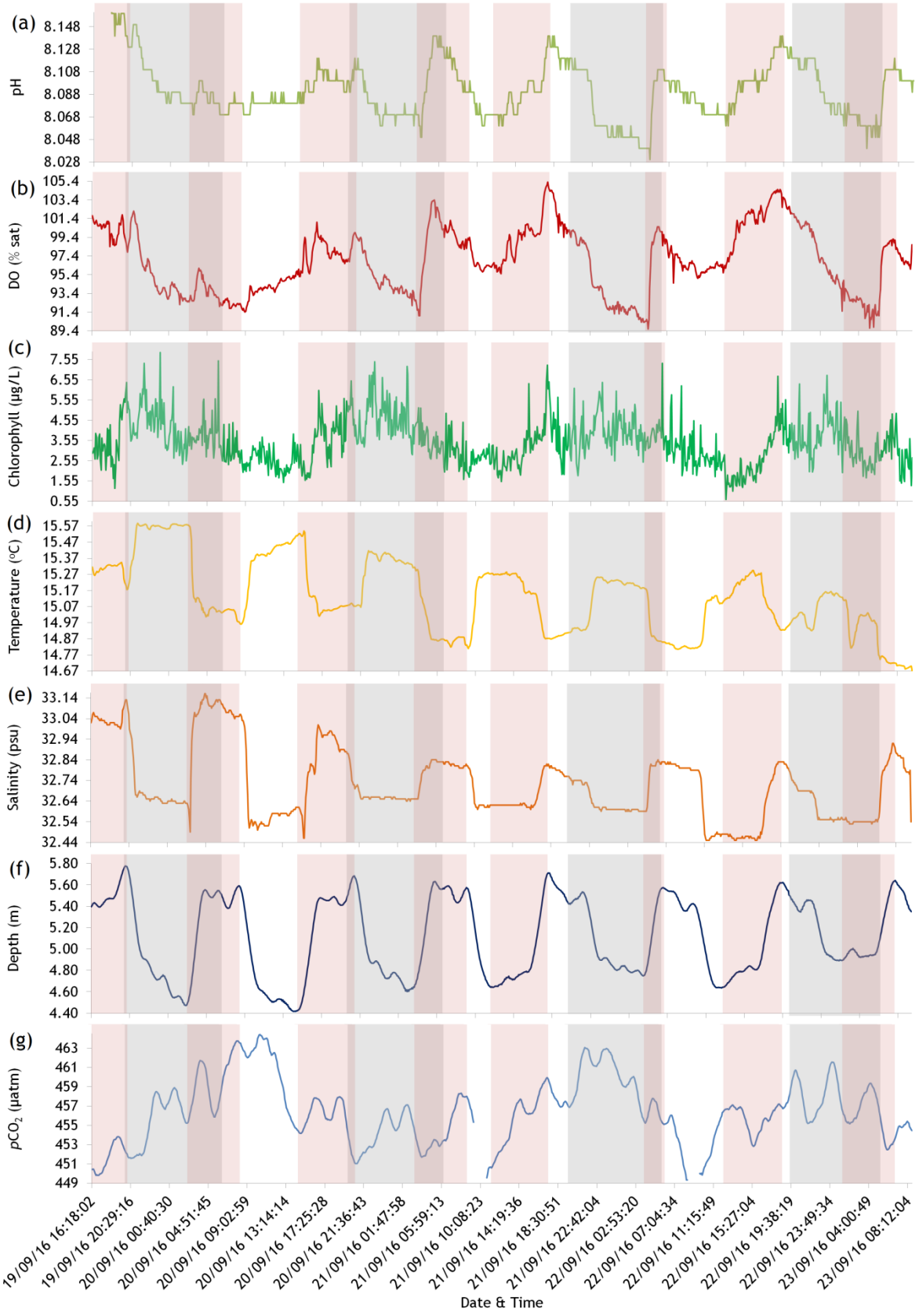

Figure 4.31: YSI EXO2 Sonde (a – f) and pCO_2 sensor (g) time series data from 19th to 23rd September. Summary plot and comparison of all variables. (a) pH (b) DO (c) Chlorophyll (d) Temperature (e) Salinity (f) Depth of water above sensor (g) pCO_2. There are gaps in the data (2h 45m) due to sensor maintenance. This deployment was for 89 hours 18 minutes in total. Light hours (no shade) = 46 h 38 m. Dark (grey shade) = 42 h 40 m. Flood tide is also shown (pink shade).

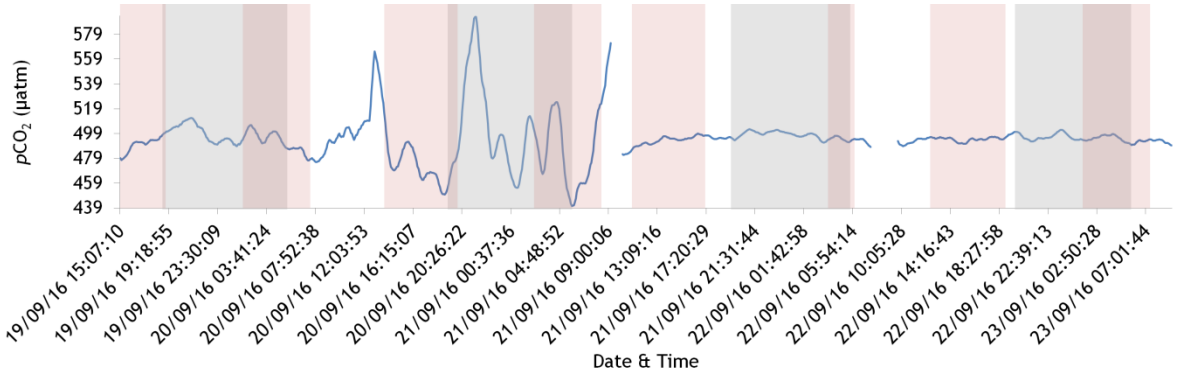

Figure 4.32: pCO_2 sensor (output voltage) data time series. There are gaps in the data (2h 45m) due to sensor maintenance. Plot shows pCO_2 data over diel cycles in Caol Scotnish from 19th to 23rd September 2016. The output voltage was later converted to a pCO_2 value. Flood tide is shown in pink shade and night cycle is shown in grey shade.

The pCO_2 time series which was converted from voltage output is shown in Figure 4.32. The results regarding this output were not what would be expected. The experiment to see if an alternative output (voltage output which was then converted to µatm) would perform well underwater (compared to µatm output) turned out to bring more problems than solutions. Succinctly, the voltage sensor produced pCO_2 data that did not correlate with any variables, concentrations that were unconventional and an unusual amount of background noise was also produced. There was no correlation with pH and the pCO_2 (voltage output). The pCO_2 scale ranged from 441 µatm to 593 µatm (ΔpCO_2 = 152 µatm). The maximum value is high and although it could possibly be a real concentration, it is likely to be erroneous due to the nature of the sudden spike in concentration followed by the sudden decrease. The first half of the deployment was a vastly different concentration scale to the second half when looking at the data provided (see Figure 4.32). The sensor was retrieved half way through the deployment for maintenance. When it was reprogrammed it produced values similar to the sensor outputting µatm. However, part-by-part, the data from the deployment was analysed and there was no correlation with any other parameter regardless of the part of cycle used. The voltage output carried a lot of background noise (which could not be effectively 'cleaned' without compromising the data) and therefore produced results that were not useable. The voltage output depends heavily on the power supplied and it is difficult to know the exact amount of power supplied when using D/C as there can be fluctuations. This is an important consideration when converting the

voltage into a pCO_2 reading. For the future tropical field work, it was concluded therefore that both sensors should only now output direct CO_2.

The diel period in September in Caol Scotnish encompassed approximately 13.5 hours of daylight and approximately 10.5 hours of darkness. In this cycle, sunset was at 19:28 at the beginning of the week and 19:20 by the end of the field week. Dusk occurred at 20:05 from the start of the week to 19:57 from the start at the end of the field week. Dawn was at 06:26 at the start of the week to 06:34 at the end of the week. Sunrise was at 07:03 at the start of the week and at 07:11 at the end of the week.

From the time series shown in Figure 4.31, as with the July deployment, it is clear that the dominant driver behind the patterns seen with the variables monitored in Caol Scotnish was tidal (with perhaps the only exception being Chl). In this area, the tide is reasonably large with a total difference from low to high tide on average being 1.36m. The tidal pattern is semi-diurnal. The depth of water above the sensor ranged from 4.42m (minimum low tide) to 5.78m (maximum high tide).

The pH in Caol Scotnish is highly influenced by tidal activity but also to a lesser extent has some superimposition with diel signals. The pH cyclical fluctuation in the deployment was from 8.03 to 8.19 (ΔpH = 0.16) with a daily pH mean of 8.097 and a nightly pH mean of 8.087. The pH pattern is mainly influenced by tidal action before any biological activity can be seen in the cycle. If a flood tide overlaps with the night cycle when you would expect low pH due to biological respiration, the pH increases and suggests that the flood tide brings higher pH water into the area. The pH reaches a peak whenever there is a flood tide. There are also pH lows during daylight hours (when highs should be expected if soley governed by biological factors due to photosynthesis) but higher pH waters are then introduced with the flood tide. The pH pattern therefore is driven mostly by the tides in the area and diel cycles are concealed when looking at the time series (biological processes can still be seen but in a secondary capacity).

The DO cyclical fluctuation over the course of the deployment was from 89.6% to 105.3% (ΔDO = 15.7%) with a daily DO mean of 97.86% and a nightly mean of 95.73%. Like the pH, the DO in September in Caol Scotnish followed a similar

correlation with tidal action. The DO has a very similar pattern to pH where DO peaks and troughs are mostly governed by the tidal action, with DO increasing with each flood tide. Again, likely biological activity would also be in the area but comes very much secondary to the influence of tides.

In Caol Scotnish, a chlorophyll sensor (on the YSI EXO2 Sonde) was only used in the September deployment and therefore no comparisons can be made between the two field trips in the area (it is used again however in Chapter 5 in the tropical deployment). The chlorophyll content varied from 0.64 µg/L to 7.9 µg/L (ΔChl = 7.26 µg/L) with a daily mean of 2.97 µg/L and a nightly mean of 4.03 µg/L. The time series of chlorophyll in Caol Scotnish shows that it is heavily correlated with light/dark cycles and shows a predominantly diel cycle. Unusually, the chlorophyll concentration (which can be used as a proxy for phytoplankton content of the water) is higher at night than it is during the day. During the day, the concentration of chlorophyll was lower than over the dark period. Light stimulates calcification in most calcareous algae (Borowitzka, 1981) and low chlorophyll concentrations during the day in Caol Scotnish may be due to calcification (Nakano and Watanabe, 2005). There will likely be extensive calcification in the area due to the large maerl beds. This could also be due however, to sun-induced quenching during the day. The chlorophyll concentration in Caol Scotnish reaches a maximum approximately around midnight. The lowest concentration occurs in the daylight period at approximately 13:00 hours. This scenario has been documented in previous work (Yentsch and Ryther, 1957; Ichimura, 1960; Glooschenko *et al.*, 1972; Le Bouteiller and Herbland, 1982) and pigment bleaching was suggested as being the driver for these low chlorophyll concentrations in the daylight cycle. The steady decrease from the maximum over the night cycle may be because of the chlorophyll cells becoming degraded in energy (Glooschenko *et al.*, 1972). Reasons as to why chlorophyll can be at its lowest concentration over the light period and reach a peak in the dark period include large light intensities causing bleaching of the pigment (Glooschenko *et al.*, 1972) and/or the photo-oxidation of pigment (Yentsch and Scagel, 1958). Depending on the accumulation and subsequent metabolism, this can create diel changes in the immediate chlorophyll content of cells of phytoplankton (Glooschenko *et al.*, 1972; Owens *et al.*, 1980). There could also be changes in the biomass of the phytoplankton

present due to the cycle of phytoplankton being grazed on by zooplankton (McAllister, 1963; Wood and Corcoran, 1966). Another factor could possibly be changes in water masses in the area although in this case, chlorophyll does not seem to be correlated to the tides. Temperature driven effects on chlorophyll in this field run seem to be negligible as similar temperatures in the day and night cycle had drastically different chlorophyll values and do not correlate. These different scenarios can make the interpretation of chlorophyll records complex but lends usefulness to interpreting the pattern that has been recorded in Caol Scotnish.

The temperature profile ranged from 14.67 ^{o}C to 15.55 ^{o}C (ΔT = 0.88 ^{o}C) with a daily mean of 15.09 ^{o}C and a nightly mean of 15.18 ^{o}C. The temperature is strongly correlated with the tides and is dictated by changes in water masses and not connected to insolation. As with the July deployment, lower temperature water masses were brought in with the flood tide.

The salinity ranged from from 32.45 psu to 33.16 psu (Δsal = 0.71 psu) with a daily mean of 32.73 psu and a nightly mean of 32.70 psu. Loch Sween is comparatively shallow and narrow and runoff combined with rainfall may keep the waters fresher than the main body of the loch. In September, there was increasing rainfall over the duration of the deployment and this appears to have affected the salinity. Monday and Tuesday had little rainfall but the most rainfall came over night on Tuesday and continued on through into late Wednesday/very early Thursday. It became much drier on Thursday with no rainfall and only sunshine. The increased rainfall over night on Tuesday and Wednesday/night is possibly the reason for the much smaller change in salinity in the middle of the run. On the drier period, there is a bigger fluctuation in the salinities with the action of the tide. The rainfall appears to act as a ‘buffer’ in diluting the higher salinity bodies of water that come into Caol Scotnish with high tide. Again, when it becomes drier at the end of the run, the salinity fluctuates slightly more than when there was heavy rainfall. Again, there is an obvious correlation with the tides and there is generally an increase in salinity with a flood tide. Salinity is further discussed in Section 4.7.4 page 215.

The pCO_2 fluctuated from 449.34 µatm to 464.41 µatm (ΔpCO_2 = 15.07 µatm) with a daily pCO_2 mean of 456.14 µatm and a nightly mean of 456.89 µatm. The pCO_2 is mainly governed by the tides but simultaneously has patterns of biological activity. Generally at night there is an increase in pCO_2 with biological respiration but also during the day there is an increase in pCO_2 with the flood tide that enters the area. This appears to be a more complex combination of both diel and tidal influences.

Some general comments are warranted before looking at correlations in more detail. Over the first day and night cycle, there is not the clear pattern that would be expected over the diel period. The pH and DO almost flatten out compared to the fluctuations over the remainder of the deployment. The opposite is true of salinity, temperature and depth in that there is a more pronounced difference from maximum to minimum over the first full day/night cycle compared to the rest of the cycle. The high tide between dawn and sunrise does not bring a large amount of oxygen into the area. This could mean other influences are acting on the DO. This part of the cycle has different water masses entering the area with the tides at this time (see Figure 4.31). These water masses contain a lower amount of oxygen. Parameters in Caol Scotnish, due to the topography and hydrography of the area, are dependent on the tide to a comparatively high extent (compare with Chapter 5 dealing with tropical field work in the Red Sea). Caol Scotnish is not a stratified water column and has different inputs that will affect the amount of DO in the body of the water. This highlights the many factors involved in characterising the water chemistry of highly mixed, dynamic coastal areas and that it is not a straightforward, simple task especially when looking at just two parameters (Rerolle *et al.*, 2014).

4.7.3.1.1 Drivers of variation in Caol Scotnish 19th to 23rd September 2016

Over the course of this deployment, the tides were the principal driving force behind the patterns in pCO_2 and most variables in Caol Scotnish. Caol Scotnish displayed strong tidal influences and any diel patterns were usually superseded by this (with a few exceptions). The tides introduced different bodies of water into Caol Scotnish. Depth was recorded for the duration of the deployment, i.e. the height of water above the sensor was measured and this provided a proxy for

tidal action. Paired variables were analysed and the most correlated are shown overleaf. The strongest correlations are visibly seen with the parallel time series and quantified through Pearson's correlation coefficient (and simultaneously with equations of a straight line). Analyses was centred around tidal (flood tide is represented in pink) and diel (night is represented in grey) patterns over the course of the deployment of the sensors. PCA was also conducted to support the previous analyses.

4.7.3.1.1.1 Variables driven by the tide

4.7.3.1.1.1.1 DO and pH

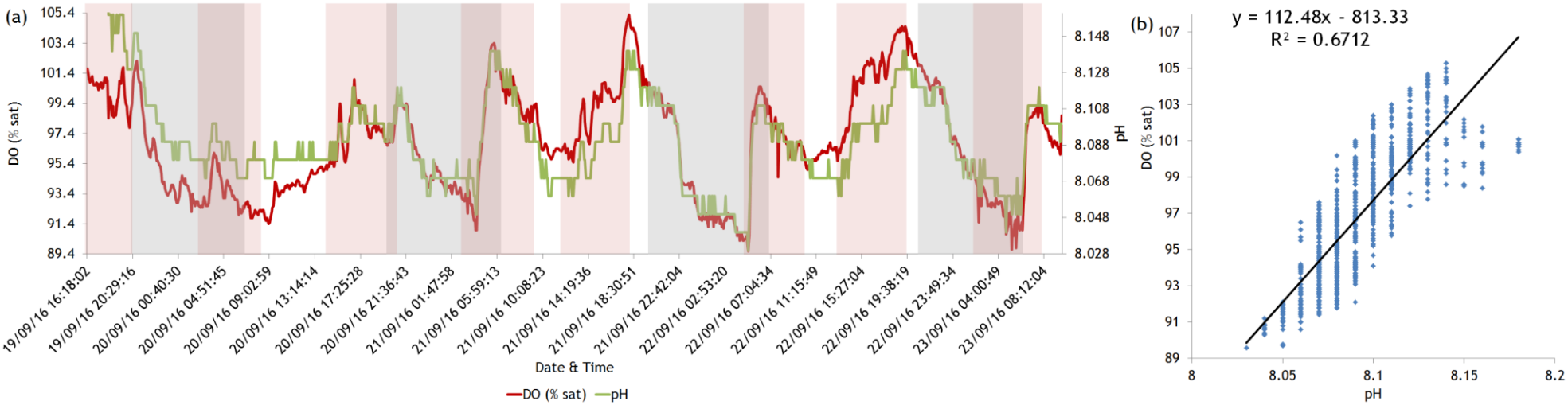

Figure 4.33: (a) parallel time series of DO and pH in Caol Scotnish from 19th to 23rd September 2016 encompassing day (no shade), night (grey shade) and flood tide (pink shade). DO; Mean = 96.8 ± 3.44 %sat. pH; Mean = 8.09 ± 0.03. (b) scatter graph of DO and pH with linear trendline. Coefficient of determination; R^2 = 0.67. Pearson correlation coefficient; r = 0.82. p < 0.001.

The parallel time series of DO and pH in Caol Scotnish is shown in Figure 4.33a. There was a significant positive correlation between DO and pH ($r = 0.82$) as shown in figure 4.33b. DO and pH are highly governed by the tides with both variables increasing with the flood tide. There is also the possibility of diel patterns being present (daytime increase of DO through photosynthesis, night-time decrease of DO through respiration) but only secondary to overwhelming tidal influence.

4.7.3.1.1.1.2 Depth and Salinity

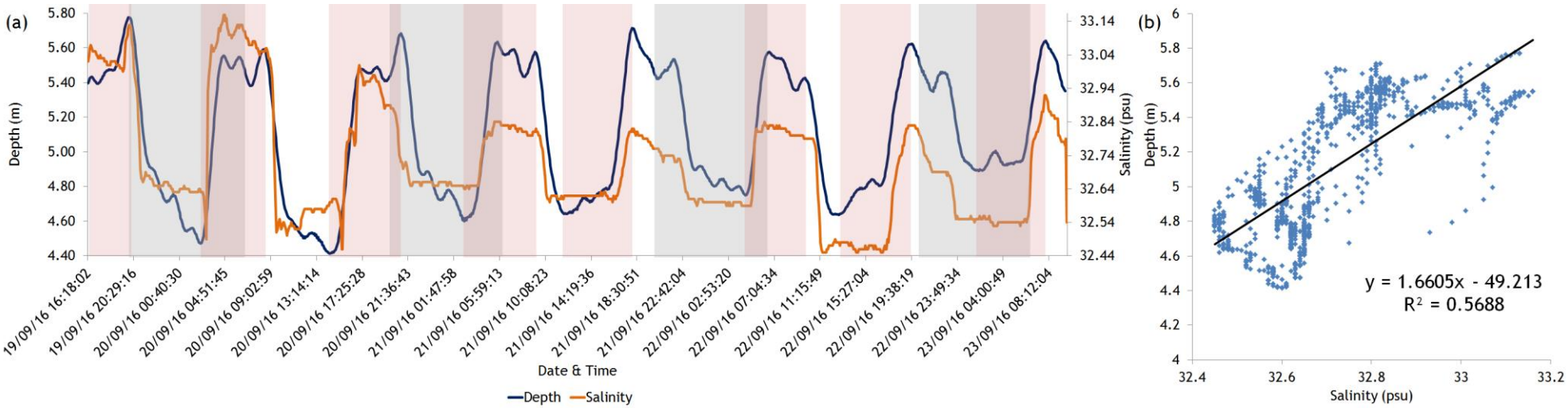

Figure 4.34: (a) parallel time series of tidal action and salinity cycle in Caol Scotnish from 19th to 23rd September 2016 encompassing day (no shade), night (grey shade) and flood tide (pink shade). Depth; Mean = 5.11 ± 0.38 m. Salinity; Mean = 32.71 ± 0.17 psu. (b) scatter graph of depth and salinity with linear trendline. Coefficient of determination; R^2 = 0.57. Pearson correlation coefficient; r = 0.75. p < 0.001.

The parallel time series of tidal action and salinity in Caol Scotnish is shown in Figure 4.34a. There was a significant positive correlation between tidal action and salinity ($r = 0.75$, $p < 0.001$) as shown in Figure 4.34b. The salinity was heavily influenced by the tidal action in the area and would generally increase in concentration with each flood tide. This would suggest higher salinity waters being introduced into the area with the incoming tide.

4.7.3.1.1.1.3 Depth and temperature

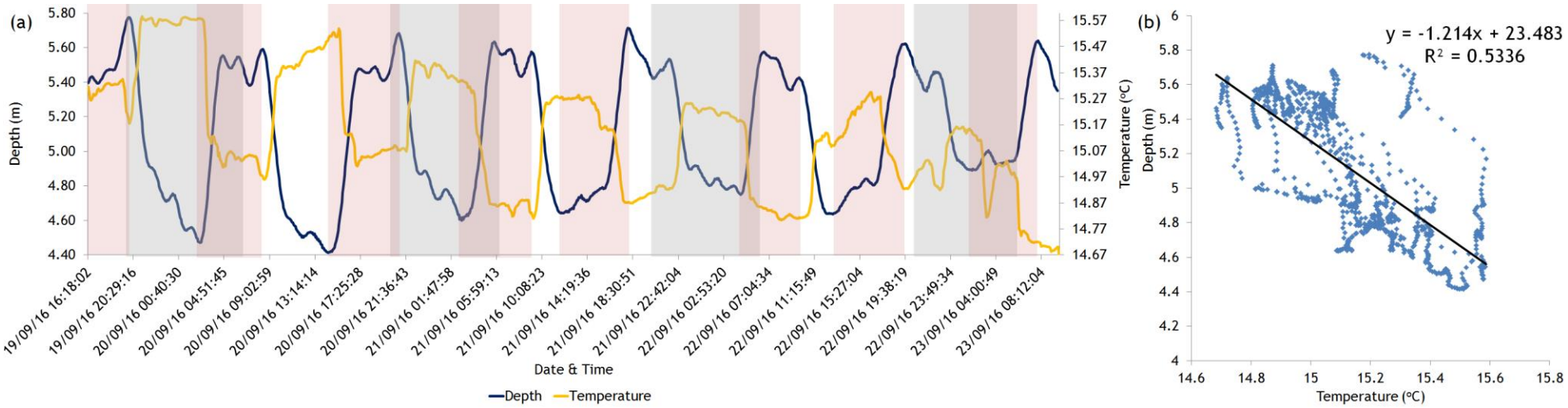

Figure 4.35: (a) parallel time series of tidal action and temperature in Caol Scotnish from 19th to 23rd September 2016 encompassing day (no shade), night (grey shade) and flood tide (pink shade). Depth; Mean = 5.11 ± 0.38m. Temperature; Mean = 15.13 ± 0.23 °C. (b) scatter graph of depth and temperature with linear trendline. Coefficient of determination; R^2 = 0.53. Pearson correlation coefficient; r = -0.73. p < 0.001.

The parallel time series of tidal action and temperature in Caol Scotnish is shown in Figure 4.35a. There was a significant inverse correlation between depth and temperature (r = -0.73) as shown in Figure 4.35b.

Temperature in Caol Scotnish is influenced more by tides rather than insolation. The greater influence of the tides is shown with the sharp temperature drops during the day which tallies the tides. There are also sharp increases in temperature in the night cycle which corresponds with the tides. The nightly mean on both deployments was higher than the daily mean and there are similar highs and lows of temperatures both in the day and the night cycle. The pattern of these two parameters suggests that the flood tide brings in bodies of water that are colder than existing water.

4.7.3.1.1.1.4 Depth and pH

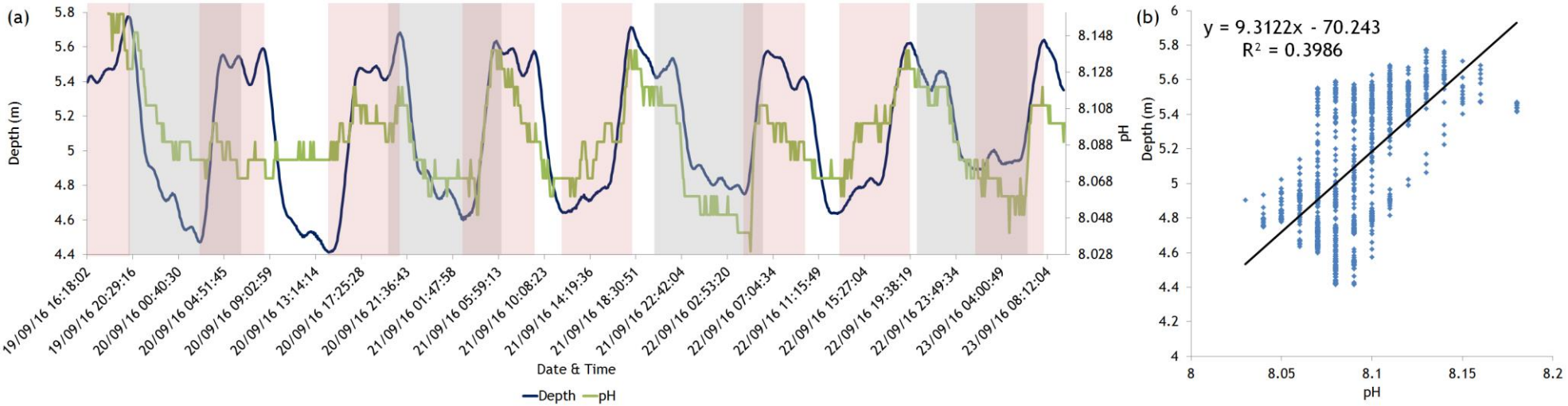

Figure 4.36: (a) parallel time series of tidal action and pH in Caol Scotnish from 19th to 23rd September 2016 encompassing day (no shade), night (grey shade) and flood tide (pink shade). pH; Mean = 8.09 ± 0.03. Depth; Mean = 5.11 ± 0.38 m. (b) scatter graph of depth and pH with linear trendline. Coefficient of determination; R^2 = 0.40. Pearson correlation coefficient; r = 0.63. p < 0.001.

The parallel time series of tidal action and pH is shown in Figure 4.36a. There is a significant positive correlation ($r = 0.63$, $p < 0.001$) as shown in Figure 4.36b. pH is heavily regulated by the tides. With the introduction of the flood tide into the area, the pH concentration increased. In addition, there may also be biological activity governing the pH pattern in places (i.e., night-time decrease of pH due to respiration and daytime increase of pH due to photosynthesis) but this again, as with other parameters, was overshadowed by the action of the tide.

4.7.3.1.1.1.5 Depth and DO

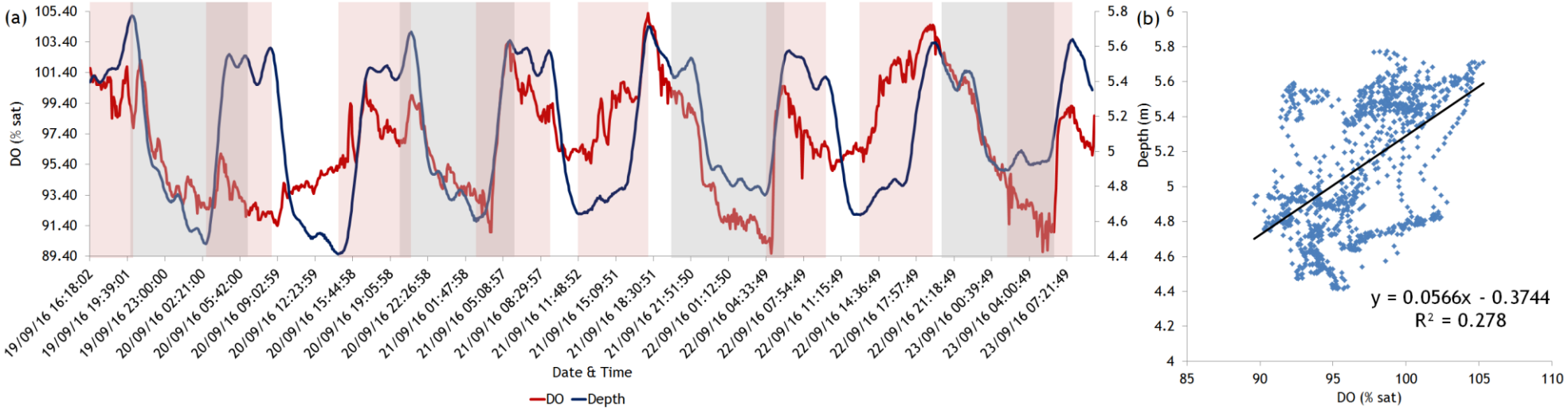

Figure 4.37: (a) parallel time series of tidal action and DO in Caol Scotnish from 19th to 23rd September 2016 encompassing day (no shade), night (grey shade) and flood tide (pink shade). Depth; Mean = 5.11 ± 0.38 m. DO; Mean = 96.8 ± 3.44 %sat. (b) scatter graph of depth and pH with linear trendline. Coefficient of determination; R^2 = 0.28. Pearson correlation coefficient; r = 0.53. p < 0.001.

The parallel time series of tidal action and DO in Caol Scotnish in September is shown in Figure 4.37a. There is a significant positive correlation between the tide and DO as shown in Figure 4.37b ($r = 0.53$, $p < 0.001$). With the flood tide, the DO would generally increase. As with pH, biological diel patterns within DO are overshawdowed by the strong tidal action in the area.

4.7.3.1.1.1.6 Salinity and pH

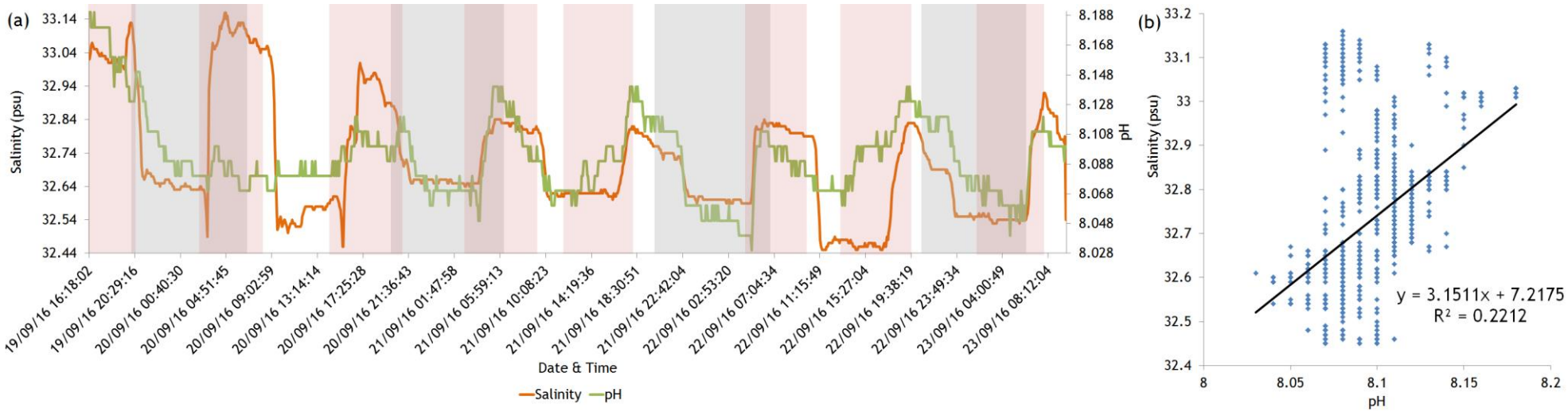

Figure 4.38: (a) parallel time series of salinity and pH in Caol Scotnish from 19th to 23rd September 2016 encompassing day (no shade), night (grey shade) and flood tide (pink shade). Salinity; Mean = 32.71 ± 0.17 psu. pH; Mean = 8.09 ± 0.03. (b) scatter graph of salinity and pH with linear trendline. Coefficient of determination; R^2 = 0.22. Pearson correlation coefficient; r = 0.47. p < 0.001.

The parallel time series of salinity and pH in Caol Scotnish is shown in Figure 4.38a. There is a significant positive correlation between salinity and pH ($r = 0.47$, $p < 0.001$) as shown in Figure 4.38b. Both variables are governed by the tide with an incoming tide increasing both the pH and the salinity. There are some possible pH diel patterns superimposed (perhaps over the first night cycle) but it is the tidal cycle predominantly forcing the pattern seen in Caol Scotnish.

T-S (temperature – salinity) diagrams can be used as a water mass tracer and this method is employed in the next section.

4.7.3.1.1.1.7 Temperature and salinity

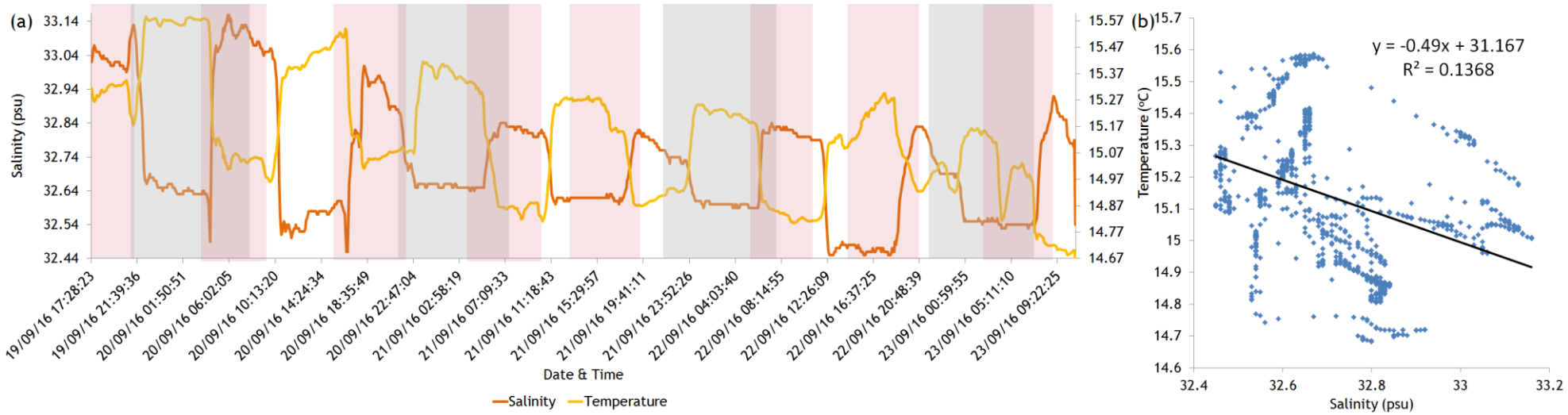

Figure 4.39: (a) parallel time series of temperature and salinity in Caol Scotnish from 19th to 23rd September 2016 encompassing day (no shade), night (grey shade) and flood tide (pink shade). Temperature; Mean = 15.13 ± 0.23 °C. Salinity; Mean = 32.71 ± 0.17 psu. (b) scatter graph of temperature and salinity with linear trendline. Coefficient of determination; R^2 = 0.14. Pearson correlation coefficient; r = -0.37. p < 0.001.

The parallel time series of temperature and salinity in Caol Scotnish in September is shown in Figure 4.39a. There is a significant inverse correlation between the two variables ($r = -0.37$, $p < 0.001$) as shown in Figure 4.39b. The T-S plot shows small temperature variations associated with certain salinities. There were clear water mass exchanges with a tidal cycle.

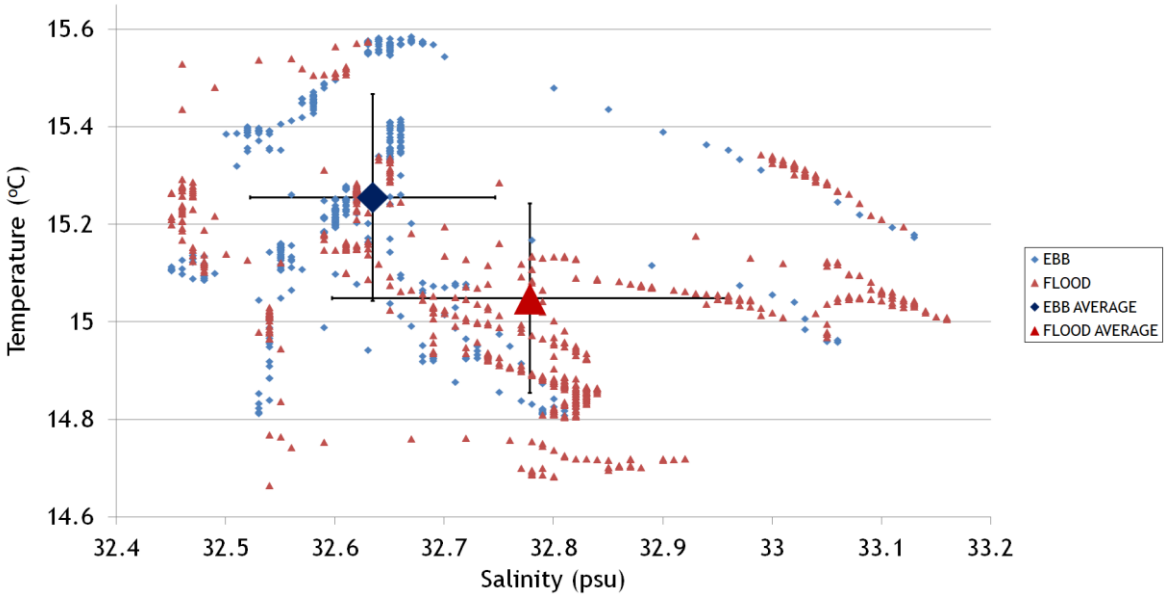

Figure 4.40: T-S diagram showing flood tide and ebb tide according to their temperature and salinity properties. Average ebb tide: Salinity = 32.634 ± 0.112 psu, Temperature = 15.26 ± 0.21 ^{o}C, Average flood tide: Salinity = 32.778 ± 0.181 psu, Temperature = 15.05 ± 0.19 ^{o}C.

Looking closely at the T-S diagram, it is possible to separate out flood and ebb tides by their temperature and salinity properties (see Figure 4.40). As with the July deployment in Caol Scotnish, this shows that on average, higher salinity and colder temperatures are brought in by the flood tide.

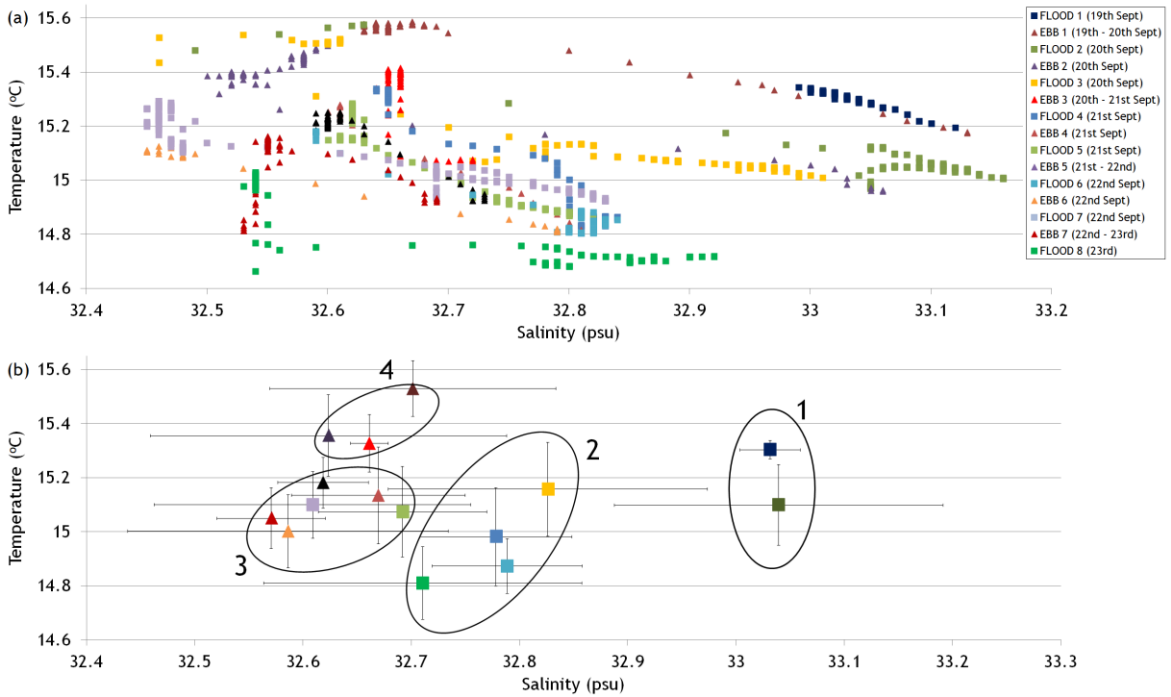

Figure 4.41: (a) T-S diagram showing each flood and ebb tide over the deployment in Caol Scotnish on 19th to 23rd September 2016 according to their temperature and salinity properties. (b) Average; Flood 1: Salinity = 33.031 ± 0.028 psu, Temperature = 15.30 ± 0.03 °C. Ebb 1: Salinity = 32.701 ± 0.132 psu, Temperature = 15.53 ± 0.10 °C. Flood 2: Salinity = 33.039 ± 0.152 psu, Temperature = 15.10 ± 0.15 °C. Ebb 2: Salinity = 32.623 ± 0.163 psu, Temperature = 15.36 ± 0.15 °C. Flood 3: Salinity = 32.826 ± 0.147 psu, Temperature = 15.16 ± 0.17 °C. Ebb 3: Salinity = 32.661 ± 0.017 psu, Temperature = 15.33 ± 0.12 °C. Flood 4: Salinity = 32.778 ± 0.070 psu, Temperature = 14.98 ± 0.18 °C. Ebb 4: Salinity = 32.669 ± 0.080 psu, Temperature = 15.14 ± 0.18 °C. Flood 5: Salinity 32.692 ± 0.078 psu, Temperature = 15.07 ± 0.17 °C. Ebb 5: Salinity = 32.618 ± 0.042 psu, Temperature = 15.18 ± 0.09 °C. Flood 6: Salinity = 32.788 ± 0.069 psu, Temperature = 14.87 ± 0.10 °C. Ebb 6: Salinity = 32.586 ± 0.148 psu, Temperature = 15.00 ± 0.14 °C. Flood 7: Salinity = 32.609 ± 0.146 psu, Temperature = 15.1 ± 0.12 °C. Ebb 7: Salinity = 32.571 ± 0.050 psu, Temperature = 15.05 ± 0.11 °C. Flood 8: Salinity = 32.710 ± 0.147 psu, Temperature = 14.81 ± 0.13 °C. Separate water masses are shown in individual circles.

Going further, as shown in Figure 4.41a, each colour represents each different flood and ebb tide in the deployment. The first two flood tides of the deployment had very similar properties of high salinity and higher temperatures and Figure 4.41b shows that they may belong to their own separate water mass. It is also evident that there were 4 separate water masses in Caol Scotnish over this deployment with. The flood tides are generally colder than the ebb tides.

Water mass	Salinity (psu)	Temperature (°C)	Water Type
1 (Flood 1, 2)	32.49 - 33.16 (μ = 33.036)	14.96 - 15.58 (μ = 15.18)	highest salinity, high-middling temperature
2 (Flood 3, 4, 6, 8)	32.46 - 33.01 (μ = 32.777)	14.67 - 15.54 (μ = 14.97)	high-middling salinity, lowest temperature
3 (Ebb 4, 5, 6, 7 & Flood 5, 7)	32.45 - 32.83 (μ = 32.629)	14.81 - 15.29 (μ = 15.09)	lowest salinity, middling-low temperature
4 (Ebb 1, 2, 3)	32.50 - 32.72 (μ = 32.663)	15.07 - 15.59 (μ = 15.41)	lower salinity, highest temperature

Table 4.7: Different water mass properties in Caol Scotnish on 19th – 23th September 2006.

Water masses were separated into specific T-S properties as shown in Table 4.7. Water mass 1 had the highest salinity with high-middling temperature. Water mass 2 contained flood tides that had the properties of high-middling salinity with the lowest temperatures. Water mass 3 contained mostly ebb waters (with the exception of the fifth flood tide and the seventh flood tide which also had these properties) which were of the lowest salinity and a middling-low temperature. Lastly, water mass 4 contained solely ebb tides with the properties of lower salinity and the highest temperatures.

The general pattern in September was similar to that of July. The flood tide would be a high salinity which would ebb to a lower salinity. Most likely due to precipitation and runoff as it is a wet area. The next flood tide would bring in higher salinity waters which again would then ebb to lower salinity waters. This

pattern was consistent throughout where each tide can be followed with each coloured data point.

4.7.3.1.1.1.8 pH and pCO_2

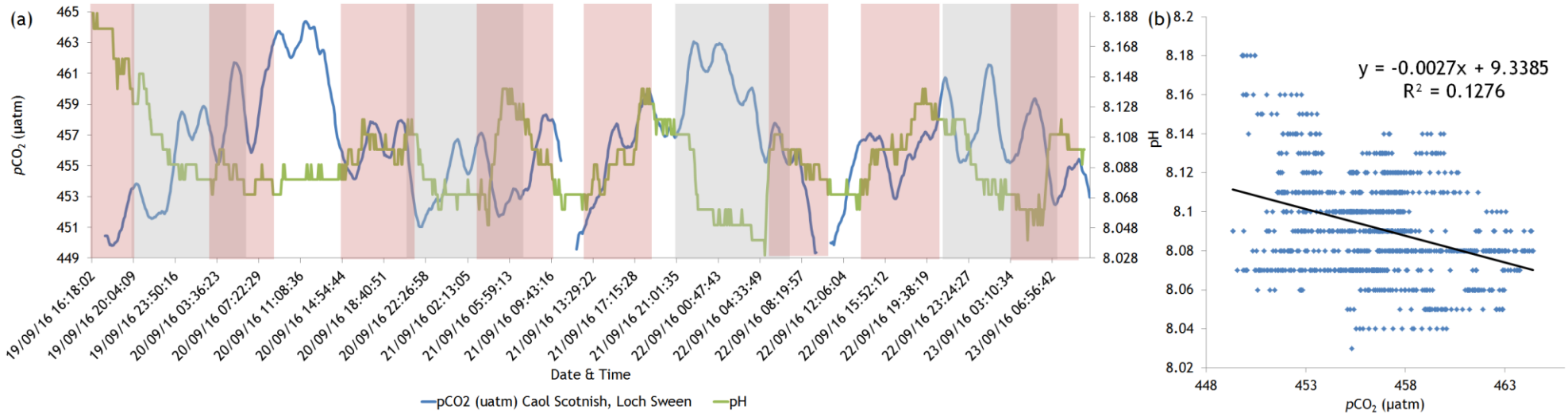

Figure 4.42: (a) parallel time series of pH and pCO_2 in Caol Scotnish from 19th to 23rd September 2016 encompassing day (no shade), night (grey shade) and flood tide (pink shade). pH; Mean = 8.09 ± 0.03. pCO_2; Mean = 457 ± 3.33 µatm. There are gaps in the pCO_2 data because of sensor maintenance during deployment. (b) scatter graph of pH and pCO_2 with linear trendline. Coefficient of determination; R^2 = 0.13. Pearson correlation coefficient; r = -0.36. p < 0.001.

The parallel time series of pH and pCO_2 is shown in Figure 4.42a. There is a significant inverse correlation between the two parameters ($r = -0.36$, $p < 0.001$) as shown in Figure 4.42b. These two parameters were governed by the tide but also showed some micro-patterns of biologically forced activity. However, as mentioned, those patterns are generally either diminished or hidden by the overwhelming dominance of tidal action. The pCO_2 has no obvious diel cycle and is perhaps more driven by tides but it is likely that both tides and diel cycles are superimposed within the pCO_2 pattern which is a complex one.

4.7.3.1.1.1.9 DO and pCO_2

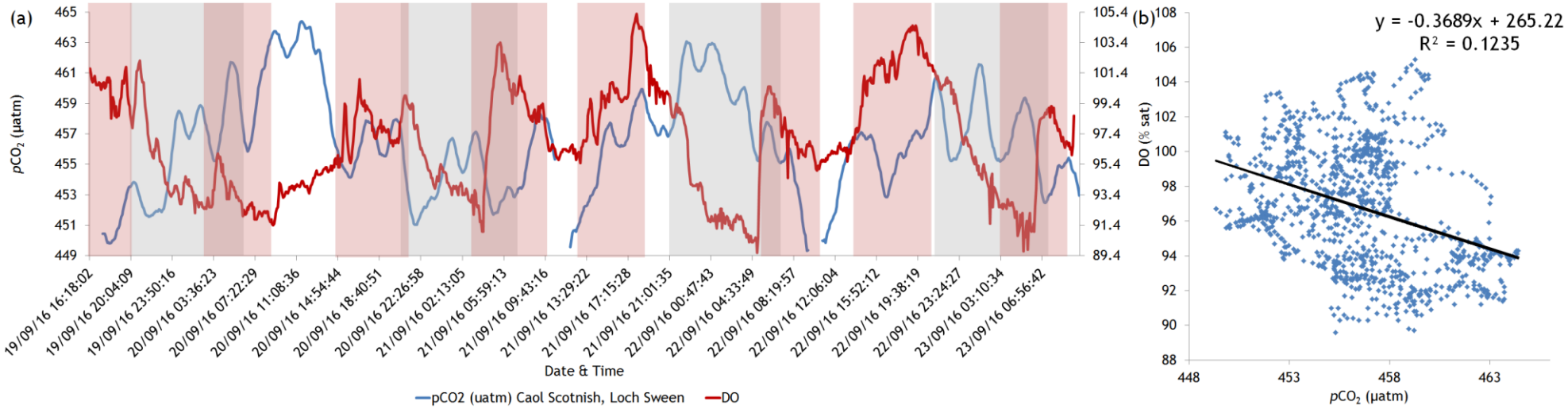

Figure 4.43: (a) parallel time series of DO and pCO_2 in Caol Scotnish from 19th to 23rd September 2016 encompassing day (no shade), night (grey shade) and flood tide (pink shade). DO; Mean = 96.8 ± 3.44 %sat. pCO_2; Mean = 457 ± 3.33 µatm. There are gaps in the pCO_2 data because of sensor maintenance during deployment. (b) scatter graph of DO and pCO_2 with linear trendline. Coefficient of determination; R^2 = 0.12. Pearson correlation coefficient; r = -0.35. p < 0.001.

The parallel time series of DO and pCO_2 in Caol Scotnish is shown in Figure 4.43a. There is a significant negative correlation between DO and pCO_2 ($r = -0.35$, $p < 0.001$) as shown in Figure 4.43b. DO and pCO_2 are both influenced by both tidal and biological processes but the dominant pattern is driven by the tides.

4.7.3.1.1.1.10 Temperature and DO

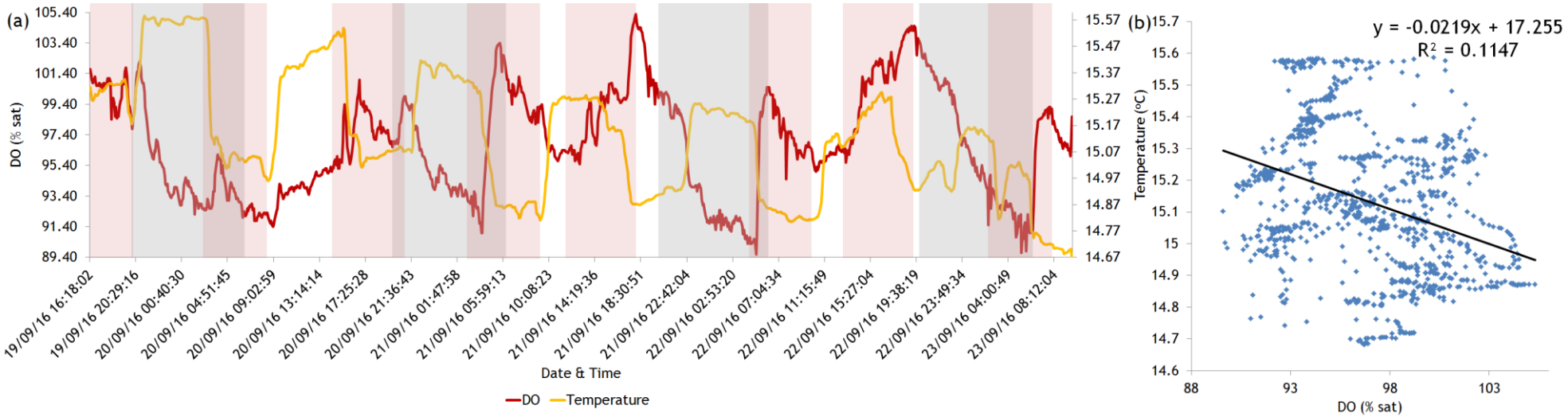

Figure 4.44: (a) parallel time series of temperature and DO in Caol Scotnish from 19th to 23rd September 2016 encompassing day (no shade), night (grey shade) and flood tide (pink shade). Temperature; Mean = 15.13 ± 0.23 °C. DO; Mean = 96.8 ± 3.44 %sat. (b) scatter graph of temperature and DO with linear trendline. Coefficient of determination; R^2 = 0.11. Pearson correlation coefficient; r = -0.34. p < 0.001.

The parallel time series of temperature and DO in Caol Scotnish is shown in figure 4.44a. There is a significant inverse correlation between temperature and DO ($r = -0.34$, $p < 0.001$) as shown in figure 4.44b. Temperature is driven by the tide as is DO but DO may also contain micro-patterns forced by biological activity.

4.7.3.1.1.1.11 Chlorophyll and pCO_2

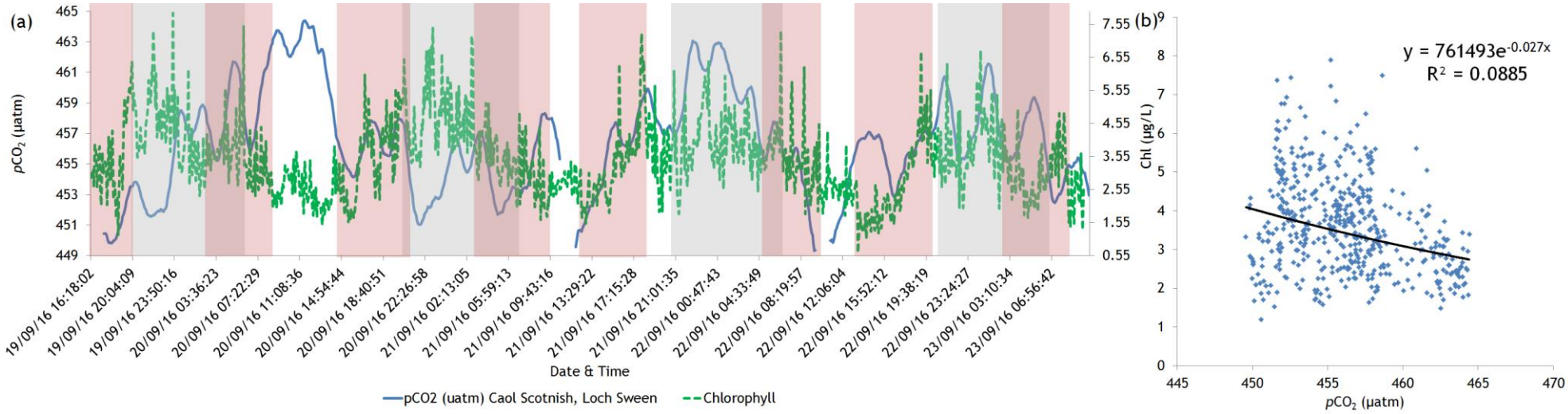

Figure 4.45: (a) parallel time series of Chl and pCO_2 in Caol Scotnish from 19th to 23rd September 2016 encompassing day (no shade), night (grey shade) and flood tide (pink shade). Chl; Mean = 3.48 ± 1.16 µg/L. pCO_2; Mean = 457 ± 3.33 µatm. There are gaps in the pCO_2 data because of sensor maintenance during deployment. (b) scatter graph of Chl and pCO_2 with linear trendline. Coefficient of determination; R^2 = 0.09. Pearson correlation coefficient; r = -0.30. p < 0.001.

The parallel time series of chl and pCO_2 in Caol Scotnish is shown in Figure 4.45a. There was a significant inverse correlation between chl and pCO_2 in Caol Scotnish ($r = -0.30$, $p < 0.001$) as shown in Figure 4.45b.

The time series shows that chl has a diel pattern which is at a maximum at night and a minimum during the day. pCO_2 shows a mainly tidal influence but also could have micro-patterns of biological forcing. As mentioned previously, the first third of the pCO_2 time series appears to be the opposite of the last two-thirds of the run. With lower concentrations of chl, there should be lower take-up of the pCO_2 by phytoplankton and therefore higher concentrations of pCO_2 in the surrounding waters (Litt *et al.*, 2010). Overall, chl in Caol Scotnish was not correlated with any parameter other than the pCO_2.

4.7.3.2 Principal Component Analysis (PCA)

As a further statistical investigation, PCA was conducted on the data from Caol Scotnish in September. The resulting correlation circle is shown in Figure 4.46.

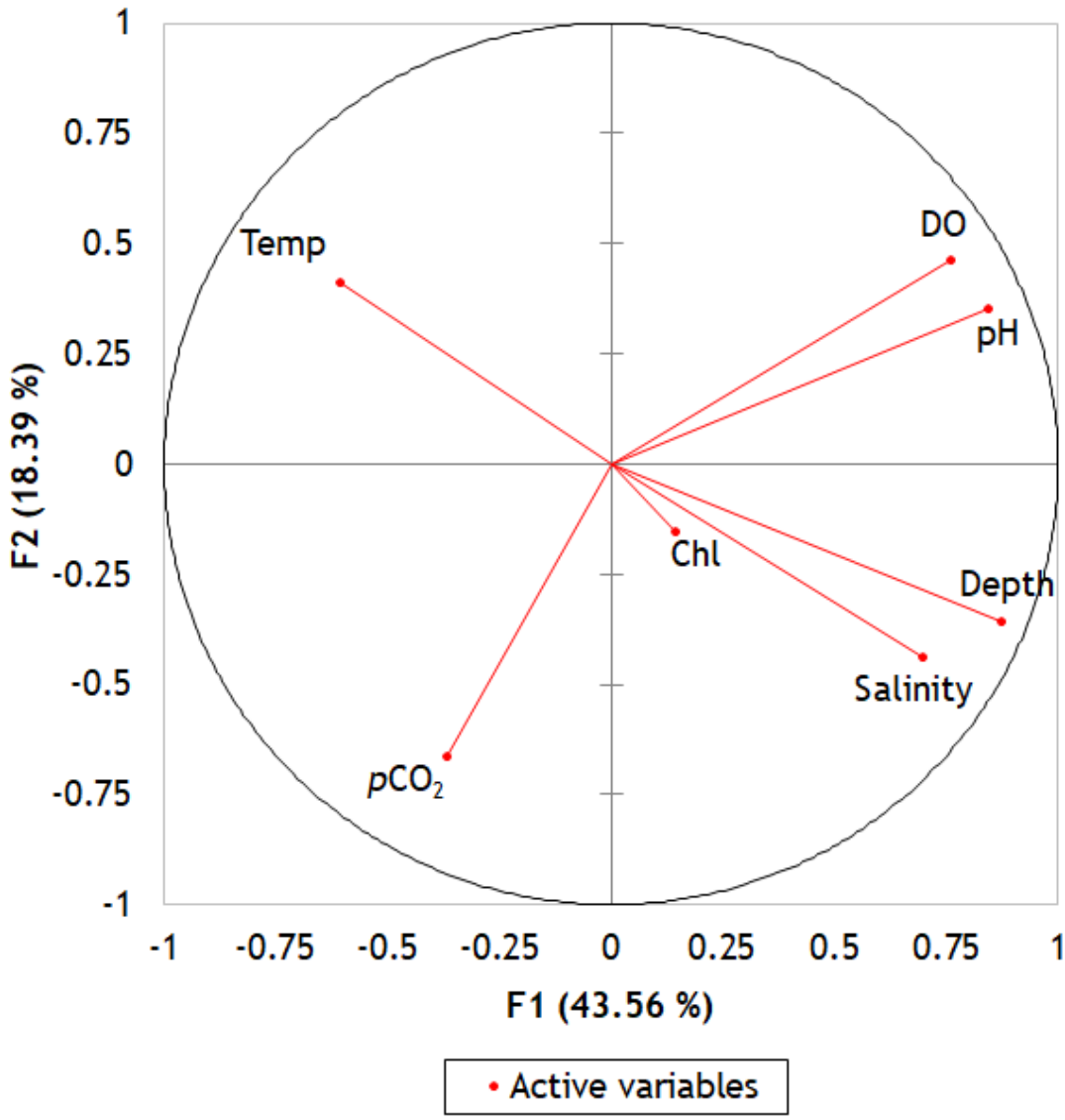

Figure 4.46: PCA showing the correlation circle from Caol Scotnish in September. If two variables are far from the centre and close to one another then they are positively significantly correlated. If two variables are orthogonal to one another then they are not related. If two variables are on opposite sides of the centre then they are negatively significantly correlated. From PCA analysis Chl is not related to any other variable.

PCA confirms the previous analyses and Figure 4.46 can be summarised as follows in Table 4.8 (which can also be used as a summary of the previous analyses).

Positively significantly correlated	Not correlated	Negatively significantly correlated
DO & pH (r = 0.82)	Chl & DO (0.00)	Depth & Temperature (-0.73)
Depth & Salinity (r = 0.75)	Chl & pCO_2 (-0.03)	Temperature & Salinity (-0.37)
Depth & pH (r = 0.63)	Chl & pH (0.09)	pH & pCO_2 (-0.36)
Depth & DO (0.53)	Salinity & pCO_2 (-0.09)	pCO_2 & DO (-0.35)
Salinity & pH (0.47)	Temperature & pCO_2 (0.03)	DO & Temperature (-0.34)
	Depth & pCO_2 (-0.11)	
	Chl & Temperature (0.12)	
	Chl & Depth (0.16)	
	DO & Salinity (0.17)	
	Chl & Salinity (0.2)	

Table 4.8: Correlated and non-correlated variables in Caol Scotnish in September according to PCA.

4.7.4 Further Discussion

4.7.4.1 Tidal influence

The tides have a strong positive correlation with pH and DO (with a flood tide there is an increase in pH and DO) and a strong negative correlation with temperature (with a high tide there is a decrease in temperature). In September, there is a strong positive correlation between the salinity and tides (this correlation is absent in July). It is difficult to separate all of these variables and pinpoint the exact drivers. pH, DO and pCO_2 are driven by biological activity which is driven by day/night cycles which are also correlated with tides. However, pH, DO and pCO_2 are also influenced by atmospheric processes, tide and current control and biological control all at the same time. It would be erroneous to say that tides are the only influence on the parameters in Caol Scotnish but that the tides overwhelmingly contribute to driving and forcing of specific parameters. The tides have an influence on most parameters monitored in this field run in Caol Scotnish. However, when the tide is not the main driver, biological activity will be the predominant influence. It is therefore conclusive to say that the patterns are not consistent in the site and the main drivers can alternate. This demonstrates the challenging nature of determining the exact drivers of different parameters in coastal chemistry. This is mainly due to the simultaneous forcing which can enhance or inhibit patterns within the different parameters. For example, pH, DO and pCO_2 are all driven by biological activity which is, in turn, driven by day/night cycles which are also correlated with the

tides (although not always). pH, DO and pCO_2 are also influenced by atmospheric processes, tide and current control and biological control all at the same time. These features will also overlap and happen simultaneously and therefore it is difficult to reduce it to single drivers especially on this time scale. Parameters cannot be looked at in an isolated manner.

The solubility of gases is affected by the salinity (Lange *et al.*, 1972; Libes, 1992; Litt *et al.*, 2010). Overall, the salinity in July is most highly correlated with DO and temperature. It has a positive correlation and a negative correlation respectively (as DO increases, salinity increases and as temperature increases, salinity decreases). Although correlation analysis does not point to a strong relationship between salinity and tides in July (there is a strong correlation between salinity and tides in September), there is a subtle salinity change with the tides but this may have been buffered by the increasing rainfall over the duration of the deployment and therefore no strong statistical correlation was identified. Overall, the salinity in Caol Scotnish in September is most highly correlated with pH, temperature and depth.

Temperature also governs the solubility of gases in a body of water. In both deployments, temperature and DO had an inverse relationship, i.e. as the temperature goes up, the concentration of DO will decrease. However, pCO_2 in Caol Scotnish also showed a positive relationship which does not follow the typical inverse relationship between gases and temperature. In September, unusually the temperature and pCO_2 do not appear to be correlated. This is due to the relationships between all the forcing factors in Caol Scotnish. Temperature on this deployment may be correlated but other drivers may also be affecting the patterns between the two parameters (although pCO_2 was correlated with temperature in July, it has an unusual positive pattern and is perhaps more influenced by other variables).

The temperature in July is most highly correlated with the tides (inverse correlation) and is also negatively correlated with the pH, DO and salinity (when temperature is raised, pH, DO and salinity are lowered) and has a positive correlation with pCO_2 (when temperature is higher, pCO_2 is also higher). There was increasing seawater temperature overnight which would suggest the temperature is driven by the tides and perhaps not directly correlated with pCO_2

in either deployment. Analysis suggests that temperature is therefore correlated with every parameter recorded in this field run in Caol Scotnish albeit indirectly via the tides and thus water masses.

DO and salinity in Caol Scotnish in July have a positive moderate correlation. An increase of DO corresponded to an increase in salinity. However, in September correlation analysis suggests there is little explicit correlation with DO and salinity. They are both part governed by the tides and aspects like freshwater input, rainfall and runoff. They are therefore most likely not explicitly related but do have common links with other driving factors. Temperature should also be taken into account when considering this relationship. The DO in Caol Scotnish is affected by the tides (positive strong relationship) with which the salinity is also correlated. DO in Caol Scotnish had an inverse relationship with the temperature. Generally, as the temperature goes up the DO will decrease. Again, temperature is influenced by the tides as is DO so there is a complex interrelationship between these variables. Mostly however, the DO is goverend by both biological activity and tidal activity which may be superimposed on one another. Temperature is influenced by tides as is DO so there is a complex dependency relationship between these parameters and knock-on effects from multiple areas.

4.7.4.2 Biological diel influences

Although tidal action had the biggest influence on variables in Caol Scotnish meaning diel patterns were subsequently superseded, it is noteworthy to mention that micro-patterns caused by biological activity may also exist. Biological drivers such as respiration, photosynthesis, calcification and remineralisation may have also had an influence in the patterns of pCO_2 and other variables seen in Caol Scotnish in both July and September.

The pCO_2 in Caol Scotnish in July was most highly correlated with the pH and tides both having a strong inverse relationship, i.e. when pCO_2 was high, there was a low tide and a low pH. pCO_2 had a negative relationship with DO, i.e. when pCO_2 was high there was low DO. September was a similar scenario with the pCO_2 in this deployment being most highly correlated with pH and DO having a strong inverse relationship. pCO_2 is also positively correlated with chlorophyll.

Metabolic processes likely affected the pCO_2 during the course of the deployment. This includes photosynthesis, respiration, calcium carbonate precipitation or dissolution. There is an increase of pCO_2 overnight which could be due to the release of pCO_2 by organisms during respiration according to Equation 33;

$$Ca^{2+} + 2HCO_3^- \leftrightarrow CaCO_3 + CO_2 + H_2O \quad (33)$$

During the night cycle in Caol Scotnish in both July and September, the pCO_2 would increase. This is also heavily influenced by the tides.

Calcification may have also contributed to the driving of the diurnal pattern of pCO_2. Generally, under high light intensity, i.e. during daylight hours, pCO_2 should decrease when photosynthesis takes place. When CO_2 is utilised by organisms in the water column during photosynthesis, the pH is increased because of a reduction in hydrogen ions (H^+) (Lucas, 1983; Cook *et al.*, 1988; Raven, 1997). Photosynthesis and calcium carbonate dissolution decrease pCO_2 according to Equation 34;

$$106CO_2 + 16HNO_3 + H_3PO_4 + 122H_2O \quad (34)$$

$$\leftrightarrow (CH_2O)_{106}(NH_3)_{16}\,H_3PO_4 + 138O_2$$

In both deployments however, there is a peak in pCO_2 in diurnal periods. In the absence of a flood tide which would increase the pCO_2, this is could be caused by calcification which may be larger than the productivity rate of the extensive maerl bed. Calcification can happen at both night (predominantly) and day (Chisholm, 2000) and this peak in pCO_2 may perhaps be a delayed biological activity when calcification takes place. When this process happens, the surrounding chemistry of the water is changed (Odhe and van Woesik, 1999) according to;

$$2HCO_3^- + Ca^{2+} \rightarrow CaCO_3 + H_2O + CO_2 \quad (35)$$

As the deposition of $CaCO_3$ occurs, DIC is used up by organisms and although this would intuitively decrease the carbon in the water column, CO_2 and H^+ ions

are released in the process (Jokiel, 2011) and the net result is a lowering of pH and an increase of pCO_2. Therefore, the process of photosynthesis which consequently decreases the pCO_2 can be buffered by other metabolic processes like calcification. When $CaCO_3$ is created, which would mostly happen during the day when photosynthesis takes place, this can increase pCO_2 concentrations which could be the reason that the pH decreases (Zeebe and Wolf-Gladrow, 2001). Since there are extensive maerl beds in Caol Scotnish, their calcification likely affect the water chemistry. Although plausible explanations, the heavy tidal influence is likely the major driver in the observed pattern of pCO_2 with an increase of pCO_2 occuring with the flood tide. This could perhaps suggest that the pelagic pCO_2 concentration of the seawater flooding into Caol Scotnish with an incoming tide contains a higher concentration of pCO_2.

The pH and pCO_2 were significantly negatively correlated, i.e. they had an inverse relationship. When the pCO_2 increased, the pH would decrease. During the night, the pCO_2 should increase through processes such as respiration and consequently the pH is lowered (Murru and Sandgren, 2004). pH can also be lowered when organisms calcify. This process releases CO_2 and H^+ ions thereby increasing pCO_2 in the water column (Jokiel, 2011). There was also a pH low during the day which corresponded to a high pCO_2 concentration. This phenomenon is confirmed on three separate sensors (pCO_2, pH and DO) and it is thus likely to be a real phenomenon and not an anomaly in the developed sensor. As previously stated, this could be because of the formation of $CaCO_3$ during the day which may be forcing the calcification rate to be higher than the rate of photosynthesis. Respiration can also happen during the day but it is unlikely that respiration would be the net biological process in the daylight cycle. It must not be ruled out however, that other organisms may be respiring to an extent that would overtake the rate at which the algae are photosynthesising and create overall net respiration at that time. However, pH and pCO_2 were also significantly correlated with the tides and it is likely that different bodies of water containing these different pH and pCO_2 concentrations were brought in by the tides rather than biological activity causing the unusual phenomena.

Coastal systems tend to have large diurnal fluctuations in pH relative to open ocean areas (Duarte and Cerbrian, 1996; Gattuso *et al.*, 1998; Anthony *et al.*,

2011; Duarte *et al.*, 2013). Caol Scotnish has a comparably low fluctuation of pH; in both deployments there was not a large difference in the pH mean at night and at day ($\Delta pH\ July_{(\mu Day - \mu Night)} = 0.01$; $\Delta pH\ Sept_{(\mu Day - \mu Night)} = 0.01$). Coastal systems can see a daily fluctuation of approximately 1 unit (Morris and Taylor, 1983; Hofmann *et al.*, 2011; Cornwall *et al.*, 2013). Large fluctuations can be considered anything above 0.25 units (Hofmann, 2011).

There may be several reasons for the relatively low fluctuation of pH in the area.

- It is possible that these pH changes are relatively small because seawater can be buffered by calcium carbonate ($CaCO_3$) and bicarbonate (HCO_3^-) content in the water. pH can be neutralised when these combine with hydrogen and hydroxyl ions (Zeebe and Wolf-Gladrow, 2001).

- There is a large window of daylight where photosynthesis will take place and the extensive maerl beds will be calcifying. Calcification happens in the daylight under high pH situations (Langdon *et al.*, 2000) and knock-on effects on the water chemistry can be exacerbated by small spatial areas (Zeebe and Wolf-Gladrow, 2001).

- There is a large volume of water exchange at this site which can cause pH concentrations to vary according to the water masses that enter or leave the site (Gattuso, *et al.*, 1998; Brown, 2008; Gasim *et al.*, 2015).

The pH and chlorophyll content in Caol Scotnish do not show any statistical correlation. At a glance of the time series of chlorophyll in Caol Scotnish, it appears to be governed by the day/light cycle and exhibits a diel pattern and although pH is also governed by the day/light cycle there are other factors which influence the pH i.e. tides, calcification, remineralisation and other biological processes. The pH also has a moderate inverse correlation with the temperature. When the temperature is at a peak, this usually corresponds with a low in the pH.

Overall, the pH in Caol Scotnish on both deployments is most highly correlated with DO, pCO_2 and tides. pH in September is correlated with salinity but this is

not replicated in July. Likewise, pH is correlated with temperature in July but not in September. This suggests a superimposition of both biological activity and tides affecting pH, DO and pCO_2.

Caol Scotnish is a narrow body of water surrounded by banks and foliage. Rainfall and runoff can be a significant influence on the chemical constitution of the water. Caol Scotnish is not a stratified water column and there is constant movement, mixing and influences on the body of water. Caol Scotnish is well oxygenated at all times with saturation concentrations always nearing 100% on both deployments. There is not a large fluctuation which suggests a good turnover of water and the area is well flushed over diurnal cycles. DO is constantly affected by physical and biological processes like air-sea flux, weather patterns, biological metabolic processes, decomposition, temperature, salinity and pressure (Barnes, 1983; Gattuso *et al.*, 1996; Zeebe *et al.*, 1999; Anthony *et al.*, 2011; Smith *et al.*, 2013; Rerolle *et al.*, 2014). Overall, the DO Caol Scotnish seems to be most highly correlated with the day/night cycles, pH, pCO_2 and the tides/different water masses (both having a positive strong relationship). Analysis suggests that DO is therefore affected by every parameter recorded in this field run in Caol Scotnish (although NOT salinity in September). Caol Scotnish is a shallow loch (~7 m); thus there may also be an influence of oxygen flux between the atmosphere and the sea surface. This, however, is unlikely to be a key driver compared to the effects of biological or physical mixing processes (Fransson *et al.*, 2004). It can be concluded that DO shows patterns of both tidal (primarily) and diel (secondary) influences.

4.7.4.3 Performance of pCO_2 sensors

The developed pCO_2 sensor had a successful first run in the field in July and produced a pattern over the period of deployment that would be expected when compared to other supporting sensor data. When comparing the pCO_2 data with that of the EXO2 Sonde, the results were very favourable. Most notably, when comparing pH and DO with pCO_2 (where the relationship should be strongly inverse), the results were agreeable. The actual concentrations of pCO_2 produced by the sensor seem to be reasonable with a minimum of 481 μatm, a maximum of 497 μatm and an overall mean of 489 μatm. Maerl is a major contributor to carbon flux concentrations and are a source of carbon in an area

through biological processes and production and dissolution of calcium carbonate (Martin *et al.*, 2007) and although these values may seem high, it would not be unexpected in an area with as an extensive bed as this. pCO_2 concentrations in areas that contain calcifying organisms vary extensively; Bates *et al*. (2001) observed a range from 73 μatm to 1068 μatm in different areas. Of course, all systems differ in terms of habitat and hydrographical influences and so values will vary accordingly. The concentrations recorded in Caol Scotnish are likely to be reasonable and what should be expected for a well-flushed, shallow area. The values are 80 – 90 μatm higher than atmospheric values and possibly reflect the large ecological community found in the area and consequently the high concentration of metabolic processes that are the main driving factor of pCO_2 in the area.

Overall, the developed sensor on both the July and September deployments gathered data of a high quality when compared to the YSI EXO2 Sonde data. There were anomalies in the run but these occurred simultaneously with the other sensors so can be identified as real events as opposed to a fault with either sensor. A maximum of pCO_2 in the daytime was always accompanied by a minimum in pH and DO. Both in July and September, the developed sensor provided data that had a strong negative correlation with the pH and DO. These three parameters should show the strongest relationship as they are heavily driven by tidal and biological processes. In terms of actual pCO_2 values, in July the range was from a low of 481.21 μatm to a high 496.99 μatm (ΔpCO_2 = 15.78 μatm). In September the range was from a low of 449.34 μatm to a high 464.41 μatm (ΔpCO_2 = 15.07 μatm). In July, the pCO_2 was therefore higher than in September by around 30 μatm. This is a reasonably small difference in pCO_2 values between the deployments. A difference in ~30 μatm between the months could be due to a number of factors specific to the time such as all the driving forces previously mention like metabolic processes, solubility, i.e. temperature, and tide and current control. It would be difficult to say that there was any clear difference in July and September for a number of reasons. Firstly, the July deployment was only for two days and two nights compared to September which was five days and four nights and it would be cautionary to compare the two in terms of absolute values. Secondly, the accuracy of the sensor is within ± 50 μatm and therefore it could be the margin of error which causes the sensor to be

giving a difference of ~30 μatm between the months. What should be noted, and is most likely the reason behind these differences, is that the means of the data were time averaged in the processing stages. Since this technique is used to smooth out short-term fluctuations in time series there may not be an exact correspondence of concentration values. Thirdly, the calibration of the sensor could not be conducted in the field as in the lab. Calibration can be conducted in the field by using general atmospheric zeroing but this is not as precise as specific gas concentration calibration. Because the deployments were months apart from each other and there were many calibrations between the field work, the small differences in values may have been a calibration issue. However, lab calibration was conducted directly before both field campaigns deployments so it is likely that Caol Scotnish in July may have slightly higher pCO_2 concentrations than Caol Scotnish in September. This is a very slight difference, however, and is not significant in terms of coastal pCO_2 values which fluctuate much more than open ocean values. In fact, the pCO_2 concentrations in Caol Scotnish are remarkably consistent between each sampling campaign. There is a reasonable amount of pCO_2 variation over both the diurnal and diel cycle.

4.7.4.4 Comparison of Caol Scotnish July and September deployments

The two deployments in Caol Scotnish produced very similar data. The most notable difference, however, was the salinity pattern. Data show that September was lower salinity with a correlation with the tides, pH and temperature. The salinity in July does not correlate with pH or tides but only with DO and temperature. Heavy rainfall and runoff may have contributed to the difference in patterns. Discharge of fresh water can lower pH (Rerolle *et al.*, 2014) and pH is lower in September. There is very little difference in temperature between the two deployments but there was a difference in fresh water input. The temperature does not change by any significant margin so this would not be a factor in the slightly different pCO_2 concentrations between deployments.

The September deployment was just over double the length of the deployment in July. In July, 72% of the data collected were in daylight hours compared to 52% of data in September. Specifically, in July there were 30 hours and 35 mins of data collected in the daytime and 12 hours collected in darkness. In

September, there were 46 hours and 38 minutes of data collected in the daytime and 42 hours and 40 minutes of data collected in the darkness. The diurnal length in July was approximately 18 hours. The diurnal length in September was approximately 13.5 hours. It can be concluded from this that there should be a higher productivity on a comparative daily basis in July than in September. This is shown in the comparison tables below (see Table 4.9).

Caol Scotnish 7th to 9th July 2016

Average concentration	Day	Night	Overall
DO (% sat)	108.03	106.31	107.61
pH	8.253	8.239	8.25
$p\,CO_2$ (µatm)	487.6	487.75	487.64

Caol Scotnish 19th to 23rd September 2016

Average concentration	Day	Night	Overall
DO (% sat)	97.86	95.73	96.85
pH	8.097	8.087	8.093
$p\,CO_2$ (µatm)	456.1	456.9	456.5

Table 4.9: Comparison of productivity from two separate deployments in Caol Scotnish in July and September. Overall mean, daylight mean and darkness mean given for DO, pH and pCO_2

PCA analysis confirmed the findings of Caol Scotnish being heavily governed by the tides.

4.8 Conclusion

This research provides novel technology for measurement of *in-situ* pCO_2. This chapter presents research on the performance of a developed pCO_2 sensor which contributed to the characterisation of the natural variability of carbonate chemistry and other parameters in a temperate marine environment in Scotland.

The sensors were able to provide pCO_2 data on numerous day/night cycles in Loch Sween. Both the July and September deployments can be deemed a success in terms of recording the concentration of pCO_2 in Caol Scotnish. There are no other records of *in-situ* pCO_2 from this area and indeed limited published *in-situ* pCO_2 data as a whole. This sensor has provided a cheap and easy way to gather pCO_2 data in coastal areas.

To accompany the *in-situ* pCO_2 data, other ancillary marine data were measured and used to support and compliment the pCO_2 data and ultimately create a full picture of the natural variability and the drivers of the diel marine cycle in Caol Scotnish. The main driver of and influence on parameters in Caol Scotnish was tidal action.

5 Characterising natural variability of coastal carbonate systems and ancillary variables in a tropical marine environment

5.1 Introduction

Although tropical areas (compared to polar or temperate waters) can be lower in nutrients and productivity in general, the direct vicinity of tropical coral reefs can host some of the most productive marine areas in the world with productivity of around 40 gC $m^{-2}day^{-1}$ compared to the surrounding open tropical water which can fall to a low of 0.01 gC m^{-2} day^{-1} (Hatcher, 1998; Hoegh-Guldberg, 1999). Coral reef habitats are some of the most biologically diverse areas on the planet (Hoegh-Guldberg, 1999). Therefore, tropical waters that contain coral reefs are important to focus on in the context of global change. This high productivity in an otherwise low productivity area is not only important to the species and the ultimate survival of these marine ecosystems but also the human communities based around these areas (Hoegh-Guldberg, 1999). Coastal communities depend on coral reefs through aspects like tourism ($1 billion USD, $1.6 billion USD and ~90 billion USD is generated from tourism in Australia, Florida and the Caribbean respectively (Jameson *et al.*, 1995; Done *et al.*, 1996; Birkeland, 1997)), providing physical protection from coastal erosion and also a direct livelihood in fishing and sustenance for the community (Carte, 1996).

Coral reefs thrive in areas which are usually typified by environmental stability including temperature, salinity and light levels which all have an influence in coral reef growth and survival (Hoegh-Guldberg, 1999). Coral reefs will generally grow in areas where there is a low thermal fluctuation both seasonally and diurnally (Hoegh-Guldberg, 1999) and proliferate in water where the temperature is 20 – 38^{o}C for the most part of the year (Nybakken and Bertness, 2005). The natural range of salinities that corals usually thrive in is 32 to 40 psu (Veron, 1986). Mortality of coral can occur if there is a rapid decrease in salinity with unusual weather occurrences like flood events (Hoegh-Guldberg and Smith, 1989). Another factor that can dictate where corals proliferate is light levels which are key for the photosynthesising zooxanthellae (Chalker *et al.*, 1988) and

consequent energy production. There is however, some flexibility in the capability of zooxanthellae to adapt to different light intensities (Hoegh-Guldberg, 1999). Under lower intensities of light, there will be a greater concentration of photosynthetic pigments, mainly chlorophyll, present in the zooxanthellae (Falkowski and Dubinsky, 1981; Porter *et al.*, 1984) and conversely, there will be a lower concentration when there is a higher light intensity (Hoegh-Guldberg, 1999). One adaption to light stressors is by a means of 'quenching' to lessen the impact of high concentrations of light (Hoegh-Guldberg and Jones, 1999; Ralph *et al.*, 1999) which is done by means of changes in xanthophylls pigments (Brown *et al.*, 1999) and production of compounds which block ultra-violet radiation (Shick *et al.*, 1996).

Tropical marine areas have experienced an increase of temperature over the last 100 years of 1- 2 ^{o}C (Bottomley *et al.*, 1990; Brown, 1997; Cane *et al.*, 1997; Winter *et al.*, 1998; Hoegh-Guldberg, 1999). In tropical environments where there have been warmer than usual waters, there have been significant effects on the organisms that inhabit these areas (Walther *et al.*, 2002). These organisms can, in some places, already be at their physiological thermal limit and a change in baseline environmental variables can have fatal consequences. In areas where there has been a sustained increase of 1^{o}C over the average summer water temperatures, corals have undergone mass bleaching (Glynn, 1991; Hoegh-Guldberg, 1999; Eakin *et al.*, 2014; Eakin *et al.*, 2016) and in some cases complete destruction of reefs (Brown, 1997; Hoegh-Guldberg, 1999; Spencer *et al.*, 2000; Mumby *et al.*, 2001; NOAA, 2017). These types of mass coral bleaching are not just happening at a greater rate but also at a greater intensity (Hoegh-Guldberg, 1999). These thermal anomalies from the usual environmental baseline can cause fundamental ecological community shifts like removing smaller, thin-tissued corals which are then replaced by bigger ones. In certain cases, all species present can be decimated (Loya *et al.*, 2001; Mumby *et al.*, 2001). The main variables that can be drivers of coral bleaching is reduced salinity (Goreau, 1964; Egana and DiSalvo, 1982), higher or lower than average light intensities (Hoegh-Guldberg and Smith, 1989; Lesser *et al.*, 1990; Gleason and Wellington, 1993) and temperature (Jokiel and Coles, 1990; Glynn and D'Croz, 1990). The introduction of agricultural chemicals like pesticides and herbicides can also be a factor in bleaching as can biological anomalies like

bacteria (Kushmaro *et al.*, 1996; Jones and Steven, 1997; Jones and Hoegh-Guldberg, 1999).

While there is stability in the nature of tropical areas (i.e., no sudden short-term variations compared to polar or temperate areas), the large biodiversity and complicated state of trophic interactions in reef environments are undergoing widespread changes due to climate change (Bryant *et al.*, 1998; Convey, 2001). Climate change is affecting all marine areas but the different geographical areas will be affected in different ways because of their unique ecological and hydrographical properties (Walther *et al.*, 2002). Coral reefs have been identified as being one of the most vulnerable areas under threat from climate change (Hoegh-Guldberg, 1999). Anthropogenic activities have been directly linked to the decline of between 50 – 70 % of corals worldwide (Goreau, 1992; Sebens, 1994; Wilkinson and Buddemeier, 1994; Bryant *et al.*, 1998; De'ath *et al.*, 2012; Hoegh-Guldberg *et al.*, 2017; Richmond *et al.*, 2018). Some of these activities include eutrophication and destructive fishing/tourist activities along with the wider threat of increased CO_2 in the atmosphere from industrial activities (Sebens, 1994; Hoegh-Guldberg *et al.*, 2017; Richmond *et al.*, 2018).

This chapter focuses on deployment of the sensors in a tropical environment – El Quseir, Egypt in the Red Sea. El Quseir is in the north western part of the Red Sea and is an area that has been reported as being highly affected by anthropogenic influences like oil spills, eutrophication induced by agriculture and sewage and wastewater from industrial activities (Abou-Aisha *et al.*, 1995; Nassar *et al.*, 2014). An increase of tourism developments around Hurghada has led to the degradation of coral reefs from 1987 onwards (El-Askary *et al.*, 2013). The Red Sea is an important study area for several reasons; in comparison to most marine areas it is generally a source for CO_2 to the atmosphere as opposed to a sink for CO_2 from the atmosphere (Elsheikh, 2008), the area is an important one for calcifying organisms and is also an area that has been highlighted to be highly vulnerable to climate change due to the high productivity and large biodiversity of organisms of which several species are endemic (Baars *et al.*, 1998).

The Red Sea extends from the Strait of Bab Al Mandab (which is the only direct link to the Indian Ocean) in the south-east at the Gulf of Aden up in a north-westerly direction to the south of the Sinai Peninsula which then forks into the Gulf of Suez to the NW and the Gulf of Aqaba to the NE. Typically there is very low rainfall in the area and therefore very little input of freshwater or discharge from rivers with runoff being negligible (Sofianos *et al.*, 2002). The Red Sea is climatologically classed as a tropical area lying between arid land, desert and semi-desert (Rasul and Stewart, 2015) which is a product of two different monsoon areas. One monsoon area originates in the northwest as a result of eastern Mediterranean climate systems (Pedgley, 1974) and another in the southeast which originates from the Indian Monsoon system. These weather systems are important in the context of water masses within the Red Sea and it is the wind that governs the movement of these bodies of water (Patzert, 1974; Honjo and Weller, 1997). Water masses formed in the Gulf of Aden have a large influence on the water masses in the Red Sea specifically Gulf of Aden Surface Water (GASW) and Gulf of Aden Intermediate Water (GAIW). GASW and GAIW contribute to the constitution of the Red Sea particularly in winter and summer respectively. Within the Red Sea there are four main water masses; Red Sea Surface Water (RSSW) which is formed from GASW, Red Sea Water (RSW) which is formed from RSSW, Red Sea Deep Water (RSDW) formed by evaporation of RSSW and Red Sea Outflow Water (RSOW) which is made up of RSW and RSDW and exits the Red Sea at the Strait of Bab Al Mandab (Souvermezoglou *et al.*, 1989; Smeed, 1997; Pratt *et al.*, 1999; Sofianos *et al.*, 2002).

Surface currents in the Red Sea are formed from complex interactions of density forcing and wind strength and direction (Sofianos and Johns, 2003). Subsurface circulation is forced mainly by seasonal flux of the monsoon (Eshel *et al.*, 1994).

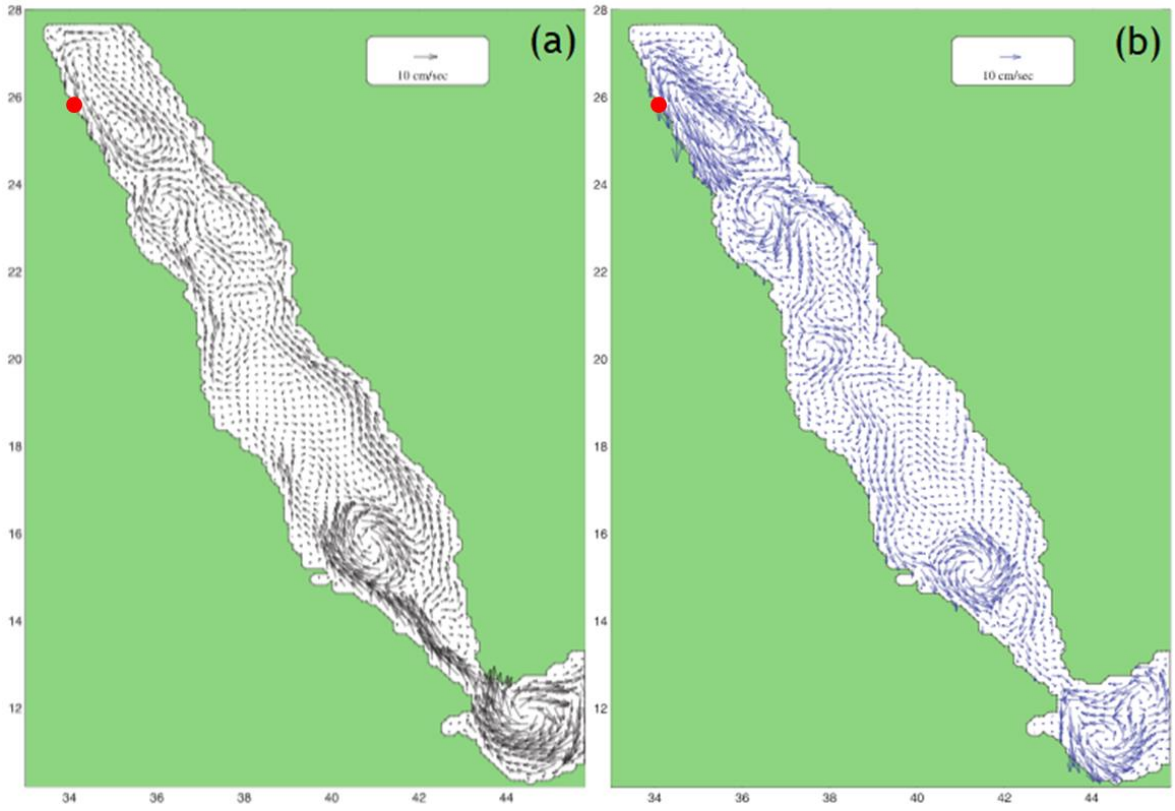

Figure 5.1: Mean surface circulation in the Red Sea. Red dot shows the location of study site. (a) During winter there is a significant surface inflow from the Indian Ocean which is created by strong SEE winds with the mean surface circulation towards the north (b) During summer there is a reversal of wind direction in the south and surface flow is also reversed (Figure adapted from Sofianos and Johns, 2003)

The Red Sea is a strategically important body of water for the people of north-eastern Africa and the Arabian Peninsula for numerous purposes including tourism, trade and sustenance (Longhurst, 2007; Belkin, 2009). The Red Sea has an abundant marine biodiversity and is an oceanographically important area because of the physical topography and hydrography whereby it is relatively cut-off from the wider Indian Ocean (Rasul and Stewart, 2015). One of the defining features of the Red Sea is the abundance of coral reefs along with the associated organisms relying on the reefs for habitat. Coral reefs are ubiquitous in the Red Sea but the majority are situated to the north (Schulz and Riebesell, 2013).

The main water mass exchanges occur at the southerly point of the Red Sea where the strait of Bab Al Mandeb meets the Gulf of Aden which is connected to the open Indian Ocean via the Arabian Sea. Although the Gulf of Suez in the north of the Red Sea connects to the Mediterranean Sea, the exchange here is minimal compared to at the Gulf of Aden (Sofianos and Johns, 2002).

The salinity of the Red Sea increases from south to north (36 to >41 psu) as shown in Figure 5.2(a) and is one of the highest salinity areas over the worlds seas and oceans (Rasul and Stewart, 2015). SST is also relatively high with the average summer temperature in the north being 26°C and 30°C in the south (Sofianos and Johns, 2002). As shown in Figure 5.2(b), there is a variation in the temperature over the whole of the Red Sea. Winter mean temperatures only decrease by around 2°C from the summer mean (Sofianos and Johns, 2002). A minimum temperature of ~21°C is situated at the extreme north and south of the Red Sea. A maximum of ~34°C can be found just below the middle regions which appear to be as a result of comparatively weak wind speeds in this area (Sofianos and Johns, 2002).

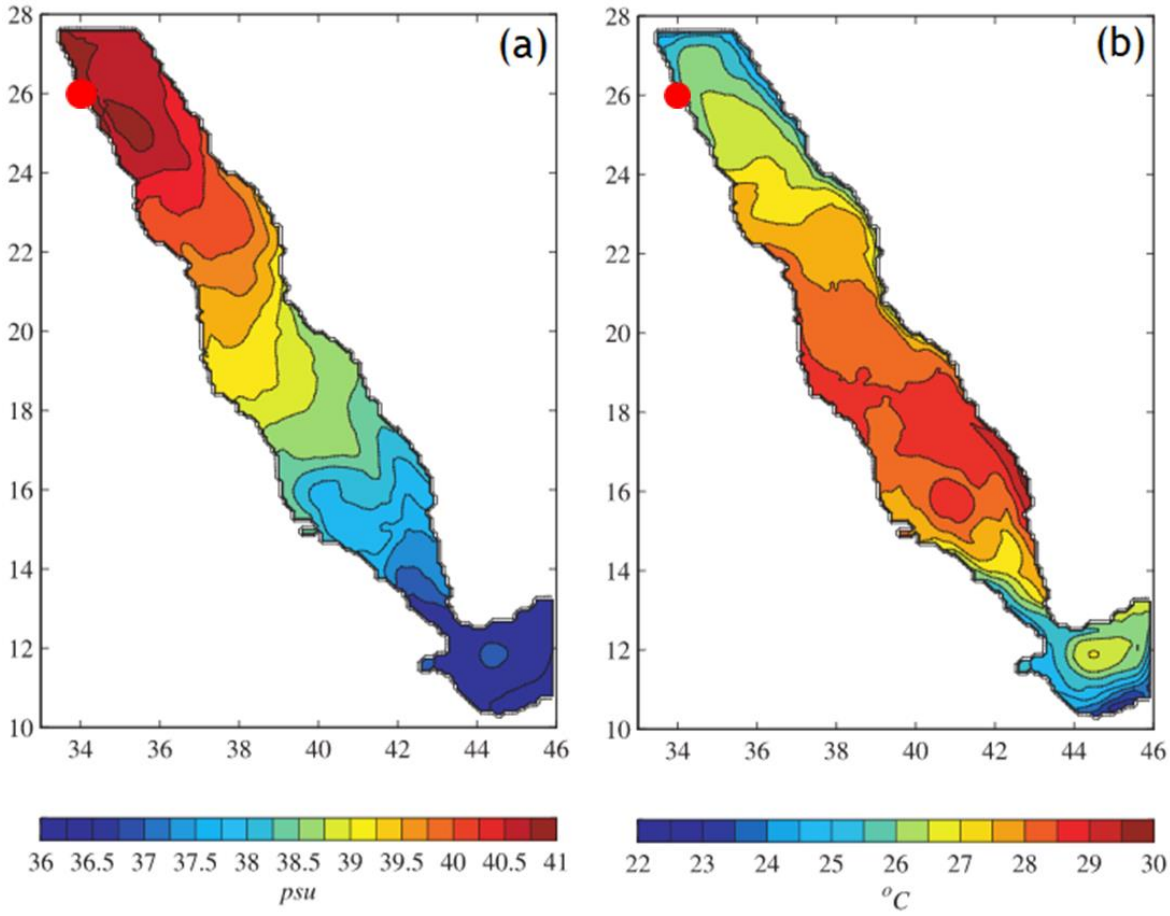

Figure 5.2: Annual mean (a) salinity (b) SST in the Red Sea. Red dot shows the study site (Figure adapted from Sofianos and Johns, 2002).

5.2 Motivation

The site chosen was a biogenic reef in a tropical coastal area. The area was chosen for several reasons;

(1) The coral reef where the sensors were deployed should create an area of fluctuating carbonate chemistry over the diel cycle and a corresponding variation of pCO_2 concentrations. These differentials will be experienced over small spatial but a large temporal scales (6 diel cycles).

(2) This area would be a significant test for the developed sensor with constantly changing carbonate chemistry (net community metabolism) compared to an area with little biological activity.

(3) If a baseline is established, then such data can be used to determine how much of a stressor changing atmospheric pCO_2 concentrations in the future (i.e. ocean acidification caused by climate change) may be for tropical, coastal biogenic reefs. Or indeed, if and how the reef is able to cope and adapt to large fluxes in concentrations over small temporal scales already.

5.3 Aims

The objectives of this field work were to characterise the natural variability of carbonate chemistry and other ancillary parameters in a coastal tropical area characterised by autotrophic biota and to evaluate the performance of pCO_2 sensors in a tropical field environment. This was conducted with the developed pCO_2 sensors, supporting sensors and with collection and analyses of discrete seawater samples.

The aims of this chapter were to:

(1) Test the functionality and performance of the newly developed pCO_2 sensor(s) in a tropical field environment over numerous day/night cycles in the Red Sea.

(2) Characterise the natural variability in a tropical environment of pCO_2 in the Red Sea in March (a transition month from winter to summer in Egypt) using the newly developed sensor.

(3) Characterise the natural variability of other marine parameters in the Red Sea (dissolved oxygen, chlorophyll, salinity, temperature, tidal action, PAR, A_T and DIC) to create a comprehensive record of the area.

Utilising the sensor allowed the following hypotheses to be tested; (1) the developed pCO_2 sensor would be a valuable supporting tool in the characterisation of the natural variation in carbonate chemistry in a tropical biogenic reef system due to the natural variability in many physicochemical parameters, (2) the seawater samples and other sensor readings would corroborate and also contribute to the creation of multiple diel patterns of marine parameters in the area, (3) the area would be heavily influenced by diel cycles.

This chapter deals with the characterisation of the natural variability of coastal carbonate systems and ancillary parameters in a tropical marine environment. The driving forces behind these parameters will be looked at and the interrelationships between them will be determined. This was the first tropical deployment of the developed pCO_2 sensors and along with the YSI EXO2 Sonde and analysis of seawater samples, high volume data was able to be collected from the site.

5.4 Site description

Field work was conducted in El Quseir, in Eastern Egypt situated on the Red Sea coast (26°28’41.3”N, 34°18’06.5”E) in March 2017.

Figure 5.3 Red Sea field site, Egypt showing a variety of weather conditions experienced over the week of deployment (a) panoramic view of site, clear calm conditions (b) sandstorm conditions (c) overcast and windy conditions.

The field site was near El Quseir on a coral reef flat. It is an open site and has fairly simple topography. There are no inputs from rivers and typically there is very low rainfall in the area. The weather was, however, exceptional during sampling and deployment in that it was very windy for the majority of the week complete with a dust storm lasting 24 hours. The water clarity was generally good with the exception of the period around the dust storm. The Red Sea coast is characterised by shallow submarine shelves. The reef grew directly from the shoreline, i.e. a fringing reef and the sensors were placed on the seabed approximately 4 m in depth near the coral shelf. The coral in the area should play an important role in carbon cycling and therefore may be a significant driving force for the carbonate chemistry. This will be commented on later in the chapter.

The deployment in the Red Sea lasted for 116.5 hours or approximately 5 nights/4.5 days from the 15th to the 20th March 2017.

5.5 Methods: tropical deployment

5.5.1 Sensor measurement

The deployed sensors included the YSI EXO2 Sonde (which measured DO, chlorophyll, salinity, temperature, depth of sensor), a PAR (Photosynthetically Active Radiation) meter, a separate temperature sensor and the two developed pCO_2 sensors (both programmed to output pCO_2 in μatm). The sensors were deployed by snorkelling. Due to essential maintenance, i.e. changing batteries and operational checks, there are small, inconsequential gaps in the data when the sensors were recovered.

5.5.2 Data processing

Data processing mirrors that in Chapter 4, Section 4.5.2, page 137.

5.5.3 Calibration of sensors

Calibration of sensors mirrors that in Chapter 4, Section 4.5.3, page 137.

5.5.4 Sensor deployment

5.5.4.1 15th – 20th March 2017

After calibration, the sensors were programmed to record one reading every five minutes. The sensors, including the two developed sensors, the YSI EXO2 Sonde, PAR meter and extra temperature sensor were deployed on the morning of 15th March 2017 at 11:30 to a depth of 4.1 m by snorkelling. The sensors were tied to the reef by placing them in a mesh bag which was then secured to the reef with cable ties (N.B. the mesh bags did not appear to affect the performance). The pCO_2 sensors were retrieved 48 hours later (all other sensors remained in place) at 12:00 on 17th March to check that they were recording adequately. The sensors were then redeployed to the same place on the reef at 13:30 hours on the same day. They were retrieved, finally, on Monday 20th at 09:00.

Figure 5.4: Sensors deployed on coral reef flat in the Red Sea 15th March 2007

Figure 5.5: EXO1 Sonde, PAR meter, temperature sensor and two *p*CO_2 sensors deployed on coral reef flat in the Red Sea on 15th March 2017.

5.5.5 Wet chemistry

Seawater samples were used to validate the sensor pCO_2 readings against the analysed seawater wet chemistry. Samples were taken directly adjacent to the sensors to ensure the same body of water that passes over the sensors was collected. The samples were also used to characterise two carbonate chemistry parameters, A_T and DIC in the sea which will be mentioned in detail later.

5.5.5.1 Water sample collection

Discrete water samples were collected in the Red Sea in accordance with standard protocols (Dickson *et al.*, 2007). Specific details for the collection are described below.

Samples were taken a minimum of once a day (on the last morning of deployment) and a maximum of three times a day. Sample times were 0900, 1200 and 1500 in accordance with the rules of the hosting dive company (night diving was restricted and weather conditions also prevented certain sampling times). Samples for A_T and DIC were collected in triplicate via snorkelling with borosilicate glass syringes (see Figure 5.6). The seawater was then transferred to 12 ml borosilicate vials. Minimal gas exchange with the atmosphere was ensured by transferring the seawater slowly and smoothly into the vials directly from the syringe. This meant that no air bubbles were introduced into the sample. A slight overflow of water was left to further ensure this. They were then poisoned with 10 µL of mercuric chloride ($HgCl_2$) to prevent any further biological activity inside the vial which would alter the carbonate chemistry in the sample. The lids were carefully placed on the vials, again ensuring no air bubbles were present in the sample. The vials were then stored in a fridge in the laboratory on-site before being transported back to The University of Glasgow for analyses.

Figure 5.6: Sensors on the coral reef with seawater samples being taken with borosilicate syringes

5.5.5.2 A_T analysis

See Chapter 4, Section 4.5.6.2, page 141 for details of A_T analysis.

5.5.5.3 DIC analysis

See Chapter 4, Section 4.5.6.3, page 141 for details of DIC analysis.

5.5.5.4 *p*CO_2 calculation from water chemistry

See Chapter 4, Section 4.5.6.4, page 141 for details of *p*CO_2 calculation from water chemistry.

5.6 Results & Discussion

5.6.1 Seawater wet chemistry

For details of the times of sample collection see Table 5.1. Seawater samples were analysed for A_T and DIC and used in conjunction with the measured pH, salinity and temperature to compute *p*CO_2.

5.6.1.1 Water chemistry

Time of sample	Salinity (psu)	T(°C)	A_T (µmol/kg⁻SW)	DIC (µmol/kg⁻SW)
Wednesday 15/3/17				
1145	40.56	22.61	2396 (σ = 49; CV = 2.1%)	2042 (σ = 14.8; CV = 0.73%)
1500	40.5	22.87	2383 (σ = 19; CV = 0.8%)	2002 (σ = 9.1; CV = 0.5%)
Thursday 16/3/17				
0900	39.64	22.13	2418 (σ = 19.4; CV = 0.8%)	2072 (σ = 3.7; CV = 0.2%)
1200	39.54	22.49	2417 (σ = 12.1; CV = 0.5%)	2033 (σ = 7.9; CV = 0.4%)
1458	39.53	22.87	2401 (σ = 14.2; CV = 0.6%)	2014 (σ = 7.8; CV = 0.4%)
Friday 17/3/17				
0900	39.45	22.25	2421 (σ = 11.6; CV = 0.5%)	2038 (σ = 14.5; CV = 0.7%)
1155	39.48	22.90	2396 (σ = 4.7; CV = 0.2%)	2067 (σ = 22; CV = 1.1%)
1455	39.37	22.57	2420 (σ = 11.9; CV = 0.5%)	2119 (σ = 6.3; CV = 0.3%)
Saturday 18/3/17				
0905	39.36	22.23	2399 (σ = 30.8; CV = 1.3%)	2154 (σ = 10.8; CV = 0.5%)
1156	39.45	22.74	2415 (σ = 8; CV = 0.3%)	2096 (σ = 18.6; CV = 0.9%)
1457	39.38	22.95	2388 (σ = 14.7; CV = 0.6%)	2068 (σ = 2.6; CV = 0.1%)
Sunday 19/3/17				
0908	39.26	22.08	2379 (σ = 36; CV = 1.5%)	2147 (σ = 9.4; CV = 0.4%)
1155	39.18	22.26	2430 (σ = 24; CV = 1%)	2131 (σ = 9.9; CV = 0.5%)
1454	39.17	22.46	2191 (σ = 69; CV = 3.2%)	2106 (σ = 13.7; CV = 0.6%)
Monday 20/3/17				
0853	39.06	22.13	2414 (σ = 18; CV = 0.8%)	2127 (σ = 26; CV = 1.2%)

Table 5.1: Analysis of A_T and DIC from water samples taken from the Red Sea 15th to 20th March 2017. Date and time of samples with accompanying measurements of temperature and salinity from YSI EXO2 Sonde and the resultant A_T and DIC concentrations from analyses in the laboratory. σ = standard deviation of the reading while CV is the coefficient of variation

The A_T in the Red Sea remains fairly constant throughout the deployment (2379 – 2414 µmol kg^{-1} with the exception of one outlier). There were no night time samples so it is not possible to comment on the overall day/night cycle. The DIC content of the water increased in the second half of the deployment as shown in Figure 5.7.

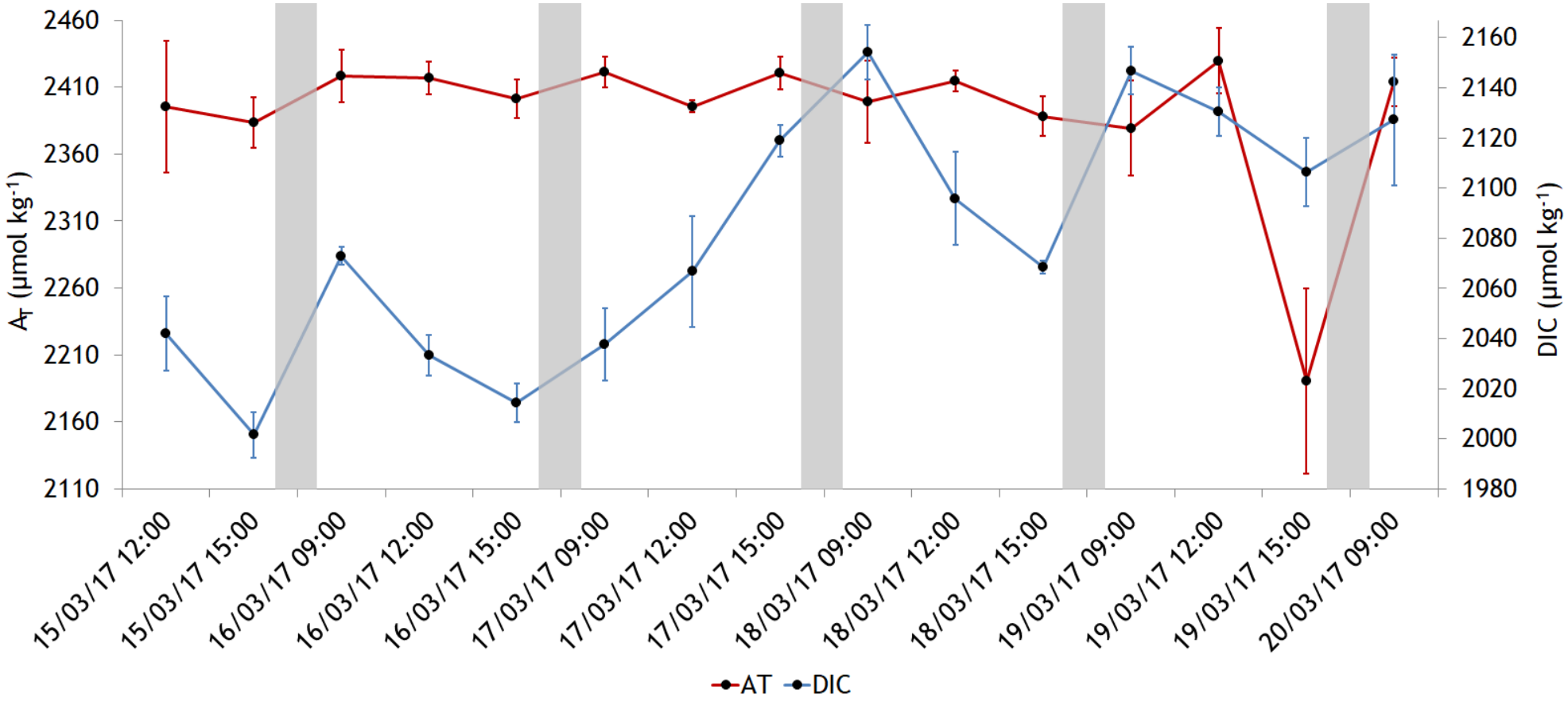

Figure 5.7: A_T and DIC in the Red Sea 15th to 20th March 2017. Data presented as a mean with ±SD. A_T did not show a strong variation throughout the six days. DIC, however, increased gradually. Samples were only taken during the day. Night hours are roughly represented by grey shading.

The A_T over the course of the deployment stayed relatively stable (only daylight samples were taken). The main influences upon A_T in an area are salinity variations and $CaCO_3$ content (Lee *et al.*, 2006). Salinity was relatively constant and A_T was also relatively constant. There was one A_T data point exception however which was much lower than the rest. If this point is a true value, then it could suggest that on this day (15:00 on 19th) there was a large increase in the formation of $CaCO_3$ which would decrease the A_T due to removal of carbonate or bicarbonate ions from the water to form $CaCO_3$ (Bates *et al.*, 1996; Feely *et al.*, 2004; Iglesias-Rodriguez *et al.*, 2008; Jones and Lu, 2003; Kinsey, 1978). CO_2 is also produced in this process ($2HCO^-_3 + Ca^{2+} \rightarrow CaCO_3 + H_2O + CO_2$) and could also explain the unusually high pCO_2 data recorded on this day.

The correlation between DIC, salinity and temperature and A_T, salinity and temperature is shown in Figure 5.8. There is a strong negative correlation between both DIC and salinity and DIC and temperature. The same analysis was conducted with A_T but there was found to be little correlation.

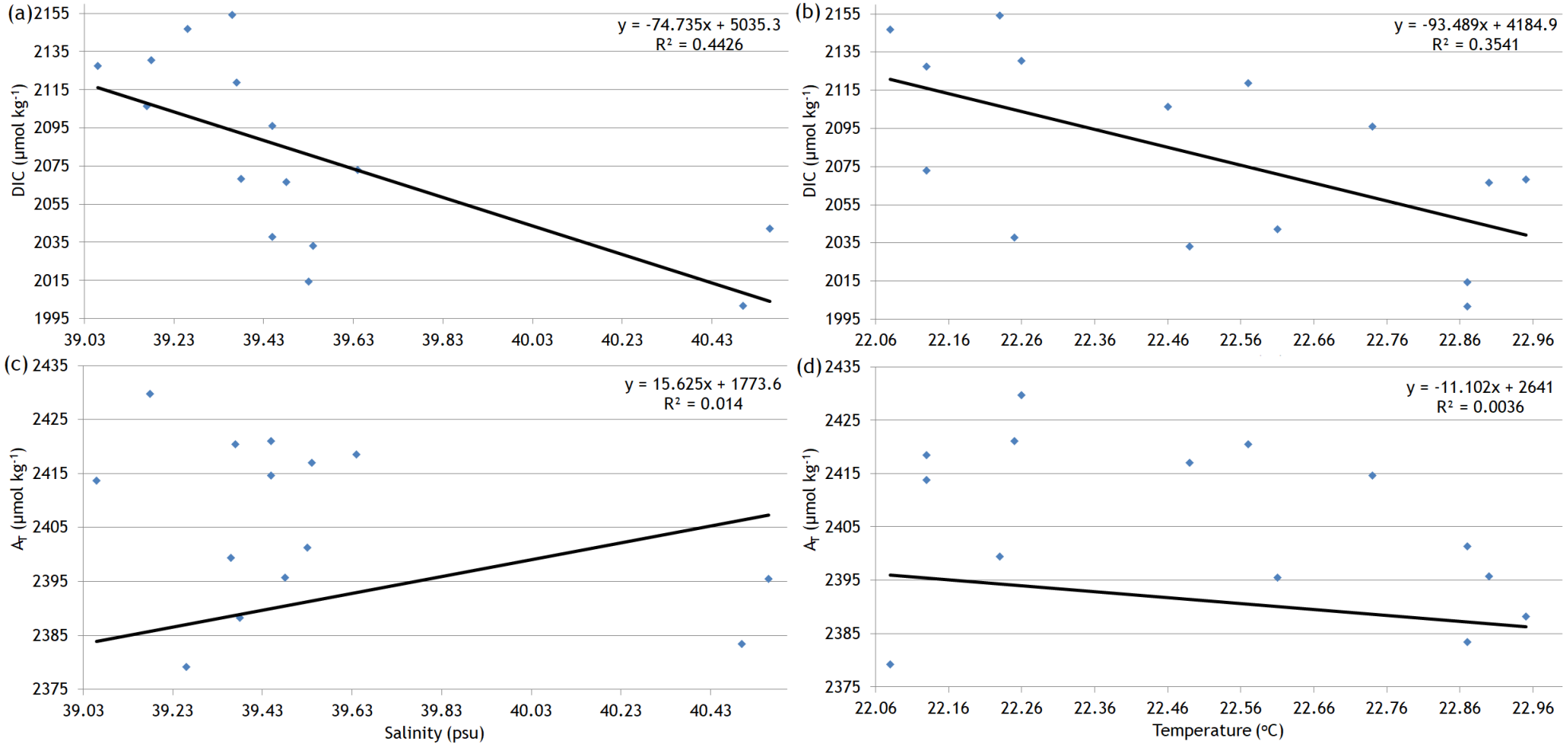

Figure 5.8: Scatter graph with linear trendline (a) DIC and salinity. Pearson correlation coefficient; r = -0.67, p = 0.007. (b) DIC and temperature. Pearson correlation coefficient; r = -0.60, p = 0.019. (c) A_T and salinity. Pearson correlation coefficient; r = 0.12, p = 0.67. The small range of salinity may be the main reason behind the lack of correlation (d) A_T and temperature. Pearson correlation coefficient; r = -0.06; p = 0.83.

5.6.2 Comparison of pCO_2 data from sensor and pCO_2 data calculated from CO2SYS

DIC, A_T and ancillary data was used to calculate the pCO_2 concentrations from the water samples with CO2SYS as shown in Table 5.2.

Input Conditions				Output Conditions					
Salinity	T(°C)	A_T (µmol/kg$^-$ SW)	DIC (µmol/kg$^-$ SW)	pH	pCO_2 (µatm)	HCO_3^- (µmol/kgSW)	CO_3^{2-} (µmol/kgSW)	Ω_{Ca}	Ω_{Ar}
40.56	22.61	2396	2042	8.072	360.4	1792.0	242.5	5.55	3.65
40.5	22.87	2383	2002	8.115	315.7	1731.8	261.0	5.98	3.93
39.64	22.13	2418	2072	8.079	359.6	1820.2	241.1	5.56	3.65
39.54	22.49	2417	2033	8.131	308.7	1758.3	265.6	6.14	4.03
39.53	22.87	2401	2014	8.132	304.9	1738.1	267.0	6.17	4.06
39.45	22.25	2421	2038	8.133	307.4	1763.7	265.2	6.13	4.02
39.480	22.90	2396	2067	8.046	390.8	1825.7	229.2	5.32	3.50
39.370	22.57	2420	2119	8.003	445.8	1892.7	213.2	4.93	3.24
39.360	22.23	2399	2154	7.930	541.2	1946.0	182.9	4.23	2.78
39.450	22.74	2415	2096	8.030	412.5	1859.6	224.3	5.19	3.41
39.380	22.95	2388	2068	8.033	403.9	1832.2	224.1	5.18	3.41
39.260	22.08	2379	2147	7.895	590.5	1960.6	168.7	3.91	2.56
39.18	22.26	2430	2131	8.005	445.9	1905.4	212.3	4.92	3.23
39.17	22.46	2191	2106	7.566	1279.5	1987.0	81.1	1.88	1.23
39.06	22.13	2414	2127	7.991	461.6	1909.0	204.2	4.74	3.11

Table 5.2: *In-situ* parameters (input conditions) used to calculate ancillary data (output conditions) from seawater samples in the Red Sea in March 2017. Salinity, temperature, A_T and DIC were used in CO2SYS to calculate concentrations of pH, pCO_2 (µatm), bicarbonate (HCO_3^-), carbonate (CO_3^{2-}), calcite saturation state (Ω_{Ca}) and aragonite saturation state (Ω_{Ar}). pCO_2 values are highlighted in yellow.

The pCO_2 concentrations from CO2SYS were then compared to the pCO_2 concentrations from the sensor as shown in Figure 5.9. This gives an average sensor percentage error of ±13.0% (or without the outlier ±9.4%).

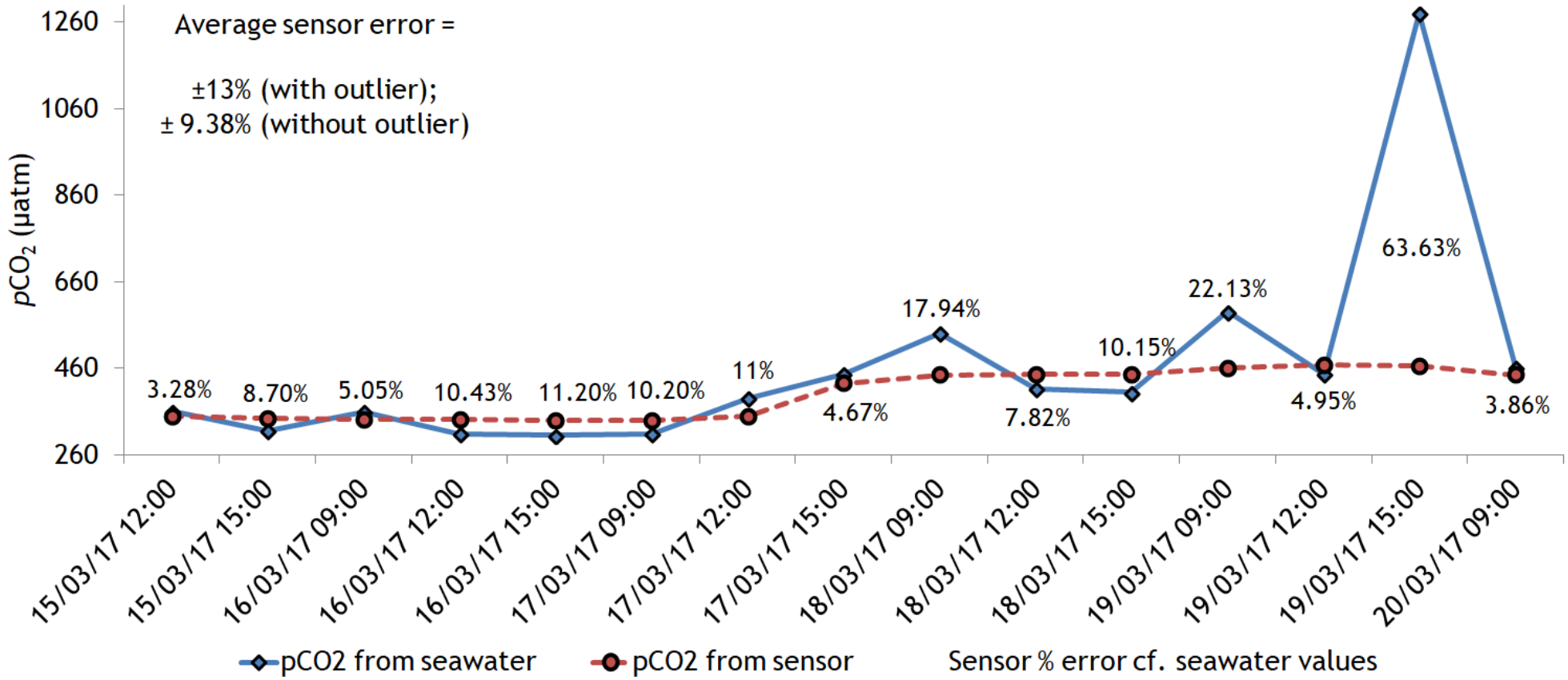

Figure 5.9: A comparison of CO2SYS pCO_2 concentration from seawater analyses and *in-situ* sensor pCO_2 concentration. Percentage error of the sensor when compared with the seawater concentration is shown beside each point. The overall sensor error was ±13.0% (with outlier) or ±9.38% (without outlier)

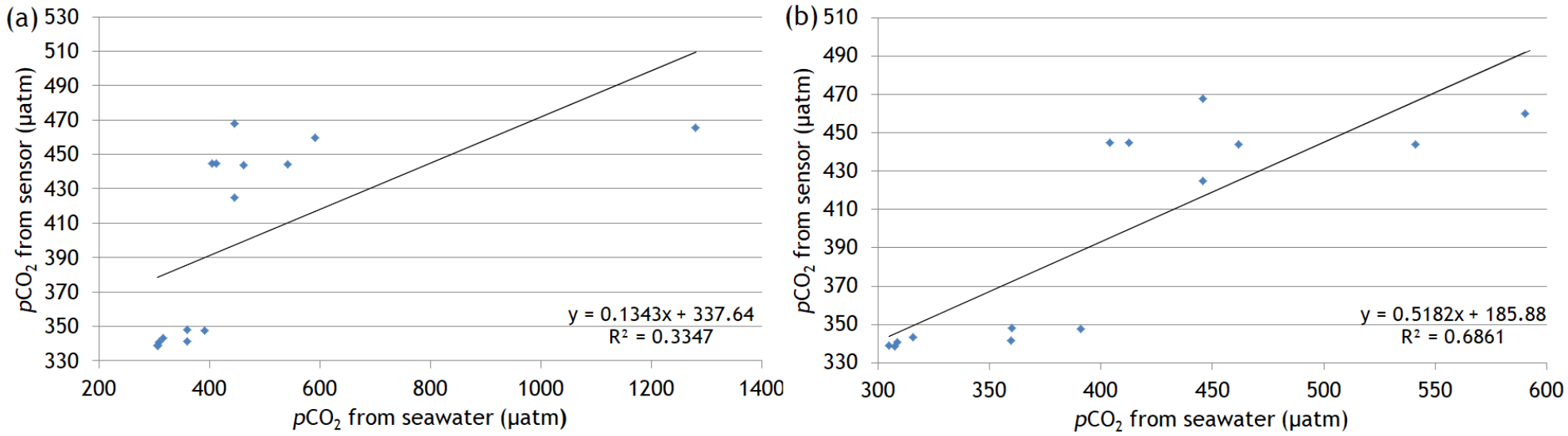

Figure 5.10: Scatter graphs comparing the pCO_2 concentration from the sensor and the pCO_2 concentration from the seawater analyses. (a) scatter graph with pCO_2 seawater possible outlier included. Pearsons correlation coefficient r = 0.58 (b) scatter graph with pCO_2 seawater analyses possible outlier taken out. Pearsons correlation coefficient r = 0.83.

A direct comparison of pCO_2 values from the sensor at the exact times samples were taken show an average concentration of 395 ± 55 μatm from the sensor and an average concentration of 403 ± 88 μatm from the seawater samples (these figures have the seawater sample outlier taken out and the corresponding pCO_2 sensor concentration value taken out). This shows a good agreement between both the samples and the sensor. Both sets of data have a strong correlation coefficient of 0.83, p = 0.0003 (n = 14) between them (see Figure 5.10).

5.6.3 Characterisations of carbonate parameters in El Quseir, Red Sea with sensor measurements

In-situ field measurements of the following parameters were made; pCO_2 (with the developed pCO_2 sensor), dissolved oxygen, chlorophyll, salinity, temperature, PAR and depth. The pH sensor unfortunately failed and could not be repaired in the field.

5.6.3.1 Natural variability of carbonate chemistry and other physicochemical variables in El Quseir, Red Sea 15th – 20th March 2017

A comparison of the time series of all variables recorded in the Red Sea is shown overleaf in Figure 5.11. The diel period in March at El Quseir encompassed approximately 12 hours of daylight and approximately 12 hours of darkness. Sunset was around 18:00 hours on each night with sunrise occurring around 06:00 hours every morning.

Overall, the main drivers behind the patterns exhibited by the various parameters recorded in El Quseir were biological activity, temperature and weather conditions. Photosynthetically active radiation has a large bearing on the variables in El Quseir and ultimately is interlinked with all drivers of the diel pattern shown.

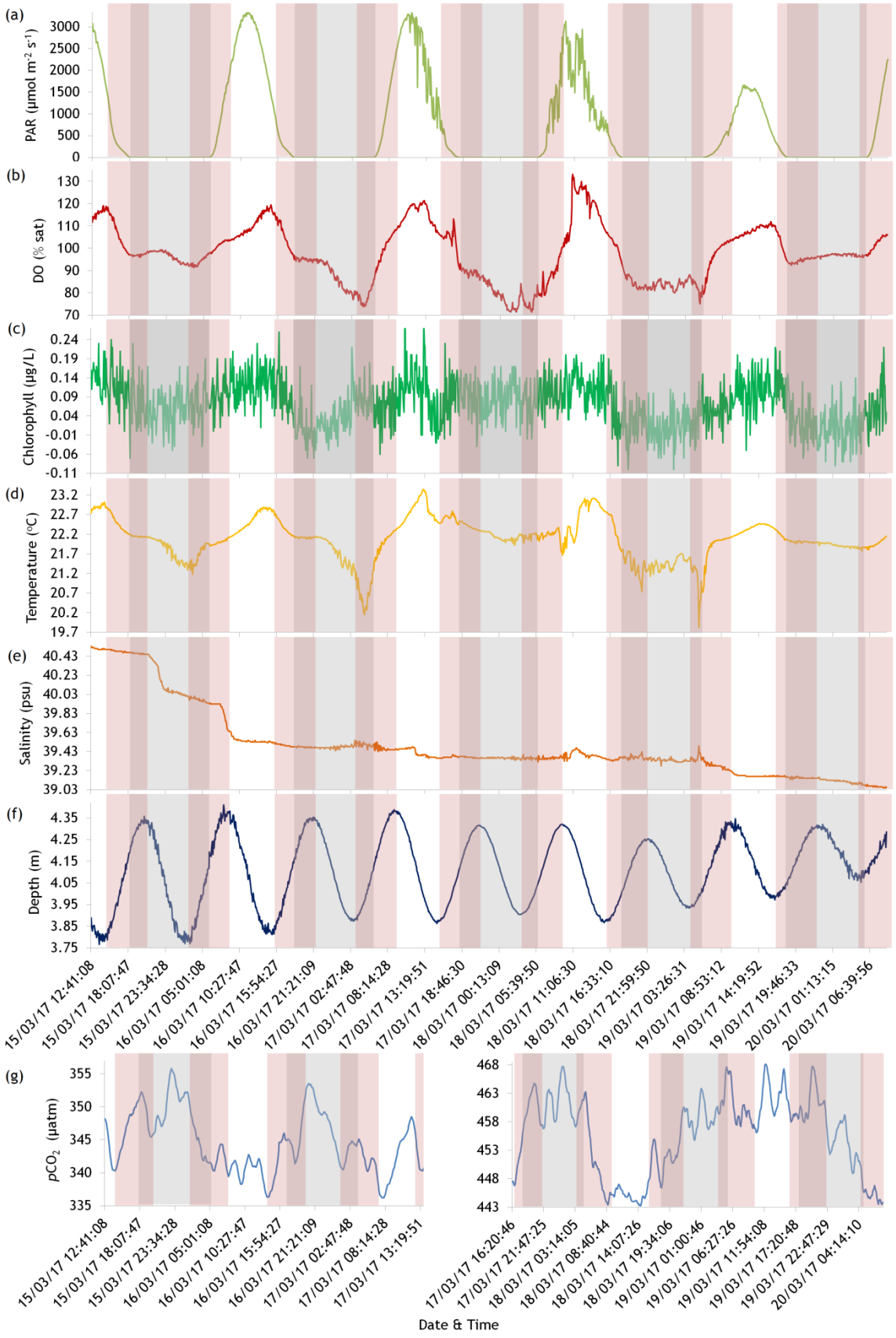

Figure 5.11: Summary plot and comparison of time series of all variables in El Quseir. Odyssey submersible measured PAR (a), YSI EXO2 Sonde measured DO (b), Chl (c), Temperature (d), Salinity (e) depth of water above sensor (f) and developed sensor measured pCO_2 (g). This deployment was for 116 hours 25 minutes in total. Light hours = 56 h 25 m. Dark hours (grey shade) = 60 h. Flood tide is shown in the pink shaded areas. See Figure 5.12 for further information on pCO_2 data.

5.6.3.1.1 pCO_2 data from sensor

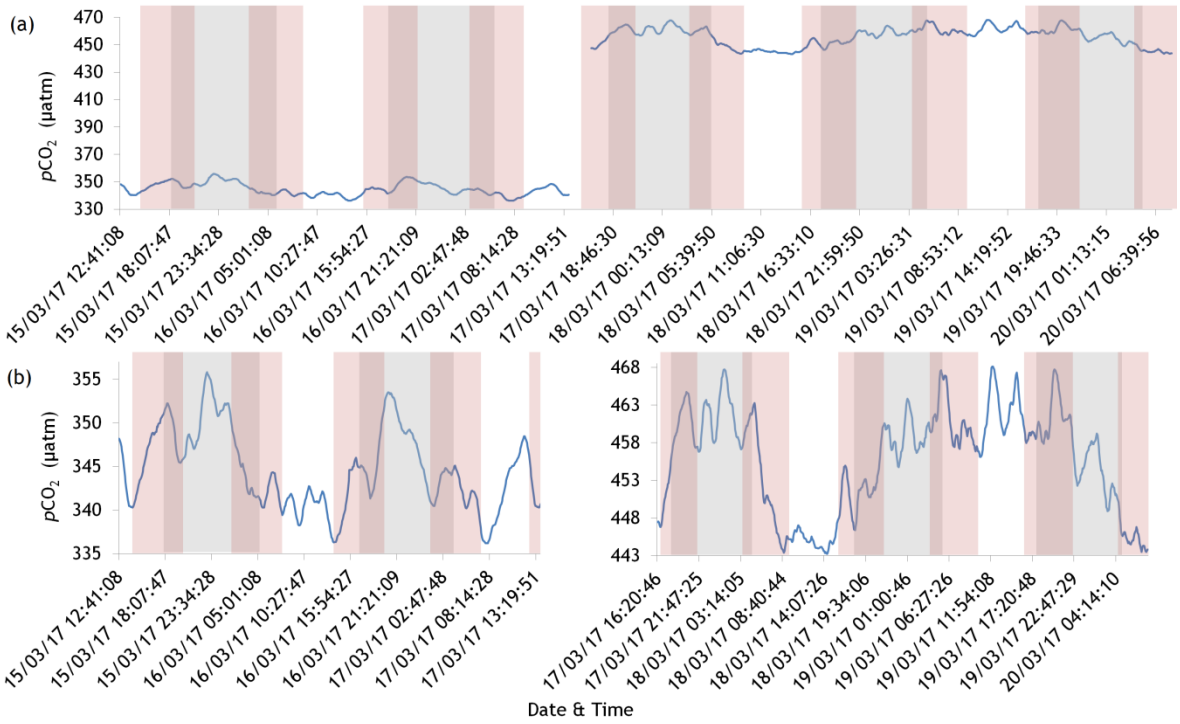

Figure 5.12: pCO_2 sensor data time series. There is a gap in the data due to sensor maintenance. Plot shows pCO_2 data over 5 diel cycles in El Quseir from 15th to 20th March 2017. (a) Plot showing the scale of change in pCO_2 over the deployment. The change was most likely due to extreme weather changes (b) Plots showing the more detailed pCO_2 pattern on separate y-axes over the course of the deployment. N.B. The "jump" in concentration of pCO_2 on the sensor simultaneously happens with the seawater sample pCO_2 concentrations which will be seen later.

There are many potential drivers of pCO_2 in the vicinity of the site at El Quseir. Coral reefs are extensive along with other organisms including pelagic algae utilising the reefs which influence the carbonate chemistry of the surrounding seawater (e.g., Gatusso *et al.*, 1998; Anthony *et al.*, 2011). The biological drivers of respiration, photosynthesis, calcification and remineralisation were some of the main drivers behind the diel patters of pCO_2 on the tropical reef (Anthony *et al.*, 2011). Over the first two days of deployment, the pCO_2 recorded from the sensor was on average a concentration of 345 µatm. However, during the next few days, the pCO_2 was an average concentration of 455 µatm. This is a difference of 110 µatm. The pCO_2 calculated from the discrete *in-situ* seawater samples also exhibit this pattern, with the samples from the first two days having an average concentration of 335 µatm and the pCO_2 concentration of the last three days being 472 µatm. The higher pCO_2

concentration in the latter part of the deployment could be a consequence of several factors. In this instance, the weather appears to have played a significant role in changing the carbonate chemistry of the surface seawater.

The pCO_2 concentrations were lower during the day than they were at night due to metabolic processes, e.g., photosynthesis during the day and respiration at night. Other biological factors also affect the pCO_2 levels and these can include calcification (increase pCO_2) or dissolution (decrease pCO_2). These have been written about in detail in Chapter 4. There was an exception over the deployment when on the 19th March (the day after the heavy sandstorm) where, compared to previous days, light levels were very low, DO concentration was lower and pCO_2 remained high over the course of the day. This would suggest that, post-sandstorm, the light levels were low and therefore there was lower primary productivity. The DO was lower than previously and it could be the case that respiration was the net biological activity due to low light levels. Formation of $CaCO_3$ could also be happening here since pCO_2 is high, A_T deceases and the DIC is consistently high here also. This would usually be expected to happen at night but it would appear that the variables are governed by the low light levels on this unusual day after the sand storm.

DO decreased after sunset when DO is utilised by organisms through respiration and no photosynthesis takes place. The DO pattern in El Quseir was as expected but there were interesting points to discuss due to the weather events. The input of dust into the area appears to have affected the chemical composition of the water with increased nutrients in the vicinity of the sensors (more detail is given about this in the duration of this chapter). DO levels increased to a higher concentration (compared to previous daily cycles) during the sandstorm in daytime and decreased to a lower concentration (compared to the previous night cycles) during the night time. This could be due to the increased primary and secondary production by organisms in the area because of the input of nutrients due to the dust storm.

The site in El Quseir was relatively open compared to the temperate site in Loch Sween which was surrounded by banks and foliage. As discussed in Chapter 4, DO is constantly affected by numerous physical and biological processes like air-sea flux, weather patterns, biological metabolic processes, decomposition,

temperature, salinity and pressure (Barnes, 1983; Gattuso *et al.*, 1996; Zeebe *et al.*, 1999; Anthony *et al.*, 2011; Smith *et al.*, 2013; Rerolle *et al.*, 2014). Specifically in this research, the DO in El Quseir was governed by temperature and biological processes. The DO was also affected by the sand storm weather event. The DO is highest in the middle of the daylight cycle where there will usually be an accumulation of photosynthetic activity. Peak DO is actually approximately 2 hours behind peak light concentrations. This could suggest an optimum condition for photosynthesis where light levels are slightly lower than their maximum in El Quseir (Burdett *et al.*, 2013).

Chlorophyll can be used as a proxy for phytoplankton present in the water column. However, it must be noted that chlorophyll is not a direct measurement of phytoplankton biomass. Temperature and PAR affect PP rates but standing stock is a function of such aspects as light, nutrients, mixing and stratification (Geider *et al.*, 1998). Chlorophyll in El Quseir is heavily correlated with day/night cycles and generally had a pattern of a minimum at night and a peak during the day. Often during dark hours the chlorophyll would reach a negative value. This coincides with the oxygen depletion and the concurrent lack of photosynthesis (Papageorgiou and Govindjee, 2004). The concentration in El Quesir is much lower than temperate areas because tropical waters are generally oligotrophic.

5.6.3.1.2 Drivers of variation in the Red Sea 15th to 20th March 2017

Over the course of this deployment, diel cycles were prominent in every variable recorded. Biological activity, temperature and weather phenomena were a principle driving force behind the patterns in pCO_2 (compared to tidal influences in previous field work). A dust storm towards the second half of deployment was influential in light levels, nutrient input and productivity levels. Paired variables were analysed and the most correlated are shown overleaf. The strongest correlations are visibly seen with the parallel time series and quantified through Pearson's correlation coefficient (and simultaneously with equations of a straight line). Analyses has been centred around tidal (flood tide is represented in pink) and diel (night is represented in grey) patterns over the course of the deployment of the sensors. PCA was also used to corroborate previous analyses.

5.6.3.1.2.1 Variables driven by diel cycle

5.6.3.1.2.1.1 DO and temperature

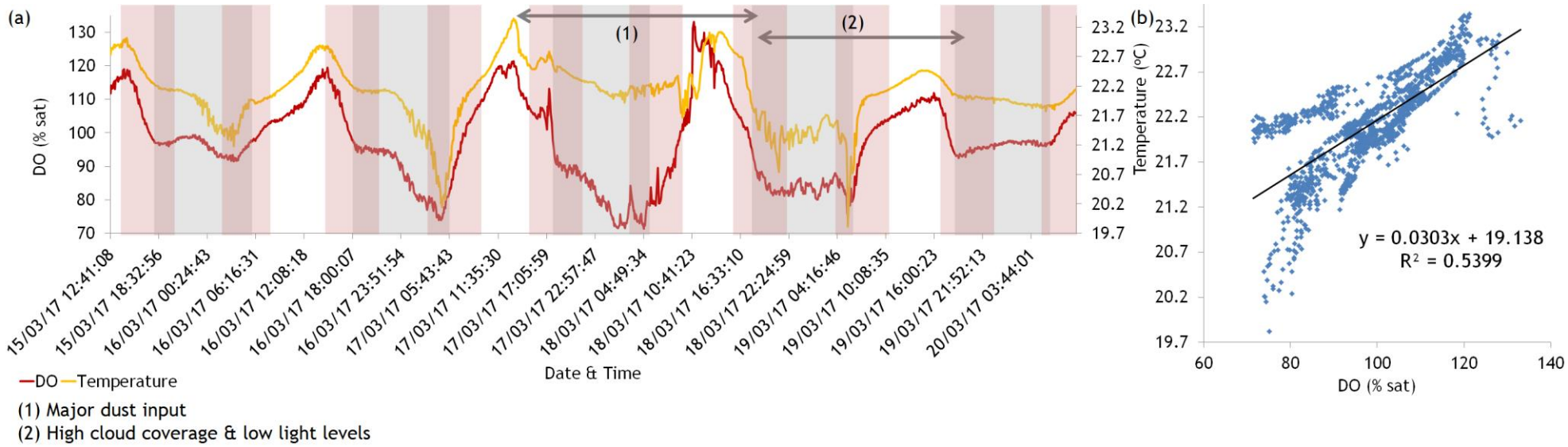

Figure 5.13: (a) parallel time series of DO and temperature in El Quseir from 15th to 20th March 2017 encompassing day (no shade), night (grey shade) and flood tide (pink shade). Arrow 1 represents the duration of major dust input and arrow 2 represents the duration of high cloud coverage and low light levels. Temperature; Mean = 22.09 ± 0.51 °C. DO; Mean = 97.57 ± 12.38 %sat. (b) scatter graph of DO and temperature with linear trendline. Coefficient of determination; R^2 = 0.54. Pearson correlation coefficient; r = 0.73. p < 0.001.

The parallel time series of DO and temperature is shown in Figure 5.13a. The DO cyclical fluctuation in El Quseir was from 71.4 to 133.7% (ΔDO = 62.3%) with a daily mean of 106.8% and a nightly mean of 88.9%. The temperature ranged from 19.82^{o}C to 23.34^{o}C (ΔT = 3.52^{o}C) with a daily mean of 22.40^{o}C and a nightly mean of 21.80^{o}C. There is a significant positive correlation ($r = 0.73$, $p < 0.001$) between DO and temperature in El Quseir (Figure 5.13b).

DO is highly positively correlated with temperature in El Quseir and they both follow a very similar pattern throughout the deployment. The temperature reached a maximum in the middle of each diurnal cycle (the water was the warmest at the hottest part of the day) as did the DO (due to biological activity). The parallel time series of DO and temperature (Figure 5.13a) exhibits such a similarly interlinked pattern that that these two variables appear to be explicitly linked rather than the coincidental occurrence of the highest temperature coinciding with the peak photosynthesis time.

The positive correlation between DO and temperature in El Quseir is the opposite of what would be expected according to gas laws, i.e. usually a decrease (or increase) in temperature would increase (decrease) the solubility of DO (Bakker *et al.*, 1999; Wetzel, 2001) which would show an inverse correlation. This would suggest that the relationship is more one of DO being strongly linked with light and also, temperature being strongly linked to insolation. Therefore, light is the key driver of DO and also temperature in this research.

5.6.3.1.2.1.2 Chlorophyll and temperature

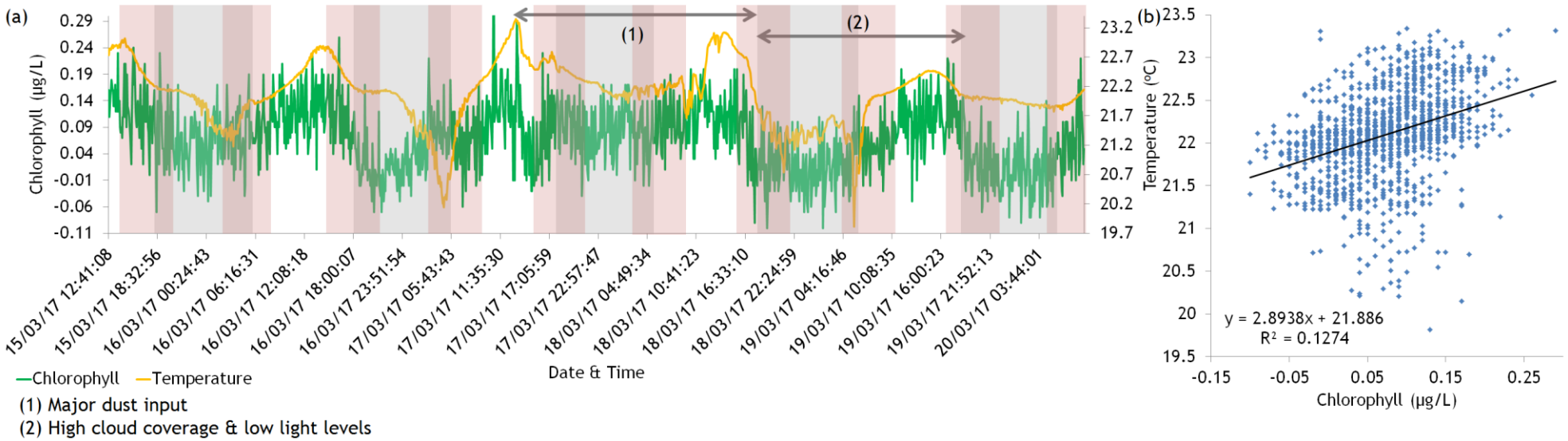

Figure 5.14: (a) parallel time series of chlorophyll and temperature in El Quseir from 15th to 20th March 2017 encompassing day (no shade), night (grey shade) and flood tide (pink shade). Arrow 1 represents the duration of major dust input and arrow 2 represents the duration of high cloud coverage and low light levels. Chlorophyll; Mean = 0.07 ± 0.06 µg/L. Temperature; Mean = 22.09 ± 0.51 °C. (b) scatter graph of chlorophyll and temperature with linear trendline. Coefficient of determination; R^2 = 0.13. Pearson correlation coefficient; r = 0.36. p < 0.001.

The parallel time series of chlorophyll and temperature in El Quseir is shown in Figure 5.14a. The chlorophyll cyclical fluctuation in El Quseir was from -0.1 to 0.29 μg/L (ΔChl = 0.31) with a daily mean of 0.098 and a nightly mean of 0.045 μg/L. There is a significant positive correlation ($r = 0.36$, $p < 0.001$) between chlorophyll and temperature in El Quseir (shown in figure 5.14b). Temperatures would typically be the highest at the part of the day when the most photosynthesis was taking place and therefore it would be expected that a positive correlation would be seen between these two variables.

5.6.3.1.2.1.3 Chlorophyll and DO

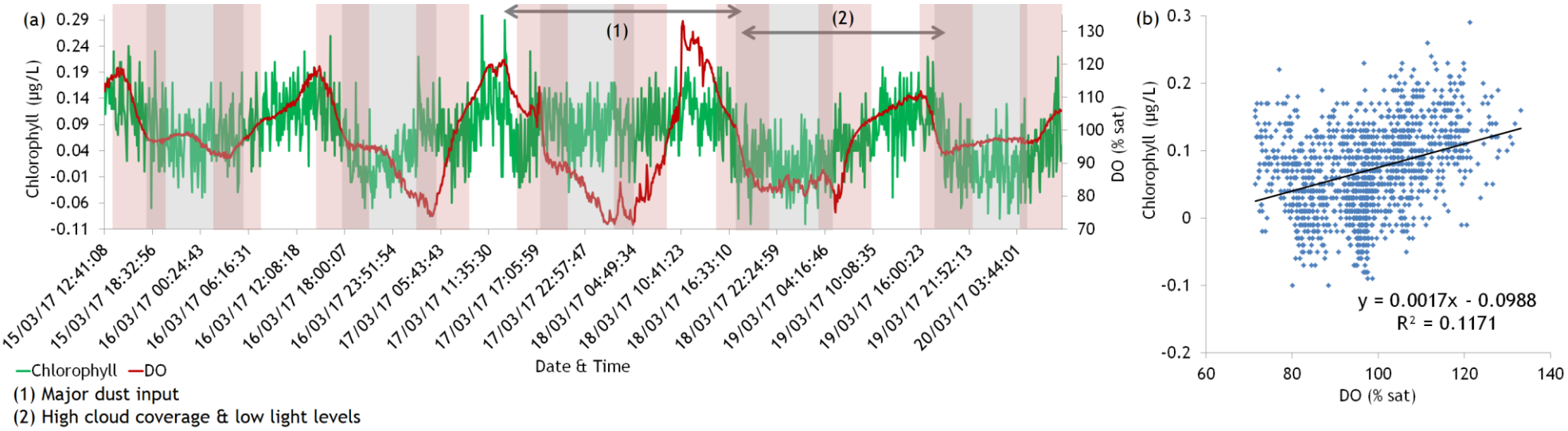

Figure 5.15: (a) parallel time series of chlorophyll and DO in El Quseir from 15th to 20th March 2017 encompassing day (no shade), night (grey shade) and flood tide (pink shade). Arrow 1 represents the duration of major dust input and arrow 2 represents the duration of high cloud coverage and low light levels. Chlorophyll; Mean = 0.07 ± 0.06 µg/L. DO; Mean = 97.6 ± 12.4 %sat. (b) scatter graph of chlorophyll and DO with linear trendline. Coefficient of determination; R^2 = 0.12. Pearson correlation coefficient; r = 0.34. p < 0.001.

The parallel time series of chlorophyll and DO in El Quseir is shown in Figure 5.15a. There is a significant positive correlation ($r = 0.34$, $p < 0.001$) between chlorophyll and DO in El Quseir (as shown in Figure 5.15b). A positive correlation would be expected due to photosynthesis occuring during daylight hours.

5.6.3.1.2.1.4 Chlorophyll and PAR

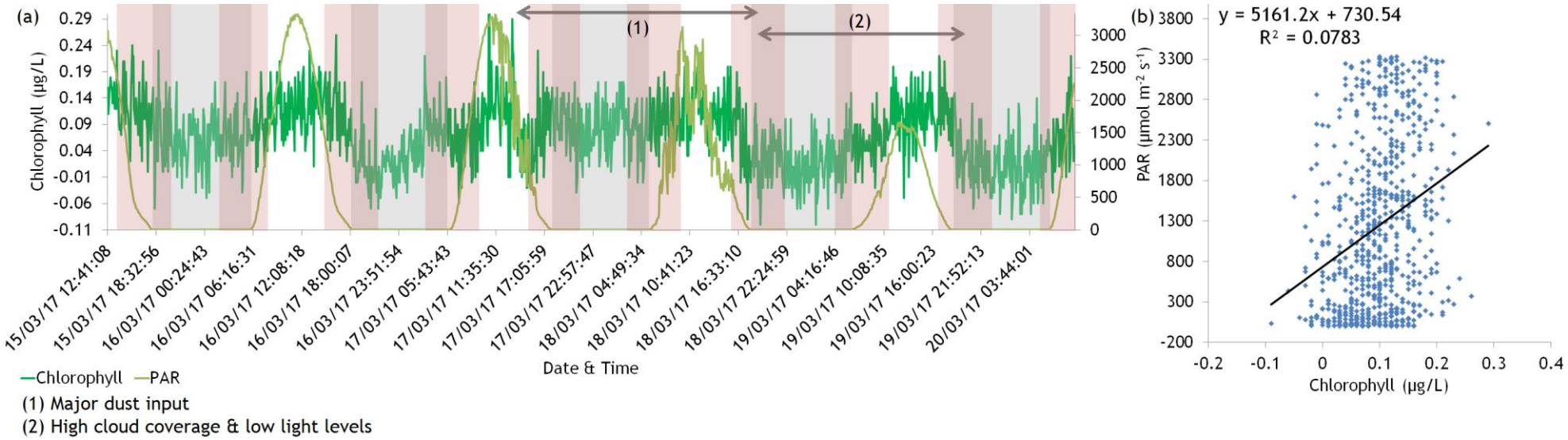

Figure 5.16: (a) parallel time series of chlorophyll and PAR in El Quseir from 15th to 20th March 2017 encompassing day (no shade), night (grey shade) and flood tide (pink shade). Arrow 1 represents the duration of major dust input and arrow 2 represents the duration of high cloud coverage and low light levels. Chlorophyll; Mean = 0.07 ± 0.06 µg/L. Mean daily PAR levels are shown in Figure 5.17. (b) scatter graph of chlorophyll and PAR with linear trendline. Coefficient of determination; R^2 = 0.08. Pearson correlation coefficient; r = 0.28. p < 0.001.

The parallel time series of chlorophyll and PAR is shown in Figure 5.16a. There is a positive correlation ($r = 0.28$, $p < 0.001$) between chlorophyll and PAR in El Quseir (Figure 5.16b).

The four full diurnal cycles (Wednesday and Monday were shorter than a full diurnal cycle because the sensors were deployed and retrieved on these days) saw the light levels drop over the duration of the deployment with the lowest being an average of 734 µmol m^{-2} s^{-1} on Sunday which coincides with the sandstorm which started on Saturday and the effect lasted until the end of Sunday (see Figure 5.17).

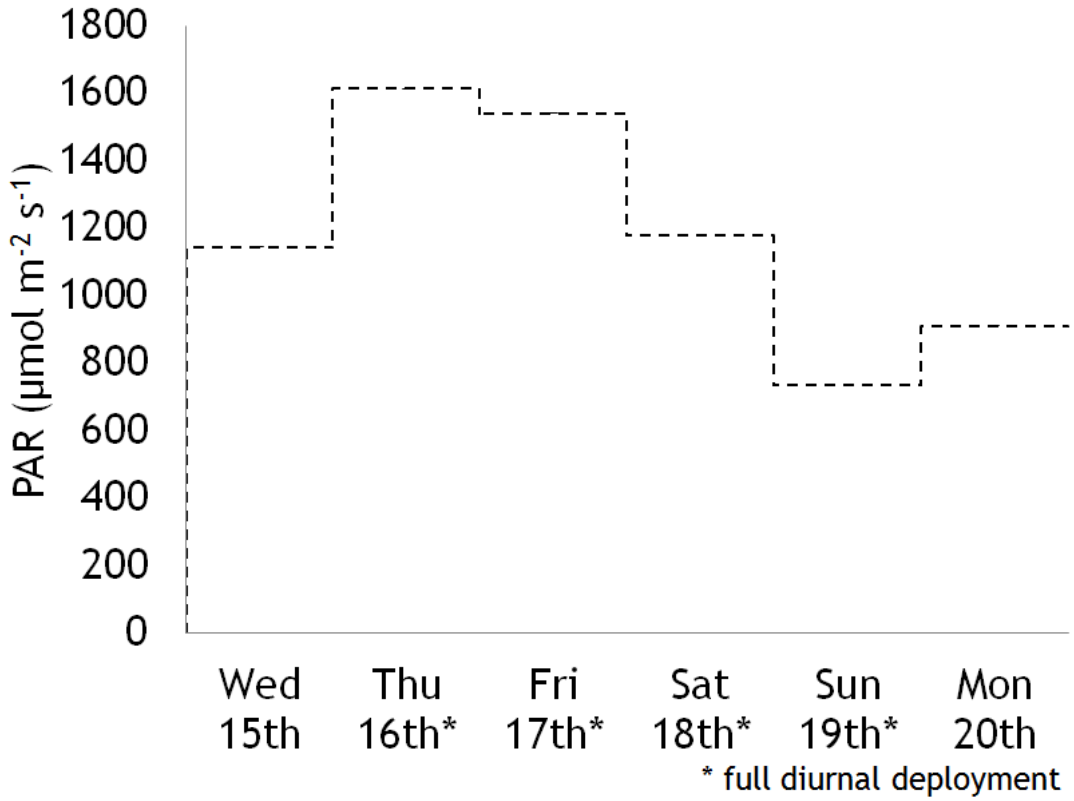

Figure 5.17: Average concentration of photosynthetically available radiation on each day of deployment.

5.6.3.1.2.1.5 DO and pCO_2 from sensor

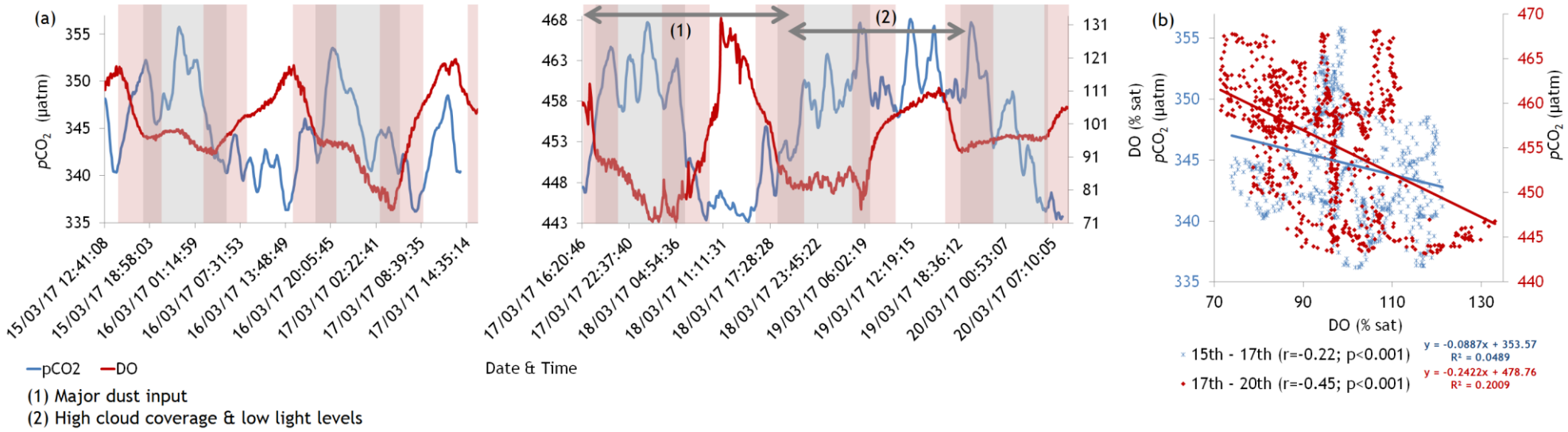

Figure 5.18: (a) parallel time series of DO and pCO_2 in El Quseir from 15th to 20th March 2017 encompassing day (no shade), night (grey shade) and flood tide (pink shade). Arrow 1 represents the duration of major dust input and arrow 2 represents the duration of high cloud coverage and low light levels. DO; Mean = 97.6 ± 12.4 %sat. pCO_2; Mean = 407 ± 55 µatm. There is a gap in the pCO_2 data because of sensor maintenance during deployment. (b) scatter graph of DO and pCO_2 with linear trendline. Coefficient of determination; (15th – 17th) R^2 = 0.05, (17th – 20th) R^2 = 0.20. Pearson correlation coefficient; (15th – 17th) r = -0.22, (17th – 20th) r = -0.45. p < 0.001.

The parallel time series of DO and pCO_2 in El Quseir is shown in Figure 5.18a. The pCO_2 fluctuated from 336.20 to 468.08 µatm (ΔpCO_2 = 131.88 µatm) with a daily pCO_2 mean of 400.22 µatm and a nightly mean of 413.75 µatm. There is a negative correlation between pCO_2 and DO in El Quseir. A stronger correlation is found from 17th to 20th as compared to 15th – 17th March (Figure 5.18b). Data for analysis was split at this point due to two different y-axes pCO_2 concentrations induced by extreme environmental conditions experienced at the site during deployment on the 17th – 20th (see Figure 5.12a where all the pCO_2 data plotted on the same y-axis is presented). Looking at the data according to similar y-axes pCO_2 concentrations was to avoid erroneous trends or correlations. It must be noted now that this phenomenon was seen in both the pCO_2 concentrations produced by the sensor and the pCO_2 concentrations calculated from the seawater samples, i.e. sensor concentrations were corroborated by seawater calculations.

Overall, pCO_2 was negatively correlated with DO which reflects the roles of respiration and photosynthesis of the organisms at night and at day respectively (Morris and Taylor, 1982). It was also predictably strongly negatively correlated with PAR which itself drives the energy for photosynthesis and respiration.

5.6.3.1.2.1.6 Chlorophyll and pCO_2 from sensor

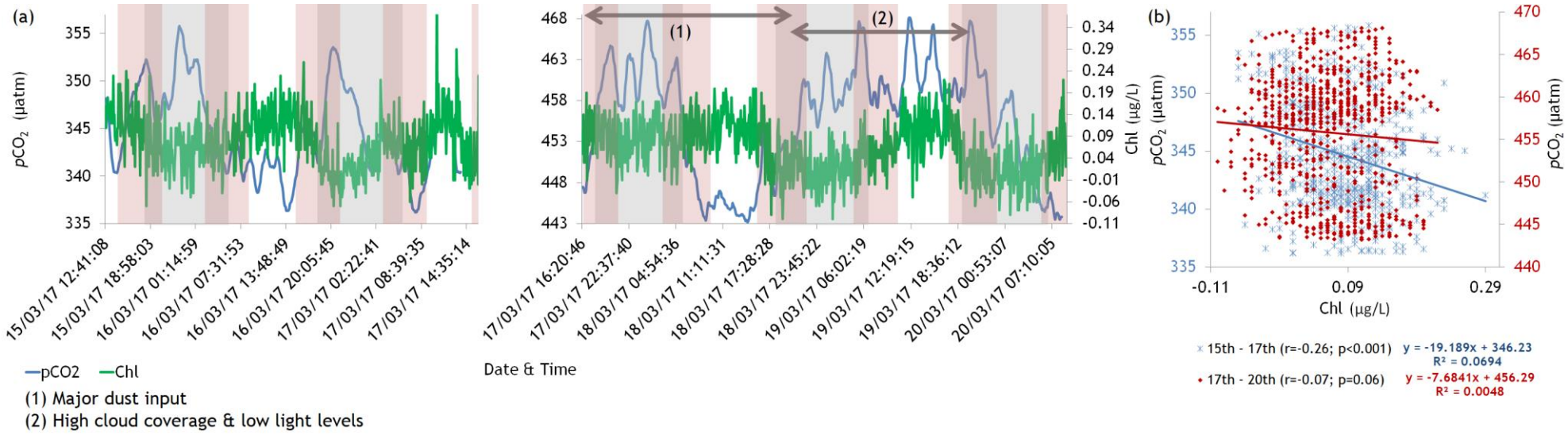

Figure 5.19: (a) parallel time series of chlorophyll and pCO_2 in El Quseir from 15th to 20th March 2017 encompassing day (no shade), night (grey shade) and flood tide (pink shade). Arrow 1 represents the duration of major dust input and arrow 2 represents the duration of high cloud coverage and low light levels. Chlorophyll; Mean = 0.07 ± 0.06 µg/L. pCO_2; Mean = 407 ± 55 µatm. (b) scatter graph of chlorophyll and pCO_2 with linear trendline. Coefficient of determination; (15th – 17th) R^2 = 0.07, (17th – 20th) R^2 = 0.005. Pearson correlation coefficient; (15th – 17th) r = -0.26, (17th – 20th) r = -0.07

The parallel time series of Chl and pCO_2 is shown in figure 5.19a. There is an inverse correlation between pCO_2 and Chl in El Quseir but only during the first part of the deployment (15th to 17th) although the statistics for 17th to 20th March (Figure 5.19b) had a high p-value.

At the start of the deployment before the sandstorm, there was an inverse relationship between Chl and pCO_2. With lower concentrations of Chl at night, this will coincide with higher respiration levels and therefore there will be higher levels of pCO_2 in the surrounding water (Litt *et al.*, 2010). However, this pattern does not continue from the sandstorm to the end of deployment where nutrients and light levels affect Chl and pCO_2 respectively and the two variables become decoupled as these other factors drive them.

The next section deals with an investigation of different water masses entering and leaving the site over the course of the deployment and unlike Caol Scotnish, this analysis suggests water masses did not have a large influence in El Quseir.

5.6.3.1.2.1.7 Temperature and salinity

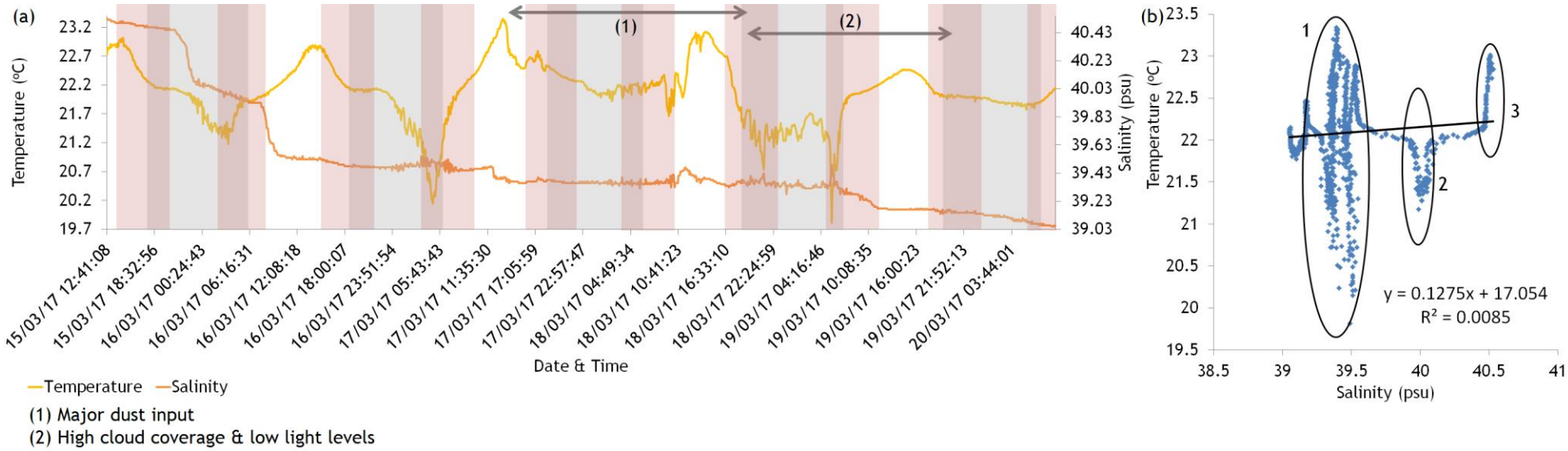

Figure 5.20: (a) parallel time series of temperature and salinity in El Quseir from 15th to 20th March 2017 encompassing day (no shade), night (grey shade) and flood tide (pink shade). Temperature; Mean = 22.09 ± 0.51 °C. Salinity; Mean = 39.50 ± 0.37 psu. (b) scatter graph of temperature and salinity with linear trendline. Coefficient of determination; R^2 = 0.01. Pearson correlation coefficient; r = 0.09. p < 0.001. The circled areas show the different water masses identified in the El Quseir site area. The three water masses all have a different combination of temperature and salinity concentrations.

The parallel time series of temperature and salinity in El Quseir in March is shown in Figure 5.20a. The salinity varied from 39.05 to 40.53 psu (Δsal = 1.48 psu). The daily mean was 39.49 and the nightly mean was 39.50 psu. There was no correlation ($r = 0.09$, $p < 0.001$) between temperature and salinity in El Quseir for the duration of this deployment (most likely due to the diel range being affected by insolation) but this was still included to show the different water masses (if any).

Water mass	Salinity (psu)	Temperature (°C)	Water Type
1	39.06 - 39.59 (μ = 39.33)	23.34 - 19.82 (μ = 21.58)	low salinity, wide-ranging temperature
2	39.59 - 40.24 (μ = 39.92)	22.012 - 22.060 (μ = 22.04)	middling salinity, middling temperature
3	40.24 - 40.53 (μ = 40.39)	22.060 - 22.844 (μ = 22.45)	high salinity, high temperature

Table 5.3: Water masses and their temperature-salinity characteristics in El Quseir from 15th to 20th March 2017. Water mass 1 contains low salinity and a wide-range of temperature which encompasses most of the deployment from approximately midday on the 16th right through until the end of deployment on the 20th. Water mass 2 has middling salinity and middling temperature which occurs half way through the first night cycle to midday on the 16th. Water mass 3 has both high salinity and high temperature (this can be seen at the start of deployment until approximately half way through the first night cycle).

Water mass 1 appears to contain both day and night temperatures but water mass 2 and water mass 3 contains only night temperatures and only day temperatures respectively. This would suggest that water mass 3 is the start of the deployment during the day on the 15th, water mass 2 is the transition to middling salinity in the dark period over the early hours of the 16th and water mass 1 represents the rest of the deployment.

5.6.3.1.2.1.8 PAR and pCO_2 from sensor

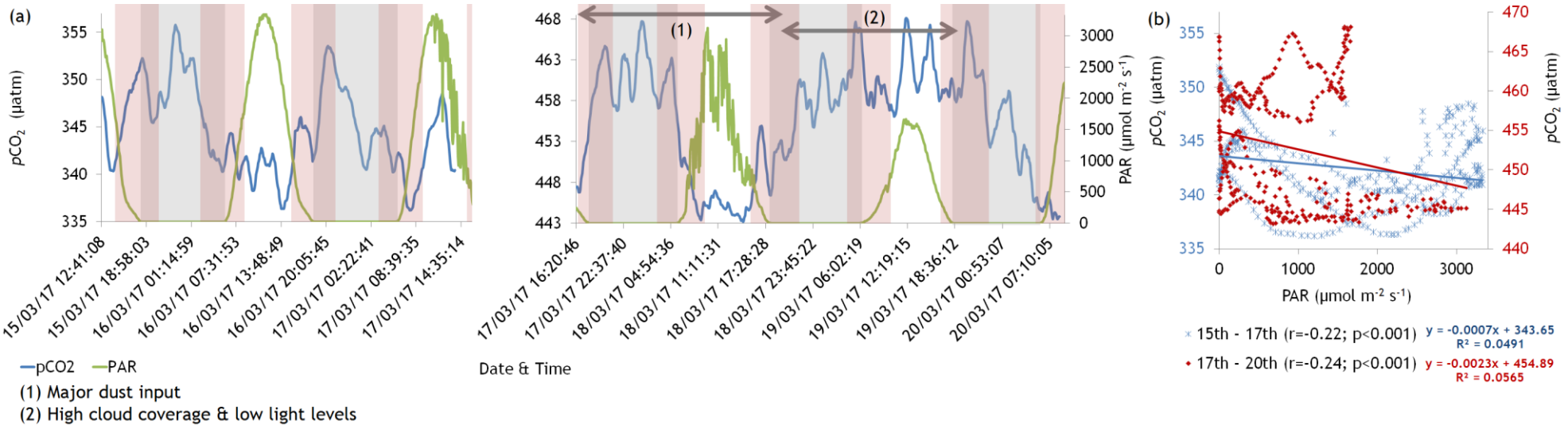

Figure 5.21: (a) parallel time series of PAR and pCO_2 in El Quseir from 15th to 20th March 2017 encompassing day (no shade), night (grey shade) and flood tide (pink shade). Arrow 1 represents the duration of major dust input and arrow 2 represents the duration of high cloud coverage and low light levels. pCO_2; Mean = 407 ± 55 µatm. There is a gap in the pCO_2 data because of sensor maintenance during deployment. (b) scatter graph of pCO_2 and PAR with linear trendline. Coefficient of determination; (15th – 17th) R^2 = 0.05, (17th – 20th) R^2 = 0.06. Pearson correlation coefficient; (15th – 17th) r = -0.22, (17th – 20th) r = -0.24. p < 0.001.

The parallel time series of PAR and pCO_2 in El Quseir is shown in Figure 5.21a. There is a significant negative correlation between PAR and pCO_2 throughout the deployment as shown in Figure 5.21b.

5.6.3.1.2.1.9 Temperature and pCO_2

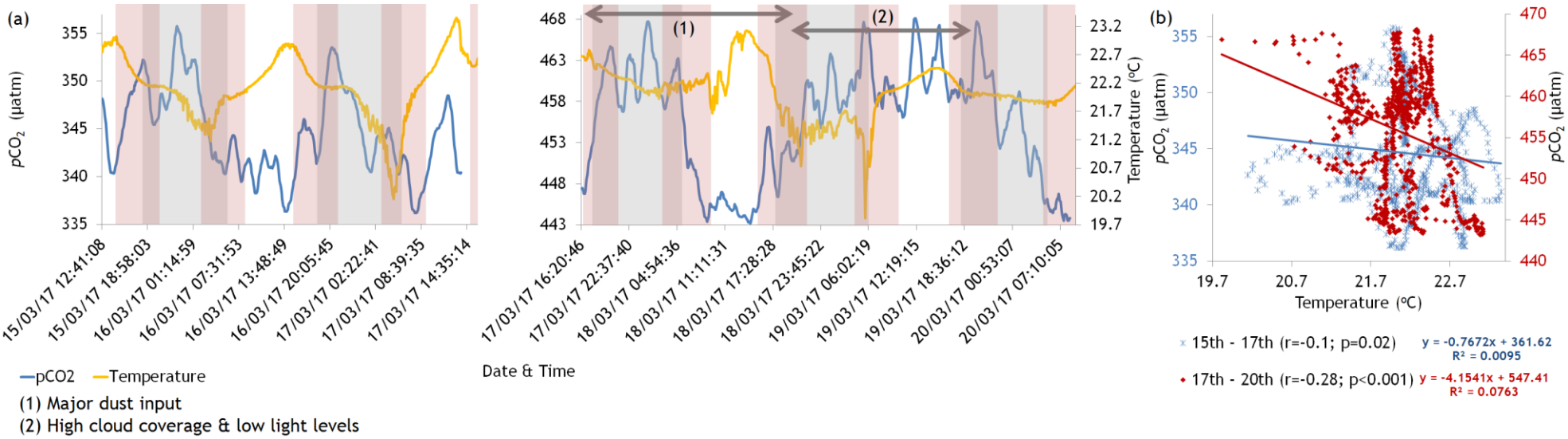

Figure 5.22: (a) parallel time series of temperature and pCO_2 in El Quseir from 15th to 20th March 2017 encompassing day (no shade), night (grey shade) and flood tide (pink shade). Arrow 1 represents the duration of major dust input and arrow 2 represents the duration of high cloud coverage and low light levels. Temperature; Mean = 22.09 ± 0.51 ^{o}C. pCO_2; Mean = 407 ± 55 µatm. There is a gap in the pCO_2 data because of sensor maintenance during deployment. (b) scatter graph of temperature and pCO_2 with linear trendline. Coefficient of determination; (15th – 17th) R^2 = 0.01, (17th – 20th) R^2 = 0.08. Pearson correlation coefficient; (15th – 17th) r = -0.10, (17th – 20th) r = -0.28. p < 0.001.

The parallel time series of temperature and pCO_2 in El Quseir is shown in Figure 5.22a. There is a significant negative correlation between temperature and pCO_2 although only from 17th to 20th whereas there is no real correlation from 15th to 17th as shown in Figure 5.22b.

5.6.3.1.2.1.10 Salinity and pCO_2

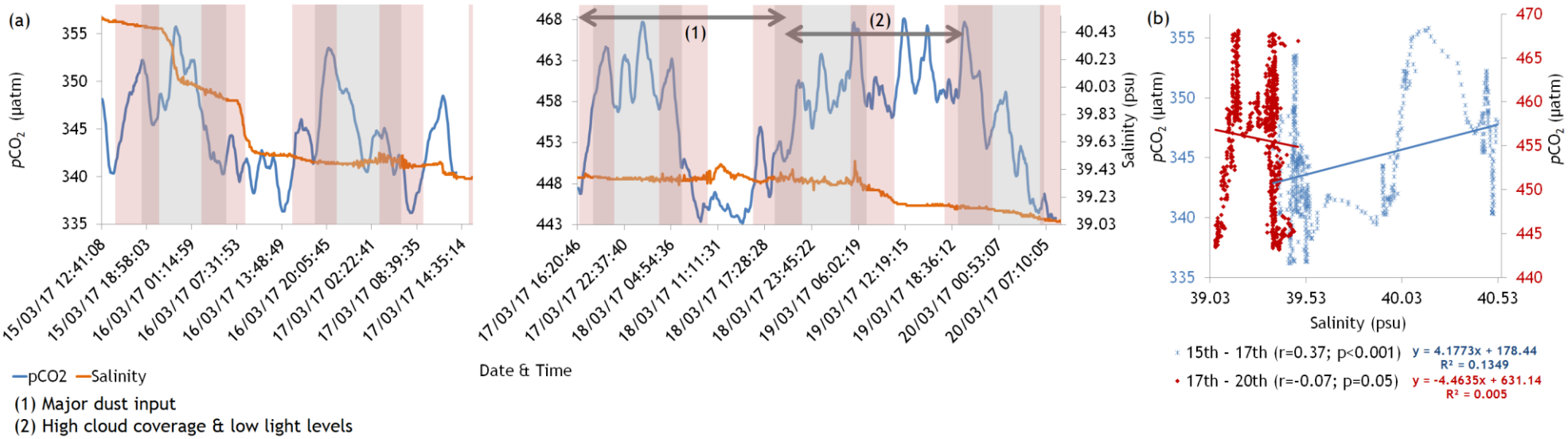

Figure 5.23: (a) parallel time series of salinity and pCO_2 in El Quseir from 15th to 20th March 2017 encompassing day (no shade), night (grey shade) and flood tide (pink shade). Arrow 1 represents the duration of major dust input and arrow 2 represents the duration of high cloud coverage and low light levels. Salinity; Mean = 39.50 ± 0.37 psu. pCO_2; Mean = 407 ± 55 µatm. There is a gap in the pCO_2 data because of sensor maintenance during deployment. (b) scatter graph of salinity and pCO_2 with linear trendline. Coefficient of determination; (15th – 17th) R^2 = 0.13, (17th – 20th) R^2 = 0.01. Pearson correlation coefficient; (15th – 17th) r = 0.37, (17th – 20th) r = -0.07. p < 0.001.

The parallel time series of salinity and pCO_2 in El Quseir in March is shown in Figure 5.23a. From the 15th to 17th, there is a significant positive correlation between pCO_2 and salinity, however, for the remainder of the deployment there is no correlation between the two variables as shown in Figure 5.23b.

DIC in El Quesir seems to have been affected by the unusual weather conditions. During the dust storm, there was an increase in concentrations of DIC (just as the pCO_2 increased). It is useful to show a time series of all variables with DIC concentrations in the site and the correlations between them (as shown in Figure 5.24).

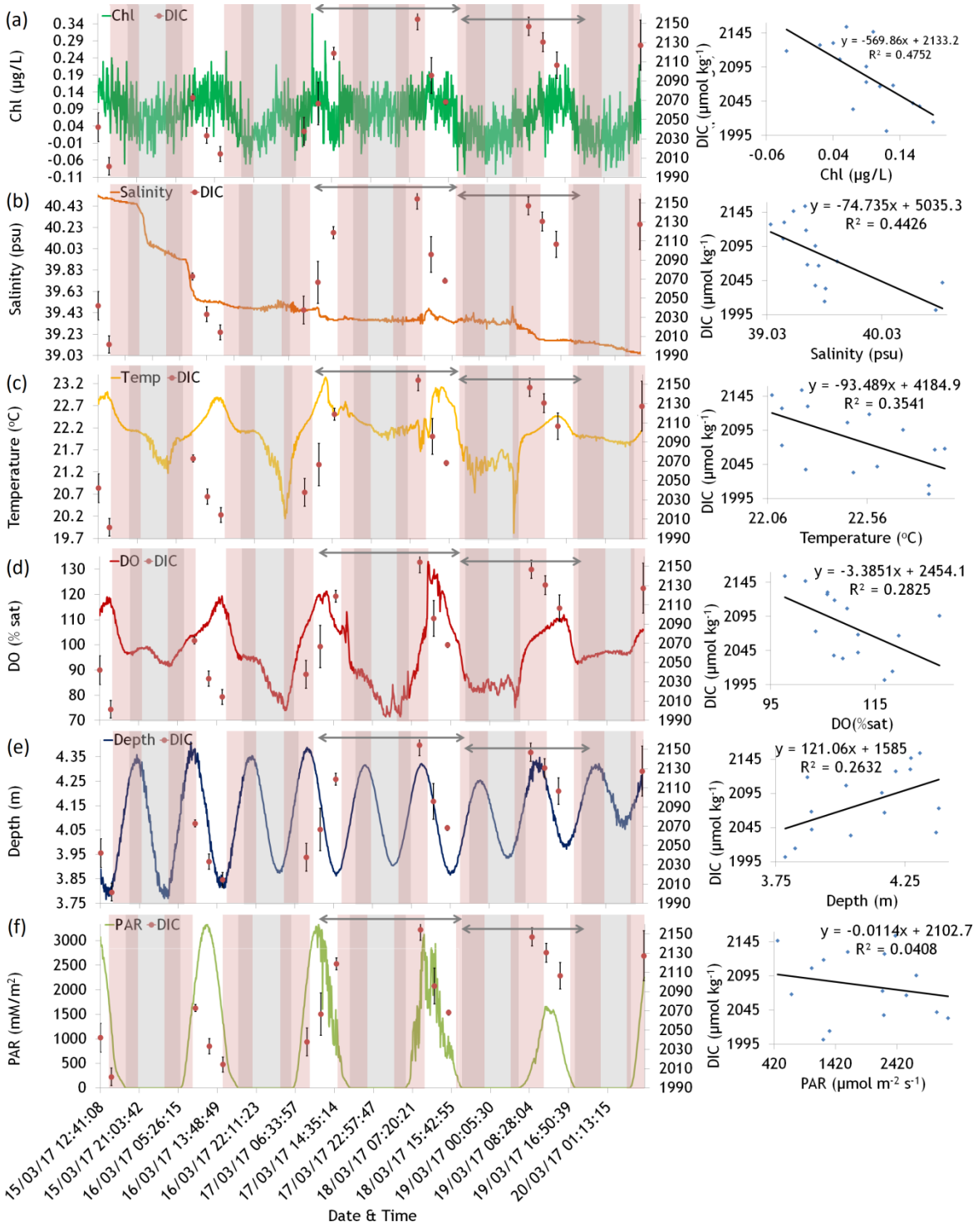

Figure 5.24: Summary plot and comparison of time series of all variables with calculated DIC in water samples. (a) Chl & DIC (Pearson correlation coefficient r = -0.69) (b) Salinity & DIC (r = -0.66) (c) Temperature & DIC (r = -0.59) (d) DO & DIC (r = -0.53) (e) Depth & DIC (r = 0.51) (f) PAR & DIC (r = -0.20). It has to be noted that the sample size for DIC was much smaller in that there were only 15 DIC samples to be compared directly to the corresponding variable. Light hours = 56 h 25 m. Dark hours (grey shade) = 60 h. Flood tide is shown in the pink shaded areas. See Figure 5.25 for further information on pCO_2 data.

5.6.3.1.2.1.11 DIC and pCO_2

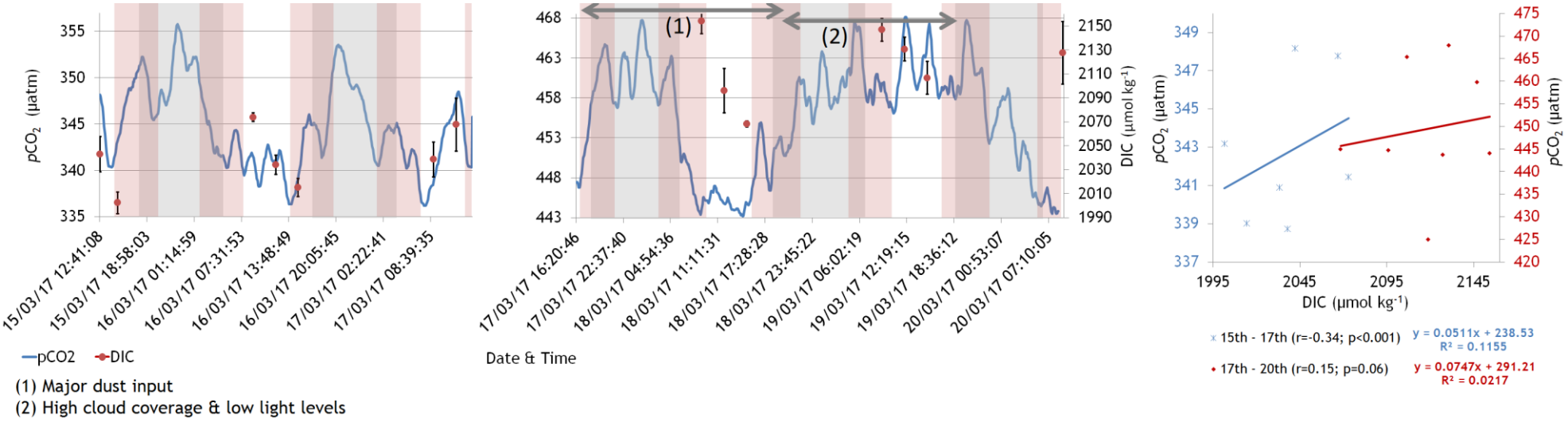

Figure 5.25: (a) parallel time series of DIC and pCO_2 in El Quseir from 15th to 20th March 2017 encompassing day (no shade), night (grey shade) and flood tide (pink shade). Arrow 1 represents the duration of major dust input and arrow 2 represents the duration of high cloud coverage and low light levels. There is a gap in the pCO_2 data because of sensor maintenance during deployment. This parallel time series is notable for the coordination of the increase in both the pCO_2 concentrations on the sensor and the increase in concentration of DIC in the water samples (b) scatter graph of DIC and pCO_2 with linear trendlines. Coefficient of determination; (15th – 17th) R^2 = 0.12, (17th – 20th) R^2 = 0.02. Pearson correlation coefficient; (15th – 17th) r = 0.34, (17th – 20th) r = 0.15. p < 0.001.

Data for DIC only included samples taken in the daylight hours so it is not possible to comment on the diel cycles. However, the notable aspects of the DIC data recorded is that it increases significantly on the 17th and stays higher compared to the 15th and 16th for the remainder of the deployment. DIC concentration is usually heavily dependent on biological activity in the water column with DIC being released when respirations occurs. DIC uptake occurs when photosynthesis takes place (Schulz and Riebesell, 2013). Other factors that affect DIC is evaporation and mixing and also the flux between atmosphere and the sea surface (Schulz and Riebesell, 2013). However, air-sea flux can be ruled out as the main driver of this quick increase of DIC as equilibration between the surface of the water and the atmosphere can take time. The flux between the atmospheric CO_2 and the concentration of the sea surface of carbon parameters is a comparatively slow equilibration process and can generally be overshadowed by other processes which act upon the DIC or CO_2 (Bakker *et al.*, 1999).

Predictably, the DIC was highly correlated the most with with pCO_2 readings from the sensor as pCO_2 and DIC are inextricably linked through the mass conservation equation (Williams and Fallows, 2011);

$$DIC = [CO_2^*] + [HCO_3^-] + [CO_3^{2-}] \quad (36)$$

As mentioned, for the final three days in the deployment, both the DIC and pCO_2 rise to concentrations that were significantly higher than in the first two days of deployment. DIC concentration over the first two days spanned 2001.53 – 2072.93 μmol kg^{-1} and had an average concentration of 2038.35 μmol kg^{-1}. The DIC concentration over the final three days spanned 2068.3 – 2154.22 μmol kg^{-1} and had an average concentration of 2118.55 μmol kg^{-1} (ΔDIC = 80.2 μmol kg^{-1}). The steady increase of DIC coincides with a decrease in salinity over the course of the deployment ($r = -0.67$; $p = 0.007$). However, other factors appear to be heavily involved. For example, although the salinity concentration levels out to near constant, variables like DIC and pCO_2 still keep to their particular cycle. The standout environmental factor which coincides with the steep rise in DIC

and pCO_2 concentrations is the sandstorm and very high winds which occurred in El Quseir in the early hours of the 18th March.

5.6.3.1.2.1.12 Lack of tidal influence

Depth was used as a proxy for tidal depth as in Chapter 4. The tides did not have any correlation with other variables throughout this study. This would also explain the lack of evidence of different water bodies through investigation of the temperature and salinity (N.B., there *are* different water bodies which are exchanged in the Red Sea as a whole as described in the introduction but in this particular site, the tides do not appear to introduce different water bodies). There were two low tides and two high tides over 24 hours split into two during daylight hours and two during darkness. There was no correlation of the tides to any variable in El Quseir as shown in Figure 5.26 (perhaps with the exception of PAR which had a Pearson correlation coefficient of r = 0.24, although this is still weak).

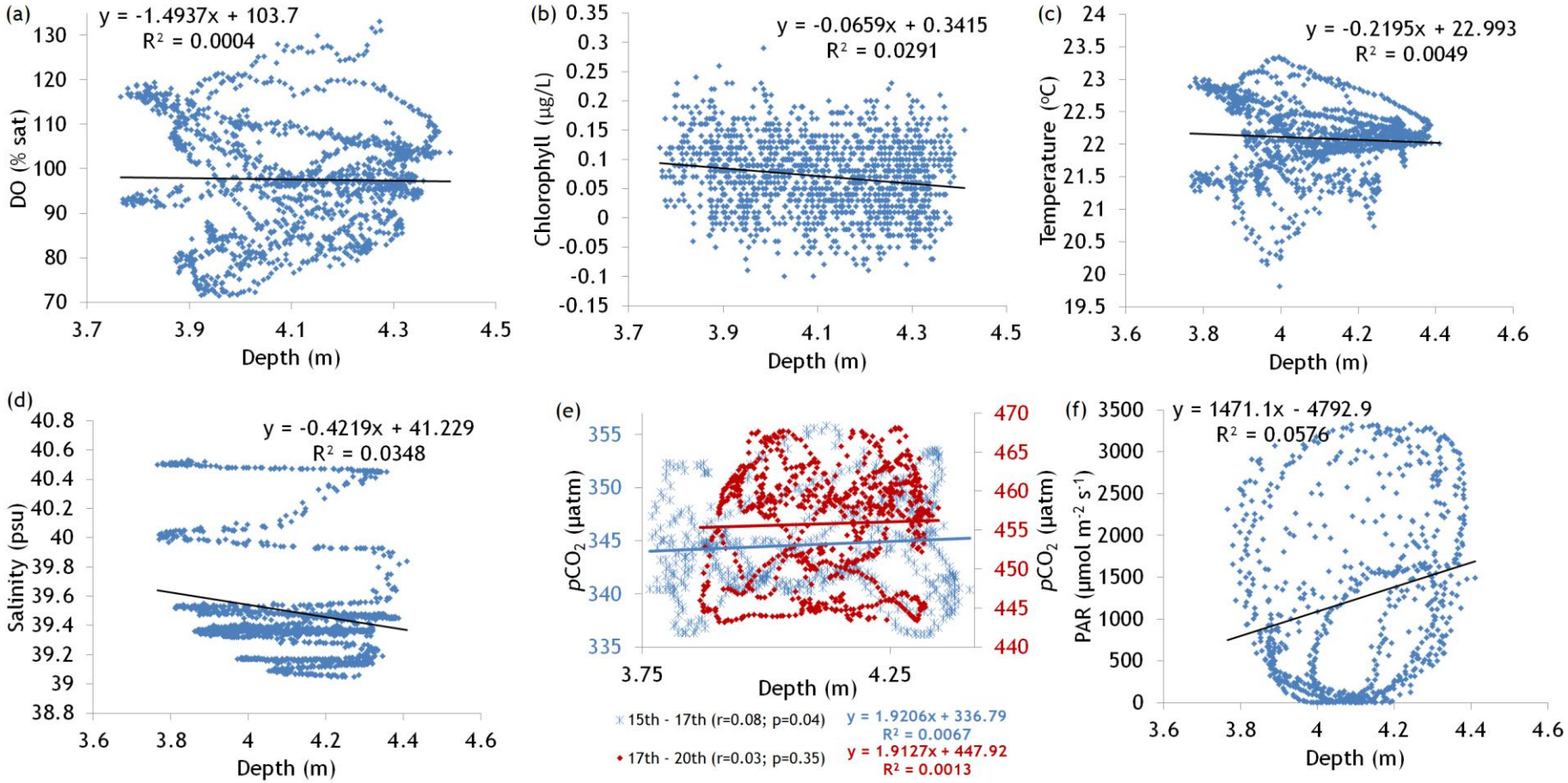

Figure 5.26: Scatter graphs with linear trendline showing depth against (a) DO (r = 0.02) (b) Chl (r = -0.17) (c) Temperature (r = -0.07) (d) Salinity (r = -0.17) (e) pCO_2 (15^{th} – 17^{th}; r = 0.08, 17^{th} – 20^{th}; r = 0.04) (f) PAR (r = 0.24). The tides have little influence in El Quesir.

5.6.3.2 Principal Component Analysis (PCA)

As a further statistical investigation, PCA was run on the data from El Quseir. The resulting correlation circle is shown in Figure 5.27.

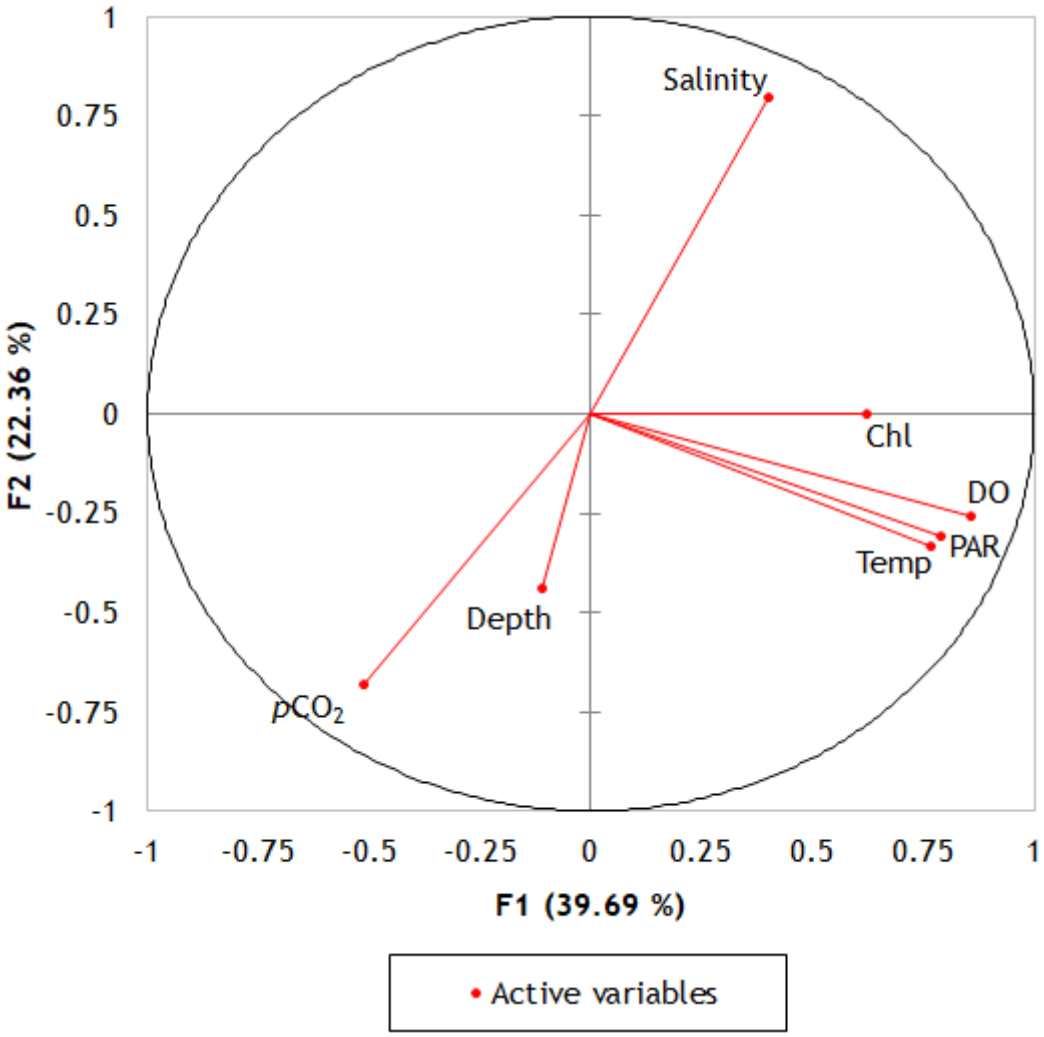

Figure 5.27: PCA showing the correlation circle from El Quseir. If two variables are far from the centre and close to one another then they are positively significantly correlated. If two variables are orthogonal to one another then they are not related. If two variables are on opposite sides of the centre then they are negatively significantly correlated.

PCA confirms the previous analyses and Figure 5.27 can be summarised as follows in Table 5.4.

Positively significantly correlated	Not correlated	Negatively significantly correlated
DO & Temperature (r = 0.73) PAR & DO (0.69) PAR & Temperature (0.52) Chl & PAR (0.43) Chl & Temperature (r = 0.37) Chl & DO (r = 0.36)	No variables were correlated with depth Salinity was only correlated with pCO_2	pCO_2 & Salinity (-0.66) pCO_2 & PAR (-0.28) pCO_2 & DO (-0.27)

Table 5.4: Correlated and non-correlated variables in Caol Scotnish in El Quseir according to PCA.

It must be noted that for previous analysis of PAR, zero levels were taken out and only light levels that registered above zero were included in any correlation analysis. With PCA, this was unable to be done and therefore PAR PCA should be disregarded in this instance (with the exception of the chlorophyll and PAR correlation which, when zeros were removed in previous analysis, was still correlated with PAR). PCA does not show a correlation between Chl and pCO_2 unlike previous analysis. With the exception of this however, there is a general agreement on the correlation of variables in El Quseir between previous analyses and PCA.

5.6.4 Weather conditions

There were notable weather conditions that should be commented on which affected several of the recorded variables. A sandstorm occurred on the 18th March which is reflected by the PAR data where lower light levels were recorded around the time of this weather phenomenon. This coincides with a levelling out of both chlorophyll and temperature where increased cloud cover perhaps kept the temperature more steady. The salinity starts at an elevated concentration at the start of the deployment. The salinity gradually decreased and levelled out by the second half of 16th March with no particular day or night pattern.

CO_2 in surface waters can change due to mixing (Bekker *et al.*, 1999; McGillis *et al.*, 2001). The highstorm winds that occurred could therefore be a driving factor behind the surface seawater pCO_2 concentrations in the area although unlikely to be a major factor. Dust storms are notable in changing the chemistry of seawater due to large input of organic and inorganic material (Jickells, 1999;

Griffin and Kellogg, 2004) both in short- and long-term time frames (Griffin and Kellogg, 2004). Young *et al*. (1991) documented a large increase in primary production amidst the Asian dust storms of 1986. This occurred due to the deposition of dust in the ocean. The high primary productivity rates, particularly in oligotrophic seawater, during and after dust storms were also confirmed by Bonnet and Guieu (2004). Bishop *et al*. (2002) saw an increase in the biomass of carbon in the North Pacific after a dust storm introduced a higher than usual concentration of iron (macro nutrients). Micronutrients such as phosphorus and nitrogen are also deposited with dust to surface waters (Tan *et al*., 2013). This happened on time scales of only a few hours to days.

The major dust input was on the 18th March but the weather was disruptive (high winds, low light levels) from the second half of daylight hours on the 17th and appeared to have affected numerous variables. The dust storm finished by the 19th but light levels were very low from the aftermath. This part of the deployment is distinctive from the previous two diel cycles in the same deployment. The evidence of primary productivity increasing with the input of dust into the marine environment appears to be shown in the recorded DO data notably with the start of the storm where DO has a higher peak and a lower low in comparison to the previous days and perhaps indicated higher productivity where during the day more DO is produced with photosynthesis and during the night more DO is taken-up through respiration. The day where light levels were unusually low (19th), the DO range was small most likely due to less productivity post-sandstorm because of the decrease in available light. During the dust input, chlorophyll does not reach the usual minimum at night and stays at a comparatively constant concentration suggesting the nutrient input from the dust storm kept the chlorophyll levels higher than usual. The dust storm also seemed to affect the pCO_2 pattern recorded in the area. pCO_2 stays high in the day cycle when it should be lower. This is likely due to there being very low light levels on this day post-sandstorm and therefore the possibility of photosynthesis being outperformed by respiration. Additionally, heterotrophs may be respiring more than normal. High pCO_2 may also be an indication of more calcification taking place.

5.6.5 Temperature and salinity

There is high salinity in El Quseir in comparison to many places in the global ocean which shows a high level evaporation rather than precipitation (Libes, 1992; Khomayis, 2002; Schumann *et al.*, 2006). Salinity in El Quseir is only very weakly correlated with any variables. Salinity showed a gradual decrease over the course of the deployment and there were no diel patterns of note. Only over the first night until the start of the second day was there any change in the salinity with a large decrease (cf. the rest of the deployment) from 40.48 to 39.54. The salinity then levelled out with only very gradual decreases until retrieval of the sensor. With the exception of the first couple of days, the salinity stayed relatively stable and did not fluctuate. This could possibly be due to overall less evaporation over the course of the deployment as the weather conditions changed from very clear and dry to mass cloud cover, high winds and the sand storm. Clouds brought more precipitation (there was a small amount of rain) and therefore this could be behind the decrease in salinity. A gradual change of water mass would also produce this phenomenon.

From the 15th to 17th, there was a positive correlation between pCO_2 and salinity however, for the remainder of the deployment there was no correlation between the two variables as shown in Figure 5.23. This suggests that after the first two days, other factors have an influence on both of these parameters. Salinity changes because of less evaporation (the influence of weather) and pCO_2 will also have factors such as light levels (weather conditions) and biological activity (sand storm nutrient input and increased/decreased primary productivity) influencing it differently in this section of the deployment.

As with salinity, pCO_2 and temperature had a changing relationship throughout the deployment. Before the sandstorm, there was no correlation. However, there was a negative correlation during and after the sandstorm. This could be a coincidental relationship however, with pCO_2 being high at night because of biological processes and the temperature naturally being low at night because of the lack of solar energy available for heating the water (it could be via the influence of salinity on A_T but as there was no change in A_T this is unlikely). The surface water in El Quseir was heavily influenced by solar radiation as indicated by the temperature and PAR data collected. The

temperature and pCO_2 may not be specific drivers of each other however as on the 19th the pCO_2 remained high in the diurnal period and the temperature was also at its peak. Temperature and pCO_2 may be affected by association with other drivers, e.g., photoperiod and biological activity, rather than being a directly driven by one another.

Temperature governs the solubility of gases in a body of water. Temperature and DO were highly positively correlated in El Quseir which is not the typical inverse relationship between gases and temperature. The highest peaks of both temperature and DO occurred in the middle of the diurnal cycle and both minimums occurred at the end of the darkness, just before dawn. Both these maxima and minima coincide with biological activity, i.e., photosynthesis and respiration and also the presence (or lack of) solar radiation. On the 19th, the light was lower than any other day during the deployment and the DO and temperature both react to this with smaller maximum and minimums. Rather than an explicit correlation, there appears to be a complex dependency between these parameters and a consequential knock-on effect from multiple drivers.

Temperature and chlorophyll were positively correlated in El Quseir. Looking at the time series, it is clear that chlorophyll is correlated with light/dark cycles (chlorophyll content being higher during the day than at night). Lower chlorophyll concentration coincides with lower temperatures.

Overall, temperature was a large influence in El Quseir and most parameters (excluding salinity and tides) were correlated either moderately or strongly with it.

As a whole, the Red Sea has a semi-diurnal tide (Frihy *et al.*, 2004). The nature of the area, an open wide sea, means there will not be a major input of freshwater or dynamically different water bodies being introduced (compared with previously detailed Caol Scotnish in Chapter 4) (Madah *et al.*, 2015). The tidal range is small in the area with the difference between high and low tide never being above 0.64 m and with the final night cycle the change is only 0.20 m. There are two high and two low tides over the diel period. The tides in the Red Sea can be regarded as relatively small (Madah *et al.*, 2015) and clearly, in

the El Quseir area this is also the case. Overall, the tides do not have a large impact on the different variables in the area.

5.6.6 Performance of the pCO_2 sensor

The pCO_2 sensor had a successful run in a tropical environment and produced a pattern over the period of deployment as would be expected when comparing with that of the YSI EXO2 Sonde data, e.g. the pCO_2 data had an inverse pattern with the DO data as should be expected. Comparison with the seawater wet chemistry analyses was also favourable.

Coral reefs appear to be a large contributor to the fluctuation of carbon in the El Quseir site. This is because of the biological processes that take place and also the production and dissolution of $CaCO_3$ (Martin *et al.*, 2007). There was an average concentration of 407 μatm over the course of the deployment but the values ranged from 336 to 468 μatm with higher pCO_2 values corresponding with respiration and/or remineralisation and the lower pCO_2 values corresponding with photosynthesis and/or calcification. These higher concentrations of pCO_2 would suggest a large amount of CO_2 being released during respiration. In the second half of deployment, higher carbon levels may have been forced by an input of dust as previously commented on.

The concentrations of CO_2 recorded in El Quseir are likely to be reasonable and what should be expected for a coral reef area and one which has very open conditions c.f. with the narrow, fjordic Caol Scotnish. Values were found to range from below atmospheric value (~60 μatm below) to above atmospheric value (~70 μatm above) but the overall average was just above sea-air equilibrium conditions (407 μatm). Values quoted from the literature include the pCO_2 ranges in the Red Sea as 310 to 420 μatm (Elsheikh, 2008), Poisson *et al*. (1984) records a value of 330 μatm on the surface water of the Red Sea because of "CO_2 escaping into the atmosphere" and Rasul and Stewart (2015) measured a surface value of 344 μatm. These values are all in agreement with the pCO_2 concentrations that both the sensor and the wet chemistry analyses presented with "normal" conditions being a lower pCO_2 concentration compared to the higher concentration of the sandstorm conditions.

5.6.6.1 Comparison of pCO_2 sensor concentrations with pCO_2 wet chemistry concentrations

When the values of the sensor against the water chemistry analyses were compared, each value, with the exception of an outlier in the wet chemistry analysis, was very similar and had the same distinctive pattern of an increase during the second half of the deployment. The advantages to *in-situ* measurement is obvious with 1358 data points of pCO_2 being recorded by the sensor compared to 15 seawater samples and consequent pCO_2 calculation over the deployment. The higher frequency of data point recordings from the sensor can be seen as a big advantage in analysing the short-term variability of seawater pCO_2 where otherwise would be missed with only sporadic sampling. Subtleties in the pCO_2 diel cycle can be displayed to a much better effect as can be seen in the time series from the sensor. Overall, the sensor pCO_2 values compared favourably with the calculated pCO_2 values from the seawater samples with 11 of the 15 readings being within 10% of each other.

5.7 Conclusion

This chapter presents research on the performance of a developed pCO_2 sensor which contributed to the characterisation of the natural variability of carbonate chemistry and other parameters in a tropical marine environment in Egypt.

Overall, the performance of the developed sensor on the tropical deployment can be deemed a successful one with data produced which accords to supporting data from additional sensors and also the analyses from seawater samples. The sensor was able to provide pCO_2 data on numerous day/night cycles in the Red Sea, El Quseir and has provided a cheap and easy way to gather pCO_2 data in coastal areas. The advantages over wet chemistry samples are vast and are discussed in Chapter 6.

To accompany the *in-situ* pCO_2 data, other ancillary marine data were measured and used to support and compliment the pCO_2 data and ultimately create a full picture of the natural variability and drivers of the diel marine cycle in El Quseir. Therefore, in addition to developing a working pCO_2 sensor, this research also provided an extensive data set to summarise the controlling processes on marine CO_2.

6 General discussion

6.1 Introduction

This project aimed to produce a low-cost, low-power, autonomous marine pCO_2 sensor which would aid in the ease of characterisation of coastal marine pCO_2. This, ultimately, will help with constructing and adding to a database of the natural variation in carbonate fluxes and their drivers over varying temporal and spatial timescales. It will also highlight areas which may be affected by anthropogenic climate change. The research within this project had the following objectives:

1. Produce a working low-cost, low-power coastal marine pCO_2 sensor (Chapter 2 & 3).

2. Produce temporal characterisations of various coastal marine parameters using different marine sensors (pH, DO, chlorophyll, temperature, salinity, depth) (Chapter 4 & 5) and identify the drivers of these variables, i.e. tidal (Caol Scotnish) vs diurnal (Egypt) systems.

There is a lack of direct comparisons of diurnal patterns in different coastal areas (Dai *et al.*, 2009). This study began to address this with a direct comparison of carbonate chemistry and other variables in a tropical and temperate coastal environment (Section 6.5). There is also a paucity of data on diurnal to diel variations of carbonate chemistry (Dai *et al.*, 2009) which this research also addresses. This work will contribute to a wider comprehension and understanding of the drivers behind what controls this diurnal/diel variability.

6.2 Effectiveness of developed pCO_2 sensor

6.2.1 Usage

The sensor was designed to be 'plug-and-play' for any user. Both the developed software and hardware allow for simple deployment. The code was easily preloaded onto the electronics and the sensor was placed in the secure housing to easily safeguard it. The sensor can be deployed with SCUBA or snorkelling or even paddling. This ease of use is of benefit not only to scientists

and industry but also to the interested layperson where no amount of expertise is needed.

6.2.2 Performance

The developed sensor performed well in each field test when compared with both seawater samples and ancillary sensor data. Although there was disagreement between sensor values and seawater analyses in Caol Scotnish, the samples were likely compromised in storage and their analyses would suggest that they were producing erroneous results (See comments of effectiveness of seawater sampling in Section 6.3). However, when compared with the ancillary sensors that were deployed in Caol Scotnish, the pCO_2 sensor performed well. In El Quseir, the sensor concentrations compared well with the seawater concentrations. This was also true for the laboratory experiments. Due to the warmer water, the batteries when used in El Quesir lasted longer than in Caol Scotnish. The exact length of time the batteries would have run in the warmer water is unknown as the sensor needed to be retrieved before they had discharged. They were still fully working when the sensor was retrieved.

In the laboratory, the percentage error of the sensor when compared with seawater samples was an average of just ± 1.07%. The same comparison when in the field was ± 9.38%. These percentage values show a good accuracy which would generally be within the COZIR quoted value of ± 50 μatm.

6.3 Effectiveness of seawater sampling and analysis for comparative use

Seawater analyses involve several steps until a final answer is ascertained. This can create several issues in the final result, e.g. human error in sampling and error propagation within analyses.

6.3.1 Error propagation and human error

With each step of seawater analysis where the end result will eventually produce a calculated pCO_2 concentration, there will be a degree of error propagation which will accumulate through each stage. The propagation of errors throughout each stage of analyses is an important aspect to take into

account and what implications this may have on the absolute end value that is reached (Riebesell *et al.*, 2010). The equilibrium constants previously mentioned within this work (See Chapter 1, Section 1.2, page 5) will also introduce more uncertainty when combining each component for end results (Riebesell *et al.*, 2010).

Considering the steps involved, firstly the collection of seawater needs to be a careful one and the introduction of human error into each process should be minimised as much as possible, i.e., there needs to be no (or as little as possible) contact with the atmosphere when the seawater is collected so as to prevent contamination of the sample with oxygen. Errors like this can happen when decanting the sample into vials, when poisoning the samples to stop any further biological activity, in the storage of the samples, when the samples are opened and ultimately when the samples go through the multistage analysis in A_T and DIC machines. Human error is involved in each step (collection and analyses) but machine error should be taken into account also. There will be human error in calibration and also mechanical errors and including both separate errors in A_T and DIC to calculate the pCO_2, these factors will have an effect on the accuracy of the final value of pCO_2.

The error propagation when using different carbonate parameters to calculate another are shown in Table 6.1. A_T and DIC is shown in row 3.

Pair of parameters	Relative uncertainty	Reference methods	State-of-the-art (using RMs)*	Other techniques (using RMs)
pH, A_T	$u_c([CO_2^*])/[CO_2^*]$ $u_c([CO_3^{2-}])/[CO_3^{2-}]$	2.6% 3.6%	2.9% 3.7%	6.1-8.7% 5.1-6.5%
pH, DIC	$u_c([CO_2^*])/[CO_2^*]$ $u_c([CO_3^{2-}])/[CO_3^{2-}]$	2.4% 4.1%	2.6% 4.2%	5.6-8.0% 5.7-7.3%
A_T, DIC	$u_c([CO_2^*])/[CO_2^*]$ $u_c([CO_3^{2-}])/[CO_3^{2-}]$	4.9% 0.6%	5.4% 1.7%	5.8-9.3% 2.2-5.5%
pH, $p(CO_2)$	$u_c([CO_2^*])/[CO_2^*]$ $u_c([CO_3^{2-}])/[CO_3^{2-}]$	0.6% 5.3%	0.8% 5.7%	1.5-2.9% 10.6-15.0%
A_T, $p(CO_2)$	$u_c([CO_2^*])/[CO_2^*]$ $u_c([CO_3^{2-}])/[CO_3^{2-}]$	0.6% 3.3%	0.8% 3.3%	1.5-2.9% 3.4-3.8%
DIC, $p(CO_2)$	$u_c([CO_2^*])/[CO_2^*]$ $u_c([CO_3^{2-}])/[CO_3^{2-}]$	0.6% 4.0%	0.8% 4.1%	1.5-2.9% 4.2-4.9%

Table 6.1: Estimate of errors when using different carbonate parameters to characterise the carbonate system (Table from Riebesell *et al*., 2010). These figures are found using estimated measurement uncertainties of single parameters (e.g., A_T, DIC, pH, pCO_2) by Riebesell *et al*., (2010) which are then used along with estimations of the sensitivity coefficients by Dickson and Riley (1978) to calculate the relative uncertainties.

Various studies have cited disagreements between direct *in-situ* concentrations measured by sensors and concentrations from calculations (Wanninkhof *et al*., 1999; Lee *et al*., 2000; Lueker *et al*., 2000; Millero *et al*., 2002; Sejr *et al*., 2011; Hoppe *et al*., 2012). As with Chapter 4, there were abnormal pCO_2 concentrations that go beyond the uncertainties in the dissociation constants or natural fluxes of carbonate chemistry. These anomalies also coincide with A_T measurements that were abnormally low. Alkalinity measurement can often be correlated with subsequent error in carbonate calculations. These A_T errors can be forced by chemically reactive carbonate particles (Sejr *et al*., 2011) and organic matter (Caol Scotnish may have high concentrations of organic matter) within the sample (Kim *et al*., 2006). What must also be noted is that there is some dispute around the use of the current dissociation constants (K_1 and K_2) (Orr and Epitalon, 2015). Millero (2010) used measurements by Luker *et al*. (2000) from Mehrbach *et al*. (1973) along with his own measurements (Millero *et al*., 2006) which are used to apply to scenarios of a wide temperature (0 – 50°C) and salinity (1 – 50 psu) range. However, the measurements by Luker *et al*. (2000) should only apply to situations of temperatures between 2 and 35 °C and salinities between 19 and 43 psu. Orr and Epitalon (2015) suggest that better

formulations of the dissociation constants need to be used in less uniform areas i.e., coastal areas. Therefore it is clear that the comparison between calculated concentrations and *in-situ* concentrations must be treated with caution. In the context of this work, in the field the sensor performed with a 9.4% concentration uncertainty when compared with the seawater sample concentrations. This is better than the manufacturing company states on their data sheet concerning the original atmospheric CO_2 sensor. For this work, the final sensor uncertainty shall be taken as 9.4% (assuming the water sample concentrations are the absolute correct concentrations).

6.4 Comparisons of key features of developed sensor with other commercially available sensors

The key features of the developed pCO_2 sensor in this research are;

- it is low-cost;
- it is operable on low-power;
- it accurately measures marine pCO_2;
- it is practical to use in a marine field environment, i.e. compact, lightweight and portable;
- it is able to log data autonomously, i.e. data is downloaded and retrievable once recovered;
- it can be programmed for different measuring needs; and
- it is suitable for the marine environment, i.e. durable and able to withstand saltwater submersion, corrosion and biofouling.

Below is a comparison of the developed sensor to commercially available sensors (see Table 6.2).

Model	Measurement method	Precision (µatm)	Accuracy (µatm)	Response time	Power consumption	Dimensions (mm)	Weight (kg)	Measurement range (µatm)	Maximum deployment depth (m)
Contros Hydro-CO2	NDIR	< 1	5 (at surface)	130-210 s	1-7 W	90 x 530	5.5	200 - 1000	0 - 6000 m
Pro-Oceanus CO2-Pro	NDIR	0.01	2 - 8	120 s	4.8 - 7.2 W, 18W during start-up	190 x 330	5.5	0 - 2000	0 - 110 m
Sunburst SAMI-CO2	SPM	1	2	5 m	14 A-h	152 x 550	7.6	200 - 600	0 - 600 m
Aanderaa Optode	Optode	2	2-75	88 s	80 mW	36 x 86		0 - 50000	0 - 6000 m
MAPCO2	NDIR	0.6	0.3	30 m	2.43 kW-h		80	0 - 1000	Moored buoy
p CO_2 sensor developed at The University of Glasgow	NDIR	1	± 9.4 %	< 10 s (atmosp.) < 2 m (marine)	0.14 W (sensor plus boards)	90 x 197	1.2	0 - 2000	0 - 25 m

Table 6.2: Comparison of commercially available *p*CO_2 sensors and the developed sensor within this research.

The main difference in the developed sensor with the sensors already on the market is the price. The sensor was able to be developed at a very low cost (~£300/~$395). Compared to the other sensors available whose cost is anything between $20000 – $50000 on the whole (and even reaching up to $100000), this is a clear advantage. The low price is beneficial because it allows institutions and industry to buy in bulk to give high spatial and temporal coverage of certain coastal areas that are under investigation. Although low-cost, the sensor still has various features of the more expensive sensors, i.e. ability to record and store data autonomously depending on use, e.g. it can be set to record as many or as few times as required on any deployment, high (if not higher) response time, runs on very low-power (if not lower) and spans a large range of concentration measurements.

The accuracy of the sensors also differs; there is a higher accuracy in the expensive models. However, as this sensor was designed for coastal environments, very small accuracy of ± 1-2 μatm was not needed due to the high variability of pCO_2 in these areas. The COZIR sensor was tested by Gibson and MacGregor (2013) and they found the sensor to be accurate to within ± 3% of the reading. The accuracy is adequate for the specific purpose of this marine sensor. The accuracy from the experiments within this research approximately agree with this figure. Sensor percentage error when compared with seawater samples was between ± 1 – 9%. The higher sensor error percentage values tended to coincide with anomalous A_T seawater concentrations. A decision key is presented in Table 6.3 as a guide for when to use the UofG developed sensor versus when to use the more expensive, currently commercially available ones.

Decision key

	Budget	Area	Measurement criteria	Deployment length
UofG $p\,CO_2$ sensor	Low	Coastal, shallow (< 25m)	Variable chemistry	Short - Mid
Competitors $p\,CO_2$ sensor	High	Pelagic, deep (> 25m)	Stable chemistry	Short - Long

Table 6.3: Criteria of when to choose the developed sensor versus competitor's sensors.

6.5 Comparison of temperate (tidal) vs tropical (non-tidal) areas

6.5.1 Main drivers

There were several differences between both sites. Although both sites consisted of calcifying fauna (along with other organisms), their biological influence was very different due to different environmental factors.

The main drivers behind the variability of carbonate chemistry in Caol Scotnish were the tides which introduced different water masses of different chemical properties into the area. The main drivers in El Quseir were biological activity but also notable weather events. The different hydrography in each area governed different patterns of each variable. Caol Scotnish is a narrow body of water which is surrounded by banks and foliage and parameters like salinity, DO, pH and pCO_2 were all affected by this. Rainfall also has an influence in the measured constituents of the water in the area. The tides were relatively large in the small area and have a great influence in terms of introducing different water masses into the vicinity. Antithetically, the wide and open nature of the site in El Quseir does not have large tides and the climate very rarely allows for precipitation. In fact, the area has some of the highest salinity concentrations of any seawater body in the world because of this. The open area does not contain any fresh water run-off from land. The deployment in Egypt was a fairly exceptional one in terms of weather events. There was indeed some precipitation over the course of the week (albeit a comparatively small amount). The dust storm also changed the composition of the marine variables that were being measured in the seawater with an evident increase in the carbon content. Although with different outcomes, weather in both areas had a large effect on the marine variables recorded in both areas. There was not a large influence in variability with the tides in El Quseir as there was in Caol Scotnish. In fact, the body of water in El Quseir was much more stratified than in Caol Scotnish and had a relatively stable salinity (with the exception of the input of precipitation seen). The difference in terms of the influence of tides between the two areas was substantial. With incoming tide in Caol Scotnish, there would likely be a change in the composition of the surrounding water whereas the constitution of the water would not change according to the tides in El Quseir. There was a

higher overall concentration of pCO_2 in Caol Scotnish compared to El Quseir. This again could be due to hydrography and the relatively narrow area which Caol Scotnish inhabits. The large bed of calcifying algae in a comparatively small area compared to El Quseir may be the reason for the higher overall pCO_2 that was recorded in Caol Scotnish. Of course, other influences in each area were also acting on the absolute value of pCO_2. A summary of the main drivers is shown in Table 6.4.

Main drivers		
Order of influence	Temperate	Tropical
1	Tides	Weather events
2	Biological activity	Biological activity
3	Weather events	Temperature

Table 6.4: Comparison of the main drivers in tropical El Quseir, Egypt and temperate Caol Scotnish, Scotland and their order of influence in the coastal system over their specific time of deployment. N.B. weather was exceptional in the tropical area during this specific field work and without the dust storm, biological drivers would be the main influence.

6.6 Is OA only a problem for the open pelagic ocean?

This research focused on marine coastal areas which already exhibit pH concentration fluctuations of the magnitude which are projected for the open ocean due to anthropogenic emission of CO_2 (Duarte *et al.*, 2013). As seen throughout this research, these concentration fluctuations in coastal areas are forced through natural processes like biological activity of organisms (which can yield a pH fluctuation of approximately 0.3 units) and hydrography which together can drive a pH change of 0.5 pH units (and up to 1 pH unit) over a small (hourly to diel) temporal scale (Duarte *et al.*, 2013). Naturally high coastal fluctuations may suggest that coastal areas will be more likely to cope with heightened pCO_2 concentrations (but can also suggest that even more pressure will be placed on these systems if concentrations increase). In contrast, the open ocean pH is comparatively stable and varies less than 0.1 pH units during a yearly timescale (Doney *et al.*, 2009). The pH fluctuation, however, was relatively low in Caol Scotnish compared to other coastal systems (the difference in average day/night concentrations in both the July and September

deployments was just 0.01 units) and therefore may be more affected by a future increase in anthropogenic acidification as would the open ocean. The forcing of pCO_2 in the area by the biota due to biological processes including respiration and calcification (and the hydrography of the area) means that the concentration stays relatively high (~ 480 µatm in July and ~ 450 µatm in September but with a low fluctuation of ~13-15 µatm) and therefore any anthropogenic increase may put added pressure on the area. Diel fluctuations of pCO_2 in Eqypt were larger than Caol Scotnish at ~ 25+ µatm (but concentration is consistently lower at ~ 407 µatm) which may suggest that this area would be able to adapt to anthropogenic acidification perhaps more adequately than Caol Scotnish as the organisms can already adapt on a daily level to higher diel fluctuations. However, it is clear that increasing acidity levels would be a potentially harmful event for any calcifying organism regardless.

Therefore, from these relatively contrasting coastal environments, it is evident that anthropogenic open ocean acidification and the effects it may have and how it is mitigated cannot be directly transposed to just any coastal ocean situation. Additionally, the effects of anthropogenic acidification will likely be exaggerated and of more pressing concern in coastal areas because of this natural variability but conversely these areas may be able to cope more due to the naturally large fluctuations (depending on the area). Future research should be focussed on not only easier and increased characterisation of the variability of coastal oceans but also overall OA models should be able to incorporate coastal areas that contain the full span of variabilities.

6.7 Direction for future research

This research has created a fundamental basis for further developing a novel, efficient and useful low-cost sensor for monitoring the pCO_2 of marine coastal areas. The sensor is still effectively a prototype and there are several directions in which to further enhance the sensor. Future work would include development of several aspects of the whole set-up.

6.7.1 Electronic platform

Modification of the electronic hardware would be the immediate work. The Arduino boards would be stripped down removing all superfluous components that drain power, i.e. LED lights and other aspects of the generalised board. Within this research, there were three electronic set-ups developed:

1. The Arduino Uno board and shield (used within this project),

2. A stripped down clone Arduino made with separate components,

3. 'TinyDuino' board and shields (a pre-constructed, commercially available clone).

The two alternative set-ups had been established but time was a constriction in running them smoothly within the timeframe of this project having already produced a working set-up. Further research would include either (2) or (3) being the main electronic base which would allow for even lower power and therefore longer deployment.

There are shields that can be used with Arduino that could enable communication from the sensor to a remote laptop using Bluetooth. This would solve the problem of knowing whether the sensor is working or corrupting under the water. However, this would also come with a power trade-off which would need to be addressed. Again, this was started during the course of the project but due to time constraints could not be completed. To protect the electronics, an epoxy would also be prepared for the final design.

6.7.2 Software

The alternative electronic set-up would incorporate the development of new code which in turn would also help with longer deployments. Battery power could be further conserved with the development of a modified code which can put the Arduino to 'sleep' and interrupt this when it needs to be turned on again, i.e. between readings when the sensor is idle, it can be put to sleep. It can then be turned on again to commence the next reading when needed. This is done via the two 'interrupt' pins of the ATMEGA328 which are used to 'wake'

the Arduino. Using a sleep code will only however cut a few mA's off the total consumption of power (should have around a 30% reduction) but combined with the stripping of the electronic hardware, this should enable the sensor to run for anything up to one year (depending on usage and battery choice). As before, time constraints impeded the development of this within this project but this would be a priority for continued work on the sensor.

6.7.3 Housing

Although during this project, there was no issue with biofouling in the relatively short deployments, for longer deployments spanning several weeks to months, this may become a pertinent concern. This would be easily prevented however with copper wiring fitted around the housing. The design could also be modified to limit the need to open the housing but commercial development would be needed to address this.

7 Conclusion

7.1 Chapter 2: Research and development of pCO_2 sensor

The aim of this research was to develop a low-cost, low-power pCO_2 sensor that could be used in a marine coastal environment. This was achieved through research and development of electronics, code and housing.

The key outcome to this chapter was the successful production of a pCO_2 sensor.

7.2 Chapter 3: Laboratory performance evaluation of pCO_2 sensor

The aim of this chapter was to assess and evaluate the effectiveness of the previously developed pCO_2 sensor with laboratory experiments in both atmospheric and marine environments. The key processes and findings were:

1. The sensor was able to recognise and record differences in pCO_2 accurately with the ability to store data in an autonomous manner.

2. Potential issues, i.e. drift/noise were identified and data processing procedures were familiarised with.

3. Practical quality control procedures were familiarised with by collection of seawater and preservation of samples.

4. Procedure for and analyses of seawater was undertaken to obtain concentrations of A_T and DIC and these data were utilised to obtain a calculation of seawater pCO_2 to be compared to the *in-situ* sensor data.

5. pCO_2 concentrations for seawater samples compared favourably with *in-situ* pCO_2 concentrations from the sensor.

7.3 Chapter 4: Characterising natural variability of coastal carbonate systems and ancillary variables in a temperate marine environment

The aim of this chapter was to characterise the natural variability of carbonate chemistry and other ancillary parameters in a coastal temperate area (Caol Scotnish, Loch Sween, Scotland) characterised by autotrophic biota and to evaluate the performance of the developed pCO_2 sensor in a temperate environment. The key findings were:

1. The developed sensors performed well in a temperate marine environment when the data were compared to ancillary sensor data.

2. Voltage output of the sensor was found to be unreliable as a means of measuring pCO_2 and would not be used again in any experimental capacity of the pCO_2 sensors.

3. The main driver in Caol Scotnish was tidal action which influenced every variable in the area.

4. High pCO_2 concentration and low pH fluctuation may be due to high amount of calcification from the maerl beds.

5. Different water masses are introduced into Caol Scotnish by tidal action. The incoming water masses contain higher salinity and lower temperatures than the existing water.

7.4 Chapter 5: Characterising natural variability of coastal carbonate systems and ancillary variables in a tropical marine environment

The aim of this chapter was to characterise the natural variability of carbonate chemistry and other ancillary parameters in a coastal tropical area (El Quseir, Egypt) characterised by autotrophic biota and to evaluate the performance of the developed pCO_2 sensor in a tropical environment. The key findings were:

1. The developed sensor performed well in a tropical marine environment when the data were compared to ancillary sensor data and seawater samples

2. The main drivers in El Quseir were biological activity from organisms, temperature and weather conditions.

3. Sandstorm conditions affected the carbonate chemistry with an increase in carbon input and cloud cover affecting primary productivity.

7.5 Wider applications of this research and concluding remarks

Sensors such as the one developed within this research will have an important role to play in climate research. For example, a multitude of these sensors can be utilised in areas such as CCS sites but also in general coastal sites where there is a paucity of data.

A novel sensor which was developed during this research was able to effectively characterise and identify a number of factors that drive the marine variables in coastal areas. This sensor demonstrated that innovative and unique technology can be utilised for ease of quantification and qualification of marine biogeochemistry parameters to help in the determination of what future implications climate change will have on the coastal areas of the oceans.

References

ABOU-AISHA, K. M. KOBBIA, I. A., EL ABYAD, M. S., SHABANA, E. F., & SCHANZ, F. (1995). Impact of phosphorus loadings on macro-algal communities in the Red Sea coast of Egypt. *Water, Air and Soil Pollution*, 83, 285-297.

ALVAREZ, M., RIOS, A. F. & ROSON, G. (2000) Spatio-temporal variability of air-sea fluxes of carbon dioxide and oxygen in the Bransfield and Gerlache Straits during austral summer 1995-96. *Deep-sea research part II*, 49, 643-662.

ANDERSON, D. M., BURKHOLDER, J. M., COCHLAN, W. P., GILBERT, P. M., GOBLER, C. J., HEIL, C. A., KUDELA, R., PARSONS, M. L., RENSEL, J. E. J., TOWNSEND, D. W., TRAINER, V. L., & VARGO, G. A. (2008). Harmful algal blooms and eutrophication: examining linkages from selected coastal regions of the United States. *Harmful Algae*, 8, 39-53.

ANDERSSON, A. J., MACKENZIE, F. T. & BATES, N. R. (2008). Life on the margin: implications of ocean acidification on Mg-calcite, high latitude and cold-water marine calcifiers. *Marine Ecology Progress Series*, 373, 265-273.

ANDERSSON, A. J., KUFFNER, I. B., MACKENZIE, F. T., JOKIEL, P. L., RODGERS, K. S., TAN, A. (2009). Net loss of $CaCO_3$ from a subtropical calcifying community due to seawater acidification: mesocosm-scale experimental evidence. *Biogeosciences*, 6, 1811-1823.

ANTHONY, K. R. N., KLINE, D. I., DIAZ-PULIDO, G., DOVE, S., HOEGH-GULDBERG, O. (2008). Ocean acidification causes bleaching and productivity loss in coral reef builders. *Proceedings of the National Academy of Sciences of the USA*, 105, 17442-17446.

ANTHONY, K., KLEYPAS, J. A., & GATTUSO, J. P. (2011). Coral reefs modify their seawater carbon chemistry – implications for impacts of ocean acidification. *Global Change Biology*. 17(12), 3655-3666.

APOSTOLAKI, E. T., VIZZINI, S., HENDRICKS, I., OLSEN, Y. S. (2014). Seagrass ecosystem response to long-term high CO_2 in a Mediterranean volcanic vent, *Marine Environmental Research*, 99, 9-15.

ARONSON, R. B., THATJE, S., CLARKE, A., PECK, L. S., BLAKE, D. B., WILGA, C.

D. & SEIBEL, B. A. (2007). Climate change and invisibility of the Antarctic benthos. *Annual Review of Ecology, Evolution and Systematics*. 38, 129-154.

BAGGINI, C., SALOMIDI, M., VOUTSINAS, E., BRAY, L., KRASAKOPOULOU, E. & HALL-SPENCER, J. M. (2014). Seasonality affects macroalgal community response to increases in pCO_2. *PLoS ONE*, 9(9).

BAKKER, D. C. E., DE BARR, H. J. W., & DE JONG, E. (1999). The dependence on temperature and salinity of dissolved inorganic carbon in East Atlantic surface waters. *Marine Chemistry*, 65(3-4), 263-280.

BARNES D. J. (1983). Profiling coral reef productivity and calcification using pH and oxygen electrodes. *Journal of Experimental Marine Biology and Ecology*, 66, 149-161.

BARNES, D. J., & CHALKER, B. E. (1990). Calcification and photosynthesis in reef-building corals and algae. In: Dubinsky, Z. (Ed) Coral Reefs. Ecosystems of the World, 25, 109-131.

BARNES, D. K. A. & PECK, L. S. (2008). Vulnerability of Antarctic shelf biodiversity to predicted regional warming. *Climate Research*, 37, 149-163.

BARRS, M. A., SCHALK, P. H., & VELDHUIS, M. J. W. (1998). *Seasonal fluctuations in plankton biomass and productivity in the ecosystems of the Somali Current Gulf of Aden and Southern Red Sea*. Sherman et al. (Eds.), Large Marine Ecosystems of the Indian Ocean: Assessment, Sustainability, and Management, Blackwell Science, Oxford, pp. 143-174.

BASS, A. M., BIRD, M. I., MUNKSGAARD, N. C., & WURSTER, C. M. (2012). ISO-CADICA: Isotopic – continuous, automated dissolved inorganic carbon analyser. *Rapid Communications in Mass Spectrometry*, 26, 639-644.

BATES, N. R., SAMUELS, L., & MERLIVAT, L. (2001). Biogeochemical and physical factors influencing seawater fCO_2 and air-sea CO_2 exchange on the Bermuda coral reef. *Limnology and Oceanography*, 46, 833-846.

BAUMANN, H., WALLACE, R. B., TAGLIAFERRI, T., & GOBLER, C. (2015). Large natural pH, CO_2 and O_2 fluctuations in a temperate tidal salt marsh on diel, seasonal, and interannual time scales. *Estuaries and Coasts*, 38(1), 220 – 231.

BEATLEY, T. (1991). Protecting biodiversity in coastal environments: Introduction and overview. *Coastal management*, 19(**1**), 1-19.

BEHRENFELD, M., O'MALLEY, R., SIEGEL, D., MCCLAIN, C., SARMIENTO, J., FELDMAN, G., MILLIGAN, A., FALKOWSKI, P., LETELIER, R., & BOSS, E. (2006). Climate-driven trends in contemporary ocean productivity. *Nature*, 444, 752-755.

BEHRENFELD, M. J., SIEGEL, D. A., O' MALLEY, R. T., & MARITORENA, S. (2009). Global ocean phytoplankton. *Bulletin of the American Meteorological Society*, 90(**8**), S68-S73.

BELKIN, I. M. (2009). Rapid warming of large marine ecosystems. *Progress in Oceanography*, 81, 207 – 213.

BELL, G. & COLLINS, S. (2008). Adaption, extinction and global change. *Evolutionary Applications*, 1, 3-16.

BENSOUSSAN, N., & GATTUSO, J-P. (2007). Community primary production and calcification in a NW Mediterranean ecosystem dominated by calcareous macroalgae. *Marine Ecology Progress Series*, 334, 37-45.

BERNER, R. A. (1990). Atmospheric carbon dioxide levels over Phanerozoic time. *Science*, 249:1382-1386.

BIALKOWSKI, S. (2006). Carbon dioxide and carbonic acid. Chemistry 3650; Environmental Chemistry.

BIOMAERL, BARBERA, C., BORDEHORE, C., BORG, J. A., GLEMAREC, M., GRALL, J., HALL-SPENCER, J. M., DE LA HUZ, C., LANFRANCO, E., LASTRA, M., MOORE, P. G. MORA, J., PITA, M. E., RAMOS-ESPLA, A. A., RIZZO, M., SANCHEZ-MATA, A., SEVA, A., SCHEMBRI, P. J., & VALLE, C. (2003). Conservation and management of northeast Atlantic and Mediterranean maerl beds. *Aquatic Conservation: Marine and Freshwater Ecosystems,* 13, S65-S76.

BIRKELAND, C. (ed) (1997). *Life and death of coral reefs.* Chapman and Hall: New York.

BISHOP, J. K. B., DAVID, R. E., & SHERMAN, J. T. (2002). Robotic observations of dust storm enhancement of carbon biomass in the North Pacific. *Science*, 298(5594), 817-821.

BLACKFORD, J. C., JONES, N., PROCTOR, R. & HOLT, J. (2008). Regional scale impacts of distinct CO_2 additions in the North Sea. *Marine Pollution Bulletin*, 56(**8**), 1461-1468.

BLACKFORD, J., STAHL, H., BULL, J. M., GERGES, B. J. P., CEVATOGLU, M.,

LICHTSCHLAG, A., CONNELLY, D., JAMES, R. H., KITA, J., LONG, D., NAYLOR, M., SHITASHIMA, K., SMITH, D., TAYLOR, P., WRIGHTS, I., AKHURST, M., CHEN, B., GERNON, T. M., HAUTON, C., HAYASHI, M., KAIEDA, H., LEIGHTON, T. G., SATO, T., SAYER, M. D. J., SUZUMURA, M., TAIT, K., VARDY, M. E., WHITE, P. R., & WIDDICOMBE, S. (2014). Detection and impacts of leakage from sub-seafloor deep geological carbon dioxide storage. *Nature Climate Change*. 4, 1011-1016.

BOCLMON, E. E., & DICKSON, A. G. (2015). An inter-laboratory comparison assessing the quality of seawater carbon dioxide measurements. *Marine Chemistry*, 171, 36-43.

BOGRAD, S. J., CASTRO, C. G., DI LORENZO, E., PALACIOS, D. M., BAILEY, H., GILLY., W., & CHAVEZ, F. P. (2008). Oxygen declines and the shoaling of the hypoxic boundary in the Californian Current. *Geophysical research Letters*, 35, L1 2607.

BONNET, S., & GUIEU, C. (2004). Dissolution of atmospheric iron in seawater. *Geophysical Research Letters*, 31, 3303.

BORGES, A. V. & GYPENS, N. (2010). Carbonate chemistry in the coastal zone responds more strongly to eutrophication than to ocean acidification. *Limnology and Oceanography*, 55(1), 346-353.

BOROWITZKA, M. A. (1981). Photosynthesis and calcification in the articulated coralline red algae *Amphiroa anceps* and *A. Foliacea*. *Marine Biology*, 62, 17-23.

BOTTOMLEY, M., FOLLAND, C. K., HSIUNG, J., NEWELL, R. E., & PARKER, D. E. (1990). Global ocean surface temperature atlas (GOSTA).

BOYD, P. W., STRZEPEK, R., FU, F-X. & HUTCHINS, D. A. (2010). Environmental control of open ocean phytoplankton groups: now and in the future. *Limnology and Oceanography*, 55, 1353-1376.

BOZEC, Y., THOMAS, H., SCHIETTECATTE, L-S., BORGES, A. V., ELKALAY, K. & DE BAAR, H. J. W. (2006). Assessment of the processes controlling the seasonal variations of dissolved inorganic carbon in the North Sea. *Limnology and Oceanography*, 51, 2746-2762.

BROWN, B. E. (1997). Coral bleaching: causes and consequences. *Coral reefs*, 16, 129 – 138.

BROWN, B. E., AMBARSARI, I., WARNER, M E., FITT, W. K., DUNNE, R. P., GIBB,

S. W., & CUMMINGS, D. G. (1999). Diurnal changes in photochemical efficiency and xanthophylls concentrations in shallow water reef corals: evidence for photoinhibition and photoprotection. *Coral reefs*, 18, 99-105.

BROWN, C. (2008). Factors influencing trends in pH in the Wootton *et al.*, (2008) dataset. U. S. Environmental Protection Agency, Washington, DC EPA/600/R/12/676, 2012.

BRYANT, D., BURKE, L., MCMANUS, J., & SPALDING, M. (1998). *Reefs at risk: a map-based indicator of threats to the world's coral reefs*. World Resources Institute, Washington DC.

BUCHAN, A., LECLEIR, G. R., GULVIK, C. A., & GONZALEZ, J. M. (2014). Master recyclers: features and functions of bacteria associated with phytoplankton blooms. *Nature reviews microbiology*, 12, 686-698.

BURDETT, H. L., KEDDIE, V., MACARTHUR, N., MCDOWALL, L., MCLEISH, J., SPIELVOGEL, E., HATTON, A. D., & KAMENOS, N. A. (2014). Dynamic photoinhibition exhibited by red coralline algae in the red sea. *BMC Plant Biology*. 14, 139.

BYRNE, R. H. (2014). Measuring ocean acidification. New technology for a new era of ocean chemistry. *Environmental Science and Technology*, 48, 5352-5360.

CALDEIRA, K & WICKETT, M. E. (2003) Oceanography: anthropogenic carbon and ocean pH. *Nature*, 425.6956, 365-365.

CALL, M., SCHULZ, K. G., CARVALHO, M. C., SANTOS, I. R., & MAHER, D. T. (2017). Technical note: Coupling infrared gas analysis and cavity ring down spectroscopy for autonomous, high-temporal-resolution measurements of DIC and δ^{13}C-DIC. *Biogeosciences*, 14, 1305-1313.

CANE, M. A., CLEMENT, A. C., KAPLAN, A., KUSHNIR, Y., POZDNYAKOV, D., SEAGER, R., ZEBIAK, S. E., & MURTUGUDDE, R. (1997). Twentieth century sea surface temperature trends. *Science*, 275, 957-960.

CAO, L., & CALDEIRA, K. (2008). Atmospheric CO_2 stabilization and ocean acidification. *Geophysical Research Letters*, 35, L19609.

CAPONE, D., & HUTCHINS, D. (2013). Microbial biogeochemistry of coastal upwelling regimes in a changing ocean. *Nature geosciences*, 6, 711-7171.

CARILLO, C. J., SMITH, R. C. & KARL, D. M. (2004). Processes regulating

oxygen and carbon dioxide in surface waters west of the Antarctic Peninsula. *Marine chemistry*, 84, 161-179.

CARTE, B. K. (1996). Biomedical potential of marine natural products. *BioScience*. 46, 271 – 286.

CHALKER, B. E., BARNES, D. J., DUNLAP, W. C., & JOKIEL, P. L. (1988). Light and reef-building corals. *Interdisciplinary science reviews*, 13(**3**), 222-237.

CHEN, C. T. A., & HSING. L. Y. (2005). Degree of nutrient consumption as an aging index of upwelling or vertically mixed water in the northern Taiwan Strait. *Acta Oceanologica Sinica*, 24, 115-124.

CHISHOLM, J. R. M. (2000). Calcification by crustose coralline algae on the northern Great Barrier. *Limnology and Oceanography*, 45(7), 1476 – 1484.

CLARK, D., LAMARE, M., & BARKER, M. (2009). Response of sea urchin pluteus larvae (Echinodermata: Echinoidea) to reduced seawater pH: a comparison among a tropical, temperate, and a polar species. *Marine Biology*, 156, 1125-1137.

CLARKE, J. S., ACHTERBERG, E. P., CONNELLY, D. P., SCHUSTER, T., & MOWLEM, M. (2017). Developments in marine pCO_2 measurement technology; towards sustained in situ observations. *Trends in Analytical Chemistry*, 88, 53-61.

COHEN, A. L., HOLCOMB, M. (2009). Why corals care about ocean acidification. *Oceanography*, 22, 118-127.

COMEAU, S., GORSKY, G., JEFFREE, R., TEYSSIE, J. L., & GATTUSO, J. P. (2009). Impact of ocean acidification on a key Arctic pelagic mollusc (*Limacina helicina*). *Biogeosciences*, 6, 1877-1882.

CONNELL, D. W., & MILLER, G. J. (1984). Chemistry and ecotoxicology of pollution. John Wiley and Sons, N. Y.

CONNELL, S. D., & RUSSELL, B. D. (2010). The direct effects of increasing CO_2 and temperature on noncalcifying organisms: increasing the potential for phase shifts in kelp forests. *Proceedings of the Royal Society B: Biological Sciences*, 277, 1409-1415.

CONVEY, P. in *"Fingerprints" of climate change – adapted behaviour and shifting species ranges* (eds Walther, G-R., Burga, C. A. & Edwards, P. J.) 17 – 42 (Kluwer Academic, New York, 2001).

COOK, C. M., LANARAS, T., & ROUBELAKIS-ANGELAKIS, K. A. (1988).

Bicarbonate transport and alkalization of the medium by four species of *Rhodophyta*. *Journal of Experimental Botany*, 39, 1185-1198.

COPIN-MONTEGUT, C. (1988). A new formula for the effects of temperature on the partial pressure of CO_2 in seawater. *Marine Chemistry*, 25, 29-37.

CORNWALL, C. E., HEPBURN, C. D., MCGRAW, C. M., CURRIE, K. I., PILDITCH, C. A., HUNTER, K. A., BOYD, P. W., & HURD, C. L. (2013). Diurnal fluctuations in seawater pH influence the response of a calcifying macroalga to ocean acidification. *Proceedings of the Royal Society B: Biological Sciences*, 280(1772), 20132201.

CORNWALL, C. E., BOYD, P. W., MCGRAW, C. M., HEPBURN, C. D., PILDITCH, C. A., MORRIS, J. N., SMITH, A. M. & HURD, C. L. (2014). Diffusion boundary layers ameliorate the negative effects of ocean acidification on the temperate coralline macroalgae *Arthrocardia corymbosa*. *PLoS ONE* 9(5).

CORNWALL, C. E., COMEAU, S., DECARLO, T. M., MOORE, B., D'ALEXIS, Q., & MCCULLOCH, M. T. (2018). Resistance of corals and coralline algae to ocean acidification: physiological control of calcification under natural pH variability. *Proceedings of the Royal Society B. Biological sciences*. 285(1884).

COWART, D., ULRICH, P., MILLER, D., & MARSH, A. (2009). Salinity sensitivity of early embryos of the Antarctic sea urchin, Sterechinus neumayeri. *Polar Biology*, 32, 435-441.

CRAWLEY, A., KLINE, D., DUNN, S., ANTHONY, K., DOVE, S. (2010). The effect of ocean acidification on symbiont photorespiration and productivity in *Acropora formosa*. *Global Change Biology*, 16, 851-863.

DAI, M., LU, ZHONGMING, L., ZHAI, W., CHEN, B., CAO, Z., ZHOU, K., CAI, W-J., & CHEN, C-T. A. (2009). Diurnal variations of surface seawater pCO_2 in contrasting coastal environments. *Limnology and Oceanography*, 54(**3**), 735-745.

DAVID, J. C. (1975). Minimal dissolved oxygen requirements of aquatic life with emphasis on Canadian species: a review. *Journal of the Fisheries Board of Canada*, 32, 2295-2332.

DAVIDSON, K., GOWEN, R. J., HARRISON, P. J., FLEMING, L. E., HOAGLAND, P., & MOSCHONAS, G. (2014). Anthropogenic nutrients and harmful algae in coastal waters. *Journal of Environmental Management*, 146, 206-216.

DE'ATH, G., FABRICIUS, K. E., SWEATMAN, H., & PUOTINEN, M. (2012). The 27-

year decline of coral cover on the Great Barrier Reef and its causes. *PNAS*. 1208909109.

DEGRANDPRE, M. (1993). Measurement of seawater *p*CO_2 using a renewable-reagent fibre optic sensor with colorimetric detection. *Analytical Chemistry*, 65, 331-337.

DEGRANDPRE, M. D., HAMMAR, T. R., SMITH, S. P. & SAYLES F. L. (1995). *In-situ* measurements of seawater CO_2. *Limnology and oceanography*, 40, 969-975.

DEGRANDRE, M. D., BAEHR, M. M., & HAMMER, T. R. (1999). Calibration-free optical chemical sensors. *Analytical Chemistry*, 71(6), 1152-1159.

DHAKWEER, L. (2003). Ecological and fishery investigations of Nozha Hydrome near Alexandria 2000 – 2001. 1. Chemistry of Nozha Hydrome water under conditions of fertilizers applications. *Bulletin of National Institute of Oceanography. Fish*, 29, 387-425.

DICKEY, T. D. (2004). Exploration of biogeochemical temporal variability. *In* M. Follows and T. Oguz [eds.], The ocean carbon cycle and climate. NATO Advanced Study Inst. Ser. Kluwer Academic.

DICKSON, A. G. (1981). An exact definition of total alkalinity and a procedure for the estimation of alkalinity and total inorganic carbon from titration data. *Deep-Sea Research*, 28A(**6**), 609 – 623.

DICKSON, A. G, & MILLERO, F. J. (1987). A comparison of the equilibrium constants for the dissociation of carbonic acid in seawater media. *Deep sea research Part A Oceanographic research papers*, 34, 1733-1743.

DICKSON, A. G. (1990). Standard potential of the reaction: $AgCl(s)+1/2H_2(g)=Ag(s)+HCl(aq)$, and the standard acidity constant of the ion HSO_4^- in synthetic sea water from 273.15 to 318.15K. *The journal of chemical thermodynamics*, 22, 113-127.

DICKSON, A., SABINE, C., & CHRISTIAN, J., editors (2007). *Guide to best practices for ocean CO_2 measurements. IOCCP REPORT No. 8.*

DONE, T. J., OGDEN, J. C., & WIEBE, W. J. (1996). Biodiversity and ecosystem function of coral reefs. In "*Functional roles of biodiversity: a global perspective*". (Eds H. A. Mooney, J. H. Cushman, E. Medina, O. E. Sala and E. D. Schulze) pp 393-429. (Wiley: Chichester).

DONEY, S. C., MAHOWALD, N., LIMA, I., FEELY, R. A., MACKENZIE, F. T.,

LAMARQUE, J-F. & RASCH, P. J. (2007). Impact of anthropogenic atmospheric nitrogen and sulfur deposition on ocean acidification and the inorganic carbon system. *Proceedings of the National Academy of Science of the USA*, 104, 14580-14585.

DONEY, S. C., FABRY, V. J., FEELY, R. A. & KLEYPAS, J. A. (2009) Ocean acidification: the other CO_2 problem. *Marine Science 1*.

DORE, J., LUKAS, R., SADLER, D., CHURCH, M., & KARL, D. (2009). Physical and biogeochemical modulation of ocean acidification in the central North Pacific. *Proceedings of the national academy of sciences of the United States of America*, 106(**30**), 12235-12240.

DUARTE, C. M., & CERBRIAN, J. (1996). The fate of marine autotrophic production. *Limnology and Oceanography*. 41(8), 1758 – 1766.

DUARTE, C. M., HENDRICKS, I. E., MOORE, T. S., OLSEN, Y. S., STECKBAUER, A., RAMAJO, L., CARSTENSEN, J., TROTTER, J. A., & MCCULLOCH, M. (2013). Is ocean acidification an open-ocean syndrome? Understanding anthropogenic impacts on seawater pH. *Estuaries and Coasts*. 36, 221-236.

DUPONT, S., HAVENHAND, J., THORNDYKE, W., PECK, L., & THORNDYKE, M. (2008). Near-future level of CO_2-driven ocean acidification radically affects larval survival and development in the brittlestar *Ophiothrix fragilis*. *Marine Ecology Progress Series*. 373, 285-294.

EAKIN, M. C., RAUENZAHN, J. L., LIU, G., HERON, S. F., SKIRVING, W. J., GEIGER, E. F., BURGESS, T. F. R., & STRONG, A. E. (2014). Will 2014-2015 be the next big El Niño? If so, what might it mean for coral reefs? *The news journal of the international society for reef studies*. 29(2), 30-35.

EAKIN, M. C., LIU, G., GOMEZ, A. M., DE LA COUR, J. L., HERON, S. F., SKIRVING, W. J., GEIGER, E. F., TIRAK, K. V., & STRONG, A. E. (2016). Global coral bleaching 2014-2017. Status and appeal for observations. *The news journal of the international society for reef studies*. 31(1), 20-25.

EDWARDS, A. & SHARPLES, F., (1986) Scottish Sea Lochs – a Catalogue. Scottish Marine Biological Association.

EGANA, A. C., & DISALVO, L. H. (1982). Mass expulsion of zooxanthellae by Easter Island corals. *Pacific Science*, 36, 61-63.

EL-ASKARY, H., ABD EL-MAWLA, S. H., LI, J., EL-HATTAB, M. M., & EL-RAEY,

M. (2013). Change detection of coral reef habitat using Landsat-5 TM, Landsat 7 ETM+ and Landsat 8 OLI data in the Red Sea (Hurghada, Egypt). *International journal of remote sensing*. 35, 2327-2346.

ELSHEIKH, A. B. (2008). The inorganic carbon cycle in the Red Sea. Master thesis in chemical oceanography. University of Bergen Geophysical Institute.

ESHEL, G., CANE, M. A., & BLUMENTHAL, M .B. (1994). Modes of subsurface, intermediate, and deep water renewal in the Red Sea. *Journal of geophysical research*, 99, 15941-15952.

FALKOWSKI, P. G., & DUBINSKY, Z. (1981). Light-shade adaption of Stylophora pistillata, a hermatypic coral from the Gulf of Eilat. *Nature*, 289, 172-174.

FALKOWSKI, P. G., BARBER, R. T., & SMETACEK, V. (1998). Biogeochemical controls and feedbacks on ocean primary production. *Science*, 281, 200-206.

FEELY, R. A., SABINE, C. I., LEE, K., BERELSON, W., KLEYPAS, J., FABRY, V. J. & Millero, F. J. (2004). Impact of anthropogenic CO_2 on the $CaCO_3$ system in the oceans. *Science*, 305, 362-366.

FEELY, R. A., SABINE C. L., HERNANDEZ-AYON, J. M., IANSON, D. & HALES B. (2008). Evidence for upwelling of corrosive “acidified” water onto the continental shelf. *Science*, 320, 1490-1492.

FEELY, R. A., DONEY, S. C. & COOLEY, S. R. (2009). Ocean acidification: present conditions and future changes in a high-CO_2 world. *Oceanography*, 22, 37-47.

FELDMAN, G., CLARK, D., & HALPERN, D. (1984). Satellite color observations of the phytoplankton distribution in the Eastern equatorial pacific during the 1982-1983 El Nino. *Science*, 226(**4678**), 1069-1071.

FENCHEL, T., KRISTENSEN, L. D., & RASMUSSEN, L. (1990). Water column anoxia: vertical zonation of planktonic protozoa. *Marine ecology progress series*, 62, 1-10.

FIEDLER, B., FIETZEK, P., VIEIRA, N., SILVA, P., BITTIG, H. C. & KORTZINGER, A. (2012). *In-situ* CO_2 and O_2 measurements on a profiling float. *Journal of atmospheric and oceanic technology*, 30, 112-126.

FINDLAY, H. S., ARTIOLI, Y., NAVAS, J. M., HENNIGE, S. J., WICKS, L. C., HUVENNE, V. A. I., WOODWARD, E. M. S. & ROBERTS, J. M. (2013). Tidal downwelling and implications for the carbon biogeochemistry of cold-

water corals in relation to future ocean acidification and warming. *Global Change Biology*, 19, 2708-2719.

FITZER, S. C., PHOENIX, V. R., CUSACK, M & KAMENOS, N. A. (2014). Ocean acidification impacts mussel control on biomineralisation. *Scientific reports* 4.

FOSTER, M. S. (2001). Rhodoliths: Between rocks and soft places. *Journal of Phycology*, 37, 659-667.

FRANK, C., FIETZEK, P., & SOBIN, J. (2014). Determination of carbonate parameters in seawater. International ocean systems.

FRANKIGNOULLE, M., GATTUSO, J. P., BIONDO, R., BOURGE, I., COPINMONTEGUT, G., PICHON, M. (1996). Carbon fluxes in coral reefs II: eulerian study of inorganic carbon dynamics and measurement of air-sea CO_2 exchanges. *Marine Ecology Progress Series*, 145, 123-132.

FRANSSON, A. M., CHIERICI, M., & ANDERSON, L. G. (2004). Diurnal variability in the oceanic carbon dioxide system and oxygen in the Southern Ocean surface water. *Deep-sea research II*, 51, 2827-2839.

FRIEDERICH, G. E., BREWER, P. G., HERLIEN, R. & CHAVEZ, F. P. (1995). Measurement of sea surface partial pressure of CO_2 from a moored buoy. *Deep-sea research*, 42, 1175-1186.

FRIHY, O. E., EL GANAINI, M. A., EL SAYED, W. R., & ISKANDER, M. M. (2004). The role of fringing coral reef in beach protection of Hurghada, Gulf of Suez, Red Sea of Egypt. *Ecological Engineering*. 22, 17-25.

FU, F-X, MULHOLLAND, M. R., GARCIA, N., BECK, A., BERNHARDT, P. W., WARNER, M. E., SANUDO-WILHELMY, S. A. & HUTCHINS, D. A. (2008). Interactions between changing pCO_2, N_2 fixation, and Fe limitation in the marine unicellular cyanobacterium *Crocosphaera*. *Limnology and Oceanography*, 53(**6**), 2472-2484.

FUHRMANN, R., & ZIRINO, A. (1988). High-resolution determination of the pH of seawater with a flow-through system. *Deep-Sea Research*, 35(**2**), 197-208.

GAGO, J., GILCOTO, M., PEREZ, F. F. & RIOS, A. F. (2003). Short-term variability of fCO_2 in seawater and air-sea CO_2 fluxes in a coastal upwelling system (Ria de Vigo, NW Spain). *Marine chemistry*, 80, 247-264.

GAO, K., ARUGA, Y., ASADA, K.., ISHIHARA, T., AKANO, T., & KIYOHARA, M.

(1993). Calcification in the articulated coralline alga *Corallina pilulifera*, with special reference to the effect of elevated CO_2 concentration. *Marine Biology*, 117, 129-132.

GAO, K., ZHENG, Y. (2010). Combined effects of ocean acidification and solar UV radiation on photosynthesis, growth, pigmentation and calcification of the coralline algae Corallina sessilis (Rhodophyta). *Global Change Biology*, 16, 2388-2398.

GARRARD, S. L., HUNTER, R., FROMMEL, A., LANE, A., PHILLIPS, J., COOPER, R., DINESHRAM, R., CARDINI, U., MCCOY, S., ARNBERG, M., RODRIGUES ALVES, B., ANNANE, S., ORTE, M.M KUMAR, A., AGUIRRE-MARTINEZ, G., MANEJA, R., BASALLOTE, M., APE, F., TORSTENSSON, A., & BJOERK, M. (2013). Biological impacts of ocean acidification: a postgraduate perspective on research priorities. *Marine biology*, 160(**8**), 1789-1805.

GARRISON, V. H., SHINN, E. A., FOREMAN, W. T., GRIFFIN, D. W. HOLMES, C. W., KELLOGG, C. A., MAJEWSKI, M. S., RICHARDSON, L. L., RITCHIE, K. B., & SMITH, G. W. (2003). *BioScience*. 53(5), 469-480.

GASIM, B. M., KHALID, N. A., & MUHAMAD, H. (2015). The influence of tidal activities on water quality of Paka river Terengganu, Malaysia. *Malaysian journal of analytical sciences*, 19(**5**), 979-990.

GATTUSO, J. P., FRANKIGNOULLE, E. M., & WOLLAST, R. (1998). Carbon and carbonate metabolism in coastal aquatic systems. *Annual Review of Ecological Systems*, 29, 405-435.

GATTUSO, J-P. (2002). Marine biogeochemical cycles: effects on climate and response to climate change. *Oceanography – Vol II*.

GAZEAU, F., QUIBLER, C., JANSEN, J. M., GATTUSO, J-P., MIDDELBURG, J. J., & HEIP, C. H. R. (2007). Impact of elevated CO_2 on shellfish calcification. *Geophysical Research Letters*, 34, L07603.

GE, X., KOSTOV, Y., HENDERSON, R., SELOCK, N. & RAO, G. (2014). A low-cost fluorescent sensor for pCO_2 measurements. *Chemosensors*, 2, 108-120.

GEIDER, R. J., MACINTRYRE, H. L., & KANA, T. M. (1998). A dynamic regulatory model of phytoplanktonic acclimation to light, nutrients, and temperature. *Limnology and Oceanography*, 43(**4**), 679-694.

GENT, P. R. (2012). Carbon cycle: Wind bias and ocean carbon uptake. *Nature Climate Change*, 2, 25-26.

GIBSON, D., & MACGREGOR, C. (2013). A novel solid state non-dispersive

infrared CO_2 gas sensor compatible with wireless and portable deployment. *Sensors*, 13(6), 7079-7103.

GIENAPP, P., TEPLITSKY, C., ALHO, J. S., MILLS, J. A. & MERILA, J. (2008). Climate change and evolution: disentangling environmental and genetic responses. *Molecular Ecology*, 17, 167-178.

GLEASON, D. F., & WELLINGTON, G. M. (1993). Ultraviolet radiation and coral bleaching. *Nature*, 365, 836-838.

GLOOSCHENKO, W. A., CURL, H. JR., & SMALL, L. F. (1972). Diel periodicity of Chlorophyll-*a* concentration in Oregon coastal waters. *Journal of Fisheries Research Board of Canada*, 29, 1253-1259.

GLYNN, P. W., & D'CROZ, L. (1990). Experimental evidence for high temperature stress as the cause of El Nino coincident coral mortality. *Coral reefs*, 8, 181-191.

GLYNN, P. W. (1991). Coral-reef bleaching in the 1980s and possible connections with global warming. *Trends in ecology and evolution*, 6, 175 – 179.

GOPEL, W., HESSE, J., & ZEMEL, J. N. (1991). Optical sensors. In *Sensors: A comprehensive survey*; Wagner, E., Dandliker, R., and Spenner, K., Eds.; VCH: New York, NY, USA, 6, 173-200.

GOREAU, T. F. (1964). Mass expulsion of zooxanthellae from Jamaican reef communities after hurricane Flora. *Science*, 145, 383-386.

GOREAU, T. J. (1992). Bleaching and reef community change in Jamaica: 1951-1991. *American Zoologist*. 32, 683-695.

GOUGH, C, & SHACKLEY, S. (2005). Tyndall Centre Tech. Rpt. 47.

GOWEN, R. J., TETT, P., KENNINGTON, K., MILLS, D. K., SHAMMON, T. M., STEWART, B. M., GREENWOOD, N., FLANAGAN, C., DEVLIN, M., & WITHER, A. (2008). The Irish Sea: Is it eutrophic? *Estuarine, Coastal and Shelf Science*, 76(**2**), 239-254.

GOYET, C., WALT, D. R., & BREWER, P. G. (1992). Development of a fiber optic sensor for measurement of pCO_2 in sea water: design criteria and sea trials. *Deep Sea Res, Part I*, 39(6), 1015-1026.

GOYET, C., & SNOVER, A. K. (1993). High-accuracy measurements of total dissolved inorganic carbon in the ocean: comparison of the alternate detection methods. *Marine Chemistry*, 44, 235-242.

GRIFFIN, D. W., & KELLOGG, C. A. (2004). Dust storms and their impact on

ocean and human health: Dust in Earth's atmosphere. *EcoHealth*, 1, 284-295.

GUADAYOL, O., SILBIGER, N. J., DONAHUE, M. J., & THOMAS, F. I. M. (2014). Patterns in temporal variability of temperature, oxygen and pH along an environmental gradient in a coral reef. *PLoS ONE*, 9(**1**), e85213.

HALES, B., TAKAHASHI, T., & BANDSTRA, L. (2005). Atmospheric CO_2 uptake by a coastal upwelling system. *Global Biogeochemical Cycles*, 19(1).

HALL-SPENCER, J. M., RODOLFO-METALPA, R., MARTIN, S., RANSOME, E., MAOZ, F., TURNER, S. M., ROWLEY, S. J., TEDESCO, D., & BUIA, M-C. (2008). Volcanic carbon dioxide vents show ecosystem effects of ocean acidification. *Nature*, 454, 96-99.

HALL-SPENCER, J. M. A., RODOLFO-METALPA, R. A. B. (2009). Using scientific diving to investigate the long-term effects of ocean acidification at CO_2 vents. *Freiberg Online Geoscience*, 22, 72–76.

HALLEGRAEFF, G. M. (2010). Ocean climate change, phytoplankton community responses and harmful algae blooms: a formidable predictive challenge. *Journal of Phycology*, 46(**2**), 220-235.

HARLEY, C. D. G., HUGHES, A. R., HULTGREN, K. M., MINER, B. G., SORTE, C. J. B., THORNBER, C. S., RODRIGUEZ, L. F., TOMANEK, L. & WILLIAMS, S. L. (2006). The impacts of climate change in coastal marine systems. *Ecology Letters*, 9, 228-241.

HASZELDINE, R. S. (2009). Carbon Capture and Storage: How green can black be? *Science*, 325(**5948**), 1647-1652.

HATCHER, B. G. (1988). Coral reef primary productivity: a beggar's banquet. *Trends in ecology and evolution*. 3, 106 – 11.

HAURI, C., GRUBER, N., PLATTNER G-K., ALIN, S., FEELY, R. A., HALES, B. & WHEELER, P. A. (2009). Ocean acidification in the Californian current system. *Oceanography*, 22, 60-71.

HAVENHAND, J. N., BUTTLER, F. R., THORNDYKE, M. C., & WILLIAMSON, J. E. (2008). Near-future levels of ocean acidification reduce fertilization success in a sea urchin. *Current Biology*, 18(**15**), R652.

HELLAND-HANSEN, B., & NANSEN, F. (1926). The eastern North Atlantic. *Geofysiske Publikasjonen*. 4, 76.

HENDRIKS, I. E., DUARTE, C. M. & ALVAREZ, M. (2010). Vulnerability of marine

biodiversity to ocean acidification: a meta-analysis. Estuarine, *Coastal and Shelf Science*, 86, 157-164.

HENDRICKS, I. E., DUARTE, C. M., OLSEN, Y. S., STECKBAUER, A., RAMAJO, L., MOORE, T. S., TROTTER, J. A. & MCCULLOCH, M. (2014). Biological mechanisms supporting adaption to ocean acidification in coastal ecosystems. *Estuarine, Coastal and Shelf Science*, 1-8.

HODGKINSON, J., & TATAM, R. P. (2012). Optical gas sensing: a review. *Measurement science and technology*, 24, 1.

HOEGH-GULDBERG, O., & SMITH, G. J. (1989). The effect of sudden changes in temperature, irradiance and salinity on the population density and export of zooxanthellae from the reef corals *Stylophora pistillata* (Esper 1797) and *Seriatopora hystrix* (Dana 1846). *Journal of experimental marine biology and ecology*. 129, 279-303.

HOEGH-GULDBERG, O. (1999). Climate change, coral bleaching and the future of the world's coral reefs. *Marine Freshwater Research*, 50, 839 – 866.

HOEGH-GULDBERG, O., & JONES, R. (1999). Diurnal patterns of photoinhibition and photoprotection. *Marine ecology progress series* (in press).

HOEGH-GULDBERG, O., MUMBY, P. J., HOOTEN, A. J., STENECK, R. S., GREENFIELD, P., GOMEZ, E., HARVELL, C. D., SALE, P. F., EDWARDS, A. J., CALDERIA, K., KNOWLTON, N., EAKIN, C. M., IGLESIAS-PRIETO, R., MUTHIGA, N., BRADBURY, R. H., DUBI, A. & HATZIOLOS, M. E. (2007). Coral reefs under rapid climate change and ocean acidification. *Science*, 318, 1737-1742.

HOEGH-GULDBERG, O., POLOCZANSKA, E. S., SKIRVING, W., & DOVE, S. (2017). Coral reef ecosystems under climate change and ocean acidification. *Frontiers in Marine Science*. 4, 158.

HOFMANN, G. E., BARRY, J. P., EDMUNDS, P. J., GATES, R. D., HUTCHINS, D. A., KLINGER, T. & SEWELL, M. A. (2010). The effect of ocean acidification on calcifying organisms in marine ecosystems: an organism-to-ecosystem perspective. *Annual review of ecology, evolution and systematics*, 41, 127-147.

HOFMANN, G. E., SMITH, J. E., JOHNSON, K. S., SEND, U., LEVIN, L. A., MICHELI, F., PAYTAN, A., PRICE, N. N., PETERSON, B., TAKESHITA, Y., MATSON, P. G., CROOK, E. D., KROEKER, K. J., GAMBI, M. C., RIVEST, E. B., FRIEDER,

C. A., YU, P. C., & MARTZ, T. R. (2011). High-frequency dynamics of ocean pH: A multi-ecosystem comparison. *PLoS One*, 6(**12**), e28983.

HONJO, S., & WELLER, R. A. (1997). Monsoon winds and carbon cycles in the Arabian Sea. *OCEANUS*, 24-28.

HOOD, E. M., MERLIVAT, L., & JOHANNESSEN, T. (1999). Variations of fCO_2 and air-sea flux of CO_2 in the Greenland Sea gyre using high-frequency time series data from CARIOCA drift buoys. *Journal of geophysical research*, 104, 20571-20583.

HOPPE, C. J. M., LANGER, G., ROKITTA, S. D., WOLF-GLADROW, D. A., & ROST, B. (2012). Implications of observed inconsistencies in carbonate chemistry measurements for ocean acidification studies. *Biogeosciences*. 9, 2401-2405.

HORWITZ, R., BORELL, E. M., FINE, M. & SHAKED, Y. (2014). Trace element profiles of the sea anemone *Anemonia viridis* living near by a natural CO_2 vent. *PeerJ*, DOI 10.7717/peerj.538.

HUNT, B. V. P., PAKHOMOV, E. A., HOISE, G. W., SIEGEL, V., WARD, P. & BERNARD, K. (2008). Pteropods in Southern Ocean ecosystems. *Progress in Oceanography*, 78, 193-221.

HUTCHINS, D. A., FU F-X., ZHANG, Y., WARNER, M. E., FENG, Y., PORTUNE, K., BERNHARDT, P. W., & MULHOLLAND, M. R. (2007). CO_2 control of Trichodesmium N_2 fixation, photosynthesis, growth rates, and elemental ratios: implications for past, present, and future ocean biogeochemistry. *Limnology and Oceanography*, 52(**4**), 1293-1304.

HUTCHINS, D. A., MULHOLLAND, M. R., & FU, F-X. (2009). Nutrient cycles and marine microbes in a CO_2-enriched ocean. *Oceanography*, 22, 128-145.

ICHIMURA, S. (1960). Diurnal fluctuation of chlorophyll content in lake water. *Botanic. Mag.*, 73, 217-224.

IGLESIAS-RODRIGUEZ, M. D., HALLORAN, P. R., RICKABY, R. E. M., HALL, I. R., COLMENERO-HIDALGO, E., GITTINS, J. R., GREEN, D. R. H., TYRRELL, T., GIBBS, S. J., VAN DASSOW, P., REHM, E., ARMBRUST, E. V., BOESSENKOOL, K. P. (2008). Phytoplankton calcification in a high-CO_2 world. *Science*, 320, 336-340.

INOUE, H., & SUGIMURA, Y. (1988). Distribution and variations of oceanic

carbon dioxide in the western North Pacific, eastern Indian and Southern Ocean south of Australia. *Chemical and physical meteorology*, 40(**4**), 308-320.

INOUE, H. Y., MATSUEDA, H., ISHII, M., FUSHIMI, K., HIROTA, M., ASANUMA, I., & TAKASUGI, Y. (1995). Long-term trend of the partial pressure of carbon dioxide (pCO_2) in surface waters of the western North Pacific, 1984 – 1993. *Tellus B: Chemical and Physical Meteorology*, 47:4, 391-413.

IPCC, 2014: Climate Change 2014: Synthesis Report. Contribution of Working Groups I, II and III to the Fifth Assessment Report of the Intergovernmental Panel on Climate Change [Core Writing Team, R.K. Pachauri and L.A. Meyer (eds.)]. IPCC, Geneva, Switzerland, 151 pp.

JAMESON, S. C., MCMANUS, J. W., & SPALDING, M. D. (1995). *State of the reefs: regional and global perspectives*. US department of state: Washington, DC.

JIANG, Z-P. (2014). Variability and control of the surface ocean carbonate system observed from ships of opportunity. University of Southampton.

JIANG, Z-P., HYDES, D. J., HARTMAN, S. E., HARTMAN, M. C., CAMPBELL, J. M., HOHNSON, B. D., SCHOFIELD, B., TURK, D., WALLACE, D., BURT, W. J., THOMAS, H., COSCA, C., & FEELY, R. (2014). Application and assessment of a membrane-based pCO_2 sensor under field and laboratory conditions. *Limnology and Oceanography: Methods*. 12, 264-280.

JICKELLS, T. D. (1999). The inputs of dust derived elements to the Sargasso sea: a synthesis. *Marine Chemistry*, 68, 5-14.

JOHNSON, K. M., KING, A., & SIEBURTH, J. (1985). Coulometric TCO_2 analyses for marine studies: An introduction, *Marine Chemistry*, 16, 61-81.

JOHNSON, K., WILLS, K., BUTLER, D., JOHNSON, W., & WONG C. (1993). Coulometric total carbon dioxide analysis for marine studies: Maximizing the performance of an automated gas extraction system and coulometric detector, *Marine Chemistry*, 44(**2-4**), 167-187.

JOHNSON, K. S., NEEDOBA, J. A., RISER, S. C. & SHOWERS, W. J. (2007) Chemical sensor networks for the aquatic environment. *Chemical Review*, 107(**2**), 623-40.

JOHNSON, Z. I., WHEELER, B. J., BLINEBRY, S. K., CARLSON, C. M., WARD, & HUNT, D. E., (2013) Dramatic variability of the carbonate system at a temperate coastal ocean site (Beaufort, North Carolina, USA) is regulated

by physical and biogeochemical processes on multiple timescales. PLoS One, 8(**12**), e85117.

JOKIEL, P. L., & COLES, S. L. (1990). Response of Hawaiian and other Indo-Pacific reef corals to elevated temperatures. *Coral Reefs*, 8, 155-162.

JOKIEL, P. L. (2011). Ocean acidification and control of reef coral calcification by boundary layer limitation of proton flux. *Bulletin of Marine Science*, 87, 639-657.

JONES, R. J., & STEVEN, A. L. (1997). Effects of cyanide on corals in relation to cyanide fishing on reefs. *Marine and freshwater research*, 48(**6**), 517-522.

JONES, R. J., & HOEGH-GULDBERG, O. (1999). Effects of cyanide on coral photosynthesis: implications for identifying the cause of coral beaching and assessing the environmental effects of cyanide fishing. *Marine ecology progress series*, 177, 83-91.

KALTIN, S. & ANDERSON, L. G. (2005). Uptake of atmospheric carbon dioxide in Arctic shelf seas: evaluation of the relative importance of processes that influence pCO_2 in water transported over the Bering-Chukchi Sea shelf. *Marine Chemistry*, 94, 67-79.

KALTIN, S., HARALDSSON, C., & ANDERSON, L. G. (2005). A rapid method for determination of total dissolved inorganic carbon in seawater with high accuracy and precision, *Marine Chemistry*, 96(**1-2**), 53-60.

KAMENOS, N. A., MOORE, P. G., & HALL-SPENCER, J. M. (2004). Nursery-area function of maerl grounds for juvenile queen scallops *Aequipecten opercularis* and other invertebrates. *Marine Ecology Progress Series,* 274, 183-189.

KAMENOS, N. A., MOORE, P. G., & HALL-SPENCER, J. M. (2004b). Small-scale distribution of juvenile gadoids in shallow inshore waters; what role does maerl play? *ICES Journal of Marine Science: Journal du Conseil*, 61, 422-429.

KAMENOS, N. A., BURDETT, H. L., ALOISIO, E., FINDLAY, H. S., MARTIN, S., LONGBONE, C., DUNN, J., WIDDICOMBE, S. & CALOSI, P. (2013). Coralline algal structure is more sensitive to rate, rather than the magnitude of ocean acidification. *Global Change Biology*, 19, 3621-3628.

KASTING, J. (1993). Earth's early atmosphere. *Science*, 259:920-926.

KAUR, J., ADAMCHUCK, V. I., WHALEN, J. K., & ISMAIL, A. A. (2015).

Development of an NDIR CO_2 sensor-based system for assessing soil toxicity using substrate-induced respiration. *Sensors*, 15, 4734-4748.

KAYANNE, H., HATA, H., NOZAKI, K., KATO, K., NEGISHI, A., SAITO, H., YAMANO, H., ISAMU, T., KIMOTO, H., TSUDA, M., AKIMOTO, F., KAWATE, K., & IWATA, I. (2002). Submergible system to measure seawater pCO_2 on a shallow sea floor. *Marine Technology Society Journal*, 36(1), 23-28.

KHOMAYIS, H. S. (2002). The annual cycle of nutrients salts and chlorophyll-a in the coastal waters of Jeddah, Red Sea. *J. KAU: Marine Science*, 13, 131-145.

KIM, J-M., LEE, K., SHIN, K., KAND, J-H., LEE, H-W., KIM, M., JANG, P-G., & JANG, M-C. (2006). The effect of seawater CO_2 concentration on growth of a natural phytoplankton assemblage in a controlled mesocosm experiment. *Limnology and oceanography*, 51(4), 1629-1636.

KIM, H.-C., & LEE, K. (2009). Significant contribution of dissolved organic matter to seawater alkalinity. *Geophysical Research Lett*ers, 36(20).

KINKADE, C. S., MARRA, J., DICKEY, T. D., LANGDON, C., SIGURDSON, D. E., & WELLER, R. (1999). Diel bio-optical variability in the Arabian Sea as observed from moored sensors. *Deep-sea research II*, 46, 1813-1832.

KLEYPAS, J. A., BUDDEMEIER, R. W., ARCHER, D., GATTUSO, J. P., LANGDON, C. & OPDYKE, B. N. (1999). Geochemical consequences of increased atmospheric carbon dioxide on coral reefs. *Science*, 284, 118-120.

KORTZINGER, A., MINTROP, L., WALLACE, D. W. R., JOHNSON, K. M., NEILL, C., TILBROOK, B., TOWLER, P., INOUE, H. Y., ISHII, M., SHAFFER, G., SAAVEDRA, R. F. T., OHTAKI, E., YAMASHITA, E., POISSON, A., BRUNET, C., SCHAUER, B., GOYET, C., & EISCHEID, G. (2000). The international at-sea intercomparison of fCO_2 systems during the R/V Meteor Cruise 26/1 in the North Atlantic Ocean. *Marine Chemistry*, 72, 171-192.

KORTZINGER, A., SEND, U., WALLACE, D. W. R., KARSTENSEN, J. & DEGRANDPRE, M. D. (2008a). Seasonal cycle of O_2 and pCO_2 in the central Labrador Sea: Atmospheric, biological, and physical implications. *Global biogeochemical cycles*, 22, GB1014.

KORTZINGER, A., SEND, U., LAMPITT, R. S., HARTMAN, S., WALLACE, D. W. R., KARTENSEN, J., VILLAGARCIA, M. G., LLINAS, O & DEGRANDPRE, M. D. (2008b). The seasonal pCO_2 cycle at $49^oN/16.5^oW$ in the northeastern

Atlantic Ocean and what it tells us about biological productivity. *Journal of Geophysical Research*, 113: C04020.

KROEKER, K. J., GAYLORD, B., HILL, T. M., HOSFELT, J. D., MILLER, S. H. & SANFORD, E. (2014). The role of temperature in determining species' vulnerability to ocean acidification: A case study using *Mytilus galloprovincialis*. *PLoS ONE*, 9(7).

KURIHARA, H., KATO, S., & ISHIMATSU, A. (2007). Effects of increased seawater pCO_2 on early development of the oyster *Crassostrea gigas*. *Aquatic biology*, 1, 91-98.

KURIHARA, H., (2008). Effects of CO_2-driven ocean acidification on the early developmental stages of invertebrates. *Marine Ecology Progress Series*, 373, 275-284.

KUSHMARO, A., LOYA, Y., FINE, M., & ROSENBERG, M. (1996). Bacterial infection and coral bleaching. *Nature*, 380-396.

KUSS, J., ROEDER, W., WLOST, K-P, & DEGRANDPRE, M. D. (2006). Timeseries of surface water CO_2 and oxygen measurements on a platform in the central Arkona Sea (Baltic Sea): seasonality of uptake and release. *Marine chemistry*, 101, 220-232.

KWON, J., AHN, G., KIM, G., KIM, J. C., & KIM, H. (2009). A study on NDIR-based CO_2 sensor to apply remont air quality monitoring system. In *Proceedings of the ICCAS-SICE*, Fukuoka, Japan, 18-21 August, 1683-1687.

LANGDON, C., TAKAHASHI, T., SWEENEY, SWEENY, C., CHIPMAN, D., GODDARD, J., MARUBINI, F., ACEVES, H., BARNETT, H., ATKINSON, M. J. (2000). Effect of calcium carbonate saturation state on the calcification rate of an experimental coral reef. *Global biogeochemical cycles*, 14(**2**), 639-654.

LANGDON, C., ALBRIGHT, R., BAKER, A. C., & JONES, P. (2018). Two threatened Caribbean coral species have contrasting responses to combined temperature and acidification stress. *Limnology and oceanography*. DOI:10.1002/lno.10952.

LANGE, R., STAALAND, H., & MOSTAD, A. (1972). The effect of salinity and temperature on solubility of oxygen and respiratory rate in oxygen-dependent marine invertebrates. *Journal of Experimental Marine Biology and Ecology*, 9(**3**), 217-229.

LE BOUTEILLER, A., & HERBLAND, A. (1982). Diel variation of chlorophyll a as

evidenced from a 13-day station in the equatorial Atlantic Ocean. *Oceanologica Acta*, 5(**4**), 433-441.

LEBRATO, M., IGLESIAS-RODRIGUEZ, D., FEELY, R., GREENLY, D., JONES, D., SUAREZ-BOSCHE, N., LAMPITT, R. S., CARTES, J. E., GREEN, D. R. H., & ALKER, B. (2010). Global contribution of echinoderms to the marine carbon cycle: a reassessment of the oceanic $CaCO_3$ budget and the benthic compartments. *Ecological Society of America*, 80(**3**), 441-467.

LEE, K., MILLERO, F. J., BYRNE, R. H., FEELY, R. A., & WANNINKHOF, R. (2000). The recommended dissociation constants for carbonic acid in seawater. *Geophysical Research Letters*, 27(2), 229-232.

LEIGH, E. G., PAINE, R. T., QUINN, J. F., & SUCHANEK, T. H. (1987). Wave energy and intertidal productivity. *Proceedings of the National Academy of Science U.S.A*, 84, 1314-1318.

LESSER, M. P., STOCHAJ, W. R., TAPLEY, D. W., & SHICK, J. M. (1990). Bleaching in coral reef anthozoans: effects of irradiance, ultraviolet radiation and temperature on the activities of protective enzymes against active oxygen. *Coral reefs*, 8, 225-32.

LIBES, S. M. (1992). An introduction to marine biogeochemistry. John Wiley & Sons, Inc.

LITT, E. J., HARDMAN-MOUNTFORD, N. J., BLACKFORD, J. C., MITCHELSON-JACOB, G., GOODMAN, A., MOORE, G. E., CUMMINGS, D. G., & BUTENSCHON, M. (2010). Biological control of pCO_2 at station L4 in the Western English Channel over 3 years. *Journal of Plankton Research*, 32(**5**), 621-629.

LONGHURST, A. R. (2007). Ecological Geography of the Sea. Second Ed, Elsevier Inc, pp. 1-542.

LOYA, Y. *et al*. (2001). Coral bleaching: the winners and the losers. *Ecol. Lett*. 4, 122 – 131.

LU, Z., DAI, M., XU, K., CHEN, J., & LIAO, Y. (2008). A high precision, fast response, and low power consumption in situ optical fibre chemical pCO_2 sensor. *Talanta*, 76, 353-359

LUCAS, W. J. (1983). Photosynthetic assimilation of exogenous HCO3 by aquatic plants. *Annual Review of Plant Physiology*, 34, 71-104.

LUEKER, T. J., DICKSON, A. G., & KEELING, C. D. (2000). Ocean pCO_2

calculated from dissolved inorganic carbon, alkalinity, and equations for K_1 and K_2: validation based on laboratory measurements of CO_2 in gas and seawater at equilibrium. *Marine Chemistry*, 70(1-3), 105-119.

LUGER, H., WALLACE, D. W. R., KORTZINGER, A. & NOJIRI, Y. (2004). The pCO_2 variability in the midlatitude North Atlantic Ocean during a full annual cycle. *Global Biogeochemical Cycles*, 18(**3**).

MARION, G. M., MILLERO, F. J., CAMOES, M. F., SPITZER, P., FEISTEL, R., & CHEN, C.-T.A. (2011). pH of seawater. *Marine Chemistry*, 126 (1-4), 89-96.

MARRA, J. (1997). Analysis of diel variability in chlorophyll fluorescence. *Journal of Marine Research*, 55, 767-784.

MARTIN, S., CLAVIER, J., CHAUVAND, L., & THOUZEAU, G. (2007). Community metabolism in temperate maerl beds. 1. Carbon and carbonate fluxes. *Marine Ecology Progress Series*, 335, 19-29.

MARTIN, S., RODOLFO-METALPA, R., RANSOME, E., ROWLEY, S., BUIA, M. C., GATTUSO, J. P., & HALL-SPENCER, J. (2008). Effects of naturally acidified seawater on seagrass calcareous epibionts. *Biology Letters*, 4, 689-692.

MARTIN, S. & GATTUSO, J. P. (2009). Response of Mediterranean coralline algae in ocean acidification and elevated temperature. *Global Change Biology*, 15, 2089-2100.

MARTINEZ, M. L., INTRALAWAN, A., VAZQUEZ, G., PEREZ-MAQUEO, O., SUTTON, P., & LANDGRAVE, R. (2007). The coasts of our world: Ecological, economic and social importance. *Ecological economics*. 63(2-3), 254-272.

MARTZ, T. R., JOHNSON, K. S. & RISER, S. C. (2008). Ocean metabolism observed with oxygen sensors on profiling floats in the South Pacific. *Limnology and Oceanography*, 53, 2094-2111.

MARUBINI, F., FERRIER-PAGES, C. & CUIF, J. P. (2003). Suppression of skeletal growth in scleractinian corals by decreasing ambient carbonate-ion concentration: a cross-family comparison. *Proceedings of the Royal Society of London B Biological Science*, 270, 179-184.

MATSON, P. G., WASHBURN, L., MARTZ, T. R. & HOFMANN, G. E. (2014). Abiotic versus biotic drivers of ocean pH variation under fast sea ice in McMurdo Sound, Antarctica. *PLoS ONE*, 9(9).

MCALLISTER, C. D. (1963). Measurements of diurnal variation in productivity at ocean station <P>. *Limnology and Oceanography*, 8, 289-292.

MCCULLOCH, M. T., HOLCOMB, M., TROTTER, J. A., & MONTAGNA, P. (2013). Resilience of coral calcification to ocean acidification: insights from boron isotopes. Twelfth Australiasian Environmental Conference. 48(38), 41-42.

MCGILLIS, W. R., EDSON, J. B., WARE, J. D., DACEY, J. W. H., HARE, J. E., FAIRALL, C. W., & WANNINKHOF, R. (2001). Carbon dioxide flux techniques performed during GasEx-98. *Marine Chemistry*, 75, 267-280.

MCNEIL, B. I. & MATEAR, R. J. (2008). Southern Ocean acidification: a tipping point at 450 ppm atmospheric CO_2. *Proceedings of the National Academy of Science of the USA*, 105, 18860-18864.

MEEHL, G. A., STOCKER, T. F., COLLINS., W. D., FRIEDLINGSTEIN, P., GAYE, A. T., et *al*. (2007). Global climate projections. Climate change 2007: The physical science basis. Contribution working group I 4th assessment report of the intergovernmental panel in climate change. 747-845. Cambridge, UK. Cambridge University Press.

MEHRBACH, C., CULBERSON, C. H., HAWLEY, J. E., & PYTKOWICZ, R. M. (1973). Measurement of the apparent dissociation constants of carbonic acid in seawater at atmospheric pressure. *Limnology and oceanography*, 18, 897-907.

MELZNER, F., GUTOWSKA, M. A., LANGENBUCH, M., DUPONT, S., LUCASSEN, M., THORNDYKE, M. C., BLEICH, M. & PORTNER, H. O. (2009). Physiological basis for high CO_2 tolerance in marine ectothermic animals: pre-adaption through lifestyle and ontogeny? *Biogeosciences*, 6, 2313-2331.

MENDES, L. B., OGINK, N. W. M., EDOUARD, N., VAN DOOREN, H. J. C., TINOCO, I. DE F. F., & MOSQUERA, J. (2015). NDIR gas sensor for spatial monitoring of carbon dioxide concentrations in naturally ventilated livestock buildings. *Sensors*. 15, 11239-11257.

MIECZNIKOWSKI, J. C., & SELLERS, K. F. (2002). Statistical analysis of chemical sensor data. *Proceedings of Advances in Chemical Sensors*. 327-347.

MILLER, R. L., BRADFORD, W. L., & PETERS, N. E. (1988). Specific conductance: Theoretical considerations and application to analytical quality control. *U. S.Geological Survey Water-Supply.*

MILLER, A. W., TEYNOLDS, A. C., SOBRINO, C., & RIEDEL, G. F. (2009).

Shellfish face uncertain future in high CO_2 world: influence of acidification on oyster larvae calcification and growth in estuaries. *PLoS One*, 4, e5661.

MILLERO, F. J., PIERROT, K., LEE, R., WANNINKHOF, R., FEELY, C. L., SABINE, KEY, R. M., & TAKAHASHI, T. (2002). Dissociation constants for carbonic acid determined from field measurements. *Deep Sea Research, Part I*, 49(10), 1705-1723.

MILLERO, F. J., GRAHAM, T. B., HUANG, F., BUSTOS-SERRANO, H., & PIERROT, D. (2006). Dissociation constants of carbonic acid in seawater as a function of salinity and temperature. *Marine Chemistry*, 100, 80-94.

MILLERO, F. J. (2007). The marine inorganic carbon cycle. *Chemical Reviews*, 107(**2**), 308-341.

MILLERO, F. J. (2010). Carbonate constants for estuarine waters. *Marine and Fresh Water Research*, 61, 139-142.

MILNE, P. H. (1972). Hydrography of Scottish west coast sea lochs. Marine Research, 1972/No. 3, HMSO, Edinburgh.

MORRIS, S., & TAYLOR, A. C. (1983). Diurnal and seasonal variation in physio-chemical conditions within intertidal rock pools. *Estuarine, Coastal and Shelf Science*, 17(**3**), 339-355.

MOY, A. D., HOWARD, W. R., BRAY, S. G., & TRULL, T. W. (2009). Reduced calcification in modern Southern Ocean planktonic foraminifera. *Nature Geoscience*, 2, 276-80.

MU, L., STAMMERJOHN, S. E., LOWRY, K.E., & YAGER, P. L. (2014). Spatial variability of surface pCO_2 and air-sea CO_2 flux in the Amundsen Sea Polynya, Antarctica. *Elementa Science of the Anthropocene*, 3, 36.

MUMBY, P. J., CHISHOLM, J. R. M., EDWARDS, A. J., CLARK, C. D., ROARK, E. B., ANDREFOUET, S., & JAUBERT, J. (2001). Unprecedented bleaching-induced mortality in *Porites* spp. at Rangiroa Atoll, French Polynesia. *Marine biology*, 139(**1**), 183 – 189.

MUNDAY, P. L., DIXSON, D. L., DONELSON, J. M., JONES, G. P., PRATCHETT, M. S., DEVITSINA, G. V., & DOVING, K. B. (2009). Ocean acidification impairs olfactory discrimination and homing ability of a marine fish. *Proceedings of the National Academy of Sciences of the USA*,106, 1848-1852.

MURRU, M., & SANDGREN, C. D. (2004). Habitat matters for inorganic carbon

acquisition in 38 species of red macroalgae (*Rhodophyta*) from Puget Sound, Washington, USA. *Journal of Phycology*, 40, 837-845.

NAKANO, Y., & WATANABE, Y. W. (2005). Reconstruction of pH in the surface seawater over the North Pacific Basin for all seasons using temperature and chlorophyll-*a*. *Journal of Oceanography*, 61, 673 – 680.

NAKANO, Y., KIMOTO, H., WATANABE, S., HARADA, K., & WATANABE, Y. W. (2006). Simultaneous vertical measurements of in-situ pH and CO_2 in the sea using spectrophotometric profilers. *Journal of Oceanography*, 62(1), 71-81.

NASSAR, M. Z., MOHAMED, H. R., KHIRAY, H. M., & RASHEDY, S. H. (2014). Seasonal fluctuations of phytoplankton community and physico-chemical parameters of the north western part of the Red Sea, Egypt. *The Egyptian Journal of Aquatic Research*, 40(**4**), 395-403.

NEMOTO, K. T., MIDORIKAWA, T., WADA, A., OGAWA, K., TAKATANI, S., KIMOTO, H., ISHII, M., & INOUE, Y. (2009). Continuous observations of atmospheric and oceanic CO_2 using a moored buoy in the East China Sea: Variations during the passage of typhoons. *Deep Sea Research, Part II*, 56(8-10), 542-553.

NOAA, 2012. OA Observations and Data [Online]. Available: https://pmel.noaa.gov/co2/story/OA+Observations+and+Data [Accessed 5th November 2017].

NYBAKKEN, J. W., & BERTNESS, M. D. (2005). *Marine Biology: an ecological approach*: Pearson/Benjamin Cummings.

OHDE, S., VAN WOESIK, R. (1999). Carbon dioxide flux and metabolic processes of a coral reef, Okinawa. *Bulletin of Marine Sci*ence, 65, 559-576.

ONI, O. E., SCHMIDT, F., MIYATAKE, T., KASTEN, S., WITT, M., HINRICHS, K-U., & FRIEDRICH, M. W. (2015). Microbial communities and organic matter composition in surface and subsurface sediments of the Helgoland Mud Area, North Sea. *Frontiers in Microbiology*, 6, 1-16.

ORR J. C., FABRY, J. C., AUMONT, O., BOPP, I., DONEY S. C., FEELY, R. M., GNANADESIKAN, A., GRUBER, N., ISHIDA, A., JOOS, F., KEY, R. M., LINDSAY, K., MAIER-REIMER, E., MATEAR, R., MONFRAY, P., MOUCHET, A., NAJJAR, R. G., PLATTNER, G.-K., RODGERS, K. B., SABINE, C. L., SARMIENTO, J. L., SCHLITZER, R., SLATER, R. D., TOTTERDELL, I. J.,

WEIRIG, M.-F., YAMANAKA, Y., & YOOL, A. (2005). Anthropogenic decline in high-latitude ocean carbonate by 2100. *Nature*, 437, 681-686.

ORR, J. C., & EPITALON, J.-M. (2015). Improved routines to model the ocean carbonate system: mocsy 2.0. *Geoscientific Model Development*, 8, 485-499.

O'SULLIVAN, D., & MILLERO, F. (1998). Continual measurement of the total inorganic carbon in surface seawater, *Marine Chemistry*, 60, 75-83.

OWENS, T. G., FALKOWSKI, P. G., & WHITLEDGE, T. E. (1980). Diel periodicity in cellular chlorophyll content in marine diatoms, *Marine Biology*, 59, 71-77.

PAPAGEORGIOU, G. C., & GOVINDJEE. (2004). Chlorophyll-*a* fluorescence: A signature of photosynthesis. Springer. New York City.

PARRY, G. (1981). The meanings of r- and K-selection. *Oecologia*, 48, 260-264.

PATZERT, W. C. (1974). Wind-induced reversal in the Red Sea circulation. *Deep Sea Research*, 21, 109-121.

PEARMAN, E. K. W., & LEUNING, R. (1980). Correction of flux measurements for density effects due to heat and water vapour transfer. *Quarterly Journal of the Royal Meteorological Society*, 106, 85-100.

PEDGLEY, D. E. (1974). An outline of the weather and climate of the Red Sea. In *L'Oceanographie Physique de la Mer Rouge*, 9-27. Cent. Natl. Pour l'Exploitation des Oceans, Paris, 1974.

PENICHON, S., JURGENS, M., & MURRAY, A. (2002). Light and dark stability of laminated and face-mounted photographs: A preliminary investigation. In *Works of Art on Paper, Books, Documents and Photographs*. Baltimore, MD: IIC Congress, 2-6 September 2002, 154-159.

PERLMAN, H. (2004). Water properties and measurements. Water Science School. Retrieved from http://nsidc.org/cryosphere/seaice/index.html.

PETIT, J. R., JOUZEL, J., RAYNAUD, D., BARKOV, N. I., BARNOLA, J.-M., BASILE, I., BENDER, M., CHAPPELLAZ, J., DAVIS, J., DELAYGUE, G., DELMOTTE, M., KOTLYAKOV, V. M., LEGRAND, M., LIPENKOV, V., LORIUS, C., PEPIN, L., RITZ, C., SALTZMAN, E., & STIEVENARD, M. (2001). Vostok ice core data for 420,000 years. *IGBP PAGES/World Data Center for Paleoclimatology Data* Contribution Series #2001-076: Boulder, CO: NOAA/NGDC Paleoclimatology Program.

PIANKA, E. R. (1970). On r- and K-selection. *The American Naturalist*, 104, 592-

597.

PIERROT, D., LEWIS, E., & WALLACE, D. W. R. (2006). CO2SYS DOS Program developed for CO_2 system calculations. ORNL/CDIAC-105. Carbon dioxide information analysis center. Oak Ridge National Laboratory, US Department of Energy, Oak Ridge, TN.

PIERROT, D., NEILL, C., SULLIVAN, K., CASTLE, R., WANNINKHOF, R., LUGER, H., JOHANNESSEN, T., OLSEN, A., FEELY, R. A., & COSCA, C. E. (2009). Recommendations for autonomous underway pCO_2 measuring systems and data-reduction routines. *Deep-sea research II*, 56, 512 – 522.

POISSON, A., MORCOS, S., SOUVERMEZOGLOU, E., PAPAUD, A., & IVANOFF, A. (1984). Some aspects of biogeochemical cycles in the Red Sea with special reference to new observations made in summer 1982. *Deep Sea Research Part A. Oceanographic Research Papers*. 31(6-8), 707-718.

PORTER, J. W., MUSCATINE, L., DUBINSKY, Z., & FALKOWSKI, P. G. (1984). Primary production and photoadaptation in light- and shade-adapted colonies of the symbiotic coral, *Stylophora pistillata*. *Proceedings of the Royal Society London B* 222, 161-180.

PORTNER, H. O. (2008). Ecosystem effects of ocean acidification in times of ocean warming: a physiologist's view. *Marine Ecology Progress Series*, 373, 203-217.

PORTNER, H. O., LANGENBUCH, M., MICHAELIDIS, B. (2005). Synergistic effects of temperature extremes, hypoxia, and increases in CO_2 on marine animals: from Earth history to global change. *Journal of Geophysical Research*, 110, C09S10.

PRATT, L., JOHNS, W., Murray. S. P. & Katsumata, K. (1999). Hydraulic interpretation of direct velocity measurements in the Bab el Mandab Strait. *Journal of Physical Oceanography*, 29, 2769-2784.

PRZESLAWSKI, R., AHYONG, S., BYRNE, M., WORHEIDE, G., HUTCHINGS, P. (2008). Beyond corals and fish: the effects of climate change on noncoral benthic invertebrates of tropical reefs. *Global Change Biology*, 14, 2773-2795.

PUTON, J., JASEK, K, SIODLOWSKI, B., KNAP, A., & WISNIEWSKI, K. (2005). Optimisation of a pulsed IR source for NDIR gas analysers. *Opto-Electronics Rev*iew, 10(**2**), 97-103.

RAHMSTORF, S. (2006). Thermohaline Ocean Circulation. *Encyclopedia of*

Quaterary Sceince. Edited by S. A. Elias. Elsevier, Amsterdam 2006.

RALPH, P. J., GADDEMANN, R., LARKUM, A. W. D., & SHREIBER, U. (1999). *In-situ* underwater measurements of photosynthetic activity of coral reef dwelling endosymbionts. *Marine Ecology Progress Series* (in press).

RASHEED, M., BADRAN, M., RICHTER, C., & HUETTEL, M. (2002). Effect of reef framework and bottom sediment on nutrient enrichment in a coral reef of the Gulf of Aqaba, Red Sea. *Marine Ecology Progress Series*, 239, 277-285.

RASUL, N. M. A., & STEWART, I. C. F. (eds). (2015). The Red Sea: The formation, morphology, oceanography and environment of a young ocean basin. Springer-Verlag Berlin Heidelberg.

RAVEN, J. A. (1997). Inorganic carbon acquisition by marine autotrophs. In: Callow J. A. (ed). Advances in botanical research. Academic Press, New York, pp 85-209.

RAVEN, J. A., & FALKOWSKI, P. G. (1999). Oceanic sinks for atmospheric CO_2. *Plant, Cell and Environment*, 22, 741-755.

RAVEN, P. H., JOHNSON, G. B., MASON, K. A., LOSO, J. B., & SINGER, S. R. (2014). The nature of molecules and properties of water. In Biology (10^{th} ed.), 17-30, New York, NY: McGraw-Hill.

RAY, G. C., HAYDEN, A. J., BULGER JR., A. J., & MCCORMICK-RAY, M. G. (1992). Effects of global warming on the biodiversity of coastal-marine zones. In Peters, R. L., and Lovejoy, T. E., (eds.). *Global warming and biological diversity*. 91-104. Yale University Press, New Haven.

REROLLE, V. M. C., RIBAS-RIBAS, M., KITIDIS, V., BROWN, I., BAKKER, D. C. E., LEE, G. A., SHI, T., MOWLEM, M. C., & ACHTERBERG, E. P. (2014). Controls on pH in surface waters of northwestern European shelf seas. *Biogeosciences Discussions*, 11, 943-974.

RICHARDSON, A. J., & SCHOEMAN, D. S. (2004). Climate impact on plankton ecosystems in the northeast atlantic. *Science*, 305(**5690**), 1609-1612.

RICHMOND, R. H., TISTHAMMER, K. H., & SPIES, N. P. (2018). The effects of anthropogenic stressors on reproduction and recruitment of corals and reef organisms. *Frontiers in Marine Science*. 5, 226.

RIEBESELL, U., ZONDERVAN, I., ROST, B., TORTELL, P. D., ZEEBE, R. E., & MOREL, F. M. M. (2000). Reduced calcification of marine plankton in response to increased atmospheric CO_2. *Nature*, 407, 364-367.

RIEBESELL, U., FABRY, V. I., HANSSON, L., & GATTUSO, J.-P. (Eds). (2010).

Guide for best practices in ocean acidification research and data reporting. Office for Official Publications of the European Union, Luxembourg.

RIES, J. B., COHEN, A. L. & MCCORKLE, D. C. (2009). Marine calcifiers exhibit mixed responses to CO_2-induced ocean acidification. *Geology*, 37, 1131-1134.

ROSA, R. & SEIBEL, B. A. (2008). Synergistic effects of climate-related variables suggest future physiological impairment in an oceanic predator. *Proceedings of the National Academy of Sciences of the USA*, 105, 20776-20780.

ROST, B., RIEBESELL, U., BURKHARDT, S., SULTEMEYER, D. (2003). Carbon acquisition of bloom-forming marine phytoplankton. *Limnology and Oceanography*, 48, 55-67.

RUBIN, S. I., & PING WU, H. (2000). A novel fiber-optic sensor for the long-term, autonomous measurement of pCO_2/Sub 2/ in seawater. OCEANS 2000 MTS/IEEE Conference and Exhibition.

RUSHDI, A. I. (2015). Calcite and aragonite saturation states of the Red Sea and biogeochemical impacts of excess carbon dioxide. In: Rasul, N., and Stewart, I. (eds). The Res Sea. Springer Earth System Sciences. Springer, Berlin, Heidelberg.

SABINE, C. L., & KEY, R. M., FEELY, R. A., & GREELEY, D. (2002). Inorganic carbon in the Indian Ocean: Distribution and dissolution processes. *Global Biogeochemical Cycles*, 16(**4**), 1067.

SABINE, C. L., FEELY, R. A., GRUBER, N., KEY, R. M., LEE, K., BULLISTER, J. L., WANNINKHOF, R., WONG, C. S., WALLACE, D. W. R., TILBROOK, B., MILLERO, F. J., PENG, T-H., KOZYR, A., ONO, T. & RIOS, A. F. (2004). The oceanic sink for anthropogenic CO_2. *Science*, 305, 367-371.

SADERNE, V., FIETZEK, P., & HERMAN, P. M. J. (2013). Extreme variations of pCO_2 and pH in a macrophyte meadow of the Baltic Sea in summer: Evidence of the effect of photosynthesis and local upwelling. *PLoS ONE*, 8(4), e62689.

SALISBURY, A., GREEN, M., HUNT, C., & CAMPBELL, J. (2008). Coastal acidification by rivers: a threat to shellfish? *EOS*, 89, 513-528.

SARMIENTO, J. L., & GRUBER, N. (2002). Sinks for anthropogenic carbon. *Physics Today*, 55, 30-36.

SCHAR, D., ATKINSON, M., JOHENGEN, T., PINCHUK, A., PURCELL, H., ROBERTSON, C., SMITH, G. J., & TAMBURRI, M. (2009). Performance demonstration statement. Sunburst Sensors SAMI-CO2. UMCES Technical report series Ref. No. [UMCES]CBL. 10-094.

SCHAR, D., ATKINSON, M., JOHENGEN, T., PINCHUK, A., PURCELL, H., ROBERTSON, C., SMITH, G. J., & TAMBURRI, M. (2010(a)). Performance demonstration statement. Contros HydroC™/CO2. UMCES Technical report series Ref. No. [UMCES]CBL. 10-091.

SCHAR, D., ATKINSON, M., JOHENGEN, T., PINCHUK, A., PURCELL, H., ROBERTSON, C., SMITH, G. J., & TAMBURRI, M. (2010(b)). Performance demonstration statement. PMEL MAPCO2/Battelle Seaology pCO_2 Monitoring System. UMCES Technical report series Ref. No. [UMCES]CBL. 10-092.

SCHAR, D., ATKINSON, M., JOHENGEN, T., PINCHUK, A., PURCELL, H., ROBERTSON, C., SMITH, G. J., & TAMBURRI, M. (2010(c)). Performance demonstration statement. Pro-Oceanus System Inc. PSI CO2-Pro. UMCES Technical report series Ref. No. [UMCES]CBL. 10-093.

SCHULZ. K. G., & RIEBESELL, U. (2013). Diurnal changes in seawater carbonate chemistry speciation at increasing atmospheric carbon dioxide. *Marine Biology*. 160(**8**), 1889-1899.

SCHUMANN, R., BAUDLER, H., GLASS, A., DUMCKE, K., & KARSTEN, U. (2006). Long-term observations on salinity dynamics in a tide less shallow coastal lagoon of the southern Baltic Sea coast and their biological relevance. *Journal of Marine Syst*ems, 60, 193-404.

SCRIPPS, THE KEELING CURVE, vol. 25, May 2016. Available from https://scripps.ucsd.edu/programs/keelingcurve/

SEBENS, K. P. (1994). Biodiversity of coral reefs: what are we losing and why? *American Zoologist*. 34, 115-133.

SEJR, M. K., KRAUSE-JENSEN, D., RYSGAARD, S., SORENSEN, L. L., CHRISTENSEN, P. B., & GLUD, R. N. (2011). Air-sea flux of CO_2 in arctic coastal waters influenced by glacial melt water and sea ice. *Tellus Series B; Chemical and Physical Meteorology, 63(5)*, 815-822.

SIGMAN, D. M., & HAIN, M. P. (2012). The biological productivity of the ocean. *Nature Education*, 3(**6**), 1-16.

SILVERMAN, J., LAZAR, B., CAO, L., CALDIERA, K. & EREZ, J. (2009). Coral

reefs may start dissolving when atmospheric CO_2 doubles. *Geophysical Research Letters*, 36, L05606.

SHI, D., XU, Y., MOREL F. M. M. (2009). Effects of the pH/pCO_2 control method on medium chemistry and phytoplankton growth. *Biogeosciences*, 6, 1199-1207.

SHICK, J. M., LESSER, M. P., & JOKIEL, P. L. (1996). Ultraviolet radiation and coral stress. *Global change biology*, 2, 527-545.

SHITASHIMA, K. (2010). Evolution of compact electrochemical in-situ pH-pCO_2 sensor using ISFET-pH electrode. *Oceans I*, 4, 20-23.

SHITASHIMA, K., MAEDA, Y., & SAKAMOTO, A. (2015). Detection and monitoring of leaked CO_2 through sediment, water column and atmosphere in a sub-seabed CCS experiment. *International Journal of Greenhouse Gas Control*, 38, 135-142.

SHORT, F., CARRUTHERS, T., DENNISON, W., & WAYCOTT, M. (2007). Global seagrass distribution and diversity: A bioregional model. *Journal of Experimental Marine Biology and Ecology*, 350, 3-20.

SKOOG, D. A., HOLLER, F. J., & CROUCH, S. R. (2006). *Principles of Instrument Analysis*, 6th Ed.: Brooks Cole: Belmont, CA, USA, 2006.

SMEED, D. A. (1997). Seasonal variation of the flow in the strait of Bab el Mandab. *Oceanological Acta*, 20(**6**), 773-781.

SOFIANOS, S. S., & JOHNS, W. E. (2002). An Oceanic General Circulation Model (OGCM) investigation of the Red Sea circulation: 1. Exchange between the Red Sea and the Indian Ocean. *Journal of Geophysical Research*, 107, 3196.

SOFIANOS, S. S., JOHNS, W. E., & MURRAY, S. P. (2002). Heat and freshwater budgets in the Red Sea from direct observations at Bab el Mandeb. *Deep sea research.*, in press, 2002.

SOFIANOS, S. S., & JOHNS, W. E. (2003). An Oceanic General Circulation Model (OGCM) investigation of the Red Sea circulation: 2.Three-dimensional circulation in the Red Sea. *Journal of Geophysical Research*, 108, 3066.

SOUVERMEZOGLOU, T., METZEL, N., & POISSON, A. (1989). Red Sea budgets of salinity, nutrients and carbon calculated in the Strait of Bab Al Mandab during summer and winter seasons. *Journal of Marine Research*, 47, 441-456.

SPENCER, T., TELEKI, T. A., BRADSHAW, C & SPALDING, M. (2000). Coral

bleaching in the southern Seychelles during the 1997 – 1998 Indian Ocean warm event. *Marine Pollution Bulletin*, 40, 569 – 586.

SPIETZ, R. L., WILLIAMS, C. M., ROCAP, G. R., & HORNER-DEVINE, C. M. (2015). A dissolved osygen threshold for shifts in bacterial community structure in a seasonally hypoxic estuary. *PLoS One*, 10(**8**): e0135731.

STEINACHER, M., JOOS, F., FROLICHER, T. L., PLATTNER, G. K. & DONEY, S. C. (2009). Imminent ocean acidification in the Arctic projected with the NCAR global coupled carbon cycle-climate model. *Biogeosciences*, 6, 515-533.

STRIEGL, R. G., DORNBLASER, M. M. AIKEN, G. R. WICKLAND, K. P., & RAYMOND, P. A. (2007). Carbon export and cycling by the Yukon, Tanana, and Porcupine rivers, Alaska, 2001-2005. *Water Resources Research*, 43(2).

SUCHANEK, T. H. (1994). Temperate coastal marine communities: biodiversity and threats. *American zoologist*, 34, 100-114.

SUTTON, A. J., FEELY, R. A., SABINE, C. L., MCPHADEN, M. J., TAKAHASHI, T., CHAVEZ, F. P., FRIEDERICH, G. E. & MATHIS, J. T. (2014). Natural variability and anthropogenic change in equatorial Pacific surface ocean pCO_2 and pH. *American Geophysical Union*, doi: 10.1002/2013GB004679.

SUZUKI, A., & KAWAHATA, H. (2003). Carbon budget of coral reef systems: an overview of observations in fringing reefs, barrier reefs and atolls in the Indo-Pacific regions. *Tellus B*, 55, 428-444.

SVERDRUP, H. U., JOHNSON, M. W., & FLEMING, R. H. (1942). The Oceans: Their physics, chemistry and general biology. Prentice-Hall. pp1087.

SWANSON, A. K. & FOX, C. H. (2007). Altered kelp (*Laminariales*) phlorotannins and growth under elevated carbon dioxide and UV-B treatments can influence associated intertidal food webs. *Global Change Biology*, 13, 1696-1709.

TAKAHASHI, T., OLAFSSON, J., GODDARD, J. G., CHIPMAN, D. W., & SUTHERLAND, S. C. (1993). Seasonal variation of CO_2 and nutrients in the high-latitude surface oceans: A comparative study. *Global Biogeochemical Cycles*, 7(**4**), 843-878.

TAKAHASHI. T., FEELY, R. A., WEISS, R. F., WANNINKHOF, R. H., CHIPMAN, D.

W., SUTHERLAND, S. C., & TAKAHASHI, T. T. (1997). Global air-sea flux of CO_2: An estimate based on measurements of sea-air pCO_2 difference. *Proceedings of the National Academy of Science USA*. 94, 8292-8299.

TAKAHASHI, T., SUTHERLAND, S., SWEENEY, C., POISSON, A., MTZL, N., TILBROOK, B., BATES, N., WANNINKHOF, R., FEELY, R., SABINE, C, OLAFSSON, J., & NOJIRI, Y. (2002). Global sea-air CO_2 flux based on climatological surface ocean pCO_2 and seasonal biological and temperature effects. *Deep-Sea Research II*, 49, 1601-1622.

TAKAHASHI, T., SUTHERLAND, S. C., WANNINKHOF, R., SWEENY, C., FEELY, R. A., CHIPMAN, D. W., *et al*. (2009). Climatological mean and decadal changes in surface ocean pCO_2, and net sea-air CO_2 flux over the global oceans. *Deep-Sea Research Part II*, 56, 554-577.

TAKESHITA, Y., MCGILLIS, W., BRIGGS, E. M., CARTER, A., DONHAM, E., MARTX, T. R., PRICE, N. N., & SMITH, J. E. (2016). Assessment of net community production and calcification of a coral reef using a boundary layer approach. *Journal of Geophysical Research: Oceans*.

TALLEY, L. D., & PICKARD, G. L. (2011). Descriptive physical oceanography (sixth edition). Elsevier Ltd.

TALMAGE, S. C. & GOBLER, C. J. (2009). The effects of elevated carbon dioxide concentrations on the metamorphosis size and survival of larval hard clams (Mercenaria *mercenaria*), bay scallops (*Argopecten irradians*), and Eastern oysters (*Crassostrea virginica*). *Limnology and Oceanography*, 54, 2072-2080.

TAN, S. C., YAO, X., GAO, H. W., SHI, G. Y., YUE, X. (2013). Variability in the correlation between Asian dust storms and chlorophyll *a* concentration from the north to equatorial Pacific. *PLoS ONE*. 8(2): e57656.

THOMAS H. & SCHNEIDER, B. (1999). The seasonal cycle of carbon dioxide in Baltic Sea surface waters. *Journal of Marine Systems*, 22, 53-67.

THOMAS, H., BOZEC, Y., ELKALAY, K., DE BAAR, H. J. W. (2004). Enhanced open ocean storage of CO_2 from shelf sea pumping. *Science*, 304, 1005-8.

THUNNELL, R., ANDERSON, D., GELLAR, D., & MIAO, Q. (1994). Sea-surface temperature estimates for the tropical western Pacific during the last glaciations and their implications for the Pacific warm pool. *Quaternary Research*. 41, 255-264.

TIMMS, G. P., DE SOUZA, P. A. JR., REZNIK, L., & SMITH, D. V. (2011).

Automated data quality assessment of marine sensors. *Sensors*, 11, 9589 – 9602.

TURNER, J & OVERLAND, J. (2009). Contrasting climate change in the two polar regions. *Polar Research*, 28, 146-164.

UPSTILL-GODDARD, R. C. (2006). Air-sea gas exchange in the coastal zone. *Estuarine, Coastal and Shelf Science*, 70(**3**), 388-404.

VERON, J. E. N. (1986). *"Corals of Australia and the Indo-Pacific"*. Angus and Robertson: London/Sydney.

VISSER, M. E. (2008). Keeping up with a warming world; assessing the rate of adaptation to climate change. *Proceedings of the Royal Society*, 275, 649-659.

WALTHER, G-R., POST, E., CONVEY, P., MENZELS, A., PARMESAN, C., BEEBEE, J-C., FROMENTIN, J-M., HOEGH-GULDBERG, O., & BAIRLEIN, F. (2002). Ecological responses to recent climate change. Nature, 419, 398 – 395.

WANG, Z. H., WANG, Y. H., CAI, W. I., & LIU, S. Y. (2002). A long pathlength spectrophotometric pCO_2 sensor using a gas-permeable liquid-core waveguide. *Talanta*, 57(1), 69-80.

WANG, Z. A., CAI, W. J., WANG, Y. C., & UPCHURCH, B. L. (2003). A long pathlength liquid-core waveguide sensor for real-time pCO_2 measurements at sea. *Marine Chemistry*, 84(1-2), 73-84.

WANG, Y., NAKAYAMA, M., TAGI, M., NISHIKAWA, M., FUKUNAGA, M., WATANABE, K. (2005). The NDIR CO_2 monitor with smart interface for global networking. *IEEE Transactions on Instrumentation and Measurements*, 54, 1634-1639.

WANNINKHOF, R. (1992). Relationship between wind speed and gas exchange over the ocean. *Journal of Geophysical Research*, 97, 7373-7382.

WANNINKHOF, R., Lewis, E., Feely, R. A., and Millero, F. J. (1999). The optimal carbonate dissociation constants for determining surface water pCO_2 from alkalinity and total inorganic carbon. *Marine Chemistry*, 65(3-4), 291-301.

WARE, J. R., SMITH, S. V., & REAKA-KUDLA, M. L. (1992). Coral reefs: sources or sinks of atmospheric CO_2? *Coral Reefs*, 11, 127-130.

WATSON, A. J., ROBINSON, C., ROBINSON, J. E., WILLIAMS, P. J. B., & FASHAM, M. J. R. (1991). Spatial variability in the sink for atmospheric carbon dioxide in the North Atlantic. *Nature*, 350, 50-53.

WATSON, R., HOUGHTON, J. & YIHUI, D. (2001). Climate change 2001: The

Scientific Basis. Intergovernmental Panel on Climate Change. Cambridge University Press, Cambridge.

WAYNE, R. P. (2000). Chemistry of atmospheres, 3rd edition. Oxford University Press.

WEISS, R. F. (1974). Carbon dioxide in water and seawater: The solubility of a non-ideal gas. *Marine Chemistry*, 2(**3**), 203-15.

WESSLANDER, K., HALL, P. O. J., HJALMARSSON, S., LEFEVRE, D., OMSTEDT, A., RUTGERSSON, A., Sahlee, E., & Tengberg, A. (2011). Observed carbon dioxide and oxygen dynamics in a Baltic Sea coastal region. *Journal of Marine Systems*, 86, 1-9.

WETZEL, R. G. (2001). Limnology: Lake and river ecosystems (3rd ed.). San Diego, CA: Academic Press.

WIEDEMANN, A. M., & PICKART, A. J. (2004). Temperate zone coastal dunes. *In* Coastal Dunes, Ecology and Conservation, Martinez, M. L., and Psuty, N. P. [eds.]. Ecological Studies, 171. Springer-Verlag Berlin Heidelberg.

WILKINSON, C. R., & BUDDEMEIER, R. W. (1994). Global climate change and coral reefs: implications for people and reefs. Report of the UNEP-IOC-ASPEI-IUCN global task team on the implications of climate change on coral reefs. IUCN, Gland, Switzerland, 124 pp.

WILKINSON, M., HASZELDINE, R. S., MACKAY, E., SMITH, K. & SARGEANT, S. (2013). A new stratigraphic trap for CO_2 in the UK North Sea: Appraisal using legacy information. *International Journal of Greenhouse Gas Control*, 12, 310-322.

WILLIAMS, R. G., & FOLLOWS, M. J. (2011). Ocean dynamics and the carbon cycle. Cambridge University Press.

WINTER, A., APPELDOORN, R. S., BRUCKNER, A., WILLIAMS, E. H. JR, & GOENAGA, C. (1998). Sea surface temperatures and coral reef bleaching off La Parguera, Puerto Rico (northeastern Caribbean Sea). *Coral Reefs*, 17, 377-382.

WOLF, A., & CLARK, J. (2014). Le Chatelier's Principle. UCDavis Chemwiki.

WOLF-GLADROW, D. A., ZEEBE, R. E., KLAAS, C., KORTZINGER, A., & DICKSON, A. G. (2007). Total alkalinity: The explicit conservative expression and its application to biogeochemical processes. *Marine Chemistry*, 106(**1-2**), 287-300.

WOOD, E. J. F., & CORCORAN, E. F. (1966). Diurnal variation in

phytoplankton. *Bulletin of Marine Sci*ence, 16, 383-403.

WOOTTON, J. T., PFISTER, C. A. and Forester, J. D. (2008). Dynamic patterns and ecological impacts of declining ocean pH in a high-resolution multi-year dataset. *Proceedings of the National Academy of Science of the USA*, 105(48), 18848-18853.

WURTS, W. A. & DURBOROW, R. M. (1992). Interactions of pH, carbon dioxide, alkalinity and hardness in fish ponds. *SRAC Publications*, 464, 1-4.

YAMAMOTO-KAWAI, M., MCLAUGHLIN, F. A., CARMACK, E. C., NISHINO, S., SHIMADA, K. (2009). Aragonite undersaturation in the Arctic Ocean: effects of ocean acidification and sea ice melt. *Science*, 326, 1098-1100.

YAO, W. & BYRNE, R. H. (1998). Simplified seawater alkalinity analysis: Use of linear array spectrometers. *Deep-Sea Research I*. 45, 1383-1392.

YATES, K. K., & HALLEY, R. B. (2006). CO_3^{2-} concentration and pCO_2 thresholds for calcification and dissolution on the Molokai reef flat, Hawaii. *Biogeosciences*, 3, 357-369.

YENTSCH, C. S., & RYTHER, J. H. (1957). Short-term variations in phytoplankton chlorophyll and their significance. *Limnology and Oceanography*, 2, 140-142.

YENTSCH, C. S., & SCAGEL, R. F. (1958). Diurnal study of phytoplankton pigments: an *in situ* study in East Sound, Washington. *Journal of Marine Rese*arch, 17, 567-583.

YODER, J. A., & KENNELLY, M. A. (2003). Seasonal and ENSO variability in global ocean phytoplankton chlorophyll derived from 4 years of SeaWiFS measurements. *Global Biogeochemical Cycles*, 17(**4**), 1112.

YOUNG, R. W., CARDER, K. L. BETZER, P. R., COSTELLO, D. K., DUCE, R. A., DI TULLO, G. R., TINDALE, N. W., LAWS, E. A., UEMATSU, M., MERRILL, J. T., & FEELY, R. A. (1991). Atmospheric iron inputs and primary productivity: phytoplankton responses in the North Pacific. *Global Biogeochemical Cycles*, 5, 119-134.

YOU-WEN, S., YI, ZENG, Y., WEN-QING, L., PIN-HUA, X., KA-LOK, C., XIAN-XIN, L., SHI-MEI, W., & SHU-HUA, H. (2012). Cross-interference correction and simultaneous multi-gas analysis based on infrared absorption. *Chinese Physical Society B*. 21(**9**), 090701-1.

ZANG, C., HUANG, S., WU, M., DU, S., SCHOLZ, M,. GAO, F., LIN, C., GUO, Y., &

DONG, Y. (2011). Comparison of relationships between pH, dissolved oxygen and chlorophyll *a* for aquaculture and non-aquaculture waters. *Water, Air and Soil Pollution*, 219, 157-174.

ZEEBE, R. E. & WOLF-GLADROW, D. A. (2001). CO_2 in seawater: Equilibrium, Kinetics, Isotopes. *Elsevier Oceanography Series*. Amsterdam.

ZHANG, Z., FALTER, J., LOWE, R., & IVEY, G. (2012). The combined influence of hydrodynamic forcing and calcification on the spatial distribution of alkalinity in a coral reef system. *Journal of Geophysical Research*, 117, CO4034.

ZONDERVAN, I. (2007). The effects of light, macronutrients, trace metals and CO_2 on the production of calcium carbonate and organic carbon in coccolithophores – a review. *Deep-Sea Research II*, 54, 521-537.

Appendix

Calibration of pCO_2 sensor

1. Using the COZIR USB cable with the COZIR sensor connected to the other end, plug into computer that has COZIR Sensor 2.0 software downloaded onto it.

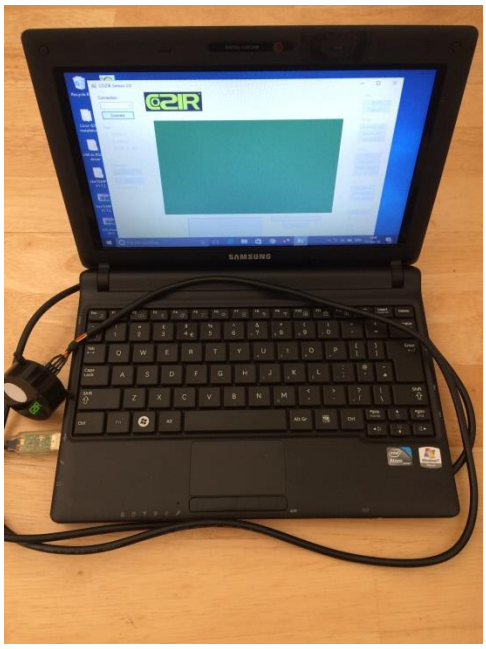

2. At the top left, select the correct port (only one should be available) and then press *Connect*.

3. The sensor should now be connected to the software and a humidity (or temperature) reading plus a CO_2 reading should be scrolling. If this is not happening, press *Stream (K1)* in the Mode category to the right of the screen.

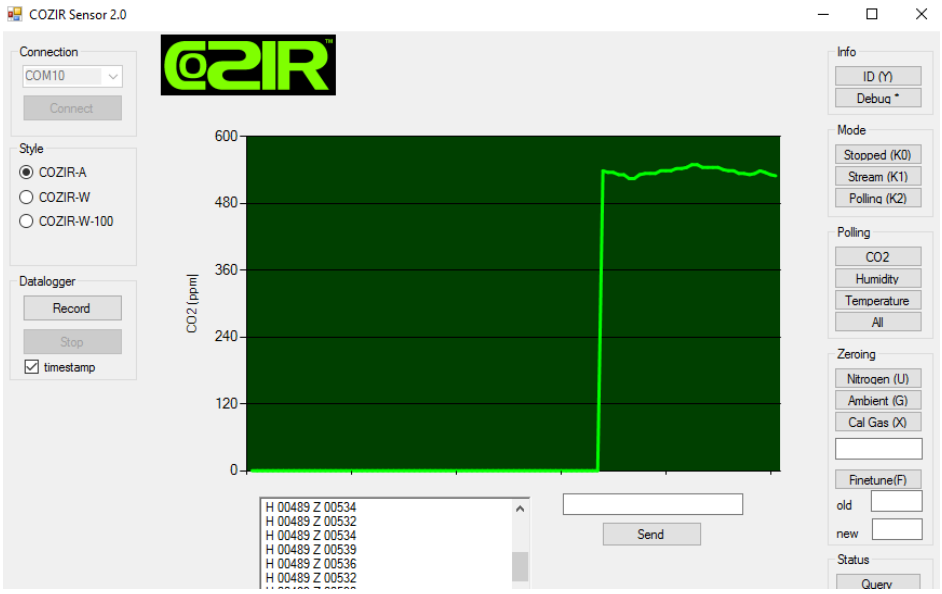

4. Ideally the sensor should be calibrated with known gases. Place the sensor in calibration housing where gases can be injected. Inject gas (e.g., 1000 ppm) and allow sensor to settle. If sensor is not accurate, proceed to next step.

5. In the Zeroing box on the right, press *Cal Gas (X)*.

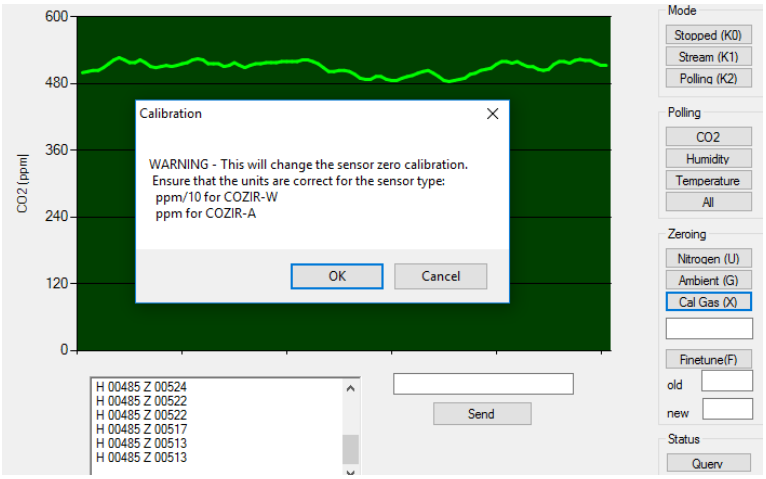

6. This will zero the sensor

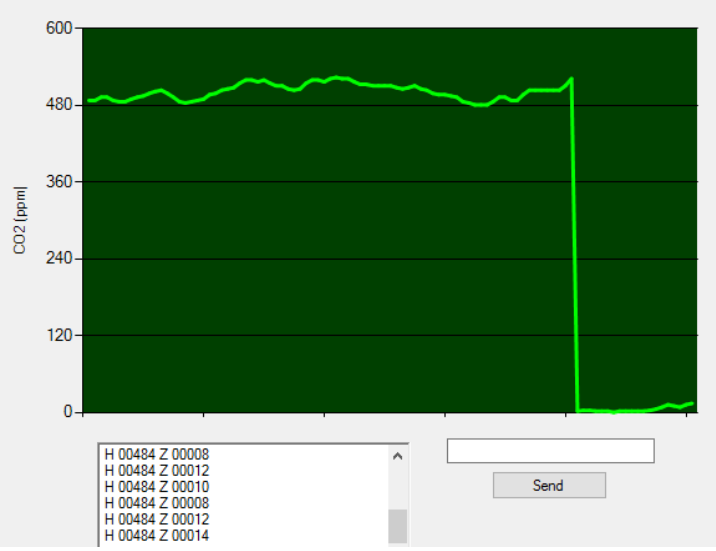

7. Make sure gas flushes through chamber and sensor settles. Input gas concentration in box (i.e. 1000 ppm) and press *Cal Gas (X)* again. The sensor should now be reading the correct concentration of the calibration gas.

8. You should then move onto the next concentration of calibration gas and test the reading from the sensor. The more calibration gases that can be used, the better.

Code

RTC (RTC_code)

```
#include <Wire.h>
const int DS1307 = 0x68;
const char* days[] =
{"Sunday", "Monday", "Tuesday", "Wednesday", "Thursday", "Friday", "Saturday"};
const char* months[] =
{"January", "February", "March", "April", "May", "June", "July",
"August","September", "October", "November", "December"};


byte second = 0;
byte minute = 0;
byte hour = 0;
byte weekday = 0;
byte monthday = 0;
byte month = 0;
byte year = 0;

void setup() {
  Wire.begin();
  Serial.begin(9600);
  delay(2000);

  Serial.print("The current date and time is: ");
  printTime();
  Serial.println("Please change to newline ending the settings on the lower right
of the Serial Monitor");
  Serial.println("Would you like to set the date and time now? Y/N");

  while (!Serial.available()) delay(10);
  if (Serial.read() == 'y' || Serial.read() == 'Y')

  {
    Serial.read();
    setTime();
    Serial.print("The current date and time is now: ");
    printTime();
  }


  Serial.println("Thank you.");
}

void loop() {
}
byte decToBcd(byte val) {
  return ((val/10*16) + (val%10));
}
byte bcdToDec(byte val) {
```

```
  return ((val/16*10) + (val%16));
}

void setTime() {
  Serial.print("Please enter the current year, 00-99. - ");
  year = readByte();
  Serial.println(year);
  Serial.print("Please enter the current month, 1-12. - ");
  month = readByte();
  Serial.println(months[month-1]);
  Serial.print("Please enter the current day of the month, 1-31. - ");
  monthday = readByte();
  Serial.println(monthday);
  Serial.println("Please enter the current day of the week, 1-7.");
  Serial.print("1 Sun | 2 Mon | 3 Tues | 4 Weds | 5 Thu | 6 Fri | 7 Sat - ");
  weekday = readByte();
  Serial.println(days[weekday-1]);
  Serial.print("Please enter the current hour in 24hr format, 0-23. - ");
  hour = readByte();
  Serial.println(hour);
  Serial.print("Please enter the current minute, 0-59. - ");
  minute = readByte();
  Serial.println(minute);
  second = 0;
  Serial.println("The data has been entered.");

  Wire.beginTransmission(DS1307);
  Wire.write(byte(0));
  Wire.write(decToBcd(second));
  Wire.write(decToBcd(minute));
  Wire.write(decToBcd(hour));
  Wire.write(decToBcd(weekday));
  Wire.write(decToBcd(monthday));
  Wire.write(decToBcd(month));
  Wire.write(decToBcd(year));
  Wire.write(byte(0));
  Wire.endTransmission();
  // Ends transmission of data
}


byte readByte() {
  while (!Serial.available()) delay(10);
  byte reading = 0;
  byte incomingByte = Serial.read();
  while (incomingByte != '\n') {
    if (incomingByte >= '0' && incomingByte <= '9')
      reading = reading * 10 + (incomingByte - '0');
    else;
    incomingByte = Serial.read();
  }
  Serial.flush();
  return reading;
```

```
}


void printTime() {
  char buffer[3];
  const char* AMPM = 0;
  readTime();
  Serial.print(days[weekday-1]);
  Serial.print(" ");
  Serial.print(months[month-1]);
  Serial.print(" ");
  Serial.print(monthday);
  Serial.print(", 20");
  Serial.print(year);
  Serial.print(" ");
  if (hour > 12) {
    hour -= 12;
    AMPM = " PM";
  }
  else AMPM = " AM";
  Serial.print(hour);
  Serial.print(":");
  sprintf(buffer, "%02d", minute);
  Serial.print(buffer);
  Serial.println(AMPM);
}


void readTime() {
  Wire.beginTransmission(DS1307);
  Wire.write(byte(0));
  Wire.endTransmission();
  Wire.requestFrom(DS1307, 7);
  second = bcdToDec(Wire.read());
  minute = bcdToDec(Wire.read());
  hour = bcdToDec(Wire.read());
  weekday = bcdToDec(Wire.read());
  monthday = bcdToDec(Wire.read());
  month = bcdToDec(Wire.read());
  year = bcdToDec(Wire.read());
}
```

pCO_2, humidity and/or temperature code (*Cozir_sensor_example_CO2Meter_v4)*

```
#include <Time.h>

#include <SPI.h>

#include <SoftwareSerial.h>
```

```
#include <SD.h>
#include <Time.h>
#include <Wire.h>
#pragma GCC diagnostic ignored "-Wwrite-strings"
#include <DS1307RTC.h>

SoftwareSerial mySerial(2,3);


String fileName;
File myFile;


String val="";
double co2=0;

double multiplier=10;


uint8_t buffer[40];
int ind=0;
char cmd[15];
char output;

int imeas=0;

char fName[14];


void setup()
{



  Serial.begin(9600);
  delay(3000);

  Serial.println(F("CO2meter.com Cozir example"));
  Serial.println(F("Setup"));


 setSyncProvider(RTC.get);
  if(timeStatus()!= timeSet)
     Serial.println("Unable to sync with the RTC");
  else
     Serial.println("RTC has set the system time");


  mySerial.begin(9600);


  sprintf(cmd, "K %u", 0);
  Serial.println(cmd);
```

```
 Command(cmd);
 delay(600);
 Serial.println(mySerial.available());
 Serial.print(F("Response from K 0 "));
 while (mySerial.available() > 0) {
   output = mySerial.read();
   Serial.print(output);
 }
 Serial.println(" ");


 Command("Y");
 delay(600);
 Serial.println(mySerial.available());
 Serial.print(F("Response from Y "));
 while (mySerial.available() > 0) {
   output = mySerial.read();
   Serial.print(output);
 }
 Serial.println(" ");


 sprintf(cmd, "K %u", 2);
 Serial.println(cmd);
 Command(cmd);
 delay(600);
 Serial.print(F("Response from K 2 "));
 while (mySerial.available() > 0) {
   output = mySerial.read();
   Serial.print(output);
 }
 Serial.println(" ");
   sprintf(cmd, "M %u", 4100);    // for Humidity input 4100, for Temp input 68
 Serial.println(cmd);
 Command(cmd);
 delay(600);
 Serial.print(F("Response from M"));
 while (mySerial.available() > 0) {
   output = mySerial.read();
  Serial.print(output);
 }
Serial.println("");

 Serial.print(F("Initializing SD card..."));



 pinMode(10, OUTPUT);

 if (!SD.begin(10)) {
   Serial.println(F("initialization failed!"));
   return;
 }
```

```
  Serial.println(F("initialization done."));


  }
}

void loop()

{


  if (timeStatus() == timeSet) {
    digitalClockDisplay();
  } else {
    Serial.println("The time has not been set.  Please run the Time");
    Serial.println("TimeRTCSet example, or DS1307RTC SetTime example.");
    Serial.println();
    delay(1000);
  }
  delay(600);
}

void digitalClockDisplay(){
  // digital clock display of the time
  Serial.print(hour());
  printDigits(minute());
  printDigits(second());
  Serial.print(" ");
  Serial.print(day());
  Serial.print(" ");
  Serial.print(month());
  Serial.print(" ");
  Serial.print(year());
  Serial.println();
}

void printDigits(int digits){
  Serial.print(":");
  if(digits < 10)
    Serial.print('0');
  Serial.print(digits);


  imeas++;
  Serial.print(F("imeas="));
  Serial.println(imeas);

  if (imeas == 1) {
     fileName="";
  if (day() < 10) {
     fileName.concat(F("0"));
     fileName.concat(day());
  }
```

```
  else {
     fileName.concat(day());
  }
  if (month() < 10) {
    fileName.concat(F("0"));
    fileName.concat(month());
  }
  else {
    fileName.concat(month());
  }
  if (hour() < 10) {
    fileName.concat(F("0"));
    fileName.concat(hour());
  }
  else {
    fileName.concat(hour());
  }
  if (minute() < 10) {
    fileName.concat(F("0"));
    fileName.concat(minute());
  }
  else {
    fileName.concat(minute());
  }
  fileName.concat(F(".txt"));
  Serial.println(fileName);
  fileName.toCharArray(fName, fileName.length()+1);
   Serial.print(F("Filename: "));
   Serial.println(fName);

    myFile = SD.open(fName,FILE_WRITE);
    if (!myFile) {
      Serial.println(F("File open failed"));
      return;
    }
  }

  delay(1000);
   Command("Q");



delay(300000);  //this line changes the frequency of readings

  ind=0;
  Serial.print(F("ind and buffer value "));
  Serial.print(ind);
  Serial.print(" ");
  Serial.println(buffer[ind]);

  Serial.println(F("reading line"));

  Serial.println(mySerial.available());
```

```
  while(mySerial.available() > 0)
          {
     buffer[ind]=mySerial.peek();
     output = mySerial.read();
     Serial.print(output);
     ind++;
    }
    Serial.println(F(" "));
    Serial.flush();

  report();
  myFile.flush();
  if (imeas == 20) {
     myFile.close();
     Serial.println(F("Close file"));
     imeas=0;
     delay(1000);
  }
}

void report()
{


  for(int i=0; i< ind+1; i++)
  {
    if ((buffer[i] > 47) && (buffer[i] < 58))
    {
      val += buffer[i]-48;


    }
  }

  Serial.println(F(""));

  co2=(multiplier*val.toInt());

  Serial.print(F("CO2="));
  Serial.print(co2);
  Serial.println(F("ppm"));
  Serial.flush();
  ind=0;
  val="";
  myFile.print(year());
 if (month() < 10) {
    myFile.print(F("0"));
    myFile.print(month());
  }
  else {
    myFile.print(month());
  }
  if (day() < 10) {
```

```
    myFile.print(F("0"));
    myFile.print(day());
  }
  else {
    myFile.print(day());
  }
    if (hour() < 10) {
    myFile.print(F("0"));
    myFile.print(hour());
  }
  else {
    myFile.print(hour());
  }
  if (minute() < 10) {
    myFile.print(F(" 0"));
    myFile.print(minute());
  }
  else {
    myFile.print(minute());
  }
    if (second() < 10) {
    myFile.print(F("0"));
    myFile.print(second());
  }
  else {
    myFile.print(second());
  }
  myFile.print(F(","));
  myFile.print(F("CO2"));
  myFile.print(F(","));
  myFile.print(co2);
  myFile.print(F(","));
  myFile.println(F("ppm"));
}

void Command(char* s)
{
  mySerial.print(s);
  mySerial.print("\r\n");
}
```

SOP for pCO_2 sensor

1. Download the latest version of Arduino software (IDE) from https://www.arduino.cc/en/Main/Software. This allows you to write code (sketches) and upload it to the board.

2. Open text editor box by clicking on the Arduino icon on your desktop:

3. A text editor box should appear. Delete any pre-existing text in the box and copy and paste *RTC_code* in one text editor box.

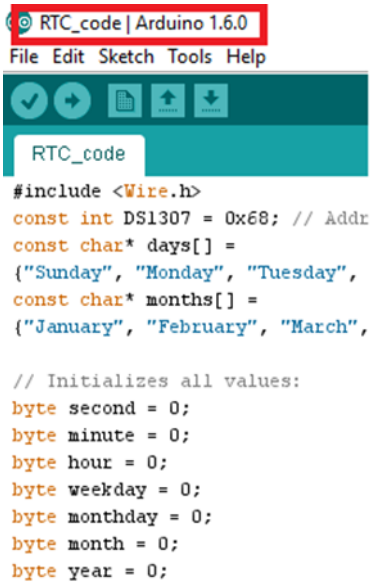

4. Whilst this text editor box is still open, click *File* then *New* to open another simultaneous text editor box. Delete any pre-existing text in the box and copy and paste *Cozir_sensor_example_CO2Meter_v4* in.

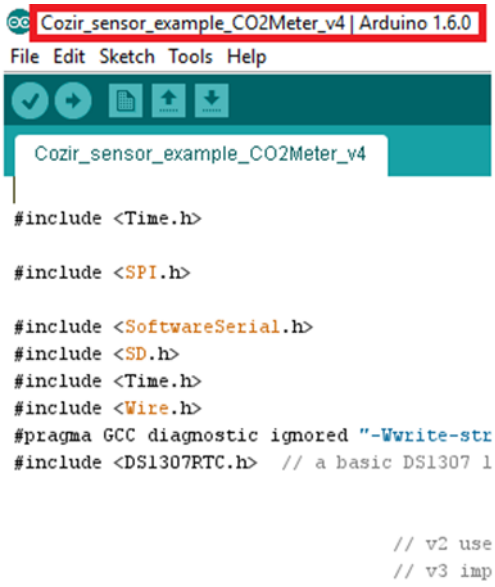

5. Connect Arduino board and sensor to laptop via USB cable. A green and a red light should appear on the electronics.

6. Ensure SD card is loaded onto the top Arduino shield (Real-Time Clock above the main Arduino board).

7. Firstly, on *RTC_code* press the arrow to upload the code onto the Arduino board

8. After a few moments, it will be compiled. Press the magnifying button at the top right corner of the Arduino programme which opens the dialogue box

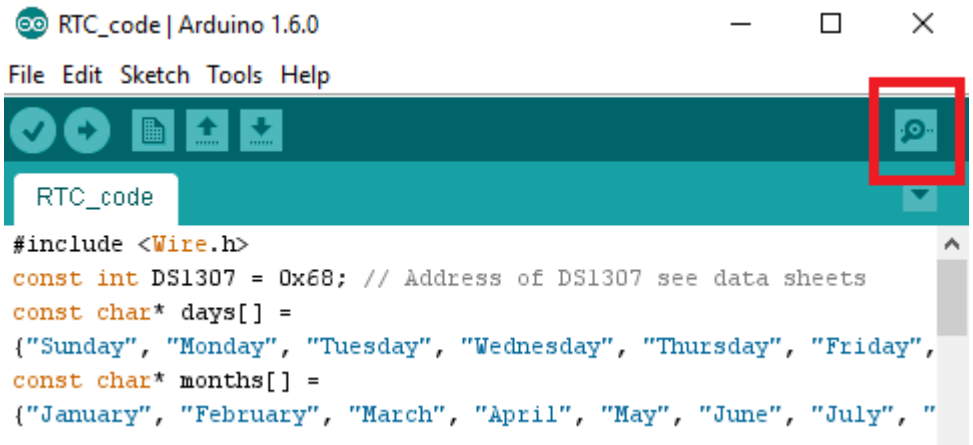

9. The dialogue box will open

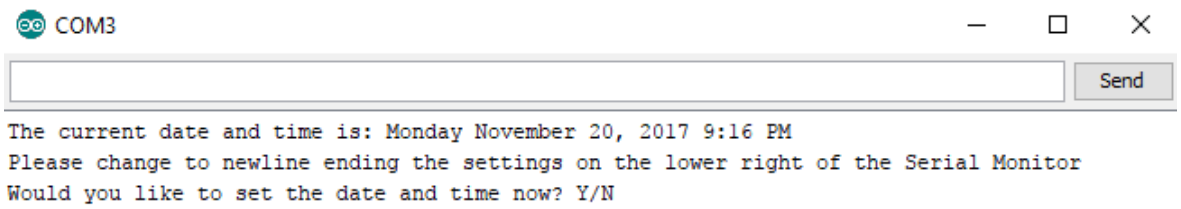

If you need to set the date and time follow the instructions in the dialogue box, i.e.

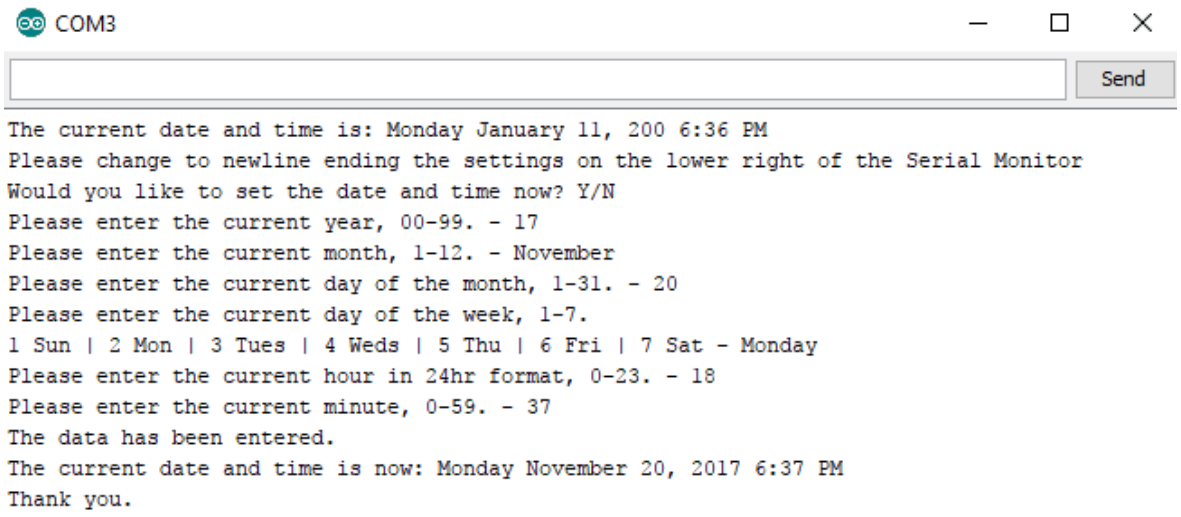

10. Next, upload the CO_2 code from the data file *Cozir_sensor_example_CO2Meter_v4*. Again, press the arrow to upload the code onto the Arduino board.

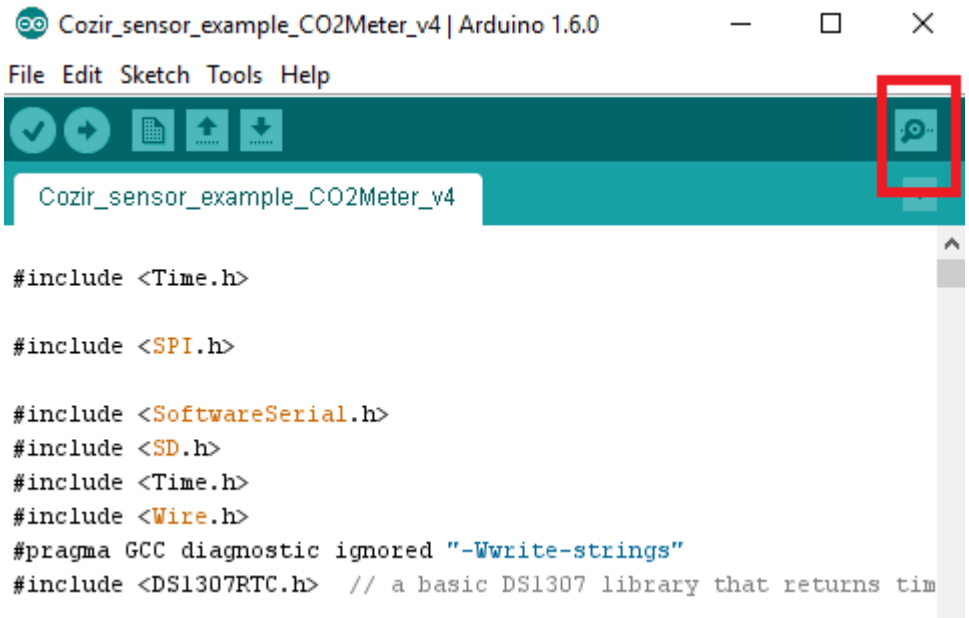

11. The dialogue box will open, and there should be readings of CO_2 plus humidity (or temperature depending on set-up). These will simultaneously be being downloaded on the SD card also.

12. Connect battery pack to Arduino board BEFORE disconnecting the sensor and electronics.

13. Disconnect sensor and electronics from the laptop via the USB cable.

14. Place sensor and electronics in the PTFE tube.

15. Make sure the o-ring is clean and free of any detritus and place a small amount of o-ring grease over the surface.

16. If possible, before deployment and when the sensor is in the PTFE tube, put a flow of air from a gas canister into the tube and quickly place the screw lid on the PFTE tube. This is to dry the air inside the PTFE tube as much as possible. Close the lid and the o-ring should create a waterproof seal.

17. The sensor is now ready to be deployed.

N.B. Within the body of code in *Cozir_sensor_example_CO2Meter_v4* there are two areas highlighted in red. The first is where to manipulate the code depending on whether you want to output CO_2 & Humidity OR CO_2 & Temperature. Change the highlighted red number to 4100 if you wish to output CO_2 & H or change the highlighted red number to 68 if you wish to output CO_2 & T.

The next area highlighted in red is where you can change the frequency of readings, i.e. whether you would like a reading every 10 seconds or every 5 mins etc (or what is needed for your specific work). This is a simple arithmetic problem and the number can be changed accordingly, e.g.

1 Reading every:	Input number:
10s	10000
20s	20000
30s	30000
1 min	60000
2 min	120000
5 min	300000